Characterisation, Quantification and Control of Plasmid DNA Driven Immune Responses in Dendritic Cells

Sadia Yaqub

Submitted for the degree of Doctor of Philosophy

Department of Chemical and Biological Engineering

September 2023

Declaration of Originality

I, Sadia Yaqub, declare this thesis and the results presented to be solely a product of my own work, with clear reference where this is not the case. This thesis has not been submitted in whole or in part for any other degree.

Acknowledgements

First and foremost, I would like to thank my supervisor Dr Adam Brown for his never-ending support and belief in this project, even when things were going wrong. I am also grateful to my industrial supervisor Dr Carl Webster for his consistent interest and feedback.

A huge thank you to the DCJ/AJB lab group for all their comedy and wisdom, especially Dr Abayomi Johnson for teaching me everything I know about dendritic cells.

To my amazing family, thank you for all the laughs, car rides, patience, and support. A special mention to my mum, whose always been my biggest fan.

And of course, my dear friends, whether in Southampton, Leeds, Sheffield, or right at home, thank you for always understanding my absence but still saving me a seat.

And finally, to my wonderful partner, who endured endless ramblings about lab wins and lab losses, your willingness to listen (or at least pretend to) is forever appreciated.

Abstract

DNA-based therapies (vaccines/ gene therapies) utilise plasmid vectors for the delivery of potent biologics, however, their promising application remains restricted by uncontrolled host immunity. This study presents novel technologies for the quantification, characterisation, and control of these DNA-driven immune responses, facilitating the development of safer and more efficacious therapeutics.

Firstly, novel immune-profiling tool 'Nanopanel' was developed, capable of characterising plasmid DNA (pDNA) immune effects across DNA-specific response pathways in murine dendritic cells (DC). An experimental pipeline was designed, validated, and utilised, incorporating an automated analysis app to facilitate medium-throughput screening of vector immunity. Application of this technology will allow highly sensitive quantification of DNA-therapy vector immunogenicity, informing sequence-specific design and/or selection to improve their safety and efficacy.

Secondly, double-stranded DNA (dsDNA) motifs able to suppress immune genes upregulated by pDNA immunity were identified and characterised. A comprehensive library of homotypic and heterotypic constructs were designed and screened, testing 20 DNA motifs in multiple design conditions. Multiple linear regression (MLR) modelling identified six statistically significant sequences capable of gene-level suppression, and seven critical design rules. These findings provide novel insight into pDNA integrated sequence effects, informing the design of immunomodulatory vectors.

Finally, novel application of sequence-specific oligodeoxynucleotide (ODN)'s as immune suppressors of pDNA-driven responses was investigated. dsDNA screening informed the selection of six motifs which, as ODNs, exhibited potent modulatory activity across inflammatory and antiviral pathways. This established a toolbox of ODNs for the control of pDNA immunogenicity. Further optimisation identified M16, a microsatellite-derived ODN capable of counteracting vector cytosine-phosphate-guanine (CpG) stimulation, suppressing TNFa production up to ~70%. M16 expands the design space for vector CpG incorporation, enabling the use of more effective functional components (promoters/ intragenic regions) in gene therapy plasmids, without compromising safety.

Contents

List of Tables

List of Figures

Acronyms and Abbreviations

AAV	adeno-associated viruses
AIM2	absent in melanoma 2
ALI	acute lung injury
APC	antigen presenting cell
BMDC	bone-marrow derived dendritic cells
CASP-1	caspase-1
CD	cluster of differentiation
cftr	cystic fibrosis conductance regulator
cGAMP	cyclic GMP-AMP
cGAS	cyclic GMP-AMP synthase
CpG	cytosine-phosphate-guanine
DAMP	danger associated molecule pattern
DC	dendritic cell
DEAD/H	Asp-Glu-Ala-Asp/His
dsDNA	double-stranded deoxyribonucleic acid
EMA	European medicines agency
ELISA	enzyme-linked immunosorbent assays
FC	fold change
FDA	food and drug administration
FE	final expression
G	guanine
GFP	green fluorescent protein
GO	gene ontology
hrs	hours
HSV-1	herpes simplex virus-1
IBD	inflammatory bowel disease
IEDB-AR	immune epitope database–analysis resource
IFN	interferon
IL	interleukins
INH-ODN	Inhibitory-oligodeoxynucleotides
IRF	interferon regulatory factor
IRS	immunoregulatory sequence
ISD	interferon stimulatory DNA
LNP	lipid nanoparticle
MDA5	melanoma differentiation-association protein 5
MHC	major histocompatibility complex
mins	minutes

MS	multiple sclerosis
MLR	Multiple linear regression
NF-kB	nuclear factor kappa B
NK	natural killers
ODN	oligodeoxynucleotide
PAMP	pathogen associated molecular pattern
PBMC	peripheral blood mononuclear cell
pDC	plasmacytoid DC
pDNA	plasmid deoxyribonucleic acid
PO	phosphodiester
R	purine
PRR	pattern recognition receptors
PS	phosphorothioate
RA	rheumatoid arthritis
RT-PCR	reverse transcription polymerase chain reaction
RIG-1	retinoid-induced gene-1
SLE	systemic lupus erythematosus
ssDNA	single-stranded deoxyribonucleic acid
STING	stimulator of interferon genes
TCR	t cell receptor
TF	transcription factor
TGF-B	transforming growth factor-b
Th	t helper
TLR	toll like receptor
Treg	t regulatory
Y	pyrimidine

Chapter 1 : Literature Review

This study aims to quantify, characterise, and control the DC immune response to dsDNA. Current literature has been summarised in the following introductory chapter to contextualise the work presented within this thesis. This includes i) an overview of DNA-based therapeutics, highlighting the key interactions and limitations of immune detection, ii) a description of sequence-specific DNA motifs capable of stimulating and/ or suppressing various immune response pathways and iii) a discussion of current limitations in the methods used to quantify and control pDNA immunogenicity. This analysis identified two critical opportunities: the development of novel screening tool capable of precisely quantifying pDNA immunogenicity, and the application of immune-modulating motifs as a technology to control immune responses triggered by pDNA therapeutics.

1.1 DNA-driven immune responses to therapeutic vectors

1.1.1 DNA therapeutics

DNA therapeutics have transformed the field of medicine, providing a novel method for treating disease by encoding therapeutic proteins in dsDNA plasmid vectors. Once administered into patients, host cell transcriptional and translational machinery is exploited to express the encoded genes, producing therapeutics in the form of *in vivo* biologics, vaccine components and gene therapy products (Saraswat et al., 2009). As of 2023, the market for biologics (monoclonal antibodies, hormones, growth factors, and fusion proteins) was valued at over USD 401 billion, with a 9.5% growth rate, treating immune-associated diseases such as psoriasis, Crohn's disease, and rheumatoid arthritis (RA) (Biologics Global Market Report, 2023). Encoding these therapeutics within DNA vectors, as opposed to direct administration of proteins/ lipids enables safer, longer-lasting, highly specific, personalised, and broader targeting effects (Ramamoorth and Narvekar, 2015).

Vaccines

Vaccines work by introducing host cells to non-pathogenic components, typically in the form of subunit components, toxins or attenuated/ inactivated pathogens (Restifo et al., 2000). This initial interaction mimics a pathogenic infection, activating an immune response, but is engineered to be safe and non-toxic. The subsequent memory response generated is retained by the host and activated more rapidly and potently upon secondary contact with native, pathogenic strains.

As opposed to more traditional methods of direct administration, DNA vaccine platforms encode these antigenic components within dsDNA vectors offering safer, more stable and cost-effective alternatives (Prazeres and Monteiro, 2014). Over 350 different DNA vaccines are currently being tested as part of human clinical trials across the globe to treat influenza, hepatitis B, rabies, malaria, and more, with a 2020 market value estimated at USD 400 million (ClinicalTrials.gov).

The use of DNA vaccine platforms is expected to grow over the coming decades. Firstly, due to its increasing success as a cancer immunotherapy (Gary and Weiner, 2020; Pandya et al., 2023) and secondly, due to its applicability as a COVID-19, post-pandemic, vaccine technology capable of rapid design, production and distribution across the globe (Excler et al., 2021). Despite recent breakthroughs in RNA technologies, DNA vaccines provide critical advantages including i) lower production costs, ii) easier design and manufacture and iii) higher molecular stability, reducing the need for expensive -80°C transportation and long-term storage (a key barrier for the access and distribution of these therapies across developing nations) (Baghban et al., 2023; Prazeres and Monteiro, 2014).

Gene therapies

Gene therapy platforms can be broadly categorised as 'non-viral' (includes pDNA-based vectors) or 'viral' (includes lentiviruses, adeno-associated viruses (AAV), adenoviruses, and retroviruses) for the delivery of functional gene copies to patient cells. pDNA-based therapeutics encode *in vivo* biologics which typically replace the functionality of a defective host gene, offering symptomatic and curative relief from hereditary single-gene disorders. For example, cystic fibrosis (a respiratory condition with no cure affecting ~ 90,000 individuals worldwide) is often caused by mutations in the cystic fibrosis conductance regulator (*cftr*) gene, resulting in abnormally thick mucus with life-threatening effects (Schmidt et al., 2016). Clinical trials using a pDNA-encoded *cftr* gene was used to express a corrected version of this protein, restoring functionality in human patients (Alton et al., 2013).

Comparatively, viral therapeutics are better studied and clinically more successful. Zynteglo for example, is a widely available one-time treatment for the blood disorder beta thalassaemia, using *ex vivo* infusion of patient stem cells with lentiviruses encoding copies of the beta-globin gene to restore host function (Schuessler-Lenz et al., 2020). The use of AAVs however, dominates the gene therapy field due to their highly infectious but non-pathogenic/ integrative features, facilitating potent and long-lasting expression of therapeutic gene (transgene) products in host cells (Au et al., 2022). These small, single-stranded DNA (ssDNA) genomes have been used to

deliver life-saving treatments for spinal muscular atrophy (Zolgensma) and retinal dystrophy (Luxturna), with over 200 therapeutics currently in clinical trials (Bulcha et al., 2021; Dangouloff and Servais, 2019; Gao et al., 2020). Unfortunately, viral delivery technologies have several significant disadvantages regarding their safety and efficacy including; limited cargo capacity, manufacturing challenges, cancer-causing off-target insertion of lentivirus/ retroviral DNA into patient genomes and unwanted stimulation of host anti-viral inflammatory immune responses (Hamilton and Wright, 2021; Warneck, 2021). With single doses over USD 1 million, gene therapy treatments are considered some of the most expensive medications available, with a market value of almost USD 8 billion (Warneck, 2021).

Immune limitations

For DNA-based therapeutics, key immunogenic challenges have been identified. To date, no naked DNA vaccines have been approved for human use primarily due to a limited ability to trigger potent immune responses from large animals and humans (Suschak et al., 2017). Conversely for gene therapies, the danger of uncontrolled immunity cannot be understated, with adenoviral vector-triggered inflammation responsible for the death of Jesse Gelsinger during treatment in 1999, all but halting research within the field (Sibbald, 2001). pDNA platforms offer a significantly less immunogenic alternative, with safer patient outcomes, accounting for ~17% (n=442) of gene therapies in clinical trials as of 2017 (Ginn et al., 2018). Nevertheless, despite growing promise, these vectors remain a major source of immune stimulation.

The introduction of any foreign component, including pDNA, elicits strong responses from host immune cells (Ramamoorth and Narvekar, 2015). Their augmentation can be beneficial in the case of vaccines, providing adjuvant enhancing stimulation but detrimental with gene therapies, destroying transgene-containing cells and compromising the activity of these million-dollar drugs (Sack and Herzog, 2009). There is a need therefore to i) better understand DNA-driven responses within immune cells, and ii) develop strategies for the modulation and control of these complex pathways, identifying new technologies to improve the efficacy of DNA therapeutics.

1.1.2 Innate immune recognition of foreign DNA

The immune system has evolved over millennia to protect its host from foreign infectious agents (viruses, fungi, protozoa, toxins) and internal dangers (cancers, inflammation) (Chaplin, 2010). The diversity of these pathogens have driven the evolution of a complex network of cells, receptors, and signalling molecules with varying functionality to eliminate, neutralise and generate a memory of invasion (Cooper, 1992). This system can be broadly divided into innate and adaptive responses based on their function. The innate immune system comprises the first line of an organism's defence system with i) non-specific detection of foreign material known as 'antigens' using specialised receptors located on the surface, cytosolic and nuclear regions of all cells, ii) rapid elimination of pathogenic compounds using immune cells such as macrophages and neutrophils and iii) downstream activation of the adaptive immune response using antigen presenting cells (APC).

The introduction of foreign DNA (in this case therapeutic pDNA) into a host system is first recognised by pattern recognition receptors (PRR) enriched within APCs such as DCs. These cells sit at the heart of the immune response, acting as master regulators through their critical role in antigen capture during innate immunity and antigen presentation activating adaptive immunity (Mellman, 2013). Numerous PRRs have been identified within these DC sentinels allowing detection across a broad range of nucleic acid, lipid, and protein-based antigens, including both sequence-dependent and sequence-independent DNA sensors, as summarised in Figure 1.1.

Toll-like receptor (TLR) 9

TLR9 is an endosomal receptor primarily expressed by DCs and responsible for the detection of endocytosed antigens from extracellular regions. It has a sequence-dependent preference for binding unmethylated CpG dinucleotides (also known as CpG motifs) typically enriched within bacterial/ viral genomes but not vertebrate DNA (Hemmi et al., 2000). Once bound, several different signalling pathways are activated through the adaptor myeloid differentiation primary response 88 (Myd88)

adaptor. These include transcription factor (TF) interferon regulatory factor (IRF) 7 which is a master regulator of type I interferon (IFN) responses, causing upregulation of IFNa and, to a lesser extent, IFNb to promote anti-viral immunity (Honda et al., 2005). Alternatively, signalling through IRF5 and nuclear factor kappa B (NF-kB) causes nuclear translocation where these TF's promote the upregulation of proinflammatory cytokines, such as TNFa and interleukin (IL)-6, through association with different promoter binding sites (Nie et al., 2019; Takaoka et al., 2005; Zhang et al., 2022).

Asp-Glu-Ala-Asp/His (DEAD/ H) family

DNA sensors DEAH box polypeptides 9 and 36 (DHX9 and DHX36) are members of the DEAD/ H helicase family and also detect CpG motifs but, unlike TLR9, patrol intracellular cytosolic regions (Kim et al., 2010). Signalling follows similar cascades with DHX9 primarily working through NF-kB, and DHX36 through IRF7 (Gürtler and Bowie, 2013). Another DEAD/ H member includes DDX41, a receptor involved in the recognition of AT dinucleotide repeats (known as poly(dA:dT)) and herpes simplex virus (HSV-1) DNA, upregulating production of IFN-b and IL-6 (Zhang et al., 2011).

Cyclic GMP-AMP (cGAMP) synthase (cGAS)

cGAS is a cytosolic DNA receptor with a significant role in stimulating dsDNA-induced responses. Largely sequence-independent, cGAS uses electrostatic interactions between its positively charged HIN200 domain (present in all PYHIN protein family members) and the negatively charged sugar-phosphate backbone of DNA (Paludan, 2015). These interactions are length-dependent with longer fragments of >1,000bps found to be more stimulatory than shorter fragments, while requiring a minimal length of 20-400bps (Luecke et al., 2017). Upon cGAS-DNA detection, secondary messenger cGAMP is produced which in turn activates the critical adaptor; stimulator of interferon genes (STING) (Ishikawa and Barber, 2008; Wu et al., 2013). This causes downstream activation of IRF3 and NF-kB which upregulates the same cytokines as TLR9 (type I IFNs, TNFa, IL-6) but with significantly higher levels of IFNB (Kawai et al., 2005).

Absent in melanoma (AIM2)

AIM2 is another member of the PYHIN protein group, activated by cytosolic dsDNA in a sequence-independent manner (similar to cGAS) through a HIN200 domain (Hornung et al., 2009). Once detected, oligomerisation and caspase-1 (CASP-1) binding generates the inflammasome complex; a multi-protein system that stimulates production of pro-inflammatory cytokines IL-1b, IL-18 and triggering pyroptotic cell death (Hornung et al., 2009; Martinon et al., 2002).

Interferon inducible gene 16 (IFI16)

IFI16 is also a PYHIN member, responsible for surveying intracellular cytoplasmic and nuclear regions for foreign ss/ dsDNA (Unterholzner et al., 2010). Uniquely, this receptor signals through STING, generating high levels of IFNb, and the inflammasome complex, increasing IL-1b levels. Similar to cGAS, a preference for longer dsDNA sequences (>60bp) has also been reported for this receptor (Jin et al., 2001; Unterholzner et al., 2010).

Retinoid-induced gene-1 (RIG-1) and melanoma differentiation-association protein 5 (MDA5)

RIG-1 and MDA5 are cytosolic ss/ dsRNA PRRs, however reports of interactions with dsDNA (likely due to similarities in nucleotide composition and an advantageous functional overlap in the detection of DNA viruses) requires these receptors be considered when describing DC detection of DNA (Dias Junior et al., 2019; Zhao et al., 2018). Both sensors signal through IRF3/ NF-kB pathways to upregulate transcription of antiviral genes, particularly type I IFNa/ b (Rehwinkel and Gack, 2020).

Once these receptors have been stimulated, downstream maturation of DCs is initiated to increase cellular mobility, dendrite extension, cytokine production and the expression of costimulatory molecules (Patente et al., 2019). This enables activation of a large-scale DNA-driven immune response. In conclusion, antigenic DNA interacts with DC receptors in a sequence-dependent and independent manner to directly influence the selection (cocktail) of cytokines secreted into the host system.

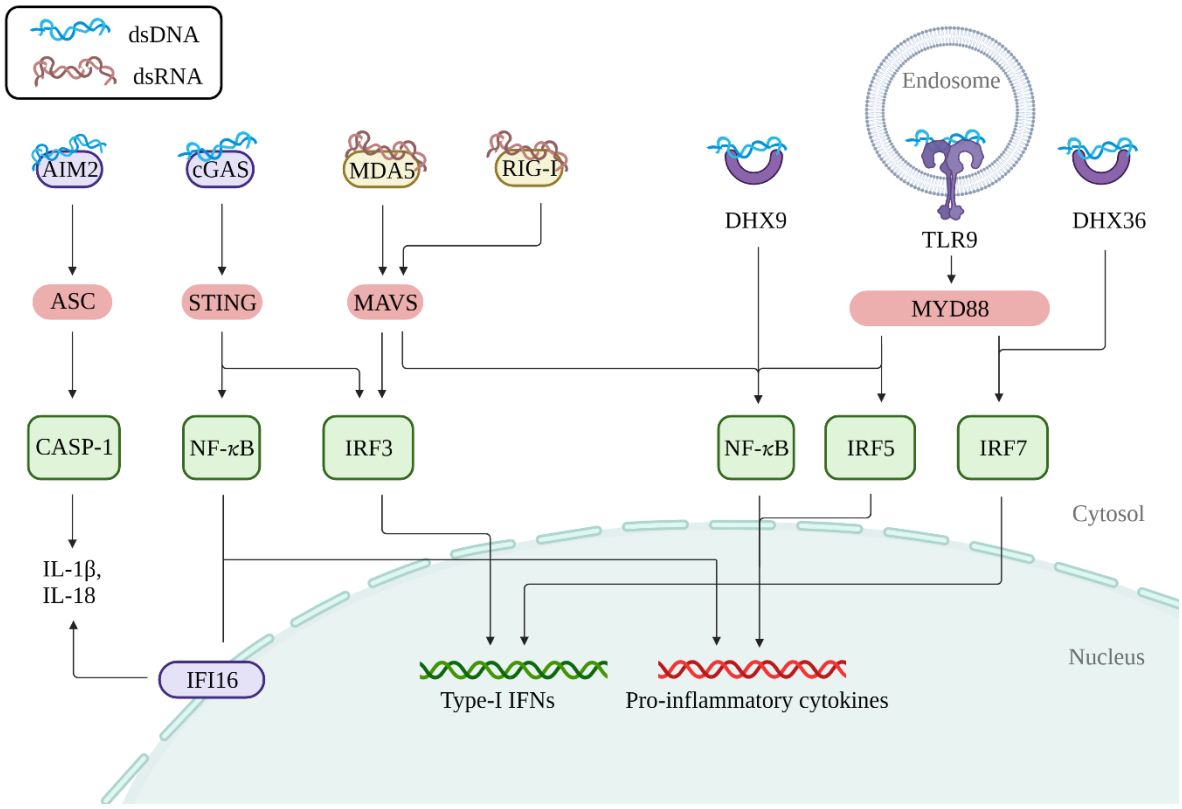

Figure 1.1) Dendritic cell activation of DNA-driven response pathways. Key receptors associated with foreign dsDNA recognition include DNA sensors AIM2, cGAS, DHX9, TLR9, DHX9, DHX36, IFI16, and RNA sensors MDA5 and RIG-1. Downstream signalling pathways involve adaptor and TF activation, resulting in the upregulation of either a type-I IFN or pro-inflammatory response *(Adapted from (Junt and Barchet, 2015), created with Biorender.com).*

1.1.3 DC-driven adaptive immune responses

The adaptive immune response is a more sophisticated, later-acting system used to generate unique, antigen-specific attacks on invading pathogens, while also retaining memory cells in case of future exposure (Chaplin, 2010). Intracellular pathogens, such as viruses and tumours, typically trigger T-cell mediated responses which involve T-lymphocytes; CD4+ T-helper (Th) and CD8+ cytotoxic T cells. Naïve CD4+ Th cells (Th0) differentiate into different subtypes depending on three DC interactions: i) direct T-cell receptor (TCR) binding with DC presented antigens (in this case dsDNA fragments) on major histocompatibility complex (MHC) proteins, ii) association with co-stimulatory molecules present at the DC-T cell interface known as cluster of differentiation (CD) receptors and iii) detection of specific DC secreted

cytokines (Bonilla and Oettgen, 2010; Grakoui et al., 1999). Two of these three T-cell activating signals are therefore dependent on the dsDNA antigen ((i) and (iii)), which influences subsequent Th0 differentiation into either Th1, Th2, Th17, or T regulatory (Treg) cell lineages. Each of these represent different arms of the immune response, associated with unique cytokine signatures and downstream functions, as summarised in Figure 1.2 (Harrington et al., 2005; O'Garra, 1998).

Th1

A Th1 response is most often triggered by intracellular bacterial/ viral infections and DC secretion of IFN-g and IL-12 (Hsieh et al., 1993). These T cells are characterised by their ability to produce IFN-g, TNFa and (to a lesser extent) IL-2, enhancing macrophage microbicidal activity and cellular phagocytosis to destroy infected cells (Suzuki et al., 1988). DNA-based therapeutics typically trigger a Th1 response due to its delivery into intracellular regions and composition of non-native foreign genetic material (Asakura et al., 2000).

Th2

In contrast, Th2 immunity is generated upon exposure to extracellular pathogens such as helminths and allergens such as pollen (Mosmann et al., 1986; Paul and Zhu, 2010). Th0 exposure to DC IL-2 and IL-4 directs differentiation into Th2 cells, characterised by their ability to produce cytokines IL-4, IL-5, IL-10, and IL-13 (Chen et al., 2004; Seder et al., 1992). Downstream activation of humoral B-cell mediated immunity induced production of IgE antibodies from B plasma cells, enhancing opsonisation and phagocytosis to eradicate pathogens (Coffman and Carty, 1986; Marshall et al., 2018). Foreign DNA exposure is predominantly intracellular however fragments within the extracellular environment may still trigger Th2-like responses.

Th17

Th17 immunity provides protection against certain extracellular bacteria and fungi that would otherwise overwhelm Th1/ Th2 responses (Harrington et al., 2005; Tesmer et al., 2008). DC secretion of transforming growth factor b (TGF-b), IL-6, IL-23 and IL-

1 induce Th0 differentiation into the Th17 lineage, characterised by its ability to produce IL-17 group cytokines and IL-22 (Langrish et al., 2005; Park et al., 2005).

Treg

Finally, the Treg response is required for the mediation of immunological tolerance, a process by which the immune response adapts to the presence of foreign antigens resulting in a non-reactive environment, actively down-regulating the activity of other Th cells (Gershon and Kondo, 1970). Differentiation is dependent on DC cytokines TGF-b and IL-10 (Jutel et al., 2003) which induce Th17 release of the same inhibitory messengers, suppressing cytokine/ chemokine cellular expression (TGF-b), and inhibiting pathogenic Th17 responses (IL-10) (Chaudhry et al., 2011; Yang et al., 2010). Other effects involve DC modulation, metabolic disruption and the induction of cell lysis (Corthay, 2009; Vignali et al., 2008).

Th inhibition is not exclusive to Treg cells. For example, the secretion of IFN-g by Th1 cells has been found to inhibit Th2 cell proliferation, while Th2 production of IL-4 has been found to suppress Th1 cells (Gajewski and Fitch, 1988; Swain et al., 1990). Further, Th17 secreted IL-17 suppresses Th1 differentiation, while Th1 IFN-g and Th2 IL-4 inhibit Th17 self-differentiation (Harrington et al., 2005; O'Connor et al., 2009) demonstrating the complex, self-regulating interplay between Th responses.

Inappropriate DC cytokine production can result in dysfunctional activation of these pathways, generating disease phenotypes such as Th1-associated organ-specific auto-inflammation, Th2 allergy, and Th17 inflammatory disease (Mbongue et al., 2014). These include, but at not limited to; multiple sclerosis (MS), RA, systemic lupus erythematosus (SLE), type I diabetes, inflammatory bowel disease (IBD), and asthma (Bonilla and Oettgen, 2010; Romagnani, 1996; Tesmer et al., 2008).

The specific pathways upregulated by DCs in response to DNA therapeutics remain to be fully understood. Given the antigen-dependent control of Th differentiation, a comprehensive map of DNA-driven responses would aid in the understanding of this complex process. This would avoid the aberrant disease phenotypes seen with viral delivery methods, aiding the development of safer and more efficacious therapies.

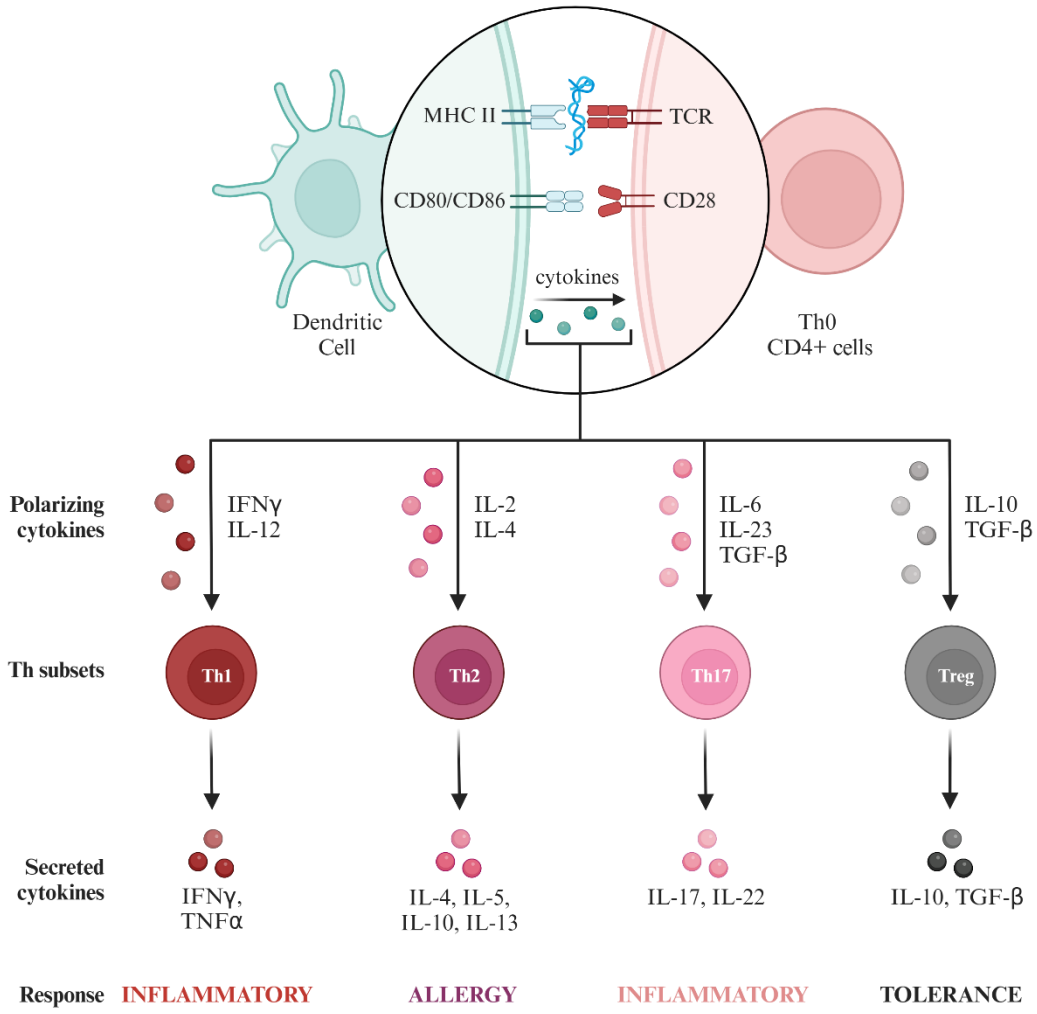

Figure 1.2) Dendritic cell mediated Th differentiation. dsDNA activated DCs interact with naïve Th0 CD4+ cells via three signals: i) DC antigenic dsDNA presentation by MHC II receptors to T-cell TCRs, ii) DC co-stimulatory CD80/ 86 interaction with T-cell CD28, and iii) secretion of antigen specific cytokines. The cocktail of DC secreted cytokines mediates Th0 differentiation into either Th1, Th2, Th17 or Treg cells which produce further cytokines to generate an inflammatory, allergy or tolerance immune response *(Adapted from (Patente et al., 2019), created with Biorender.com)*.

1.2 Immune-modulating DNA sequences

The success of DNA therapeutics lies in their ability to upregulate or downregulate immune responses to i) plasmid vectors, ii) transgene products and iii) modified cells (Arruda et al., 2009). Desired outcomes vary, with stimulatory effects preferred for vaccines but suppressive/ tolerant effects for gene therapies. Current strategies involve co-administrating adjuvants (such as aluminium) alongside vaccines and immunosuppressants alongside gene therapies, although these methods often have detrimental impacts on patient health (Arruda et al., 2009; Danielsson and Eriksson, 2021). Alternative approaches have been developed to overcome these limitations. These involve the use of specific DNA sequences with the ability to interact with immune sensors/ signalling molecules, stimulating or suppressing downstream responses.

1.2.1 Stimulatory sequences

The singular, most comprehensively characterised immune stimulatory sequence is the CpG motif. Within prokaryotic genomes, CG dinucleotides are present at expected frequencies (1 in 16) and are typically unmethylated, while vertebrates have significantly lower CG frequencies (1 in 64) at higher methylation rates (70-90%). This vertebrate phenomenon is known as CpG depletion/ suppression and is driven by an increased propensity for cytosine methylation, resulting in spontaneous deamination to generate CpG to TpG mutations (Bird, 1980; Sved and Bird, 1990). This differentiation has allowed higher organisms to develop specific receptors (TLR9 and DEAD/ H family) to specifically detect unmethylated CpG motifs, alerting host adaptive responses. Additionally, generic receptors originally thought to detect dsDNA through sequence-independent mechanisms, have been found to show preferential associations for certain repetitive sequences, as discussed in this section.

Single-stranded ODN CpG motifs

ODNs are short, ssDNA molecules commonly used as primers, probes, or therapeutic agents (Scharner and Aznarez, 2021). Their use as synthetic, 15-20bp CpG motifs with nuclease resistant backbone modifications (phosphorothioate (PS) rather than

phosphodiester (PO)) have exhibited immune-modulatory effects. Four different sub-groups have been established, with differential modulation of immune pathways (as summarised in Table 1.1) dependent on ODN sequence, structure and backbone identity (Brazolot Millan et al., 1998; Krieg et al., 1995; Verthelyi et al., 2003). A core, defining feature across these groups is the presence of at least one unmethylated CG dinucleotide, recognised as a pathogen-associated molecular pattern (PAMP) (Bauer et al., 2001). Detection is often TLR9 specific and is most effective when in the sequence context: RRCGYY (R = purine, Y = pyrimidine, CpG has been underlined), generating a Th1 biased immune response (Klinman et al., 1996; Krieg, 2006). More specifically, in mice the optimal TLR9 stimulating ligand has been identified as GACGTT, whereas in humans it is GTCGTT (Bauer et al., 2001). This distinction arises from variations in the structure of TLR9 receptors between these species (Krieg et al., 1995; Rehli, 2002).

Class A CpG ODNs (also known as D-class) are composed of a central palindromic PO CpG motif flanked by 3' polyG PS nucleotides. These ODNs activate TLR9 and are trafficked into specialised endolysosomes where they signal via IRF7 (Sasai et al., 2010). Although able to stimulate high IFN-a production from human plasmacytoid DC ((pDC) a subtype of DCs), CpG-A ODNs are poor stimulators of antibody-producing B cells (Table 1.1) (Gursel et al., 2013)

Class B CpG ODNs (also known as K-class) are characterised by a PS backbone with 1—5 CpG dinucleotides that interact with TLR9 and signal through NF-kB (Kawai and Akira, 2010). Despite interacting with the same receptor as class A ODNs, their downstream effects involve; pDC differentiation and TNFa production, B cell IL-6 and IgM production, and macrophage IL-6 and IL-12 secretion with weak IFNa stimulating abilities (Table 1.1) (Gursel et al., 2013).

Class C CpG ODNs combine characteristics of both A and B, with a complete PS backbone within a palindromic CpG motif, often forming stem-loops or dimers. These secondary structures interact with TLR9, simulating B cell IL-6 production and pDC IFN-a, producing potent proinflammatory responses (Table 1.1) (Gursel et al., 2013; Vollmer et al., 2004).

And finally, the more recently discovered Class P CpG ODNs are characterised by a double palindrome forming hairpin at their GC-rich ends (Samulowitz et al., 2010). Of all classes, these are the strongest inducers of type I IFN (and *in vivo* TNFa, IL-12, and IL-10) although they are less potent than Class C ODNs in inducing B cell proliferation and antibody production (Table 1.1) (Samulowitz et al., 2010).

Table 1.1) Comparative activity of CpG-ODN classes. Class A, B, C and P backbone structures vary between PS, PO, or a combination of both. Relative stimulation of B-cells, pDCs, IFNa and IL-6 is represented by + symbols *(Adapted from Invivogen, San Diego, CA).*

Class	Backbone	B-cells	pDCs	IFNa	IL-6
A	PS-PO	+	++++	++++	+
B	PS	++++	++++	+	+++
C	PS	+++	+++	+++	++
P	PS	++	+++	++++	++

Double-stranded DNA

Derived from the genome of *Listeria monocytogenes*, interferon stimulatory DNA (ISD) is a 45bp sequence containing multiple CpG motifs within a particular configuration, often described as the 'gold standard' for immune stimulation studies (Li et al., 2013a). It is recognised by cytosolic receptor cGAS, stimulating high levels of type I IFN from pDCs and pro-inflammatory cytokines TNF-a, IL-6, and IL-1b from other immune cells (Bode et al., 2016).

Poly(dA:dT) and poly(dC:dG) are immunogenic synthetic sequences composed of consecutive AT or GC repeats respectively. Poly(dA:dT) in particular, has been found to signal through IFI16 and RIG-1 within DCs, inducing secretion of type I IFNs and pro-inflammatory TNFa / IL-6 (Ablasser et al., 2009; Kis-Toth et al., 2011).

A number of other sequences have also been reported, including a 60bp dsDNA fragment derived from HSV-1 and a 70bp fragment from vaccina virus, both of which generated high levels of IFN-b mRNA from bone marrow derived dendritic cells (BMDCs) (Rasmussen et al., 2011; Unterholzner et al., 2010).

Although cGAS accounts for a large portion of cytosolic dsDNA immune detection in a largely sequence-independent manner, Herzner and colleagues reported sequence-specific recognition of a short dsDNA fragment (12-20bps flanked by ssDNA containing at least three guanines) to be highly stimulatory (Herzner et al., 2015). They also found high guanine content in short DNA fragments produced large quantities of IFNa and IFNb comparable to that of plasmid and genomic dsDNA. More recently, a microsatellite-derived dsDNA motif $(AATGG)_4$ was observed to specifically stimulate cGAS, suggesting this receptor, and potentially others initially thought to be sequence-independent, may in-fact possess some sequence-specific preference for binding certain DNA motifs (Gentili et al., 2019).

1.2.2 Suppressive sequences

A large-scale analysis of the literature identified >80 DNA sequences, both native and synthetic, capable of suppressing the immune response in some capacity (Appendix, Supplementary Table 1). Similar to CpG ODNs, these motifs were ~15-25bps with modified backbones to protect against nuclease degradation and aid in their downregulatory activity (Bayik et al., 2016). Their mechanism of action varies but primarily involves inhibition of TLRs (particularly TLR9), interference of stimulatory signalling cascades, CpG-ODN competition, saturation of TF binding sites, and the activation of Treg cells. ODNs were identified in the following categories: 1) g-tetrads, 2) CpG dinucleotides, 3) inhibitory ODNs (INH-IDNs), 4) immunoregulatory DNA sequences (IRS), 5) microsatellites and 6) hybrid inhibitory ODNs.

G-tetrad ODNs

Many suppressive ODNs contain a string of consecutive guanine (G) nucleotides (Gursel et al., 2003; Yamada et al., 2002). Studies have found suppressive potency to correlate with longer G runs with a minimum threshold of 3, below which motifs lose their suppressive capability (Ashman et al., 2005; Duramad et al., 2005; Gursel et al., 2003; Kaminski et al., 2013). A151 for example is an important, well-characterised, telomere-derived ODN composed of TTAGGG repeats, found to inhibit activation and differentiation across broad immune cell types (DCs, macrophages, T/ B cells (Gursel

et al., 2003). The 3 G string was found to be essential for the formation of second-order planar structures known as G-tetrads through Hoogsteen hydrogen bonds (Costa et al., 2004). Its broad inhibitory activity involves i) competing with CpG ODN for TLR9 binding, reducing IL-6, Il12, IFN-g and TNFa production, shifting from a Th1 to Th2 response (Shirota et al., 2004), ii) directly binding AIM2 to prevent recruitment and assembly of the inflammasome complex, iii) inhibiting phosphorylation of STAT molecules in Th cells and iv) promoting Th17 and Treg differentiation responses (Bode et al., 2013). Successful treatment of atherosclerosis and SLE in pre-clinical murine and human models shows promising results (Wang et al., 2023).

H154 is another well investigated G-rich ODN but is much more specific in its inhibition of TLR9, preventing activation of DCs, B-cells, and cytokine production (Yamada et al., 2002). Unlike A151 however, this ODN has a much more limited therapeutic utility, only inhibiting immune responses upregulated by TLR9 agonists. Successful reduction in inflammation, swelling, and systemic inflammatory arthritis has been reported, along with patent protection for its use in the treatment of inflammatory arthropathies (joint disease) (Bayik et al., 2016; Klinman et al., 2006; Zeuner et al., 2002).

A number of other G-rich ODNs have been reported including numerous G-tetrad forming sequences able to downregulate cytokine production by Gursel and colleagues (Gursel et al., 2003), a highly suppressive 5 G-containing sequence known as G-ODN able to inhibit IFN-a production in human pDCs (Avalos and Ploegh, 2011; Peter et al., 2008), and a 30bp string of G nucleotides capable of antagonising CpG-ODN stimulation in murine cells (Pisetsky and Reich, 2000).

CpG Dinucleotide ODNs

Although certain CpG motifs cause immune stimulation, dinucleotides in different sequence contexts or with specific base conversions (known as CpG-N) have been found to neutralise, and even suppress, immune activity. Their mechanisms usually involve TLR9 inhibition through antagonistic binding, direct competition with stimulatory CpG-ODNs, or inhibition of ssRNA detecting DNA sensors TLR7 and TLR8

(Li et al., 2011; Liu et al., 2017). This promiscuity in receptor interference is not unexpected given the similarities in DNA and RNA nucleotide structure. An in-depth sequence analysis of adenoviral DNA by Krieg and colleagues found an enrichment of CG dinucleotides preceded by a C and/ or followed by a G (e.g., CCG, CGG or CCGG) within specific serotypes compared to other sequence contexts (Krieg et al., 1998). Although CpGs are significantly underrepresented in the human genome (as described earlier) those that are present exist instead within this CpG-N context and were found to specifically antagonise the effects of stimulatory CpG motifs, reducing the production of cytokines IL-6, IL-12, and IFNg (Frazier, 2015; Krieg, 2002; Krieg et al., 1998). Examples include CpG-c41, which inhibits TLR9, TLR7 and TLR8 (Li et al., 2011; Liu et al., 2017), and murine splenocyte suppressor ODN 1953 (Krieg et al., 1998).

Conversion of the stimulatory CpG dinucleotide into GpG or GpC motifs converts these sequences into immune suppressors. GpC 1826b for example, has been found to downregulate murine pDCs through TLR7 (rather than TLR9 pathways) upregulating the production of regulatory cytokine TGF-b (Avalos and Ploegh, 2011; Volpi et al., 2012). Similarly, potent suppressor GpG 1019 inhibits TLR9, 7, and 3 (a dsRNA receptor) in mice and human cells, biasing Th2 allergy over Th1 inflammatory responses (Duramad et al., 2005; Graham et al., 2010; Ho et al., 2003, 2005).

INH-ODNs

INH-ODN are the largest group of suppressive motifs with contributions from numerous groups through iterative changes in nucleotide sequence/ backbone modifications, generating variants with differing potency and specificity (Ashman et al., 2005; Römmler et al., 2013; Stunz et al., 2002). Their mechanisms involve binding the TLR9 C-terminal domain inhibiting the conformational changes required for downstream NF-kB activation, resulting in receptor saturation, preventing other potentially stimulatory sequences from binding (Avalos and Ploegh, 2011; Stunz et al., 2002). Similar to CpG dinucleotides, observations of TLR7-dependent downregulation have also been reported, although this is thought to be due to generic PS rather than sequence-specific effects (Lenert et al., 2009; Römmler et al., 2015).

Overlap in INH-ODN categorisation was observed in many motifs containing polyG runs or CpG/ GpG/ GpC dinucleotides.

A number of prototypic INH-ODNs can be characterised by the presence of integral motif CC(T)XXX_{3}-GGG, of which the CCT and GGG motif was found to be essential for suppressive function (Duramad et al., 2005; Lenert et al., 2009). INH-ODN 2088 was one of the first characterised, with broad suppressive activity in human and mice immune cells, inhibiting pro-inflammatory and adaptive responses through TLR3, TLR7, and TLR9 inhibition (Duramad et al., 2005; Lenert et al., 2009). INH-ODN 18 is another example, inhibiting TNFa production from macrophages and IFN-a from DCs. Interestingly, IgM levels were inhibited by ~90% in both PS and PO backbone variants (although much larger PO concentrations were required due to the higher degradation rate), confirming suppression was sequence-dependent (Ashman et al., 2011; Lenert et al., 2009). Overall, INH-ODNs show more effective downregulation of humoral immunity compared to other groups.

Similar to G-rich sequences, many INH-ODNs contain polyG tracts forming G-tetrads that stack together into higher-order G-quadruplex structures. By modifying these G's (replacing strategically selected carbon atoms with nitrogen), Hoogsteen hydrogen bonds cannot form interfering with quadruplex formation. Rommler and colleagues found these modified INH-ODNs had similar effects on macrophage and DC TLR9 but were more effective at impairing TLR7-induced TNFa, Il12p40, and B cell IL-6 (Römmler et al., 2013). Other modifications include 2'-*O*-methyl-modifications within a PS context or 2′,4′-methylene nucleic acid bridging (known as locked nucleic acids) which have reported increased binding affinities and suppressive activity (Swayze et al., 2007; Yoo et al., 2004). Disadvantages of these modifications however involve increased cytotoxic effects, higher production costs, and difficulty in predicting off-target effects.

IRS ODNs

IRS sequences were designed by Barrat and colleagues to develop new ODNs capable of reducing the aberrant production of IFN-a from pDCs in SLE patients (Barrat et al.,

2005). Subgroups of IRS ODNs were identified targeting TLR7 and TLR9 either exclusively or simultaneously. IRS 869 for example is a well characterised inhibitor of human and mouse TLR9, reducing B cell proliferation and cytokine release (IL-6, IL-12, TNFa) from TLR9 stimulating agonists (Duramad et al., 2005). IRS 661 on the other hand inhibits only TLR7, reducing cytokine production and autoantibodies IgG2a and IgG2b (Barrat et al., 2005; Pawar et al., 2007). IRS 954 instead inhibits both TLRs, downregulating HSV-1 activated IFN-a production from human pDCs as well as numerous interferon stimulated genes (ISGs) such as *ifit1, isg15, isg20, cxcl10,* and cytokines TNFa and IL-6 (Barrat et al., 2005; Pawar et al., 2007). This ODN in particular shows the most promise, relieving symptoms of glomerulonephritis (kidney damage) and increasing murine SLE survival rates. As with INH-ODNs, these motifs share some similarities in nucleotide composition to previously described groups, with many ISGs containing CCT and GGG motifs and/ or polyG strings, suggesting significant redundancy in their categorisation.

Microsatellite derived ODNs

The success of telomeric A151 ODN suggests highly repetitive endogenous mammalian DNA may have suppressive capabilities. Given that ~3% of the human genome is composed of short, tandemly repeated microsatellite DNA, Hu and colleagues systematically screened the effects of 33 different monomer, dimer, trimer, tetramer, pentameter, and hexamer nucleotide repeating units (Hu et al., 2009). A number of effective sequences were identified from this study, with TLR9 dependent and independent mechanisms, generating promising pre-clinical results.

SAT05f is a 24bp ODN composed of trimeric CCT repeats, inhibiting TLR7/ 9 signalling and causing a downregulating in IFN-a production, successfully treating SLE and graft-versus-host disease (Zhang et al, 2014). Application in cytokine-mediated toxic shock models have identified a novel mechanism of action involving upregulation of surface TLR9 receptors (as opposed to endosomal/ lysosomal TLR9) located on neutrophil membranes, recruiting these cells to sites of inflammation to help counteract aberrant cytokine release (Meng et al., 2017).

During initial testing, MS19 was thought to behave as a neutral ODN (Hu et al., 2009; Sun et al., 2010). Later investigations of this AAAG tetramer however, found potent inhibition of inflammatory responses across a broad range of disease models including septic peritonitis, systemic inflammatory response syndrome, myocarditis, and acute lung injury (ALI) (Gao et al., 2017; Nie et al., 2019; Xiao et al., 2017; Zhang et al., 2022). This ODN has multiple suppressive mechanisms including i) IRF5 binding to prevent translocation into the nucleus, ii) inhibition of NF-kB phosphorylation required for activation and, iii) prevention of HMGB1 translocation from the nucleus into the cytosol/ extracellular space where it auto-stimulates sterile inflammation and TNFa release from immune cells acting as a danger associated molecule pattern (DAMP) (Gao et al., 2017; Zhang et al., 2022).

Hybrid inhibitory ODNs

The final group of suppressive motifs includes hybrid inhibitory ODNs (referred to as ISGs) which combine a 3' poly G string with the TTAGGG telomeric motif, exhibiting suppression across Th1 and Th2 immune markers (Ito et al., 2013). Reduced levels of IL-6 mRNA were detected in murine splenocytes, with functionality found to be dependent on secondary structure formation. *In vivo* oral administration of iSG3 generated potent Th2-specific suppression, reducing IL-33 levels and improving atopic dermatitis symptoms in mice models (Wang et al., 2015). Interestingly, the structure of iSG3 resembles that of INH-ODN motif CC(T)$XXX_{3\text{-}5}$GGG with a 3' CCT, followed by telomeric TTAGGG, and an additional 5' polyG string.

Overall, six different groups of suppressive ODNs have been described, with promising therapeutic applications and varying mechanisms of suppression. Although primarily examined within murine models of immune disease, it remains to be characterised whether these ODNs can control/ modulate unwanted immune stimulation from DNA therapy vectors.

1.2.3 Plasmid integrated modulatory motifs

Stimulatory sequences

The immune-stimulatory activity of CpG-ODNs have been found to translate into a plasmid integrated context with class dependent effects (Schneeberger et al., 2004). Coban and colleagues designed vectors integrated with either A-class (45bps) or B-class (31bps) CpG sequences and analysed cytokine production after transfection into human peripheral blood mononuclear cell (PBMC) (a mixture of immune cells including DC, macrophages, lymphocytes, natural killers (NK) and more) (Coban et al., 2005). They found B-class integrated plasmids generated higher levels of IL-6 and IFN-g, whilst A-class produced more IgG. This confirms i) the stimulatory effects of integrated sequences and ii) differential class-dependent activity even in a double-stranded context. These differential effects did not align with ssODN findings, for example, A-class vectors did not produce as much IFN-a or IFN-g as their single stranded counterparts, whilst the B-class plasmids produced much more than expected. These variations may be due to differing interactions between PRRs and ssODN secondary structures compared to the more rigid DNA double helix.

Later studies found CpG motif insertion into an anthrax vaccine vector enhanced its immunogenic effects, functioning as an adjuvant (Yu et al., 2015). Class B and C motifs increased IgG, IgG1, IL-6 and IFN-g levels compared to A class, contradicting earlier described studies (although vector backbones and cell models differed across experiments) (Coban et al., 2005; Yu et al., 2015). The authors also found that increasing CpG motif numbers from 5 to 40 induces stronger cell-mediated (IL-4, IFN-g) and antigen-specific humoral responses (Yu et al., 2015). Interestingly, combining different CpG class sequences had no effect on antibody levels but increasing B-class motif copy number to 20 significantly elevated antibody production, IgG1 (Th2 associated) compared to IgG2a (Th1 associated), and IL-4, suggesting a bias towards Th2 immunity.

Suppressive sequences

Unlike CpG-ODNs, investigation of plasmid integrated suppressive motifs are highly limited. One of the earliest reports by Krieg and colleagues used *in vitro* mutagenesis to progressively remove 52/ 134 CpG-N motifs within the murine hepatitis B vaccine (Krieg et al., 1998). A two-fold increase in antibody production, elevated cytotoxic T cell responses and a more Th1-like function was observed suggesting CpG-N integrated motifs were exerting Th1 suppressive effects.

A more recent study published in 2021 integrated 3 copies of telomeric TTAGGG into the single stranded genome of an AAV gene therapy vector (Chan et al., 2021). Reduced innate immune function and T cell responses were detected in murine and porcine models along with enhanced gene expression, however, higher dose administration in macaque models showed delayed but not reduced effects in a clinical uveitis (eye inflammation) disease model.

Suppressive technologies have valuable applications in the field of gene therapies, offering alternative approaches for the downregulation/ modulation of DNA-driven immune responses. Based on the literature described, it is yet to be determined whether suppressive sequences retain their functionality when integrated into a dsDNA plasmid context.

1.3 Methods of quantifying plasmid immunogenicity

All novel therapeutics require a complete immunogenic assessment to ensure patient safety. This is often conducted during the final stages of clinical trials however earlier screening during design stages is recommended by regulatory bodies, including the European Medicines Agency (EMA) and USA Food and Drug Administration (FDA), to better anticipate potential immunological side effects (Vandivort et al., 2020). Guidelines for characterising the immunogenicity of DNA vaccines are well established involving *in vitro* and *in vivo* analysis methods such as i) cell-mediated immune response screening through T-cell stimulation/ proliferation assays and ii) T-cell/ DC cytokine production analysis using enzyme-linked immunosorbent assays (ELISAs), ELISpots and flow cytometry (European Medicines Agency, 2007, FDA 2007). As interest in gene therapy and other DNA-based therapeutic technology grows, the requirement for novel tools capable of analysis that is easy, fast, and capable of more specific characterisation has emerged.

1.3.1 Immune-cell proliferation assays

Most experimental assays involve exposing DCs to the DNA therapeutic of interest for initial processing and antigenic presentation. In immune-proliferation assays, T and/ or B cells are co-incubated and undergo rapid clonal expansion required to execute their cell-mediated/ humoral functions (Chen et al., 2002). Cell proliferation assays exploit this feature, with more immunogenic stimuli activating higher levels of division, measured using radiolabelled or fluorescent nucleotides (Chattopadhyay et al., 2014). Although quick, sensitive, and easy, this method does not delineate which cells are proliferating (e.g., memory rather than Th0), nor which Th differentiation pathways/ antibody sub-types are upregulated, is labour intensive, and can produce variable results (Lašťovička et al., 2009; Phetsouphanh et al., 2015). For example, Yu and colleagues measured the immunogenicity of different CpG-modified viral pDNA vectors by exposing them to human PBMCs and measuring the proliferative response (Yu et al., 2015). Their data enabled relative comparisons of immunogenicity between constructs however specific effects across response pathways could not be characterised.

1.3.2 Cytokine quantification

Measuring the production of specific cytokines is a much more informative method to quantify immune activation and is widely used across studies (Aydin, 2015). Cytokine producing immune-cells are first exposed to DNA (or other antigenic compounds) *in vitro* or *in vivo*, with resulting secretion of chemical messengers measured to i) quantify the magnitude of immunogenicity, ii) identify which arms of the immune response have been stimulated (e.g., IFN-g from Th1, IL-4 from Th2, IL-17 from Th17 or TGF-b from Treg) and iii) speculate which DNA sensors have been activated (e.g., TNFa from TLR9, IFN-b from cGAS).

ELISAs

The process of ELISA detection involves highly specific antibody-antigen binding interactions and enzyme-based signal amplification (Engvall and Perlmann, 1971; Weemen and Schuurs, 1971). Plates coated with antibodies complementary to a cytokine/ antibody of interest, such as TNFa, are incubated with supernatant samples. Secondary antibody detection and enzyme-based amplification is then used to overexpress and quantify the level of bound antibody-TNFa complexes represented by detectable colour changes. This method is by far the most commonly used for pDNA (and other antigenic stimulant) immunogenicity analyses (Coban et al., 2005; Kawabata et al., 1999; Kojima et al., 2002; Yu et al., 2015) .

ELISpots

ELISpot assays are similar to ELISAs but instead quantify the number of cells secreting a cytokine of interest rather than the total cytokine concentration within a sample (Czerkinsky et al., 1984). Generally used alongside (rather than instead of) ELISAs, this technology quantifies the proportion/ frequency of cytokine secreting cells within a population which is particularly advantageous in heterogenous cell samples, distinguishing responsive and non-responsive cell types. For example, supernatants from mice immunised with pDNA vaccines were analysed using ELISpots to determine the proportion of T-cells producing IFN-g (Schneeberger et al., 2004).

RT-qPCR

Reverse transcription polymerase chain reaction (RT-PCR) is another method used to quantify cytokine expression in immune cells upon exposure to immunogenic pDNA. Unlike ELISAs, this assay measures absolute changes in the mRNA transcript levels of genes compared to the relative quantification of a secreted protein (Bustin, 2000). Although this platform offers a simple, sensitive, reliable and easy to multiplex assay, concerns regarding its accuracy have been reported (Bustin, 2000, 2002; Bustin et al., 2005). Although used less frequently, studies have measured gene expression levels of Th1 and Th2 cytokines *ifng, il4* and *il5* upon PBMC exposure to pDNA vaccine vectors (Fischer et al., 2000; Kawabata et al., 1999).

Limitation

Although highly informative, limitations of these technologies include i) restrictions/ high cost of multiplexing, with ELISA/ ELISpots/ RT-qPCR analysis generally limited to ~1-3 cytokines/ antibodies of interest, ii) long and laborious methods requiring multiple hours of hands-on experimental and analysis time, iii) high levels of inaccuracy and variation and iv) a requirement for pre-selecting gene/ protein (outputs) of interest which can limit the understanding of pDNA vectors on alternate and even unexpected response pathways (Bustin, 2002; Kouwenhoven et al., 2001; Sakamoto et al., 2018).

1.3.3 Transcriptomic characterisation

To overcome limitations of pre-selecting immune outputs, comprehensive transcriptomic analysis can be used instead. This technology measures whole transcriptomes through RNA-sequencing or microarray analysis.

RNA-sequencing

RNA-sequencing enables quantification of >90% of all protein coding genes within sample populations (Wang et al., 2010). Its process involves conversion of expressed mRNA transcripts into complementary DNA, subsequent sequencing using next generation technology and analysis with computational software to determine the

abundancy and identity of RNA transcripts within a sample. The ability to screen entire cellular responses provides a comprehensive and data-rich understanding of pDNA effects across all immune response pathways (Warga et al., 2023). However, the complexity of analysis and high cost significantly limits application of this method for standardised screening of vector immunogenicity.

Microarray analysis

Unlike RNA-sequencing, microarray analysis allows for more refined characterisation using immobilised, labelled cDNA to only bind RNA transcripts of interest and is therefore more commonly used in immunogenicity screens (Stetson and Medzhitov, 2006; Woo et al., 2014). Although more cost-effective and time-efficient, microarray analysis still involves quantification of thousands of genes, generating large data-rich files that require laborious processing (Jaluria et al., 2007).

1.3.4 Surface marker analysis

During immune-activation, fundamental changes in the expression of surface receptors on APCs, T-cells, and B-cells is essential for the maturation process. For example, DCs and B cells upregulate receptors CD80, CD86, and CD40, whilst T cells overexpress receptors CD25 and CD28 (see Figure 1.2) (Aalamian et al., 2001; Kaminski et al., 2012; Rea et al., 1999). Flow cytometry technology uses fluorescently labelled antibodies to measure the expression of these surface molecules, providing an effective assay for analysing pDNA vaccine effects on immune cell activation (Coban et al., 2005). Advantages of this technology include quantifying maturation levels in mixed populations, identifying the stage of activation (early, mid, late) and, single-cell analysis (McKinnon, 2019). Limitations however include high costs, complex and laborious analysis, difficulties in multiplexing, and highly sensitive sample preparation (Drescher et al., 2021).

1.3.5 Computational screens

Outside of cell-based analyses, a number of *in silico* computational tools are available to predict putative T-cell, B-cell, and MHC protein epitopes or measuring CpG

content. None, however, could directly analyse nucleotide sequences to identify immune-modulatory motifs to quantify/ characterise potential immunogenic effects.

T/ B cell epitope predictors

T and B cells interact with DC-presented antigens through the expression of highly specific and varied receptors enabling detection across a broad array of pathogens. This critical receptor-antigen interaction has been well studied and forms the basis of most antigen-predicting software. For example, the immune epitope database–analysis resource (IEDB-AR) hosts multiple prediction tools using known interactions to determine sequences with the potential to associate with T, B, and MHC receptors (Dhanda et al., 2019). Other examples include ImmuneDB, DeepImmuno, and VaxiJen (Doytchinova and Flower, 2007; Li et al., 2021; Rosenfeld et al., 2018).

CpG prediction tools

CpG motifs have critical functions in maintaining gene regulation (see 1.4.3) and so have driven the development of tools such as CpGPlot, CpGProD, CpGIS, CpGcluster, and CpGPAP to determine the presence and density of CpGs within inputted DNA sequences (Cai et al., 2020). CG dinucleotide content can therefore be used to predict relative immunogenicity given the correlation between frequency and immune stimulation (Chen et al., 2007; Pontarollo et al., 2002; Yu et al., 2015). Although useful in initial screens, prediction tools are highly limited, especially in their ability to measure sequence-dependent pDNA immunogenicity.

In summary, current pDNA immunogenicity screening assays are either i) cheap and simple, but restricted to analysing a small number of outputs, or ii) provide a data-rich overview but are limited in cost and laborious processing. Furthermore, none have been designed to specifically interrogate effects on DNA-driven immune responses. Novel tools are therefore required to quantify and characterise the impact of DNA therapeutics across different arms of the immune response. Ideally, these technologies would be quick, simple and easy-to-use, enabling medium throughput screening of plasmid vectors during early design (Vandivort et al., 2020).

1.4 Current immune-modulating strategies

Given the industrial interest in developing novel strategies for the downregulation (rather than upregulation) of immune responses by AstraZeneca, existing suppressive approaches were evaluated. The most common consequence of gene therapy stimulated immune activation involves i) cell death and eradication of foreign transgene proteins/ plasmids, ii) decreased expression of therapeutic products and, iii) uncontrolled inflammation leading to potentially fatal cytokine storms, as seen with Jesse Gelsinger (Sibbald, 2001). Key vector-based factors influencing these responses include; route of administration, dose, the pre-existing immunogenicity of targeted tissues, alterations in nucleotide sequence/ structure, and choice of regulatory features such as transgene promoters and enhancers (Bessis et al., 2004).

1.4.1 Coadministration of immune-modulating drugs

The most commonly used approach to reduce unwanted responses during gene therapy treatment involves coadministration of immunosuppressants such as glucocorticoids, antiproliferative agents, calcineurin inhibitors, and others (Arruda et al., 2009). Their mechanisms include checkpoint inhibition, TLR agonism, B-cell depletion through anti-receptor antibodies, cytokine suppression, and inhibition of T/ B-cell proliferation (Sampaolesi et al., 2006; Wang et al., 2007). Typically used to avoid allograft rejection, moderately intensive regiments have been found to induce tolerance or suppression providing a relatively safe method of improving transgene efficacy and expression duration (Arruda et al., 2009).

Fine-tuned control from combining drugs can generate environments closer to immune tolerance rather than suppression, offering more desirable outcomes, with reduced effects on wider host immune functions (Chang et al., 2000; Wu et al., 2004). However, several concerns remain regarding compromised immunity, increased susceptibility to tissue damage, drug side effects (lipid/ glucose metabolism disorders) and long-term complications with malignancies and infertility (Arruda et al., 2009). These safety concerns have led to the development of alternative methods.

1.4.2 Controlled delivery

Organ selection

For AAV-based gene therapies, the route/ tissue of administration significantly affects its immunogenicity. Within the human body, tissues such as the eye and central nervous system are considered immune-privileged due to the respective presence of retina and brain blood barriers (Muldoon et al., 2013; Perez et al., 2020). The mechanisms driving immune privilege vary but include reduced lymphatic drainage, reduced expression of MHC molecules associated with antigen display, and production of immune-suppressive cytokines like TGF-b, amongst others (Streilein et al., 1997a, 1997b). For this reason, the majority of early AAV investigations focussed on the eye, delivering retinal gene therapy through intravitreal injection (a relatively simple procedure with direct medicinal delivery into the eye area) or subretinal injection (a more specialised process requiring precise targeting to the back of the eye) (Bucher et al., 2021). These localised delivery methods are significantly superior to traditional systemic methods as they require lower vector doses resulting in substantial cost-saving and dramatically reducing the probability of an exaggerated immune response along with anti-capsid, anti-transgene, and capsid neutralising antibodies (Fitzpatrick et al., 2018). There are however, many immune-responsive organs including the skin, lungs and kidneys which limits application of these approaches due to the presence of specialised dermal DC sentinels, macrophages, T cells and other immune surveillance/ defence components (Kupper and Fuhlbrigge, 2004). Selective organ administration therefore is not an ideal solution for reducing gene therapy-stimulated responses.

Tissue-specific promoters

Given transgene expression in DCs is one of the largest contributors to activating adaptive responses (Jooss et al., 1998; Yang et al., 1996), tissue-specific promoters offer a highly selective solution with weak expression in APCs but high expression in cells of interest (Shirley et al., 2020; Weeratna et al., 2001). There are however a number of challenges associated with their use including; off-target activity, few well-

characterised promoters available from the literature, low expression efficiencies, and long-term epigenetic silencing (Cabrera et al., 2022; Mendell et al., 2010; Weeratna et al., 2001). Further research is therefore required before effective implementation of tissue-specific gene promoters.

1.4.3 Vector engineering

Removing/ methylating CpG motifs

Given a key feature of foreign prokaryotic CpGs is their unmethylated status, simply methylating these dinucleotides proposes an attractive solution (Reyes-Sandoval and Ertl, 2004). This, however, is not always effective and instead results in abolished or severely reduced transgene expression (McLachlan et al., 2000; Razin and Cedar, 1983). Despite the general depletion of CpG motifs throughout the mammalian genome, enrichment in promoters, enhancers, transcriptional start sites, and origins of replication were found to exert regulatory effects, up or downregulating gene expression, depending on the CG methylation status (Bird, 2011). For example, promoters with high CG densities, known as 'CpG islands', tend to have higher transcriptional activity, and are widely present in house-keeping and tissue-specific genes (Hartl et al., 2019; Larsen et al., 1992). However, those with lower CG densities are more prone to methylation by DNA methyltransferases, inducing gene silencing through the disruption of TF binding or recruitment of repressors/ chromatin modifiers (Figure 1.3) (Tate and Bird, 1993; Vaissière et al., 2008). Therefore, depending on the promoter and gene of interest, CpG removal can i) increase or decrease long-term transgene expression (Habib et al., 2020), ii) limit the design of synthetic promoters due to restricted use of CpG-free TF bindings sites, and iii) compromise the activity of tissue-specific promoters dependent on unique CpG methylation patterns for differential activity (Nagae et al., 2011; Rishi et al., 2010).

Similarly, intragenic CpGs also exhibit methylation-dependent regulatory activity, with variable effects on transgene expression, as summarised in Figure 1.3 (Krinner et al., 2015). CG removal from these regions has been found to interfere with host transcriptional activity, causing a reduction in mRNA copy number/ mRNA

translation, due to a lack of CpG-dependent secondary structure stabilisation (Bauer et al., 2010; Duan and Antezana, 2003). Furthermore, restrictions in codon usage during CG removal can affect ribosomal translation, causing unwanted changes in protein conformation and function as seen with the *cftr* (Kirchner et al., 2017).

Given the limitations in current suppressive strategies, a requirement for alternative technologies able to counteract CpG immunogenicity, without methylation or removal, would facilitate the development of safer and more effective gene therapies.

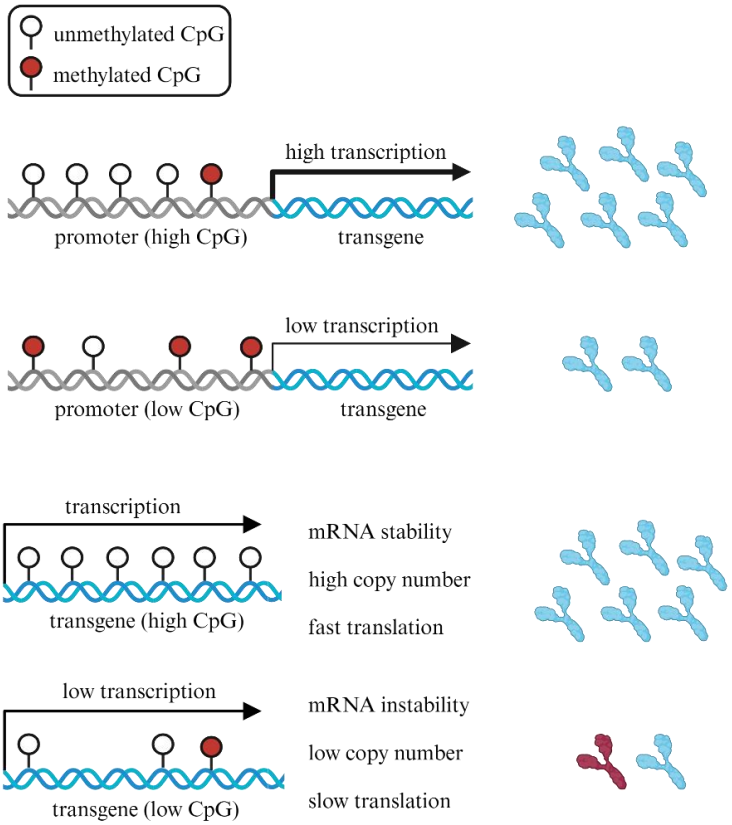

Figure 1.3) Impact of vector CpG content and methylation status on transgene production. Promoters with high CpG content form CpG islands which are predominantly unmethylated, resulting in high rates of transgene transcription resulting in high protein yields. Promoters with low CpG content are more prone to methylation resulting in reduced transcriptional activity and low protein yields. Intragenic transgene sequences with high CpG content tend to produce more stable mRNA present in larger copy numbers and more readily translated resulting in high protein yields. Intragenic transgene sequences with low CpG content are more prone to methylation resulting in reduced transcription, lower mRNA stability and copy numbers, with slower rates of ribosomal translation resulting in low protein yields that are more protein to misfolding (*Created with Biorender.com*).

1.5 Thesis Overview

Thus far, this thesis has presented an overview of i) pDNA-driven immune responses from vaccines and gene therapies, ii) the capacity for DNA sequence dependent immune modulation and iii) current limitations in the methodologies used to screen the immunogenic impact of these therapeutics. From this review, two key requirements have been identified to further the field of DNA-based therapies from an immunological perspective. 1) The design of tools capable of specifically quantifying pDNA-driven responses, characterising sequence-specific effects on different arms of immunity for use in vaccine and gene therapy immunogenicity screens. Ideally, these technologies would be comprehensive, sensitive, standardised, and automated. This would enable medium through-put screening of numerous vector designs, informing optimal selection in early design stages to develop more efficacious vaccine (more immune-stimulatory/ trigger a specific Th response) and gene therapies (more immune-suppressive). 2) Novel tools for DNA-based immune-suppression, capable of down-regulating pDNA vector immune responses. Ideally, a toolbox of well-characterised sequences with the ability to predictably modulate immune activity (with a specific focus on reducing pro-inflammatory responses) would provide a controllable approach for the scientific and industrial community.

Chapter 2 of this thesis describes the materials and methods used within the study. Chapter 3 details the development of a novel Nanostrings-based tool capable of quantitatively characterising pDNA immunogenicity for industrial application and scientific research. Literature informed bottom-up and top-down bioinformatics analysis was used to generate a comprehensive map of DNA-driven responses in DCs, including core and condition-specific genes/ proteins (also referred to as outputs). Subsequent gene filtering defined a panel of 34 key responders representing the variety in associated immune pathways whilst forming the foundation of said analysis tool. Its utility was validated by screening vectors of varying sequences, generating reproducible and accurate measures of overall immunogenicity, as well as granular quantification across the 34 representative genes. An automated analysis

app was also developed to enable simple, standardised, and direct comparison of vector immunogenicity for use in i) quantifying immunogenic activity of DNA therapeutics, ii) informing vector engineering design decisions during early development of therapeutic plasmids and iii) characterising the effects of specific sequence alterations.

Chapter 4 presents the first-ever large-scale screen of plasmid-integrated immune-suppressive DNA motifs, through the design of homotypic and heterotypic sequences. The resulting vector constructs were tested using the immune-profiling tool developed in chapter 3, consistently identifying microsatellite sequences as the most immune-suppressive, followed by CpG dinucleotides and finally G-rich motifs. MLR modelling was used to model and quantify these effects, although no suppression was detected in TNFa and IFNb protein ELISAs. The data presented here characterise a toolbox of statistically significant dsDNA suppressive motifs to inform future therapeutic vector engineering design strategies.

And finally, chapter 5 characterises the first-ever toolbox of ODNs with the capacity to predictably modulate DNA vector driven immune responses. Trends in sequence Type similar to those concluded from chapter 4 were observed. Microsatellite-derived M16 was found to exhibit the most suppression, thresholding TNFa production across multiple vectors of varying sequence, immunogenicity, and concentration. Further investigation found M16 to downregulate TNFa production by almost 70%, counteracting plasmid integrated CpG-induced responses across numerous pathways. Interrogation of the human pDC CAL-1 cell line found this model to be limited in its ability to respond to pDNA, however some CpG sequence-dependent activation was observed. The sequence specific ODN technology identified in this chapter presents a novel approach for reducing pDNA vector immune responses. This expands the design space for vector CpG incorporation, allowing more stable and longer-term expression of therapeutic transgenes.

Chapter 2 : Materials and Methods

This chapter details the materials and methods used within this thesis.

2.1 Bioinformatics analysis

2.1.1 Bottom-up literature analysis

A comprehensive review of the literature identified studies quantifying the effects of double-stranded DNA (linear or plasmid) exposed to DCs (of varying subtypes) within human or mice models. All outputs were consolidated and ranked based on the frequency of their analysis: rank 1 (5+ studies), rank 2 (3-4 studies), rank 3 (2 studies) and rank 4 (1 study) .

2.1.2 Top-down transcriptomic analysis

Microarray data measuring DC effects to dsDNA was downloaded from NCBI Gene Expression Omnibus. Dataset 1 accession number GSE2197 samples GSM40050 – GSM40056 (Stetson and Medzhitov, 2006). Dataset 2 accession number GSE61835 samples GSM1515489 - GSM1515490, GSM1515492 - GSM1515493, GSM1515495 - GSM1515496 (Woo et al., 2014). Both microarrays were conducted on the Affymetrix Mouse Genome 430 2.0 Array.

Data was imported for analysis into R using the GEOquery Bioconductor package by Sheffield University's Bioinformatics Core (Sean and Meltzer, 2007). For each data set, quality assessments were performed using boxplots and principal components analysis. If applicable, a $\log_2$ transformation was calculated to compare conditional effects. Differential expression analysis was conducted using the limma Bioconductor package, with adjusted p-values calculated from multiple t-testing and corrected using the Benjamini-Hochberg method (Benjamini and Hochberg, 1995; Ritchie et al., 2015).

2.1.3 Gene filtering approach

From the processed transcriptomic data set, a series of filtering rules were applied to bias gene selection towards the following criteria: i) high FCs, ii) high final expression (FE) values, iii) supported by high-confidence bottom-up data, iv) over-represented in dsDNA over ssDNA conditions and v) identified from more variable DNA sequences/ size conditions. This was done by firstly, identifying all statistically

significantly upregulated genes using an adjusted p-value threshold of <0.1 and log_2 FC >1, (2,067 genes). Secondly, those with an FC and FE value in the top 25% of their respective conditions were selected (98 genes). And finally, to further bias this top-down selection and incorporate key bottom-up data, filters were applied to only include genes according to the following rules:

i. shared in top-down tumour DNA conditions and at least one other,
ii. met the 25% threshold for at least one top-down DNA condition and have been reported within the literature at least three separate times,
iii. were significantly up regulated in tumour DNA conditions (but did not meet the 25% threshold) and have been reported within the literature at least three separate times.

2.1.4 Cytoscape visualisation

34 identified response genes were analysed using g:Profiler (version e109_eg56_p17_1d3191d) with a g:SCS applied q-value of 0.05 to identify over-represented biological themes (Raudvere et al., 2019). This was used to generate an enrichment map using visualisation tool Cytoscape, with q-value < 0.01 to limit node significance and a Jaccard Overlap combined coefficient of > 0.375 to prevent image over-crowding (Shannon et al., 2019). Autoannotate was used to cluster similar biological themes, these were manually re-labelled for clarity (Kucera et al., 2016).

2.2 Vector construction and preparation

2.2.1 Plasmid design

pVAX1 (Thermo Fisher, Oxford, UK) was modified to include a Turbo green fluorescent protein (GFP) (referred to as GFP) reporter protein. Immune-modulatory motifs were organised into larger suppressive or stimulatory elements and cloned 5' upstream of the cmv promoter of pVAX1 (GenScript Biotech, Piscataway, US). These included neutral control sequence 'scrambled' composed of randomly selected CpG-free sequence segments from the GFP reporter gene, a 'positive control' sequence containing a mixture of CpG-class motifs, library 1 designs and library 2 designs.

2.2.2 DNA preparation

Plasmids were amplified and isolated using the Qiagen DNA extraction kits according to the manufacturer's guidelines (Qiagen, Manchester, UK). To further reduce endotoxin, 300ul endotoxin removal solution (Merck, Kent, UK) was added (prior to the addition of binding buffer), incubated on ice for 20-30 minutes (mins), transferred to a water bath (37°C) and centrifuged (4,000xg) for 5 mins. The resulting clear upper phase was transferred into a fresh tube and the entire endotoxin removal process was repeated once more before continuation following the standard protocol.

Upon isolation of DNA, samples were resuspended and stored in cell culture grade endotoxin free water. Prior to use, DNA was further purified using an ethanol precipitation. This involved; adding 1/10 volume 3M sodium acetate and 2.5X volume 100% ethanol, freeze for >1hr at -80°C, centrifuge (15,000rpm) at 4°C for 30mins, wash with 300ul 70% ice-cold ethanol and centrifuge (15,000rpm) at 4°C for 5mins. Supernatant was removed and pellets resuspended in endotoxin free water.

2.3 Cell culture and transfection

2.3.1 DC2.4

Immortalised murine, monocyte derived dendritic cell (moDC) line DC2.4 (Merck CAT# SCC 142) was cultured in RPMI-1640 media supplemented with 20% heat inactivated foetal bovine serum (FBS), 1X L-glutamine, 1X non-essential amino acid, 1X HEPES buffer, 0.0054X β-Mercaptoethanol (Thermo Fisher, Oxford, UK) and incubated at 37°C, 5% CO_2. Media was replaced every two days, while cells were sub-cultured every third day at a 1:6 – 1:10 ratio (as per manufacturers protocols). Cell concentration and viability was analysed at each passage using a Vi-CELL cell viability analysed (Beckman-Coulter, High Wycombe, UK)

Pre-transfection, cells were grown to 60-70% confluency in T-75 flasks (Thermo Fisher, Oxford, UK), washed with 1X PBS twice, accutased for 5 mins (Thermo Fisher, Oxford, UK), neutralised with supplemented media, centrifuged at 300xg for a further 5 mins and resuspended in fresh supplemented media. For each technical replicate,

400,000 cells were transfected with pDNA at 400ng +/ - 1% diluted in endotoxin free water (or alternate concentrations where specified) in SG buffer using the Amaxa 96-well shuttle (Lonza, Slough, UK) with pulse CD147, according to the manufacturers protocol. 320,000 transfected cells were cultured in 48-well plates in a final total volume of 400ul supplemented media and incubated for 2-24 hours (hrs) depending on the downstream analysis required.

2.3.2 CAL-1

Immortalised human plasmacytoid dendritic cell line CAL-1 (DSMZ CAT# ACC 923) was cultured in RPMI-1640 media supplemented with L-glutamine 2mM, sodium pyruvate 1mM, HEPES buffer 10mM, minimum essential medium non-essential amino acids and 10% heat-inactivated FBS (Thermo Fisher, Oxford, UK). Cells were seeded at a density of 1 x10^6 in T-75 flasks and incubated at 37°C, 5% CO_2. Cultures were split every 2-3 days at a 1:2 – 1:4 ratio, with a maximal density of 1.5 x 10^6/ ml.

Pre-transfection cells were either starved (grown in supplemented media but with 0.1% heat inactivated FBS) for 16hrs overnight or non-starved (grown in standard supplemented media with 10% heat inactivated FBS). For each technical replicate, 1.5 x 10^6 cells were transfected with pDNA (ranging from 400 – 2000ng) in SF buffer using the Amaxa 96-well shuttle with pulse DN100, according to the manufacturers protocol. 320,000 transfected cells were cultured in 48-well plates in a final total volume of 400ul supplemented media and incubated for 24hrs.

2.3.3 ODN supplementation

Post-transfection

Post-transfected cells were incubated in 400ul media composed of 7% (28ul) ODN in endotoxin-free water and 93% (372ul) RPMI supplemented media for both DC2.4 and CAL-1 experiments. Controls were composed of identical solution mixtures but without any ODN. These volumes were a compromise between maintaining low levels of endotoxin free water (to ensure cells had as much media as possible) whilst ensuring ODN volumes were large enough to be accurately handled and transferred.

Co-transfection

During DC2.4 preparation for transfection, pDNA and ODN samples were pre-mixed at desired concentrations in endotoxin free water. This solution was added to SG buffer containing cells (as described in the manufacturers protocol) ensuring no change in the total volume of water added during nucleofection.

2.3.4 Statistical tests

Statistical analyses using standard, unpaired, two-tailed t-tests were performed using GraphPad Prism (version 9.5.1) with a p-value significance threshold of 0.05 where *=p≤0.05, **=p≤0.01, ***= p≤ 0.001, ****= p≤0.0001 and non-significance was denoted 'ns'. For multiple t-test comparisons, individual variance was assumed for each row (to account for normalised samples) with the Holm-Sidak method used to control for family wise error rates using a p-value threshold of 0.05 as described above.

2.4 Nanostrings analysis

2.4.1 nCoutner and nSolver processing

Transfected cells were washed, accutased and centrifuged as described in section 2.3.1, at time-points indicated (including 2hrs, 4hrs, 8hrs, 12hrs and 24hrs). Pellets were snap-frozen and stored at -80°C for no longer than 7 days. Total RNA was extracted with RNAeasy Kits (QIAGEN) according to the manufacturer's guidelines. 60ng total RNA was hybridised to a custom gene expression Codeset (34 total genes + 4 housekeepers) and analysed on an nCounter SPRINT Profiler by the University of Sheffield's Institute for Translational Neuroscience. Negative control thresholding was applied to raw counts followed by positive control normalisation and codeset content normalisation to housekeeper *g6pdx* using nSolver software, as per recommended Nanostrings analysis guidelines (Gene Expression Data Analysis Guidelines, 2017).

2.4.2 Nanopanel automated analysis app

The Nanopanel app was coded using Shiny, an open-source R package for the development of user-friendly web applications (Chang et al, 2023). For use, two data

inputs were required; 1) Nanostrings nCounter generated RCC files and 2) a csv describing each sample and its condition status. R package NACHO was used to normalise data based on positive control geometric means and facilitates selection/ prediction of housekeeping genes using NACHO functions (Canouil et al., 2019). Resulting quality control graphics can be assessed within the 'Quality Control' tab.

Differentially expressed genes present within each sample were identified as fold change (FC) ratios between sample and control conditions. A heatmap of up/ down regulated genes can be displayed within the 'Analysis' tab alongside a slider function for user determined thresholding of expression differences. The number of genes above/ below set threshold were displayed as a bar plot. Differential expression analysis was performed using the limma Bioconductor package (version 3.41) and presented in a table alongside adjusted p-values (Ritchie et al., 2015).

2.5 Protein quantification

2.5.1 GFP analysis

24-hrs post-transfection, reporter protein expression was measured using the SpectraMax iD5 Multi-Mode Microplate Reader (Avantor, Luuterworth, UK) at an excitation wavelength of 485nm and emission wavelength of 535nm for GFP detection. Bottom-reads were used for adherent DC2.4 cells whilst top-reads for suspensions CAL-1 cells. To measure transfection efficiencies, post-transfected cells were resuspended and mixed with equal volumes trypan blue stain 0.4% (20ul total) (Thermo Fisher, Oxford, UK). Samples were analysed on the Countess 3 Cell Counter (Thermo Fisher, Oxford, UK) using GFP filters at a gate of 100.

2.5.2 ELISA detection

24-hour post-transfection, supernatant samples were harvested and frozen at -20C. From DC2.4 cells, TNFa and IFNb was measured using mouse ELISA kits (Thermo Fisher, Oxford, UK) whilst CAL-1 TNFa levels were measured using human ELISA kits (Thermo Fisher, Oxford, UK) according to the manufacturers protocol. Samples were freeze-thawed no more than three times.

Chapter 3 : A Novel Tool for Quantitative Characterisation of Plasmid DNA Immunogenicity in Dendritic cells

This chapter describes the development of a novel tool, specifically designed to quantify, and characterise the effects of pDNA on DNA-driven immune response pathways, within DCs. A literature-based bioinformatics analysis was used to comprehensively map the transcriptomic effects of DC exposure to foreign DNA. Hypothesis-based filtering identified 34 key representative response genes, forming the basis of an immune profiling tool capable of detecting and quantifying pDNA sequence-specific effects. Utility was investigated by screening vectors of varying sequence/ immunogenicity and comparing outputs to traditional methods. Automated analysis app 'Nanopanel' was developed to streamline and standardise data processing. This tool presents a novel technology capable of precise, sensitive, and reproducible characterisation of pDNA immunity to facilitate early vector design screening, with applications in industrial and scientific research.

3.1 Introduction

As discussed in section 1.1.2, DNA therapeutics elicit potent responses from immune cells through detection by DNA sensors and activation of signalling pathways within APCs such as DCs. FDA and EMA guidelines require thorough immunogenic characterisation of novel therapeutics in order to ensure patient safety (European Medicines Agency, 2007, FDA 2007). Current screening methods have several drawbacks, for example, RNA sequencing offers a comprehensive and data-rich approach but is limited by cost, low throughput, and large unfocussed datasets (Bustin, 2000). ELISAs, ELISpots and RT-qPCR are more commonly used but can be time-consuming, limited in their outputs and require prior knowledge of genes/ proteins of interest (Czerkinsky et al., 1984; Kawabata et al., 1999). Furthermore, none of these methods enables characterisation of pDNA effects specifically across DNA-driven response pathways. As the field of plasmid-based DNA therapeutics continues to expand (Ginn et al., 2018; Lopes et al., 2019), regulatory bodies have recommended earlier pre-clinical immunogenicity screening (compared to current late-stage detection) to highlight safety issues (Vandivort et al., 2020).

The ability to quantify pDNA immunogenicity with high specificity and sensitivity would not only provide accurate screening tools for the community, improving patient safety, but could also inform early vector engineering design strategies, improving therapeutic efficacy. For example, pDNA-integrated immune-stimulatory motifs have been found to exhibit advantageous adjuvant effects in vaccine therapies (Mirjam et al., 2011; Schneeberger et al., 2004; Su et al., 2017; Yu et al., 2015), whilst the removal of these motifs produces safer and more effective gene therapies (Krieg et al., 1998; Yew et al., 2002). The ability to discriminate between small, sequence-specific immunogenic differences in novel vaccine/ gene therapy vectors would inform the selection of more efficacious designs capable of better stimulating (vaccines) or suppressing (gene therapies) response pathways.

In order to develop a tool capable of the above, it must i) quantify plasmid-dependent upregulation/ downregulation of DNA-specific response pathways, ii) sensitively and precisely discriminate between sequence-dependent changes in immunogenicity, iii)

offer an easy-to-use and easy-to-implement pipeline capable of standardised analysis for simple, quick and detailed comparison of vector immune-effects and iv) enable screening of murine specific responses, as early-stage designs require initial testing in mice models before human testing (AstraZeneca, Cambridge, UK).

The work in this chapter aims to:

1. Identify a panel of genes representative of DNA-driven response pathways in DCs, forming the foundation of a novel immune-profiling tool.
2. Characterise the functionality of these genes and their association with different innate/ adaptive response pathways.
3. Develop and validate a pipeline for medium-throughput DNA vector screening, quantifying representative response genes.
4. Investigate and confirm the utility of this profiling tool by screening vectors of varying sequence/ immunogenicity and comparing outputs to traditionally used assays.
5. Develop and implement an automated data-processing app, presenting quality control assessments and user-defined analysis visualisations.

3.2 Results

3.2.1 Mapping the dsDNA driven immune response in DCs

In order to develop a tool capable of characterising the impact of pDNA within DCs, a bottom-up screen of published data analysing dsDNA effects on pre-selected genes/ proteins was combined with a top-down bioinformatics analysis of pDNA-specific transcriptomic data. By integrating these methods, the numerous but focused bottom-up studies could be complemented with fewer but more in-depth top-down analyses, resulting in an unbiased and comprehensive map of pDNA driven gene responses in DCs.

Bottom-up literature-based analysis

A systematic and comprehensive evaluation of the literature identified numerous studies analysing different dsDNA sequence conformations (linear, circular,

synthetic, native) within varying DC subtypes (BMDC, pDC, moDC, conventional DCs (coDC)). Outputs in the form of key immune genes (mRNA transcript analysis) and proteins (cytokines, chemokines, cell surface receptors, signalling molecules etc.) were compiled and assembled (Table 3.1). Overall, 14 types of linear dsDNA sequences and 7 plasmids were tested, with immune-stimulating poly(dA:dT) inducing upregulation from 55/ 57 analysed outputs. Mouse models were investigated more frequently than humans (as expected), with BMDC tested most frequently given its upregulation across 53/ 57 outputs. The broad variety in sequence and cell-type highlights core genes/ proteins considered most important in immune-studies and so analysed most often in the literature.

The 57 total outputs were categorised based on how often they were quantified: rank 1 (5+ studies), rank 2 (3-4 studies), rank 3 (2 studies) and rank 4 (1 study). IFNa and IFNb were most often analysed given their critical role in mediating intracellular antiviral responses followed by inflammatory cytokines IL-6, essential for Th2 differentiation, and CXCL10, involved in Th1 activation and IFN regulation (Diehl and Rincón, 2002; Khan et al., 2000; Meager, 1998). Rank 2 outputs included TNFa, a master regulator of proinflammatory cytokine production, DC activation markers CD40 and CD86, and T-cell chemoattractant *ccl5* (Carswell et al., 1975; Culley et al., 2006; Ma and Clark, 2010). Less commonly reported outputs form ranks 3 and 4 include PRRs (*aim2, mda5, ifit205, rig1*), interleukins (*il18, il4*) chemokines (*cxcl2, cxcl9*) and transcription factors (*irf1, irf7*). Advantages of a bottom-up approach include high confidence in a small, focussed number of outputs consistently proven to show immune-associated effects. However, limitations lie in the biased detection of certain genes/ proteins based on literature consensus rather than system conditions, as well as the dependency on pre-selected outputs.

Table 3.1) Bottom-up analysis of dendritic cell responses to foreign dsDNA. Column 1 describes analysed genes/ proteins, columns 2 describes the total number of associated studies with the breakdown of genes (left) and proteins (right). Column 3 denotes output rank based on frequency of detection: rank 1 (5+ studies), rank 2 (3-4 studies), rank 3 (2 studies) and rank 4 (1 study). Highlighted (blue) boxes described dsDNA conditions, DC cell model and species analysed for each output.


Gene/ protein
Reference
Rank
DNA sequence
Linear dsDNA
plasmid DNA
DC model
Species
poly dA:dT
poly (G:dC
ISD
HT-DNA
CT DNA
dsCpG
salmon sperm
human LL37
huDNA
Mtb DNA
E. coli gDNA
Self-DNA LL37
HSV-1 60mer
VACV 70mer
pDNA
pcDNA3
CpG
pcDNA4
pcOVA
pLacZ DNA
pCMV9
BMDC
pDC
cDC
moDC
D2SC cell line
Murine
Human
Ifna, IFN-a 11 (3, 10) 1
Ifn-b, IFN-b 11 (11, 7) 1
Il-6, IL-6 6 (2, 4) 1
Cxcl10, CXCL10 5 (4, 1) 1
tnf-a, TNF-a 4 (2, 3) 2
Il-1b, IL-1b 4 (1, 3) 2
CD40 4 (4) 2
CD86 4 (4) 2
Ccl5 / RANTES 3 2
Ifih1/mda5 2 3
Casp1, Caspase 1 2 (1,1) 3
Il-12b, IL12p40 2 (1,1) 3
Ifit1 2 3
CD80 2 3
Irf7 1 4
IRF1 1 4
IFIT2a 1 4
Ddx58/RIG 1 1 4
Rsad2/viperin 1 4
Myd88 1 4
Il-18, IL-18 1,1 4
LC3 II 1 4
Ifn-g 1 4
tgfb1 1 4
tgfb2 1 4
Il-1a 1 4
Il-4 1 4
Il-13 1 4
Il-15 1 4
Il-23a 1 4
Il-33 1 4
Il-1ra 1 4
Ccl4 1 4
Cxcl1 1 4
Cxcl2 1 4
Cxcl6 1 4
Cxcl9 1 4
Ccr1 1 4
Ish15 1 4
IFNL1 1 4
Ifi204 1 4
Ifi205/mnda 1 4
Ifi47 1 4
Irf2 1 4
Irf5 1 4
aim2 1 4
mndal 1 4
tlr2 1 4
tlr3 1 4
tlr7 1 4
IkBa/nfkbia 1 4
zbp1 1 4
socs1 1 4
socs3 1 4
a20/tnfaip3 1 4
prdm1 1 4
CD25 1 4

Top-down transcriptomic analysis

To avoid bias from literature based small-scale outputs, an in-depth transcriptomics analysis of pDNA effects in DCs was conducted. Although proteomics searches yielded no results, two relevant microarray studies were found testing three different DNA conditions using lipofectamine-based transfection in BMDCs (Figure 3.1A) (Stetson and Medzhitov, 2006; Woo et al., 2014). These included tumour DNA which was highly immunogenic and variable in both sequence and length, ISD DNA composed of a 45bp sequence used as the 'gold standard' for immune-stimulation studies (Li et al., 2013b) and a CpG ssODN class-B motif. Although not dsDNA, CpG sequences have been comprehensively characterised as potent immune-stimulators and so were included to ensure their associated response pathways were included and to differentiate between dsDNA specific and non-specific upregulated genes. Differential expression analysis of both datasets compared 45,000 genes per DNA condition, assigning $\log_2$ FC and associated p-values. In ISD and CpG conditions, 1% of all genes were found to be significantly upregulated ($\log_2$ FC>1, p value<0.1) and in Tumour conditions 3%, confirming foreign DNA exposure upregulates hundreds of genes within DCs. 173 were over-expressed across all three conditions representing a core DNA-driven response independent of sequence/ backbone (Figure 1.3B).

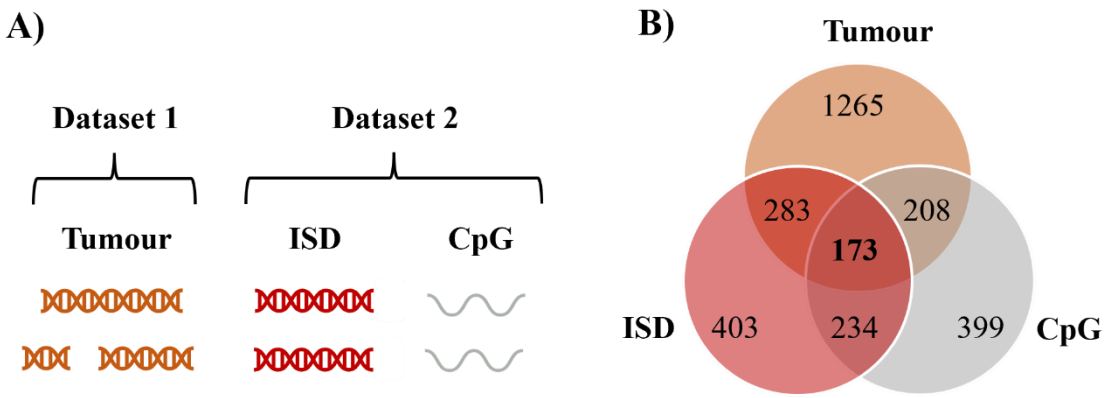

Figure 3.1) Transcriptomic dataset summary. A) DNA conditions tested in datasets 1 and 2. B) Number of statistically significant upregulated genes (log2 FC>1, q value<0.1) across individual and shared DNA conditions.

3.2.2 Identifying and characterising representative response genes

Identifying 34 key response genes using filtering rules

Over 1000 genes were found to be significantly upregulated from top-down OMICs analysis however for application as an immune-profiling tool, these were filtered to identify a smaller, representative panel capable of characterising multiple dsDNA-activated pathways. As detailed earlier in section 2.1.3, rules were applied to bias gene selection, favouring: i) high FCs, ii) high FE values, iii) support from high-confidence bottom-up data, iv) over-representation in dsDNA over ssDNA conditions and v) more variability in DNA sequence and size (summarised in Figure 3.2A). From an initial pool of 2,9657, top 25% of FC and FE expressers were filtered down to 98, of which 26 were also present in bottom-up data (Appendix, Supplementary Table 2). Further rules identified 34 genes distributed across DNA specific and non-specific conditions, with a clear bias towards core, tumour and ISD responses as expected (Figure 3.2B). These were ranked prioritising shared > single conditions, tumour > ISD > CpG and ordered based on the magnitude of their combined FC and FE (Table 3.2).

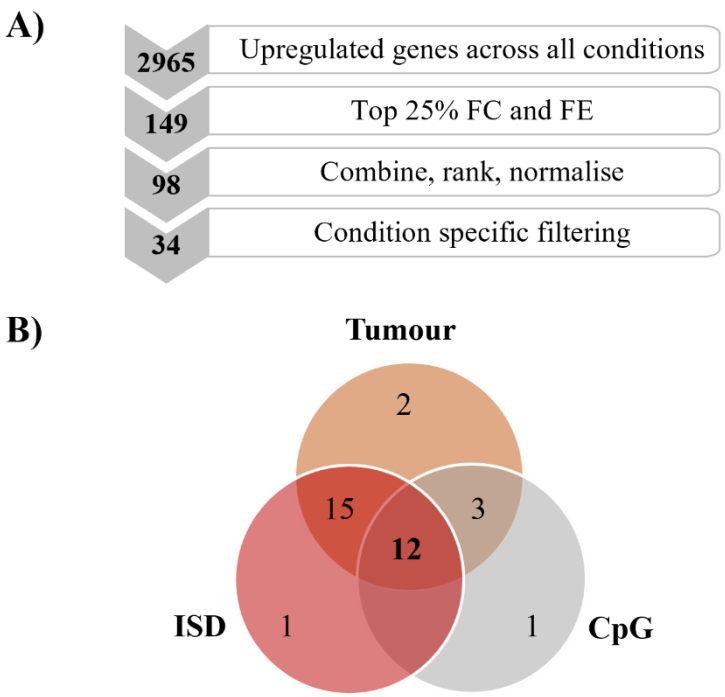

Figure 3.2) Filtering key response genes. A) Summary of filtering rules and associated gene numbers at each stage B) Distribution of final 34 response genes across DNA conditions.

Table 3.2) Top-down and bottom-up filtering identified 34 key response genes. Top-down response genes (orange) were grouped favouring conditions: shared > single and Tumour > ISD > CpG. Genes were sub-ranked based on count magnitude (combined fold change and final expression values). Genes present in bottom-up data were highlighted (blue) along with their rank and an example reference.

Top-down			Bottom-up	
Condition	**Gene**	**Count magnitude**	**Rank**	**Reference**
Tumour X ISD X CpG	*rsad2*	2,105	*4*	*(Kaminski III, 2013)*
	il6	1,508	*1*	*(Li et al, 2013)*
	cxcl10	1,484	*1*	*(Kaminski III, 2013)*
	Ifit1c	1,356		
	oasl1	1,054		
	cd69	884		
	irf7	494	*4*	*(Kaminski III, 2013)*
	tnf	374	*2*	*(Yang et al, 2020)*
	mx1	245		
	ifi205	214	*4*	*(Kaminski III, 2013)*
	ccrl2	206		
	ccl5	57	*2*	*(Zhang et al, 2013a)*
Tumour X ISD	*cxcl9*	17,130	*4*	*(Kaminski III, 2013)*
	cmpk2	5,065		
	ifnb1	4,357	*1*	*(Kaminski III, 2013)*
	ccl12	3,254		
	iigp1	1,347		
	tgtp1/2	1,182		
	fam26f	606		
	gbp6	451		
	serpina3g	456		
	ms4a4c	299		
	pyhin1	234		
	igtp	200		
	phfl1d	174		
	nt5c3	174		
	fgl2	160		
Tumour X CpG	*il12b*	1,441	*3*	*(Kaminski III, 2013)*
	cox2	1,393		
	cd40	540	*2*	*(Spies et al, 2003)*
Tumour	*ifna2*	6,275	*1*	*(Spies et al, 2003)*
	cd86	86	*2*	*(Spies et al, 2003)*
ISD	*ifih1*	308	*2*	*(Zhang et al, 2013a)*
CpG	*il1b*	331	*2*	*(Kaminski III, 2013)*

Characterising functionality and T-cell responses of 34 key response genes

A number of different tools were used to characterise the functionality of these 34 representative genes (Table 3.3). INTERFEROME screening confirmed all outputs as interferon responders (Rusinova et al., 2013) broadly categorised into: cytokines/ chemokines and their receptors, surface markers, receptors/ signalling molecules, immune-related GTPases and TFs. 16/ 34 were linked to specific T-cell response pathways with an over-representation of Th1-associated genes, followed by Th2, Th17 and Treg. This Th1 bias was expected given pDNA is transfected into the intracellular environment where it interacts with cytoplasmic and nuclear receptors similar to viral infections (Huerfano et al., 2013). A Th2 response to extracellular pathogens/ allergy was represented by *rsad2, il6, ccrl2* and *ifnb1* within the panel (Diehl and Rincón, 2002; Du et al., 2020; Hu et al., 2016; Šega et al., 2004) whilst more specialised Th17 responses to certain bacteria and fungi were represented by cytokines *il6, cxcl10, ifnb1* and *ifna2* (Korn and Hiltensperger, 2021; Li et al., 2017; Šega et al., 2004; Touzot et al., 2014). Only *fgl2* a Treg effector represented this immune-suppressive pathway (Hu et al., 2016). These findings confirmed the top-down OMICs and bottom-up literature-based gene filtering approach enabled identification of 34 response genes representative of pDNA effects in DCs, all of which were immune-associated interferon response genes representing different Th arms of the immune response.

Table 3.3) Characterising the 34 key response genes. Core gene function, Th associated responses and literature references are shown, with Th1 specific responses highlighted (grey).

Gene	Function	Th response	References
rsad2	antiviral	Th2	*(Du et al, 2020) (Touzot et al, 2014)*
il6	cytokine	Th2, Th17	*(Diehl and Rincon, 2002) (Korn and Hiltensperger, 2021)*
cxcl10	chemokine	Th1, Th17	*(Li et al, 2017)*
Ifit1c	viral inhibitor		*(Mears and Sweeney, 2020)*
oasl1	modulatory antiviral		*(Kang et al, 2018)*
cd69	activation marker	Th1	*(Dorfman and Shahsafaei, 2002)*
irf7	TF/PRR		*(Ning et al, 2011)*
tnf	cytokine		*(Carswell et al, 1975)*
mx1	immune GTPase	Th1, Th2	*(Touzot et al, 2014)*
ifi205	PRR		*(Nakaya et al, 2017)*
ccrl2	chemokine receptor	Th2	*(Yoshimura and Oppenheim, 2011)*
ccl5	chemokine	Th1	*(Lebre et al, 2005)*
cxcl9	chemokine	Th1	*(Du et al, 2020)*
cmpk2	antiviral mediator		*(Lai et al, 2021)*
ifnb1	cytokine	Th1, Th2, Th17	*(Sega et al, 2004)*
ccl12	chemokine	Th1	*(Du et al, 2020)*
iigp1	immune GTPase		*(Uthaiah et al, 2003)*
tgtp1/2	immune GTPase		*(Prajeeth et al, 2018)*
fam26f	PRR		*(Malik et al, 2016)*
gbp6	immune GTPase		*(Olszewski et al, 2006)*
serpina3g	protease inhibitor		*(Shamji et al, 2019)*
ms4a4c	membrane spanning 4a family	Th1	*(Xu et al, 2006)*
pyhin1	PRR		*(Massa et al, 2020)*
igtp	immune GTPase		*(Collaza et al, 2002)*
phfl1d	Th1 gene regulator	Th1	*(Clarke et al, 20080*
nt5c3	Nucleotidase		*(Hao et al, 2013)*
fgl2	Treg effector	Treg, Th2	*(Hu et al, 2016)*
il12b	cytokine	Th1	*(Heufler et al, 1996)*
cox2	inflammatory regulator		*(Li et al, 2013)*
cd40	activation marker		*(Ma and Clark, 2009)*
ifna2	cytokine	Th1, Th2, Th17	*(Touzot et al, 2014)*
cd86	activation marker	Th1	*(Bao et al, 2018)*
ifih1	PRR		*(Jaeger et al, 2015)*
il1b	cytokine		*(Chizzolini et al, 1997)*

Identifying enriched biological pathways from key responders using g:Profiler

To determine which biological pathways were associated with these 34 upregulated genes, a gene ontology (GO) analysis was performed. g:Profiler, a web-based tool used to identify enriched biological pathways/ molecular functions, was used to screen genes against the online KEGG database (Kanehisa and Goto, 1999; Reimand et al., 2007). 177 biological pathways and 17 molecular functions were found to be significantly enriched, all of which were associated with the activation or regulation of immunity (Appendix, Supplementary Table 3). In order to simplify and visualise these functionalities, a Cytoscape map of associated biological pathways was generated (Raudvere et al., 2019) with GO terms clustered into 10 main biological themes, these included; adaptive immune responses, cytokine/ immune receptor activation, and regulatory pathways, further characterising the broad functionality of these 34 genes across numerous immune pathways as shown in Figure 3.3. (Appendix, Supplementary Table 4)

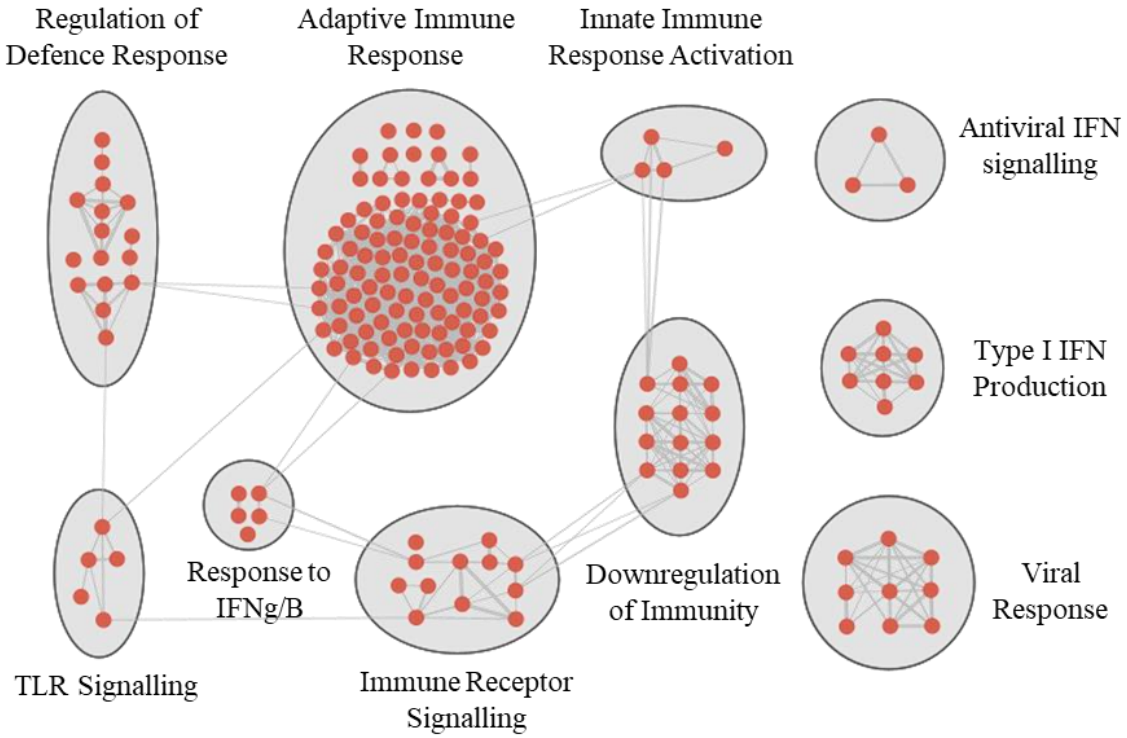

Figure 3.3) Characterising key response themes using Cytoscape. g:Profiler enriched biological pathways were clustered and visualised using Cytoscape Autoannotate function. Threshold q-value <0.01 and a Jaccard Overlap combined coefficient of >0.375 was used. Nodes (red) represent individual biological pathways while connecting lines represent associations.

3.2.3 Developing a Nanostrings based immune-profiling tool

Establishing an experimental pipeline

To develop an immune-profiling tool capable of quantifying these 34 representative genes, characterising the effects of non-coding pDNA across multiple arms of the immune response, the following experimental pipeline was developed and optimised (Figure 3.4). First, a dsDNA vector of interest was selected. Given its intended application for DNA therapeutic use, the widely available DNA vaccine vector pVAX1 was chosen with an encoded GFP reporter protein for measurement of transfection efficiency and relative expression (Invitrogen, Carlsbad, CA). Next, a nucleofection method was determined. Electroporation of pDNA in murine DC model DC2.4 was chosen based on industrial interest and well-established optimised in-house protocols, with consistent observation of transfection efficiencies >40% using 400ng pDNA (Johnson et al., 2022; Shen et al., 1997; Steinman and Cohn, 1973). A number of downstream analysis techniques were considered including multiplex ELISA, multiplex qPCR and Nanostrings (Elnifro et al., 2000; Tighe et al., 2015).

Nanostrings technology utilises specifically designed capture and reporter probes to hybridise RNA sequences of interest. The presence of colour-coded molecular barcodes on the reporter probes allows direct counting of individual RNA molecules with no amplification required. By designing different reporter probes with different molecular barcodes, this technology can be easily multiplexed. For these reasons and considering cost and tool utility, Nanostring was chosen as the immune-profiling tool analysis method providing fast, accurate, simultaneous and absolute quantification of RNA copy numbers (Kulkarni, 2011).

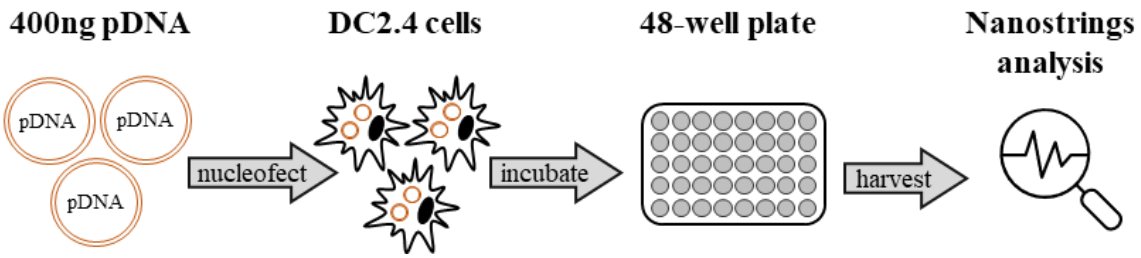

Figure 3.4) Summary of immune-profiling tool experimental pipeline. 400ng pDNA was nucleofected into 400,000 DC2.4 cells and incubated. Pellets were later harvested and RNA extracted for quantification using a Nanostrings based immune-profiling tool.

Preliminary tests were conducted to determine the optimal pDNA concentration within this system through analysis of TNFa cytokine production at 24hrs. The use of well-established pre-existing methods ensured the system was responsive before implementing a custom, novel analysis tool. A pDNA titration range between 50-800ng found TNFa levels correlated with pDNA load up to ~600ng after which values plateaued, reaching the limits of ELISA detection accuracy (Figure 3.5). These data confirm the system could detect and generate immune responses to pDNA with DC2.4 TNFa production dependent on DNA load. 400ng was determined to be an appropriate concentration producing ~15000 pg/ml TNFa. Lower concentrations may not produce detectable gene level responses whilst higher concentrations could saturate the system, masking subtle changes in response. Relative fluorescence measured from these samples exhibited a direct correlation between pDNA load and relative GFP expression, confirming nucleofection was an effective and appropriate transfection method (Appendix, Supplementary Figure 1).

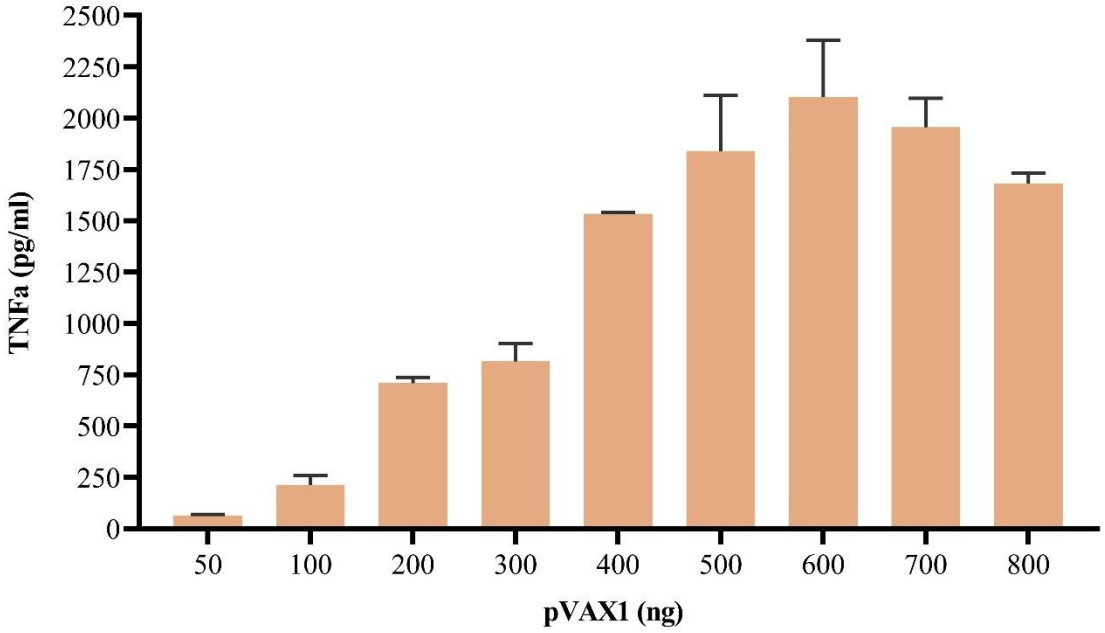

Figure 3.5 TNFa production correlated with pVAX1 DNA load up to 600ng. Vector DNA at varying concentrations were nucleofected into 400,000 DC2.4 cells and TNFa protein production quantified at 24hrs. Bars represent the mean +SD from 1 biological replicate in technical duplicate.

To ensure the response to pVAX1 was not due to GFP reporter protein immune-stimulation, a cmv excised variant 'pVAX1-cmv' was designed and similarly analysed using TNFa ELISA. Relative fluorescence measurements found no GFP protein was produced post-nucleofection whilst TNFa quantification was very similar to that of pVAX1 with a ~6% reduction (Figure 3.6). This confirmed the system was responding to dsDNA, and not GFP, immunogenic effects.

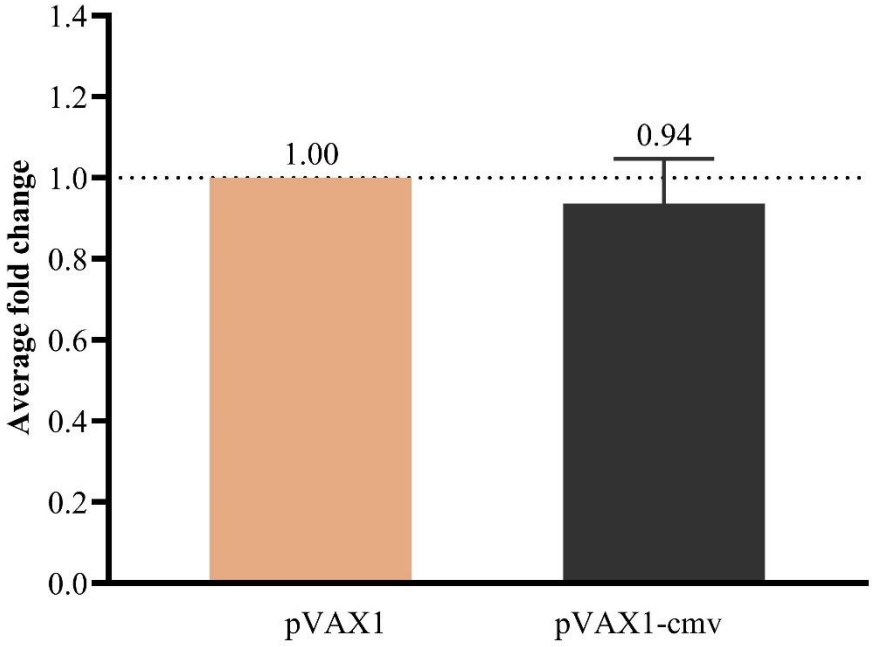

Figure 3.6) GFP production had minimal immune-stimulatory effects. 400ng vector DNA was nucleofected into 400,000 DC2.4 cells and TNFa protein production quantified at 24hrs. Bars represent the mean +SD from 3 biological replicates in technical duplicate.

Validating a Nanostrings based immune-profiling tool

Using the experimental pipeline described, a 24hrs time-course of the pDNA response in DC2.4 cells was produced (Figure 3.7). Initial analysis found 4/ 34 genes within the custom Nanostrings panel to be unresponsive to pVAX1 (*cxcl9, il12b, il1b, ms4a4c)*, leaving 30 working genes. The average expression count across these 30 genes confirmed the cellular response to electroporation with no DNA to be negligible when compared to pVAX1. Significant upregulation was observed across 2-24hrs peaking at 4hrs with an average count of >2000 mRNA copies (Figure 3.7A).

These findings confirm the Nanostrings panel worked, generating large and reproducible responses specific to pDNA across 30/ 34 immune genes over 24hrs.

A closer analysis of individual gene counts from pVAX1 samples explained some of the variability in average expression, with a clear distinction between early (expression levels peak at 2-4hrs) and late genes (peak at 4-8hrs) response genes (Figure 3.7B). *Ifnb1, tnfa, il6, ccrl2* and *cox2* were identified as 5 early responders as shown in heatmap Figure 3.7C. The former three are pro-inflammatory cytokines, regularly screened within the literature and identified during bottom-up analysis. Without incorporation of the top-down OMICs approach, core-response gene *cox2* (a key receptor associated with the regulation of DC inflammation) would not have been included within this response panel, despite showing significant upregulation within the system. Of the remaining 25/ 30 late responders, the most highly upregulated included Th2-associated *rsad2* and Th1-activating chemokines *cxcl10* and *ccl5*, all of which were top-down core-response genes also present in bottom-up data. Following these, upregulation of viral mediators *oasl1* and *cmpk2* was observed, both of which were core/ dsDNA response genes exclusive to OMICs analysis. These findings highlight the importance of a combined bioinformatics approach.

Overall, these data confirm: i) the panel of 30 genes could produce significant dsDNA specific DC responses across five orders of magnitude (*rsad2* peaking at >100,000), ii) genes found to be most upregulated were dependent on both top-down and bottom-up approaches and iii) the largest responders were associated with core/ dsDNA specific conditions, validating use of this panel.

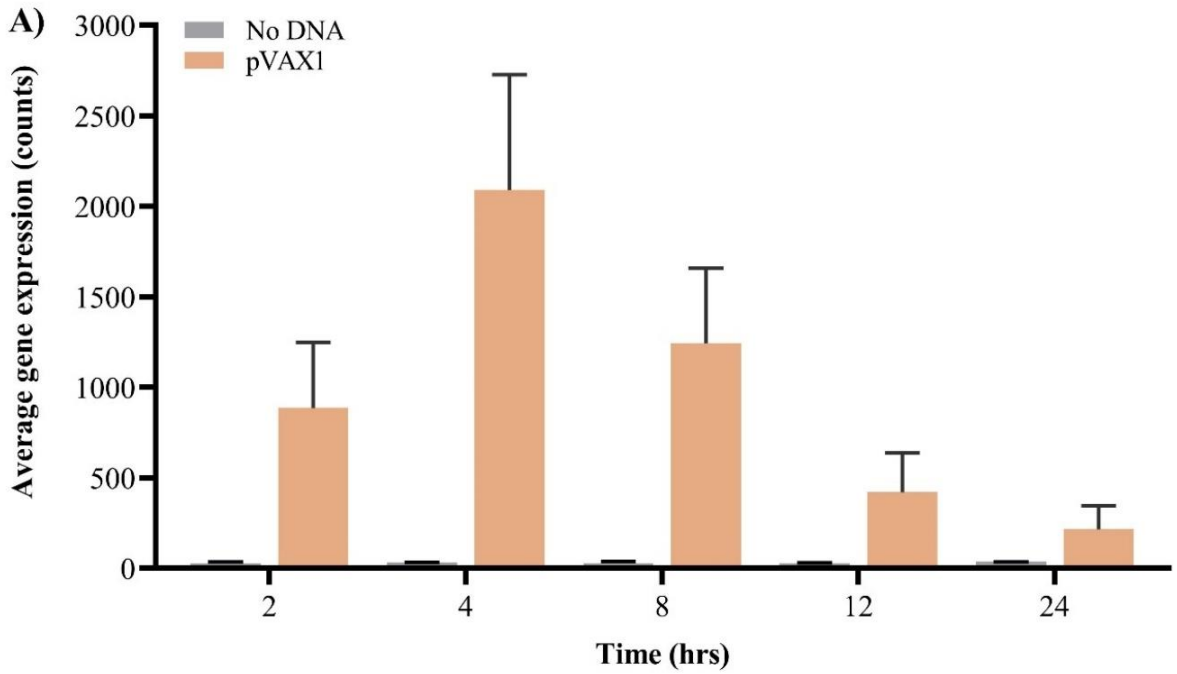
A)
No DNA
pVAX1
Average gene expression (counts)
3000
2500
2000
1500
1000
500
0
2
4
8
12
24
Time (hrs)

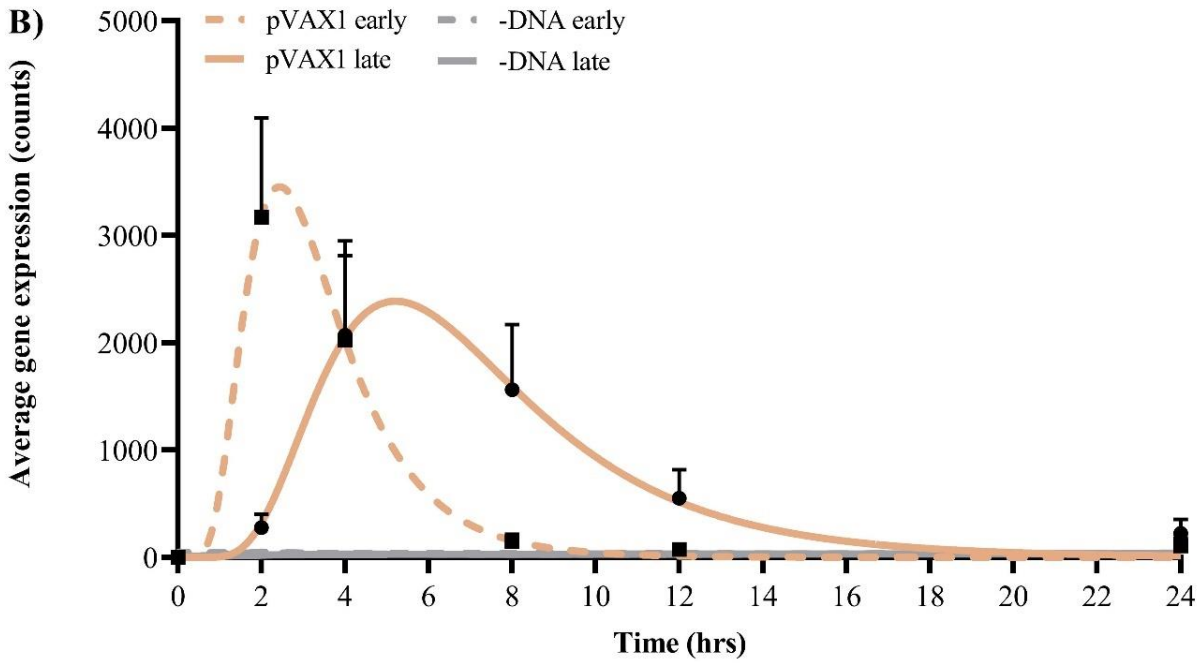
B)
pVAX1 early
pVAX1 late
-DNA early
-DNA late
Average gene expression (counts)
5000
4000
3000
2000
1000
0
0
2
4
6
8
10
12
14
16
18
20
22
24
Time (hrs)

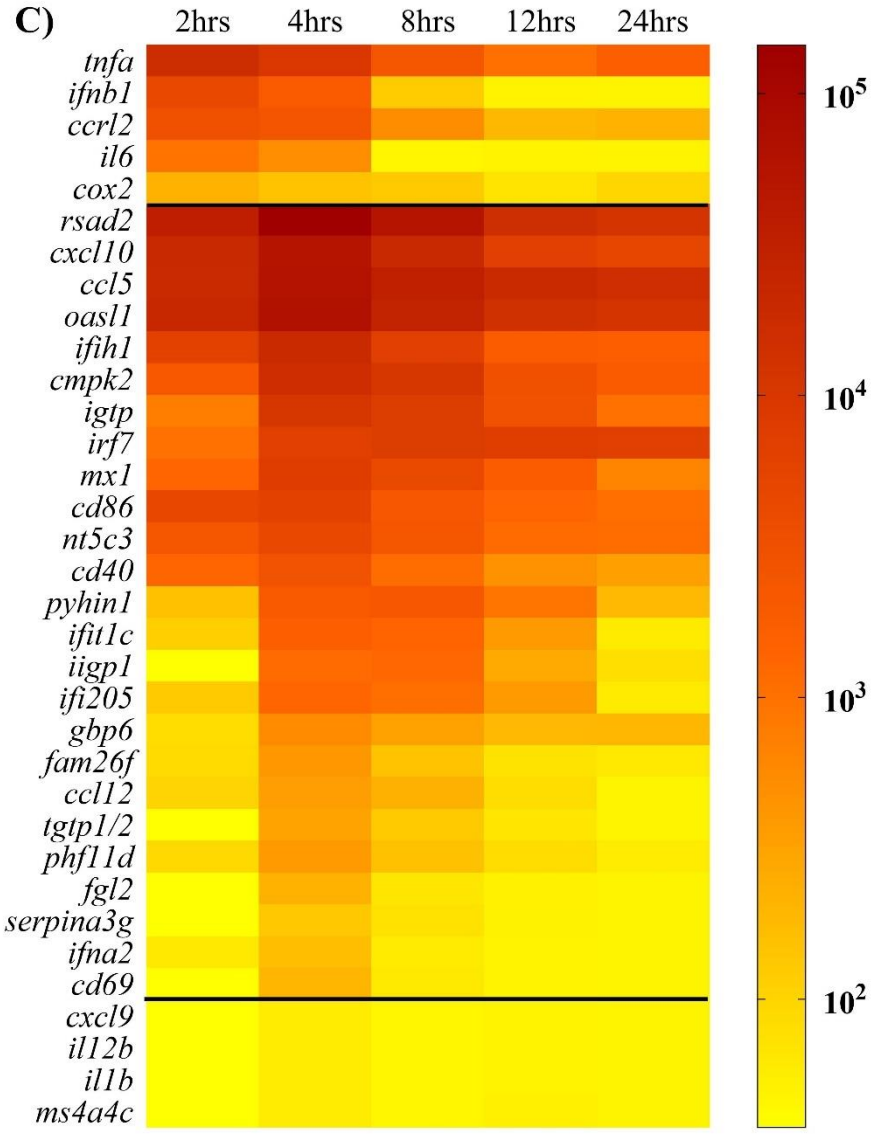

Figure 3.7) pVAX1 time-course generated significant upregulation in immune-profiling tool Nanopanel. 400ng DNA or mock transfected controls (no DNA) were nucleofected into 400,00 DC2.4 cells and analysed at varying time-points using custom Nanostrings based immune-profiling tool. A) Average 30 gene expression count from mock transfected control and pVAX1. B) Average 30 gene expression count from mock transfection control and pVAX1 with early (5/30) and late (25/30) response genes separated with a lognormal gaussian distribution curve of best fit. C) A heatmap of B) plotted on a log10 scale, with early-responders shown at the top, late-responders in the middle and non-responders at the bottom. All data represents three biological replicates tested once.

Optimising RNA harvest time

Although time-course data can be informative, in order to develop an immune-profiling tool that was both comprehensive and cost effective, a singular screening time-point was required. Time-course data from Figure 3.7 was re-analysed to determine FC values for each of the 30 individual genes within the Nanostrings panel. By applying a 20% expression threshold, the number of upregulated (FC>1.2) and downregulated (FC<0.8) genes were quantified (Figure 3.8). These data showed almost all genes to be upregulated at 2, 4, 8 and 12hrs, any of which could therefore be an appropriate selection time for RNA screening. Given that no genes were downregulated at 8hrs, the decision to use this time-point was made, with the lowest noise and highest number of consistently upregulated genes. Depending on the genes of interest however, 2 and 4hrs were also informative time-points, although 2hrs limits detection of late response genes and 4hrs shows larger variability in count values and consistent downregulation of *cox2*.

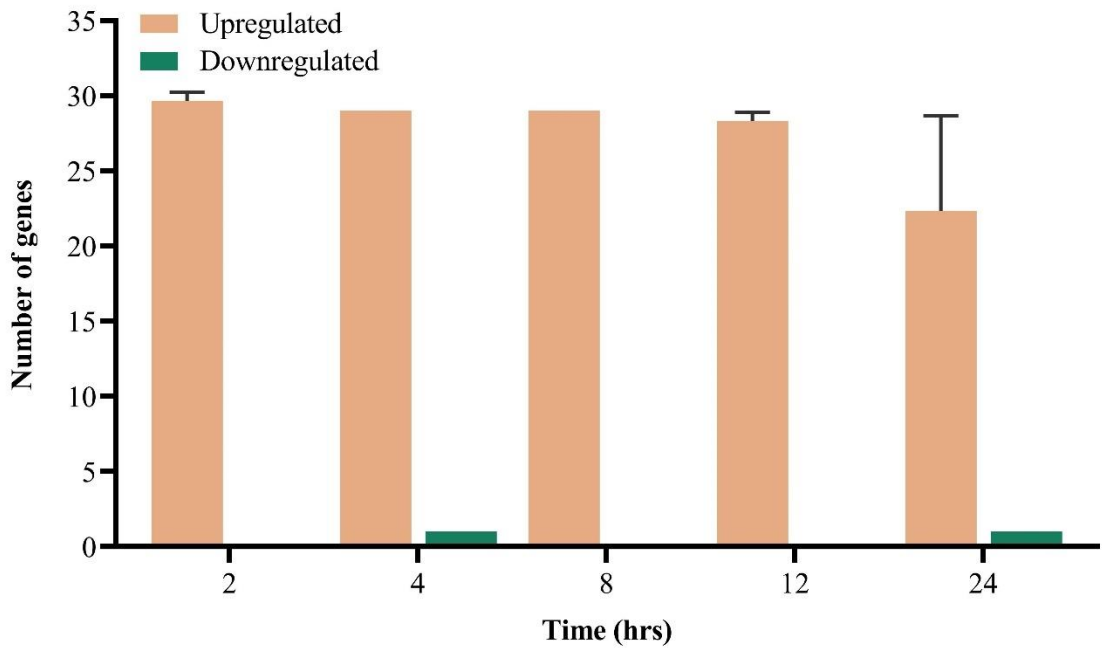

Figure 3.8) pVAX1 time-course identified multiple time-points as informative. 400ng pVAX1 or mock transfection controls (no DNA) were transfected into 400,000 DC2.4 cells and analysed at 8hrs using custom Nanostrings based immune-profiling tool. Fold change relative to no DNA with a 20% threshold was used to quantify the average number of upregulated and down-regulated genes at each time-point.

3.2.4 Investigating tool utility

Immunogenicity was quantified and compared across different vectors

A well-established relationship between plasmid CpG content and immune-activation has been described in section 1.2.1 (Bode et al., 2011; Schneeberger et al., 2004; Su et al., 2017; Yew et al., 2002; Yu et al., 2015). To develop an immune-profiling tool capable of quantifying and comparing vector immunogenicity, five synthetically engineered plasmids were designed and tested, with CG dinucleotide content ranging from 0–392 (Figure 3.9).

Two vectors with a backbone context similar to that of pVAX1 were designed and tested. These include pVAX1-Inert which had 251 CG dinucleotides but 600bp smaller than pVAX1, and pVAX1-CpG with 392 CG dinucleotides inserted upstream of the CMV promoter (Appendix, Supplementary Table 5). Two key metrics were quantified; i) average FC across all 30 genes relative to pVAX1 and ii) the number of upregulated and downregulated genes based on a 20% expression threshold (Figure 3.9A). As expected, pVAX1-Inert (251) had an average FC of ~1.01 with 3/ 30 upregulated and 1/ 30 downregulated genes, validating the sensitivity and reproducibility of the tool whilst quantifying system noise. pVAX1-CpG (392) was much more stimulatory with an average FC of ~1.3 and >15/30 upregulated genes.

Additionally, three AZ supplied vectors engineered with varying CG dinucleotide content were tested to validate tool application across different vector backbones. These included AZ CpG-H with 123 CG dinucleotides, AZ CpG-M with 42 and AZ CpG-0 with none. Immune-profiles relative to AZ CpG-H were used to quantify relative immunogenicity (Figure 3.9B). pVAX1-CpG (42) exhibited an average FC of 0.73 with 24/ 30 genes downregulated whilst pVAX1-CpG (0) had an average FC of 0.71 and 22/ 30 genes downregulated. These findings confirmed the Nanostrings based immune-profiling tool could quantify relative increases and decreases in immune-activation across different vector backbones correlating with plasmid CpG content.

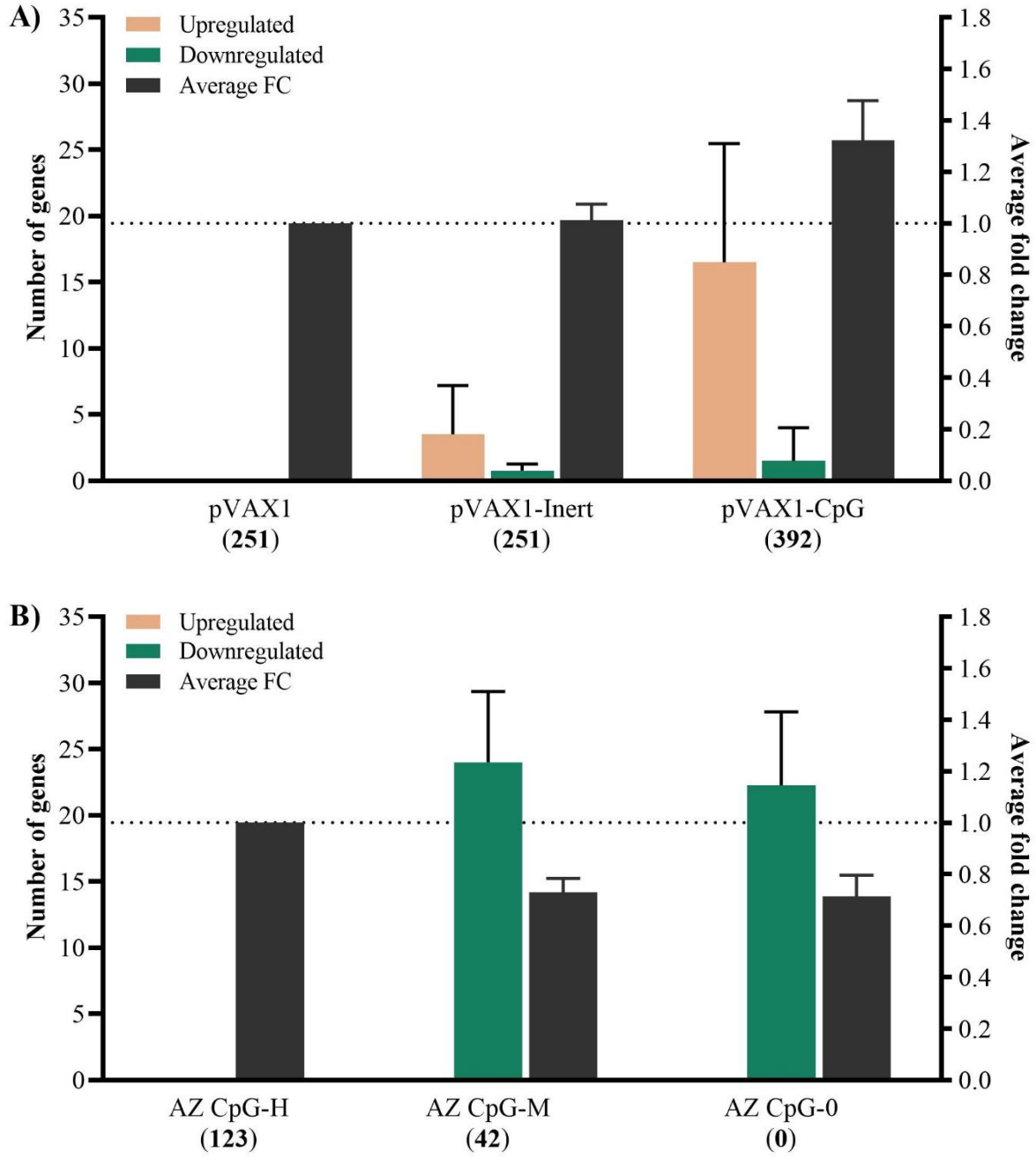

Figure 3.9) Investigating tool utility across different vectors. 400ng vector DNA was transfected into 400,000 DC2.4 cells and analysed at 8hrs using novel Nanostrings based immune-profiling tool. Overall average fold change of 30 immune-profiling genes relative to pVAX1 and the number of up/ downregulated genes (20% threshold) is shown for A) pVAX1 derived vector backbones and B) AZ derived vector backbones. The CpG content of each plasmid is denoted in brackets.

Nanostrings data aligns with traditional ELISA analysis

To ascertain whether Nanostrings immune profiling outputs aligned with standard methods of quantification, vectors were also quantified using TNFa ELISA analysis. Three key measurements were compared: i) average FC of all 30 Nanostrings immune-profiling genes at 8hrs, ii) average FC of the *tnfa* gene from Nanostrings immune-profiling at 8hrs and iii) average FC of TNFa protein production by ELISA at 24hrs (Figure 3.10). These data show larger effects in ELISA quantification compared to Nanostrings 30-gene averages for both stimulatory and suppressive plasmids. Vector pVAX1-CpG (392) for example had relative FCs of 1.3 and 2.3 for (i) and (iii) respectively, whilst AZ CpG-0 (0) had relative FCs of 0.72 and 0.57. When comparing FCs of only the TNFa gene however, these values aligned more closely with Nanostring averages for the pVAX1 derived vectors, except for ELISA TNFa FCs for AZ-CpG-M (42) and AZ-CpG-0 (0) vectors. Overall, despite some variability, Nanostring 30-gene average FCs and ELISA TNFa FCs follow similar trends, confirming this immune-profiling tool aligned with more commonly used methods. However, with the simultaneous analysis of 30x more genes and smaller standard deviations, the immune-profiling tool has the advantage of increased statistical power, precision, and reproducibility.

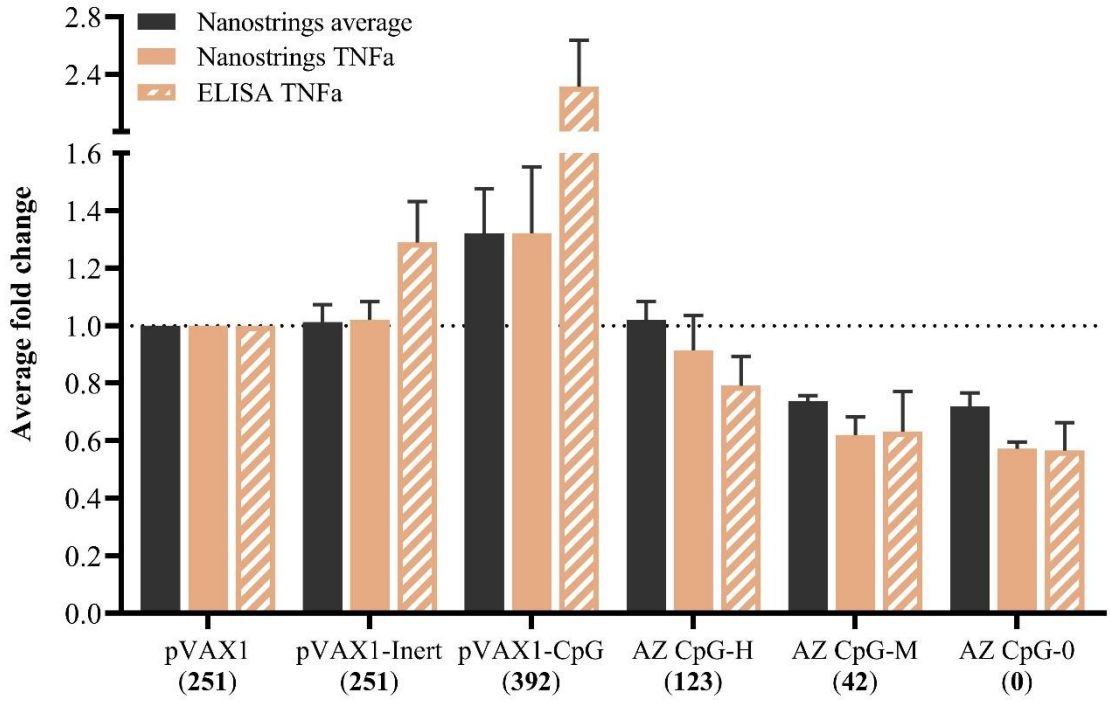

Figure 3.10) Comparing immune-profiling tool vector quantification with TNFa ELISA. 400ng vector DNA was transfected into 400,000 DC2.4 cells and analysed at 8hrs using Nanostrings based immune-profiling tool and TNFa ELISA at 24hrs. Fold change relative to pVAX1 is shown from Nanostrings immune-profiling tool are shown for A) all 30-genes (black) and B) TNFa gene only (orange) and C) TNFa ELISA (orange patterned). Bars represent mean +SD for three biological replicates in technical duplicate (immune-profiling tool) or four biological replicates in technical duplicate (ELISA).

3.2.5 Developing automated analysis app Nanopanel

To establish a versatile platform that is quick, easy-to-use and allows direct comparison of vector immunogenicity, automated analysis app Nanopanel was designed, facilitating the interpretation of nCounter RCC files to standardised outputs as illustrated in Figure 3.11. User-defined inputs required include: RCC run files, a csv describing samples as either treatment or controls and pre-selected house-keeping genes (although these can be predicted in-app) which are used to generate eight quality control visualisations using R package NACHO (Canouil et al., 2019).

a) Positive controls vs Negative controls: counts from six positive controls and eight negative controls were plotted on a log scale to display control count distribution.
b) Average counts vs Median counts: the relationship between average mean and median counts was quantified for each treatment sample to compare distribution.
c) Positive controls: count boxplots from positive control probes of known concentration (128, 32, 8, 2, 0.5 and 0.125 fM) were plotted to visualise the degree of linearity. A Pearson's correlation coefficient of >0.95 was expected with anything below flagged as a potential hybridisation issue.
d) Negative controls: probes unable to bind targets within biological samples were included as their counts approximate the general non-specific binding propensity of sequence probes (background noise).
e) Housekeeping genes: four house-keeping genes were included within the panel for normalisation, their average counts across input samples were visualised for quantification and comparison.

f) Housekeeping factor: compares the 'housekeeping factor' (calculated using the geometric mean of housekeeping counts across samples) to account for variation in gene expression levels across samples, with the 'positive factor' (calculated using the geometric mean of positive control probes) to adjust signal intensities across samples and determine background noise using negative control probes. Thresholds of 11-fold for positive-scaling factors and 4-fold for housekeeping normalised factors have been recommended by the manufacturer.

g) Binding density: this value represents the number of barcodes counted per square micron. For nCounter SPRINT systems a range of 0.1–1.8 was recommended to avoid data loss from overlapping barcodes.

h) Normalisation factor: raw counts from selected housekeeping genes across input samples are shown alongside their normalised value.

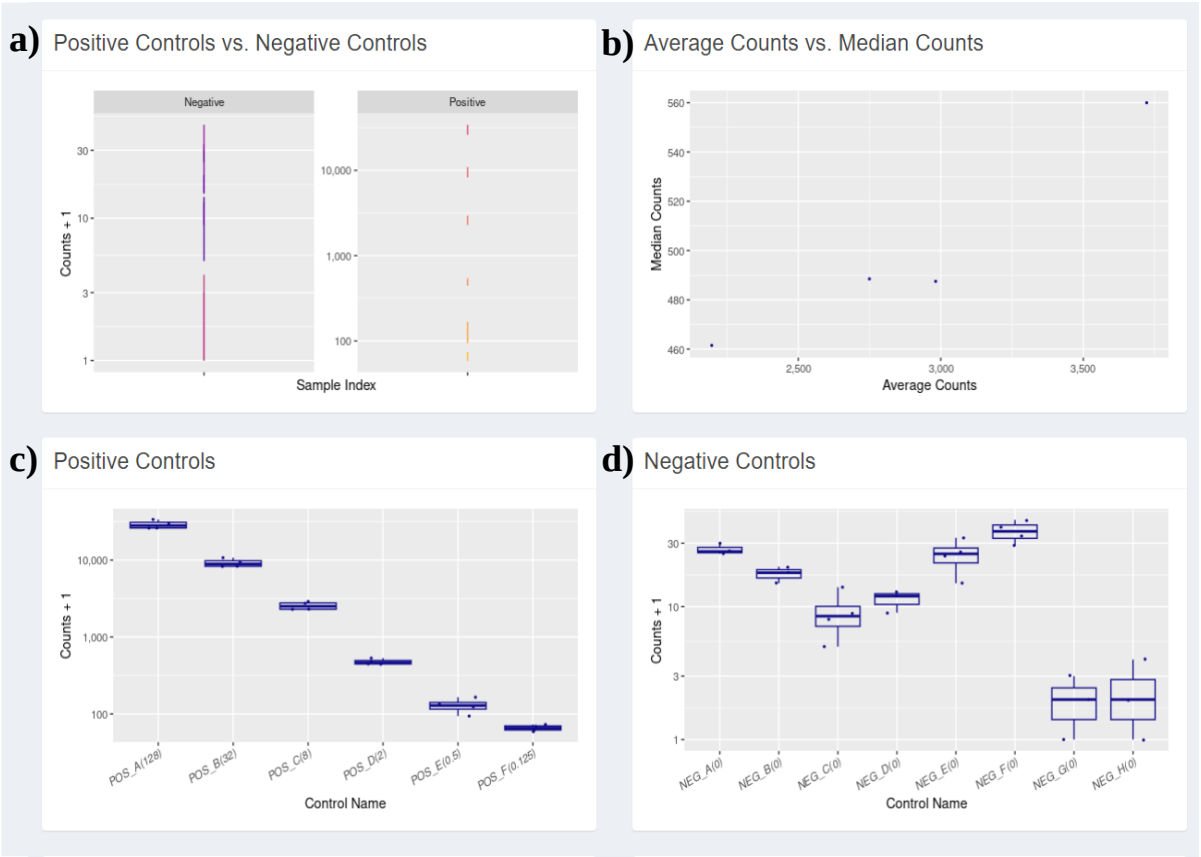

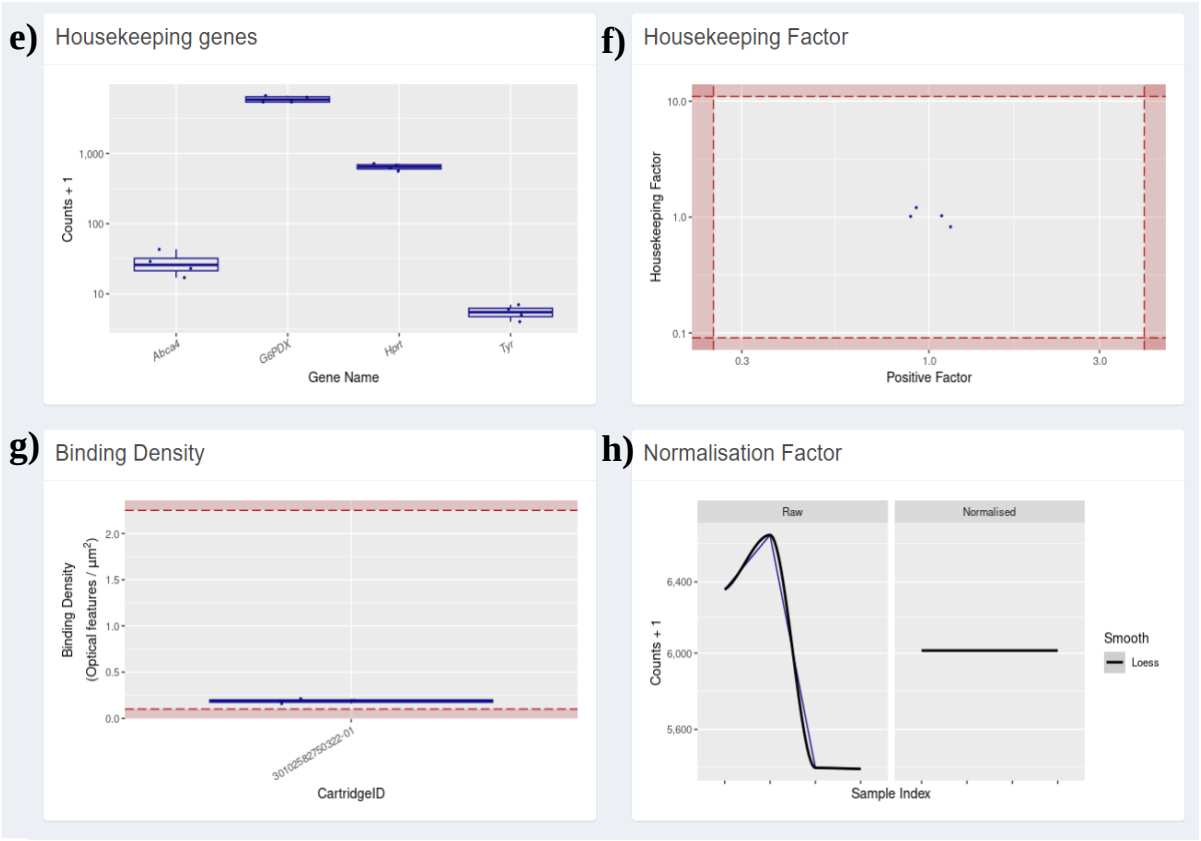

Figure 3.11) Nanopanel generates quality control visualisations. Example inputted RCC files are analysed as a group to show A) the distribution of positive and negative control counts across samples, B) the mean and median counts from each sample, C) boxplots of positive and D) negative control counts across samples, E) housekeeping gene counts across samples, F) housekeeping factor and positive control factors, G) barcode binding density per um2 and H) housekeeping gene count normalisation across samples.

Based on the analysis found to be useful within this chapter, input samples were processed to generate the following standardised outputs:

A) Average fold change (%): samples were compared against a user-defined control to determine the average fold change of all 34 differentially expression response genes with downregulation presented as a negative and percentage upregulation as a positive (Figure 3.12A).

B) Heatmap of normalised counts**:** a complete heatmap of gene expression counts within each sample across the 34 panel genes were shown with a user-defined percentage threshold between 1%-50% to highlight the upregulated (orange) and downregulated (green) genes (Figure 3.12B).

C) Number of up/downregulated genes**:** bar graph of B) (Figure 3.12C)

D) <u>Limma analysis:</u> Inputted RCC files can also be treated as a group to identify the top 10 differentially expressed genes, count difference, FCs, average count and associated t, b and p values (Ritchie et al., 2015). These metrics can be used to compare biological repeats/ identify trends across samples (Figure 3.12D)

These analyses included all 34-genes to facilitate future panel application across different murine models. In conclusion, Nanopanel integration downstream of the Nanostrings based immune-profiling pipeline automates RCC analysis providing a versatile tool for standardised quantification, characterisation, and comparison of vector DNA immunogenicity for application in vector design screens (Figure 3.12E).

A)

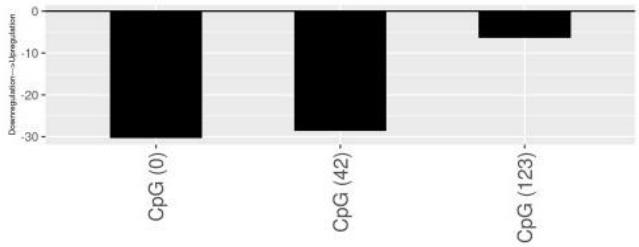

B)

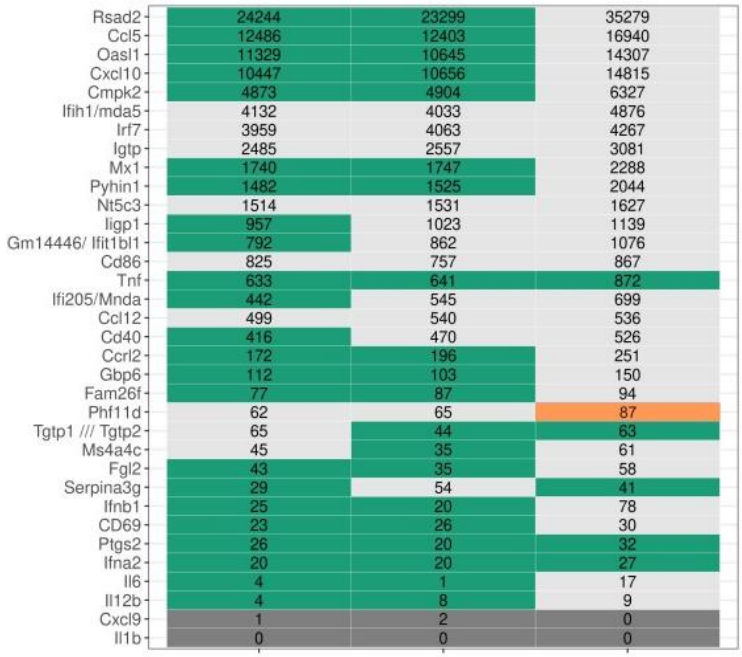

C)

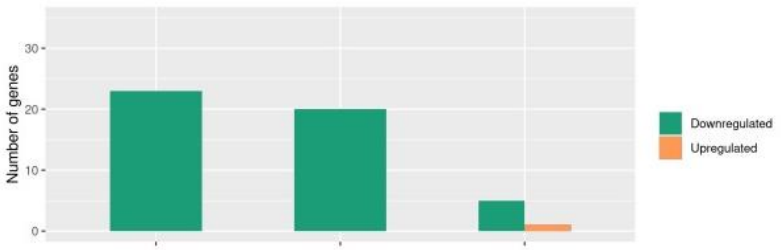

D) Differential expression in treatment samples vs control calculated by limma

Gene	Treatment - Control	AveExpr	t	P.Value	adj.P.Val	B	Control	Treatment	FC	logFC
Ptgs2	-33.00	34.25	-3.67	0.05	0.53	-4.60	59.00	26.00	0.44	-1.18
Tnf	-472.67	833.50	-3.33	0.06	0.53	-4.60	1188.00	715.33	0.60	-0.73
Fam26f	-27.00	92.75	-2.45	0.11	0.53	-4.60	113.00	86.00	0.76	-0.39
Ifna2	-15.67	26.25	-2.03	0.16	0.53	-4.60	38.00	22.33	0.59	-0.77
Cxcl10	-4951.33	13210.50	-1.93	0.17	0.53	-4.60	16924.00	11972.67	0.71	-0.50
Gbp6	-49.33	134.00	-1.84	0.18	0.53	-4.60	171.00	121.67	0.71	-0.49
Ccrl2	-75.67	225.25	-1.77	0.20	0.53	-4.60	282.00	206.33	0.73	-0.45
Iigp1	-163.33	1080.50	-1.69	0.21	0.53	-4.60	1203.00	1039.67	0.86	-0.21
Cmpk2	-1426.00	5724.50	-1.64	0.22	0.53	-4.60	6794.00	5368.00	0.79	-0.34
Mx1	-534.00	2058.50	-1.63	0.22	0.53	-4.60	2459.00	1925.00	0.78	-0.35

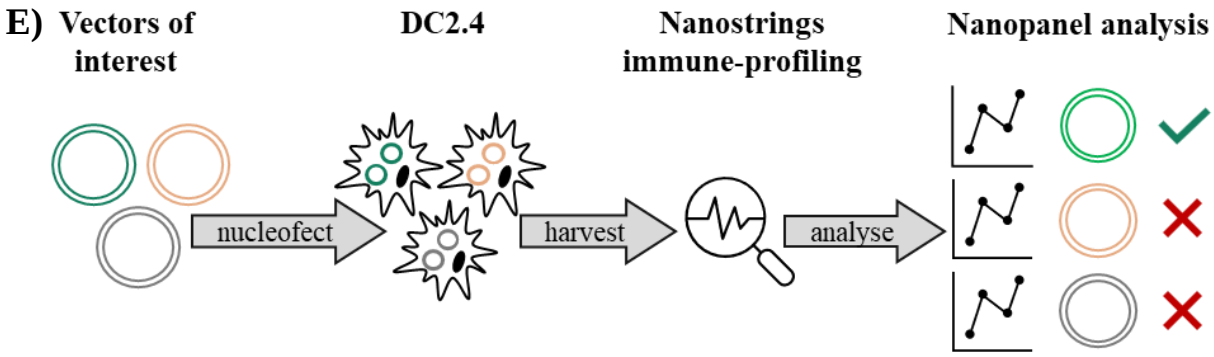

Figure 3.12) Nanopanel automated analysis of AZ CpG Vectors. 400ng vector DNA was transfected into 400,000 DC2.4 cells and analysed at 8hrs using immune-profiling tool Nanopanel. RCC files were inputted into automated analysis app Nanopanel and compared to pVAX1 to generate the following outputs. A) Average fold change of 34 immune-profiling genes. B) Heatmap of normalised expression count highlighting upregulated (orange) and downregulated (green) genes based on a user-defined threshold. C) Bar graph representing the number of up/ downregulated genes from B). D) Differential expression analysis of treatment samples compared to controls calculate by limma and E) A summary of Nanopanel incorporation into immune-profiling pipeline for application as a vector screening and selection tool.

3.3 Discussion

The work in this chapter describes development of a novel tool capable of characterising sequence-specific effects of pDNA vectors on key DNA-driven response pathways. This not only expands the technologies available for DNA therapeutic vector immunogenicity analysis, but also provides a platform capable of highly sensitive sequence-specific immune-characterisations, informing early-stage vector design choices for more immunogenic (vaccines) or immunosuppressive (gene therapy) plasmid backbones. Although pre-established immunology panels are available, they lack specificity with >500 genes assessed per screen (Nanostrings, Seattle, US), a disadvantage also inherent to RNA-sequencing/ microarray analyses. Other previously discussed drawbacks of traditional methods include a requirement for pre-selecting genes/ proteins of interest, resulting in a limited understanding of alternate and unexpected response pathways.

Use of a hypothesis and data-driven approach for the selection of key response genes allows for more relevant representation of the most essential pathways upregulated specifically by pDNA within immune cells. Integrating a bottom-up approach ensured critical response genes based on functionality were included from decades of studies whilst top-down unbiased OMICs selection incorporated the most highly upregulated FC and FE responders. For example, *cmpk2, fam26f* and *gbp6* were top-down exclusive responders with little to no literature understanding of their functionality or mechanism of action despite significant upregulation in dsDNA exclusive conditions. However, growing interest in their characterisation highlights the relevancy of these responders, for instance *ifit1c* was recently identified as equivalent to human IFIT3; a cofactor enabling IFIT1-mediated inhibition of viral RNA translation upregulated during IFN responses (Mears and Sweeney, 2020). Characterisation of the resulting 34 response genes confirmed all had immune associated functionalities with representation of different Th response pathways. Further gene ontology analysis of enriched biological pathways found innate, adaptive, and regulatory immune response pathways were upregulated by Cytoscape visualisation. This further supports the gene filtering approach used, enabling

coverage across multiple immune pathways and functions despite being restricted to only 34 genes. There were however, a number of limitation in this bioinformatics-based approach including; i) a lack of available OMICs studies particularly of pDNA conditions, ii) restrictions to lipofectamine based OMICs transfection which differs from the electroporation based method used and iii) the use of stringent screening rules limited to ~30-40 genes which likely excluded a large number of responders with smaller gene expression effects but critical roles in different arms of the immune response.

During tool development, the most appropriate method for quantification was carefully considered. Given growing popularity in the use of Nanostring technology, particularly within the field of immunology, this method was used to design a custom panel for simultaneous RNA quantification of the 34 representative response genes (Graves et al., 2023; Lee et al., 2023). OMICs-based studies performed microarray analyses at different time points, with dataset 1 screened at 4hrs and dataset 2 screened at 7hrs. An 8hr time-point was chosen given the consistent upregulation of all 30 responding immune-genes, despite increased expression between 2-6hrs. However, any time-point of interest could be examined during use of this tool and should be dictated by users' preferred genes of interest, e.g., early-responders (~2hrs), late-responders (~4hrs) or all genes (~8hrs). Median counts across the time-course were modelled using lognormal gaussian distribution curve fitting, however, this was exclusively to aid visualisation and cannot be used to predict the peak in average count for early/ late responders with confidence.

Tool utility was investigated by screening several different vectors designed to vary in their immunogenic 'power'. Currently, only the presence or absence of CG dinucleotides within a double-stranded pDNA backbone is known to affect the magnitude of immune-activation, therefore vectors with varying CpG content were tested in either a pVAX1 of AZ vector backbone context (Bode et al., 2011; Schneeberger et al., 2004; Su et al., 2017; Yew et al., 2002; Yu et al., 2015). Given the depth of data available from Nanostrings, two metrics were used to observe individual and overall gene effects i) average FC from all 34 genes and ii) the number

of up/ downregulated genes (based on a 20% threshold). As expected, the magnitude of quantified responses correlated with CpG vector content and TNA ELISA values, validating use of this tool to detect sequence-driven increases and decreases in immunogenicity and use of these metrics to quantitatively characterise immunogenicity effects from Nanostrings data. Interestingly, CpG content alone could not account for total observed immunogenicity with vectors pVAX1 (251) and AZ CpG-H (123), for example, displaying similar average FCs despite the presence of half as much CG dinucleotides. Therefore, non CpG motifs, secondary structures and vector composition likely also contribute to overall plasmid immunogenicity.

Although changes in gene expression do not always translate to protein production, the integral use of OMICs expression data and its relative affordability compared to multiplex protein quantification informed the decision to characterise gene (rather than protein) changes (Li and Xie, 2011; Olkhov-Mitsel et al., 2022). Data presented within this chapter shows a close correlation between *tnfa* RNA and protein expression, however use of Nanostrings technology offers a number of advantages over traditional ELISA methods as summarised in Table 3.4. 1) Ease of multiplexing enables detection of multiple genes, providing increased confidence in quantified immune response values compared to standard ELISA detection of only singular proteins (Leng et al., 2008). 2) Simultaneous detection of multiple outputs allows for more detailed characterisation and comparison of different response pathways, for example the upregulation of DNA sensors cGAS-STING and TLR9 can be compared through *ifnb1* and *tnfa* respectively, whilst Th biased effects can be identified through *il6* (Th2) and *tnfa* (Th1) (Iwamoto et al., 2007; Motwani et al., 2019; Xu et al., 2022). This kind of comparison is much more difficult to recapitulate using ELISA technology given the complexity of optimising multiple protein dynamic ranges within a single sample (Tighe et al., 2015). 3) Highly variable expression counts from genes can be accurately measured across five orders of magnitude, unlike the limited dynamic range of traditional ELISAs, reducing errors from dilutions and laborious optimisations (Tighe et al., 2015). 4) The effects of small, sequence-dependent changes can be delineated from highly-precise absolute quantification methods

unlike ELISAs which have high levels of sample variation (accepted error of up to <20%) (Leng et al., 2008) (Thermo Fisher, Oxford, UK). 5) Precise and reproducible count values remove the requirement for technical repeats whereas ELISAs require both experimental and plate replicates, resulting in higher costs and increased labour for sample processing (Leng et al., 2008).

Table 3.4) advantages of Nanostring technology compared to traditional ELISAs

Key Advantages	Nanostrings	ELISA	Reference
Confidence in quantified responses	Ease of multiplexing enables simultaneous quantification of 34 genes	Standard detection of singular proteins due to differing dynamic ranges	(Leng et al., 2008)
Characterisation/ comparison of different response pathways	Compares multiple genes from one sample, enabling comparison of receptor/ Th/ other responses	Difficult to optimise multiple dynamic ranges for single sample testing	(Iwamoto et al., 2007) (Motwani et al 2019) (Xu et al., 2022)
Accurate measure of outputs across large concentration range	Highly accurate absolute quantification across 5+ orders of magnitude	Errors from large dilutions and laborious optimisation requires time and resources	(Tighe et al., 2015)
Delineation of small sequence changes	Highly precise and sensitive detection of small sequence-specific changes	Accepted variation of <20% limits confidence in small expression changes	(Leng et al., 2008) (Thermo Fisher, Oxford, UK)
Experimental labour	Precise and reproducible counts do not require technical replicates	Requires standard curve for each analysis, experimental and technical replicates	(Leng et al., 2008)

Given the large number of data points generated from Nanostrings analysis per sample, a bottleneck in the time and training required to process results was identified. Given the aim was to design a tool that was both quick and easy-to-use, a platform to automate normalisation and standardise quantification directly from nCounter generated RCC files was developed. The app was successfully validated providing a screening method for the characterisation and comparison of vector immunogenicity. This can now be used to inform design decisions, quantifying the effects for small sequence-dependent changes on DNA-driven immunogenicity, facilitating selection of more immunosuppressive vectors for gene therapy application. In conclusion, this chapter describes the development, validation, and utility of a novel tool capable of quantitatively characterising pDNA immunogenicity, with an easy-to-use automated analysis platform.

Chapter 4 : Identification of Immunosuppressive DNA Motifs for Modulating Plasmid DNA Driven Responses in Dendritic Cells

This chapter described the first-ever large-scale screen of immunosuppressive DNA motifs within a pDNA integrated system, quantitatively characterising the immune-modulatory 'power' of each sequence. Individual motifs were tested using gene immune-profiling tool Nanopanel, screening homotypic and heterotypic library 1 designs to quantify the effects of individual sequences, and motif groups. Design rules based on sequence, combination, copy number and architectural arrangement were established. MLR modelling defined individual motif effects, identifying six as significantly suppressive, informing the design of heterotypic library 2 constructs. Differential effects were not detected on the protein level, nevertheless, this study characterises the first-ever toolbox of double-stranded suppressive motifs to inform future vector design strategies.

4.1 Introduction

As outlined in section 1.1, immune responses to therapeutic plasmids significantly limit therapeutic efficacy and safety. DNA vaccines for example are currently limited by insufficient activation of immunity (Suschak et al., 2017) whilst gene therapy immune-stimulation remains a major hindrance in affordability and patient welfare (Sack and Herzog, 2009). The use of engineered DNA motifs however offers a potential solution, with a well-characterised ability to upregulate immune responses to DNA vaccines using stimulatory sequences in ODN or double-stranded plasmid integrated form, significantly improving therapeutic activity (Krieg et al., 1995; Schneeberger et al., 2004). Similar approaches for down-regulating DNA-driven gene therapy responses could also improve patient safety and drug efficacy, downregulating unwanted and potentially fatal immune responses (Sibbald, 2001). Despite reports of suppressive ODNs within the literature, none have been tested in ODN or dsDNA form alongside therapeutic vectors. Given stimulatory CpG-ODN sequence-specific activity was found to translate into pDNA integrated systems (Schneeberger et al., 2004), it seems possible suppressive ODNs could do the same. This hypothesis is further supported by recently published data from Chan and colleagues, detecting immune-suppressive effects from an integrated ssODN motif, derived from thee well-established suppressive ODN sequence; A151 (Chan et al., 2021).

This chapter describes the first even screen of suppressive motifs within a dsDNA context using novel immune-profiling tool (now referred to as 'Nanopanel') to not only quantitatively characterise sequence effects on different response pathways, but to also detect small, sequence-driven changes sensitively. Given the novelty of this screen, two key challenges were identified. 1) Managing numerous testing variables, such as selecting motifs for initial screening from an ODN pool of almost 100, evaluating copy number effects, optimising pDNA: motif ratio, investigating motif architectural impacts (arrangement) within pDNA and assessing optimal sequence combinations. 2) Containing the cost of Nanostrings based immune profiling given the large number of testing variables and their associated expenses. To overcome

these limitations, an initial library of homotypic elements was analysed to screen only the most promising sequences (~20), enabling interrogation of sequence and pDNA: motif ratio effects. Simultaneously, a heterotypic library was designed to examine the effects of motif copy number, architecture, and optimal combinations. These designs were then tested only once, providing motif replicates (across constructs) but not element replicates. These effects were subsequently delineated using MLR modelling, quantifying individual motif power, and identifying statistically significant suppressive sequences. This method is limited in the number of biological replicates but was determined as the most appropriate approach for initial, comprehensive screening of potential immune-suppressive motifs (Brown et al., 2014).

The work in this chapter therefore aims to:

1. Identify a representative panel of ssODN motifs for initial screening in dsDNA form.
2. Design and construct a library of homotypic and heterotypic motif elements for quantitative characterisation using immune-profiling tool Nanopanel.
3. Identify design rules for optimal sequence, group, architectural, and combination effects.
4. Use of data modelling to quantify the immune-modulatory 'power' of individual motifs and identify those with statistically significant suppressive effects.
5. Design and screen an improved second library of heterotypic elements based on established design rules.
6. Quantify protein effects (TNFa ELISA) of the most promising constructs.

4.2 Results

4.2.1 Designing and characterising homotypic library 1 elements

Mapping the design space of immune-suppressive DNA motifs

In order to investigate the suppressive capacity of DNA motifs within a novel plasmid integrated context, a comprehensive database of all literature reported immune-suppressive DNA sequences was compiled. In total, 88 suppressive motifs were identified, all of which were ssODNs with various backbone modifications assigned to one of six groups, as described in section 1.2.2 (Appendix, Supplementary Table 1) Significant overlap was observed across these categories therefore sequences were consolidated and refined to i) include motifs with the highest reported capacity for suppression, ii) include one representative motif from sub-groups of similar sequences and iii) exclude motifs composed of complex/ varying backbone modifications.

The resulting library was formed of three representative groups (referred to as 'Types') described in Table 4.1. These include Type1 G-rich sequences, with an increased capacity for G-tetrad/ G-quadruplex secondary structure formation. For example, M1 (known in the literature as A151) was a therapeutic ODN found to be functionally dependent on G-tetrad formation, previously used to treat inflammatory and auto-immune diseases in mouse models. (Gursel et al., 2003). This group was the most well characterised and literature supported. Type2 dinucleotides include CpG mimicking ODN structures with key base pair modifications in flanking regions or within the CG dinucleotide itself (e.g., conversion to GpG or GpC) enabling suppression. For example, M14 (known as CpG-c41) behaves as a TLR9 antagonist but also inhibits intracellular TLR7/ 8 and inflammasome formation (Li et al., 2011; Liu et al., 2017). And finally, Type3 microsatellite sequences which have been reported with highly suppressive potential but limited literature-based characterisation. For example, M17 (known as MS08) down-regulates TLR9 activity but shows inconsistent effects during *in vitro/ in vivo* use (Fang et al., 2011; Hu et al., 2009; Sun et al., 2010).

Table 4.1) Refined library of immune-suppressive motifs. Sequences are grouped based on assigned Type and number, with PS backbone sequence and total nucleotide (nt) length shown. Motifs that could not be synthesised into homotypic vectors are highlighted (grey).

	Library of suppressive motifs			
	Motif number	**Motif name**	**Sequence**	**Motif length (nt)**
Type1 (G-rich)	M1	A151	TTAGGGTTAGGGTTAGGGTTAGGG	24
	M2	H154	CCTCAAGCTTGAGGGG	16
	M3	G-tetrad 1	GGGTGGGTGGGTATTACCATTA	22
	M4	iSG3	CCTCATTAGGGTGAGGG	17
	M5	G' ODN	CTCCTATTGGGGGTTTCCTAT	21
	M6	PolyG	GGGGGGGGGGGGGGGGGGGG	20
	M7	IRS 954	TGCTCCTGGAGGGGTTGT	18
	M8	INH-ODN 18	CCTGGATGGGAACTTACCGCTGCA	24
Type2 (Dinucleotides)	M9	GpC 1502	GAGCAAGCTGGACCTTCCAT	20
	M10	GpC 1826b	TCCATGAGCTTCCTAAGCTT	20
	M11	GpC 2006	TGCTGCTTTTGTGCTTTTGTGCTT	24
	M12	GpG 1019	TGACTGTGAAGGTTAGAGATGA	22
	M13	ODN 1953	TCCATGTCGTTCCGCCCGCG	20
	M14	CpG-c41	TGGCGCGCACCCACGGCCTG	20
Type3 (Microsatellites)	M15	SAT05f	CCTCCTCCTCCTCCTCCTCCTCCT	24
	M16	MS19	AAAGAAAGAAAGAAAGAAAGAAAG	24
	M17	MS08	TCTCTCTCTCTCTCTCTCTCTCTC	24
	M18	MS03	ACACACACACACACACACACACAC	24
	M19	MS28	TTTTGTTTTGTTTTGTTTTGTTTTG	25
	M20	MS13	AGGAGGAGGAGGAGGAGGAGGAGG	24

Constructing homotypic vectors

To test these non-coding motifs within a vector backbone, a synthetic homotypic library was designed. Based on similar immune-stimulatory studies, each homotypic vector was composed of a non-coding 600bp suppressive 'element' integrated upstream of the cmv promoter within pVAX1 to ensure essential secondary structures could form. This phenomenon is enabled by the transcription bubble dependent negative supercoiling of upstream DNA, resulting in separation of double-stranded DNA allowing single-stranded structures to form (Duquette et al., 2004; Yu et al., 2015). Each element contained 10 copies of the same motif, separated by a 10bp 'neutral' spacer in the form of a random CpG-free sequence selected from the pVAX1 GFP reporter as illustrated in Figure 4.1. Spacers were included to i) facilitate synthesis of highly repetitive DNA elements, ii) enable motif secondary structure

formation without interference from neighbouring motifs and iii) ensure individual motif units could interact with receptors/ signalling proteins without causing steric hinderance (Yamada et al., 2002). Despite this, M6 and M18 were too repetitive to be synthesised, therefore a total of 18/ 20 homotypic vectors were successfully synthesised and tested (Appendix, Supplementary Table 6).

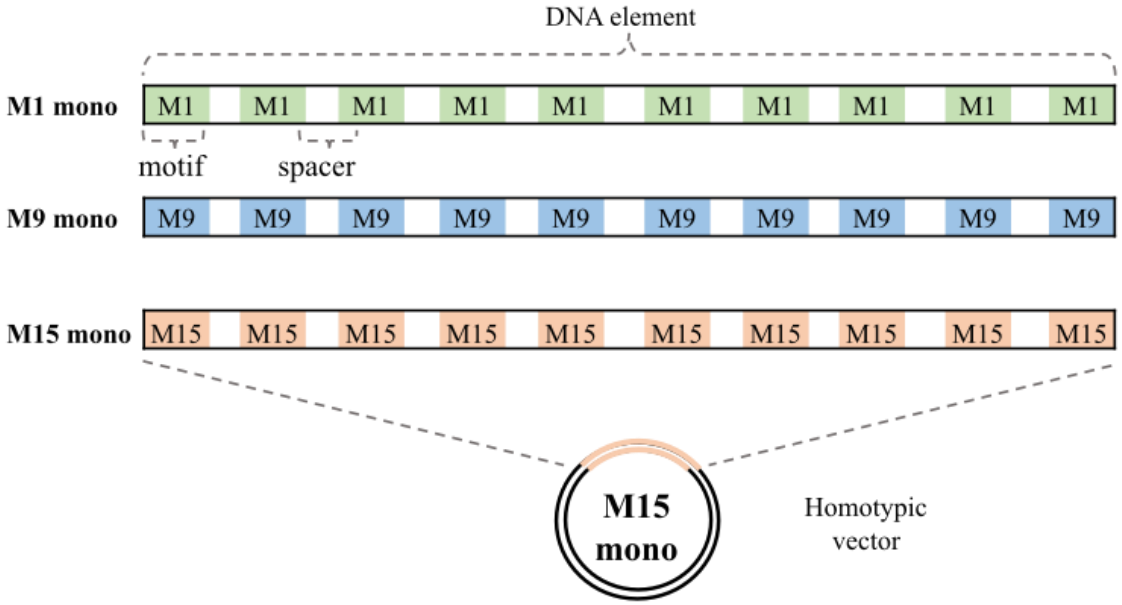

Figure 4.1) Constructing library 1 homotypic vectors. Examples of type1 (green), type2 (blue) and type3 (orange) 600bp DNA elements containing 10 identical copies of each double-stranded DNA motif. Integration of M15 mono upstream of pVAX1 represents 1/ 18 synthesised homotypic DNA vectors.

Homotypic Type3 motifs were most suppressive, followed by Type2 and Type1

Nanostrings-based immune-profiling tool 'Nanopanel' described in chapter 3 was used to quantify the immune-modulatory effects of homotypic library 1 via simultaneous quantification of 30 immune-associated genes responsive to pDNA. To observe the sequence-specific effects of these engineered elements, a scrambled control was designed to account for the generic impact of vector DNA. This was composed of a 600bp 'neutral' element containing random CpG-free sequences selected from the GFP reporter, referred to as pVAX1 for simplicity. 400ng of each vector was transfected into DC2.4 cells for 8hrs before harvesting RNA. Samples were then analysed to quantify mRNA expression of the 30 different immune-genes relative to pVAX1 control. Average FC across the panel was quantified for seven

Type1 vectors, six Type2, five Type3, a 'neutral' control (pVAX1-Inert), a 'positive control' (600bp CpG-rich immune-stimulatory element) and shown in Figure 4.2A with SEM plotted to highlight mean differences. Both the neutral (FC ~1) and positive control (FC ~1.4) behave as expected, confirming this tool could reliably detect sequence-specific immune-effects of double-stranded DNA. The majority of Type1 vectors were relatively neutral except M1 and M3 which were statistically significantly suppressive when compared to the neutral control. Unexpectedly however, M1 (A151) exhibited minimal suppression despite comprehensive support of this G-rich motif in both ssODN and ssDNA form (Chan et al., 2021; Gursel et al., 2003). As a whole, Type2 dinucleotides were more suppressive that type1's, with 5/ 6 motifs found to be statistically significantly. M12, M13 and M14 exhibited the largest relative suppression of ~10% (FC 0.9). Surprisingly however, it was the Type3 microsatellites that were the most suppressive group, with all motifs exhibiting significant suppression with ~15% (FC 0.85) reduction from M16 and M19.

From this same data, two of the most suppressive motifs from each Type were presented in more detail using two key outputs; i) the average number of genes that were up or down regulated relative to pVAX1 (a threshold of 10% was used to enable observation of small, sequence-specific changes) and ii) average percentage reduction of all 30 genes relative to pVAX1 (as described in chapter 3) (Figure 4.2B). Despite the lack of biological replicates, quantification of 30 different genes increases confidence in this analysis, for example, M1 and M3 show low levels of downregulation, with <10 genes downregulated by more than 10% and average reductions of <5%. Type2 dinucleotides however downregulate ~20/30 genes, revealing M13's slightly more suppressive effects compared to M14. Furthermore, form the Type3 microsatellites, M16 and M19 show almost identical levels of average suppression, however the number of suppressed genes vary, with 27/30 and 24/30 respectively.

These data confirm quantification using immune-profiling tool Nanostrings allows small changes in suppressive activity to be delineated with detailed characterisation using the two key analyses described above.

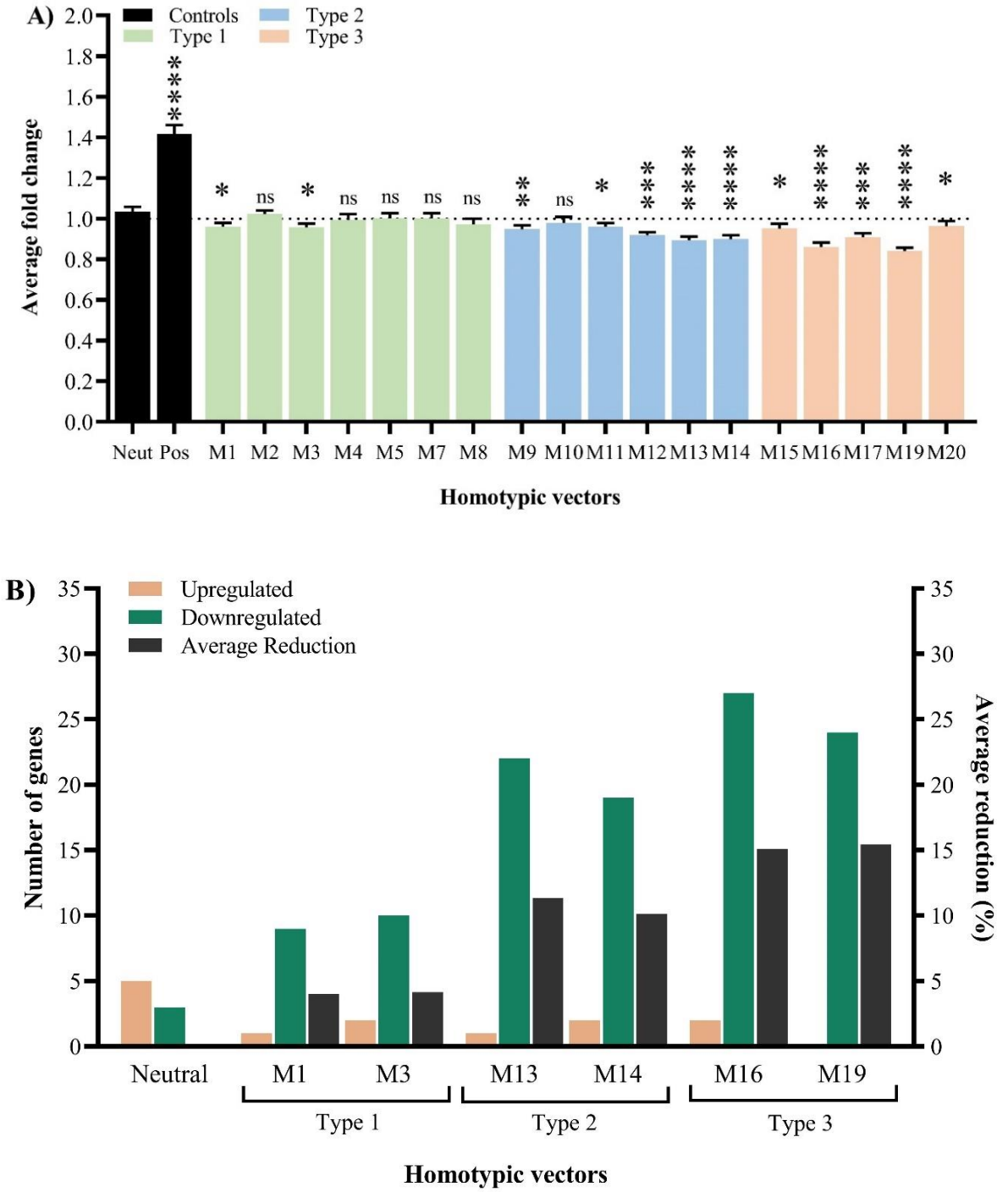

Figure 4.2) Immune-suppressive effects of library 1 homotypic vectors. 400ng of neutral (Neut), positive control (Pos) and 18 homotypic vectors were nucleofected into 400,000 DC2.4 and screened at 8hrs using immune-profiling tool Nanopanel. A) Average FC of all 30 genes relative to pVAX1 control. B) Average number of up/ down-regulated genes (10% threshold) and average reduction (%) relative to pVAX1 for the two most suppressive vectors from each type. Samples were compared to the 'neutral control' to account for error with statistical significance defined as p≤0.05 (* = p≤0.05, **=p≤0.01, ***=p≤0.001, ****=p≤0.0001) and non-significance denoted 'ns'. Bars represent the mean FC +SEM of 30 immune genes relative to pVAX1 across one biological replicate.

The number of samples that could be characterised using Nanostrings immune profiling was limited by cost, especially given the large number of vectors designed within this library. A compromise was therefore made to test as many vectors as possible using only one biological replicate by grouping Types together, enabling broader conclusion about the relative effects of each group to be made. Type1, Type2 and Type3 homotypic elements were grouped, with new averages calculated for the number of up/ downregulated genes and average reduction of each Type, displaying sample deviation as shown in Figure 4.3. As a group, Type3 motifs were found to downregulate most genes (~17/30) with an average reduction in immune response of ~10%, followed by Type2 motifs (~6%) and Type1 which were broadly neutral. Overall, these data suggest the integration of double-stranded motifs into homotypic vectors had small immunomodulatory effects detectable on the gene level. Furthermore, from an initial testing pool of 18 elements, modest but significant suppressive effects show promise for further suppression.

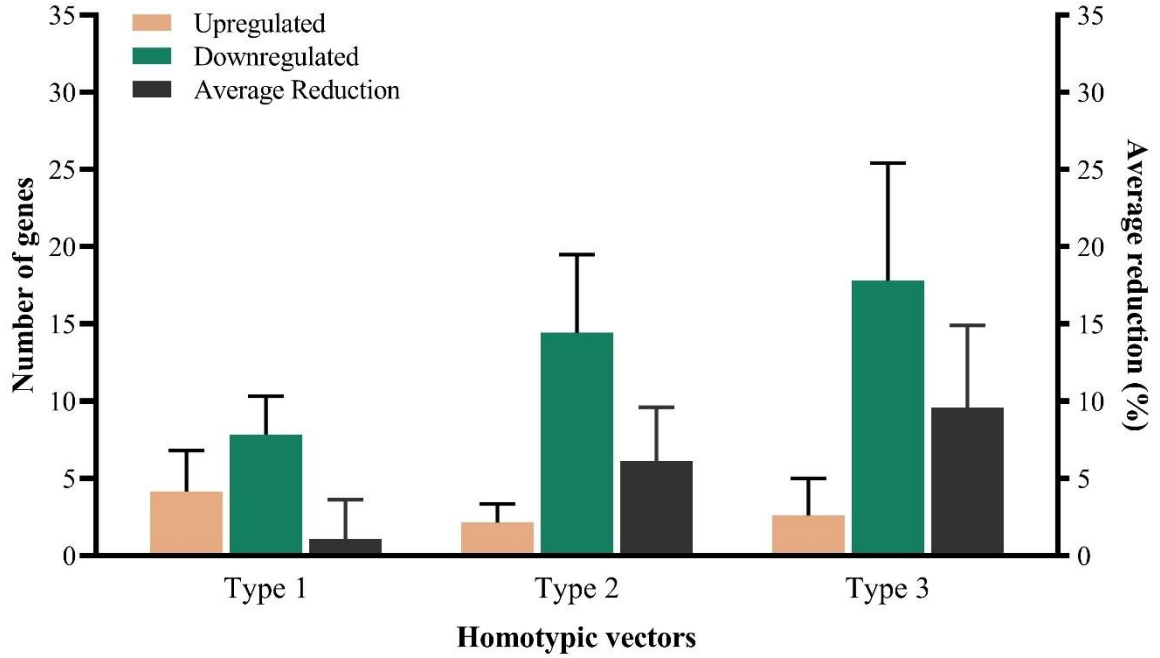

Figure 4.3) Homotypic vectors composed of Type3 motifs were more suppressive than Type2 and Type1. 18 vectors were tested using immune-profiling tool Nanopanel and grouped based on Type to determine the average number of up/ down-regulated genes (10% threshold) and average reduction (%) relative to pVAX1. Bars represent mean +SD where Type1 n=7, Type2 n=6 and Type3 n=5.

4.2.2 Designing and characterising heterotypic library 1 elements

Constructing heterotypic vectors

To investigate whether combining different motifs within the same system generated additive or synergistic suppressive effects, a synthetic heterotypic library was designed with varying motif combinations and architectural arrangements. The advantage of screening motifs within a double-stranded integrated system compared to a pDNA and ODN separated system lies in; i) understanding heterotypic motif dynamics within a novel vector backbone context and ii) screening large numbers of motif combinations and copy number variants without optimising the ODN combination formulas and transfection methods. 21 heterotypic elements were designed, 18 of which were successfully synthesised and tested (Appendix, Supplementary Table 6). As with the homotypic library, these constructs were ~600bp (593bp – 614bp) but with spacers of 1-10bp in length, depending on the level of motif repetition and overall element size, integrated 5' of pVAX1 cmv promoter.

Mono-type elements were designed to quantify and compare the suppressive strength of each Type and determine whether grouping vs dispersing motif copies, within elements, was more advantageous. These elements constituted three copies of each motif from a singular Type in architectural arrangements where copies were mixed throughout the element 'motif-mix' or grouped together 'motif-grp', generating 6 elements in total (three motif-mix architecture, one for each Type, three motif-grp architectures, one for each Type) as show in Figure 4.4 (Appendix, Supplementary Table 6). Duo-types elements were designed to; i) determine whether combining motifs from different Types had advantageous effects, ii) identify which combinations, if any, were most effective and iii) compare whether grouping vs dispersing Types within elements was more advantageous. These elements were composed of all motifs from two different Types, each present in two copies. Architectural variations involve mixing motifs from each Type 'types-mix' or grouping them 'types-grp', whilst also mixing duplicate motifs 'motif-mix' or grouping them 'motif-grp', generating 12 different elements (three duo-type combinations each in four architectures) (Figure 4.4) And finally, trio-type elements

were designed to; i) investigate whether a single copy of each motif was sufficient to exhibit suppression, ii) observe potential synergistic/ additive effects in combining motifs from all three Types and iii) determine whether the distribution of motifs effects suppression. These elements contained a single copy of each motif from the three different Types within an architecture of Types 'alternating', 'grouped' or with a 'random' distribution, generating one element per architecture (Figure 4.4).

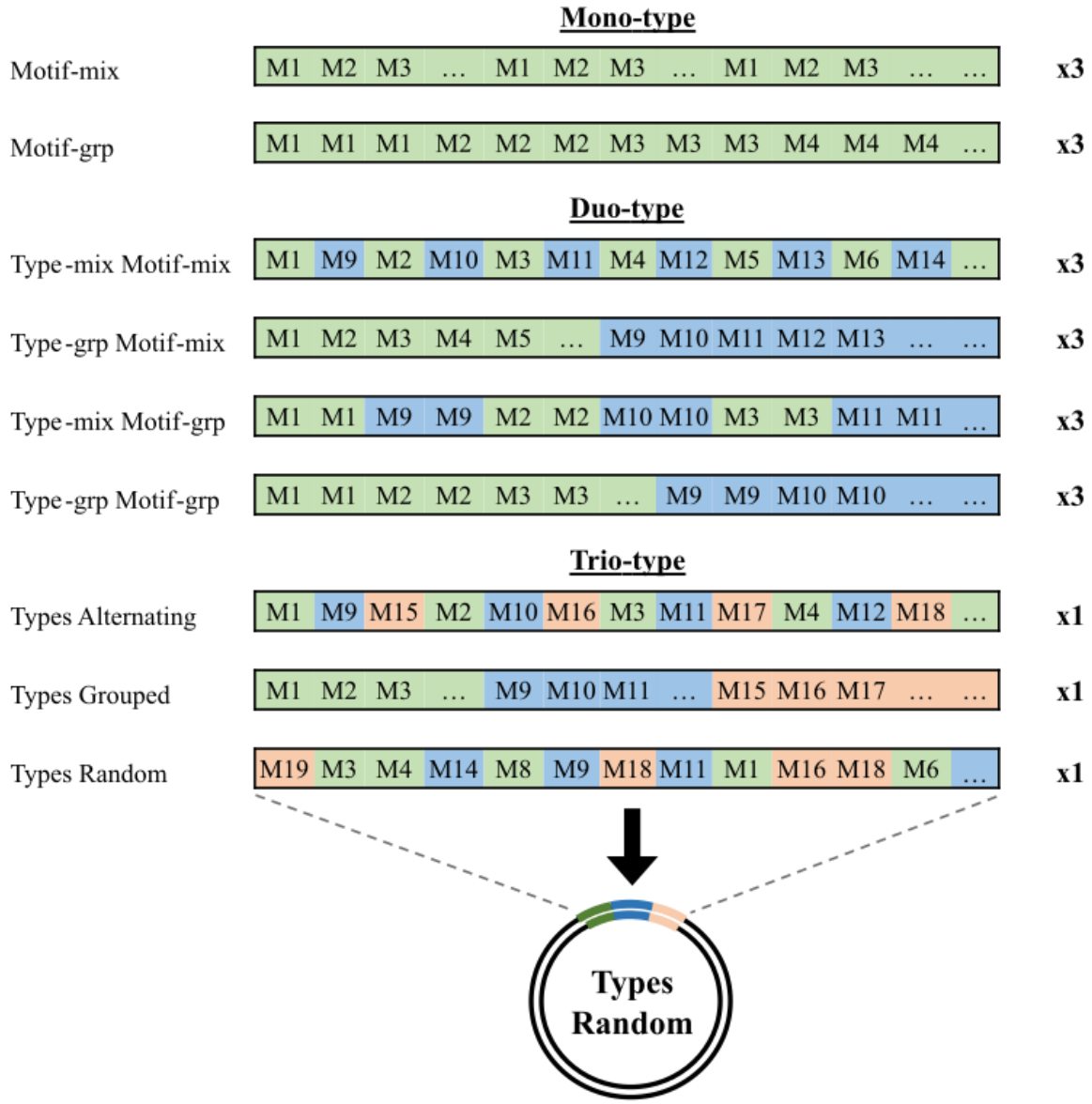

Figure 4.4) Constructing library 1 heterotypic vectors. 600bp DNA elements composed of suppressive motifs and spacer sequences were designed, synthesised, and cloned upstream of the pVAX1 CMV promoter. One example of each construct is shown for the three design groups: Type1 Mono-types (A), Type1+2 Duo-types (B) and Type1+2+3 Trio-types (C).

Mono-Type3 motifs were most suppressive, followed by Type2 and Type1

Five heterotypic mono-type vectors were screened using Nanopanel. Those composed exclusively of Type3 motifs were most suppressive (~14%) followed by type2 (~10%) and finally type1 (~7%). Only one element could be synthesised for Type1, limiting confidence in its observations (Figure 4.5) however these data do align with findings from the previous homotypic screen (Figure 4.3) but with a further ~5% reduction for each Type. As these elements contained 18 or 24 (rather than 10) motifs, we cannot discern whether the increased suppression was a result of motif variation or copy number. Nevertheless, given difficulties with synthesising highly repetitive homotypic DNA, heterotypic elements facilitate synthesis and increase the number of suppressive motifs available by decreasing spacer usage. This confirms heterotypic mono-types were more suppressive and easier to design compared to homotypic elements. No clear trend was observed between motifs mixed or grouped, suggesting motif sequence not distribution was driving suppression (data not shown).

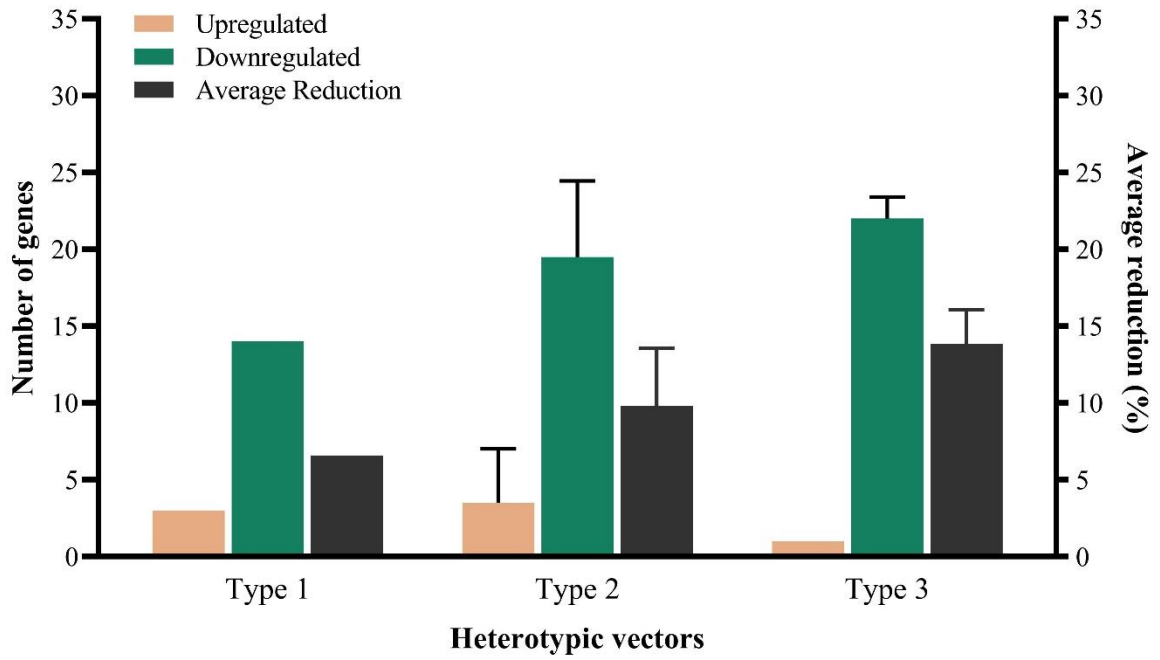

Figure 4.5) Heterotypic mono-type vectors composed of Type3 motifs were more suppressive than Type2 and Type1. Five vectors were tested using immune-profiling tool Nanopanel and grouped based on Type to determine the number of up/ downregulated genes (10% threshold) and average reduction (%) relative to pVAX1 control. Bars represents the mean +SD where Type1 n=1, Type2 n=2 and Type3 n=2.

Duo-types-grouped with motifs-mixed was an unfavourable element architecture

Of the 12 duo-type elements designed, 10 were successfully synthesised and tested using Nanopanel. These elements were grouped based on their four architectural designs to determine which, if any, were most effective (Figure 4.6). The two most suppressive architectures included elements with types-mixed and duplicate motifs-mixed or types-grouped and duplicate motifs-grouped, with an average reduction ~15% and 25/30 genes downregulated by >10% relative to pVAX1. This was interesting given their opposing designs. Elements with types-mixed and motifs-grouped were slightly less suppressive, with more variation in average reduction but a mean equal to that of the most effective designs. Elements with types-grouped and motif-mixed however were much less effective, with an 8% average reduction and 14/30 downregulated genes.

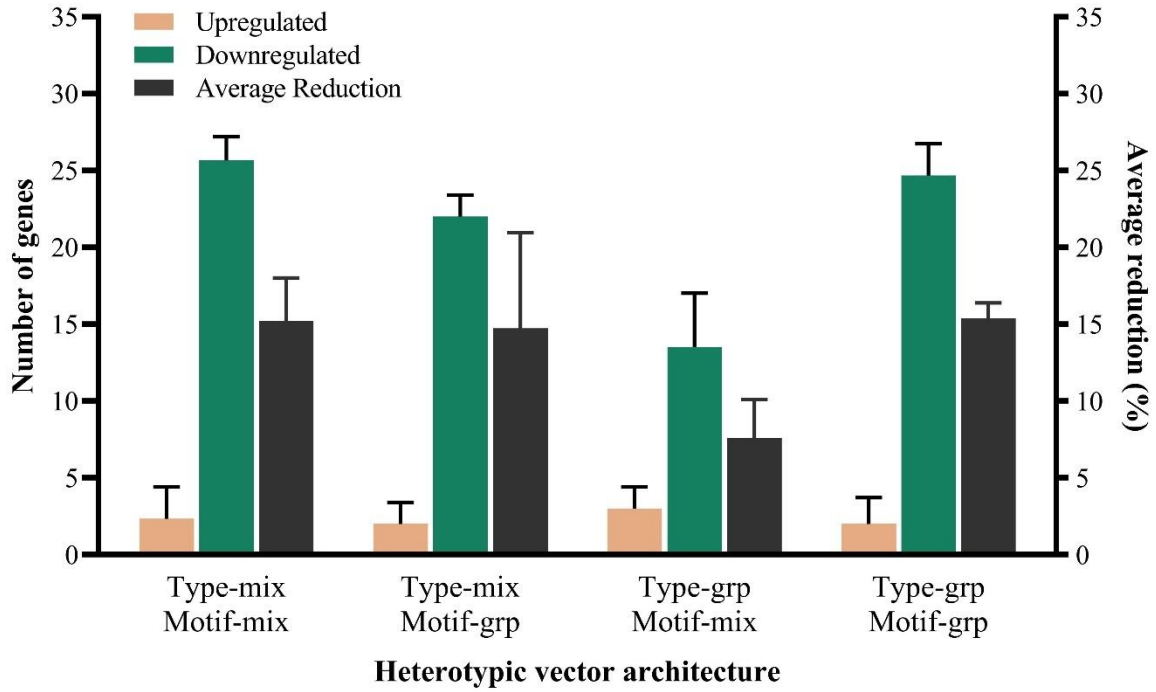

Figure 4.6) Duo-type heterotypic motif architecture affected suppression. Ten vectors were tested using immune-profiling tool Nanopanel and grouped based on architectural design to determine the number of up/ downregulated genes (10% threshold) and average reduction (%) relative to pVAX1 control. Bars represent mean +SD where Type-mix Motif-mix n=3, Type-mix Motif-grp n=2, Type=grp Motif-mix n=2 and Type-grp Motif-grp n=3.

Duo-type elements were 'stronger' than Mono-types, with Type3 combinations most suppressive followed by Type2 and Type1

The same duo-type vectors were grouped based on motif composition to observe sequence effects and enable comparison with mono-types (Figure 4.7). In order to remove architectural effects, the unfavourable design (types-grouped and motif-mixed) was removed. All duo-type combinations caused an average reduction larger than that observed in comparable mono-types (see Figure 4.5), with Type1 containing elements exhibiting the largest change from 5% average reduction (mono-type) to 14%. (duotype). To identify the most effective combination, a comparison of average reduction found Type2+3 elements were most suppressive (14.6%), followed by Type1+3 (14%) and Type1+2 (13.5%). Although the average number of downregulated genes remained ~25/30, the number of upregulated genes increased following the same trend. These data support previous findings, confirming Type3 motif containing elements were most suppressive, followed by Type2 and Type1.

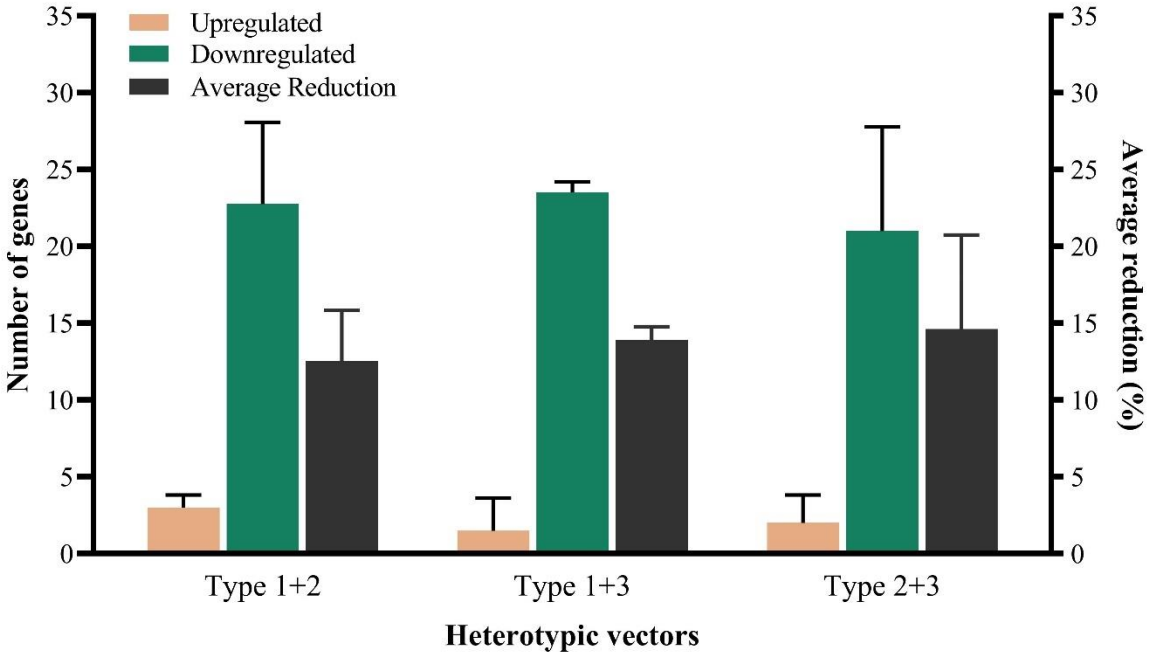

Figure 4.7) Heterotypic duo-type vectors were more suppressive than mono-type vectors. 10 vectors were tested using immune-profiling tool Nanopanel and grouped based on shared Types to determine the average number of up/ downregulated genes (threshold of 10%) and average reduction (%) relative to pVAX1 control. Bars represent the mean +SD where Type1+2 n=3, Type1+3 n=2 and Type 2+3 n=3.

Trio-type elements had minimal immune-stimulatory effects

Three trio-type elements were tested in different architectural arrangements and screened using Nanopanel (Figure 4.8). Unexpectedly, these vectors had no suppressive effects with ~5% immune-activation, 9/30 upregulated genes and 5/30 downregulated genes. No architectural differences were observed (data not shown) suggesting these effects were sequence dependent and may be explained by the presence of singular motif copies compared to previous elements with at least two duplicates of each motif. This hypothesis suggests a minimum number of motif copies may be required to exhibit downregulation. Alternatively, the presence of so many different motifs may have interfered with the suppressive activity of other sequences, inhibiting their function.

Overall, from all designed and tested library 1 vectors, duo-type elements were the most suppressive (~15% average reduction), followed by mono-types (~10% reduction) and finally trio-types with no suppressive effects (~5% immune-stimulatory). Furthermore, microsatellite motifs were consistently most suppressive, followed by the dinucleotides and finally G-rich sequences (with minimal effects).

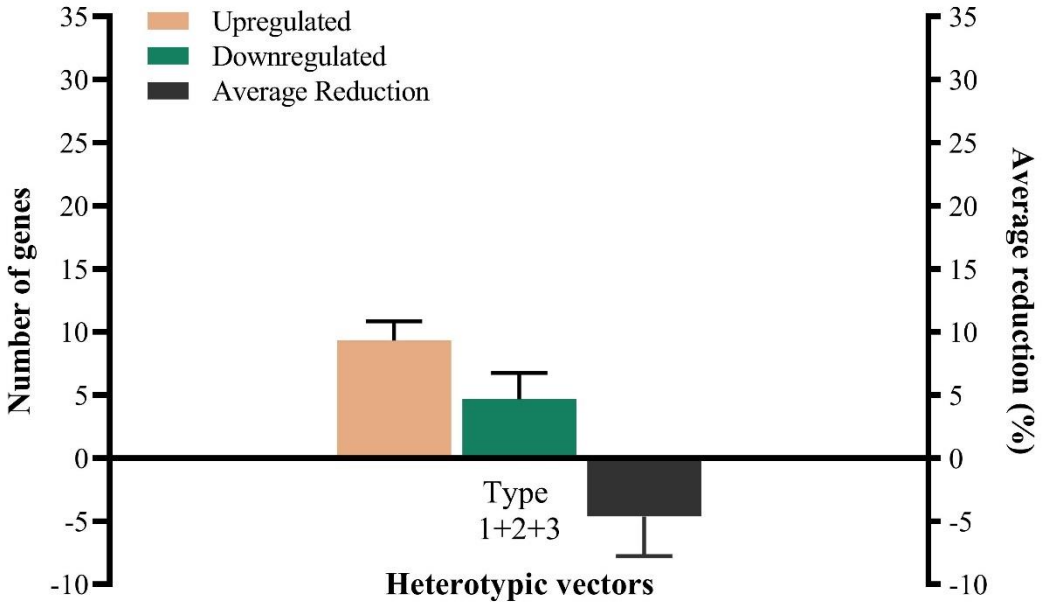

Figure 4.8) Heterotypic trio-type vectors had minimal immune-stimulatory effects. Three vectors were tested using immune-profiling tool Nanopanel and grouped to determine the average number of up/ downregulated genes (10% threshold) and average reduction (%) relative to pVAX1. Bars represent the mean +SD where n=3

4.2.3 MLR modelling of library 1 motifs

A total of 36 elements were designed and tested from library 1 including 18 homotypic, 5 mono-type and 8 duo-type heterotypics. To test as many design rules as affordable, motif replicates were compiled from different elements rather than biological repeats, using multiple linear regression modelling to derive coefficient values (comparable to immune-modulatory 'power') for individual sequences. To prevent interference from known architectural effects, the following groups were excluded: duo-type types-grouped motifs-mixed and all three trio-types. A resulting total of 31 elements were inputted to the model, generating 7 replicates per motif.

Individual elements motif composition and average percentage reduction was MLR modelled to i) identify sequences with a statistically significant effect on observed percentage reduction and ii) determine how well the model fit the input data (Appendix, Supplementary Table 7). Coefficients were calculated for all sequences identifying three Type2 motifs (M12, M13, M14) and three Type3 motifs (M16, M17, M19) with the highest coefficient values and statistically significant p-values shown in Figure 4.9A. M6 and M18 were omitted as homotypic elements could not be synthesised and tested. These observations confirm 6/20 tested motifs had small but significant suppressive effects that could be detected using immune-profiling tool Nanopanel within a plasmid context. Furthermore, with an adjusted global R^2 of 0.82 these data fit the MLR model with high confidence suggesting motif sequence and copy number account for 82% of the variation observed in percentage reduction. As expected, residuals displayed a random stochastic relationship suggesting no other predictable factor (such as architecture) was affecting suppression. The F statistic tests the significance of the model by comparing the ratio from model explained variance: unexplained variance. An F-statistic of 7.801 with a p-value 1 <0.001 was calculated for this model, confirming motif sequence significantly impacts observed reduction from Nanostrings immune-profiling 30-gene average values. Observed element suppression values were plotted against model-derived predicted values to show the close correlation in Figure 4.9B. From this, we can conclude MLR modelling provides high confidence from the data set, identifying six motifs of interest.

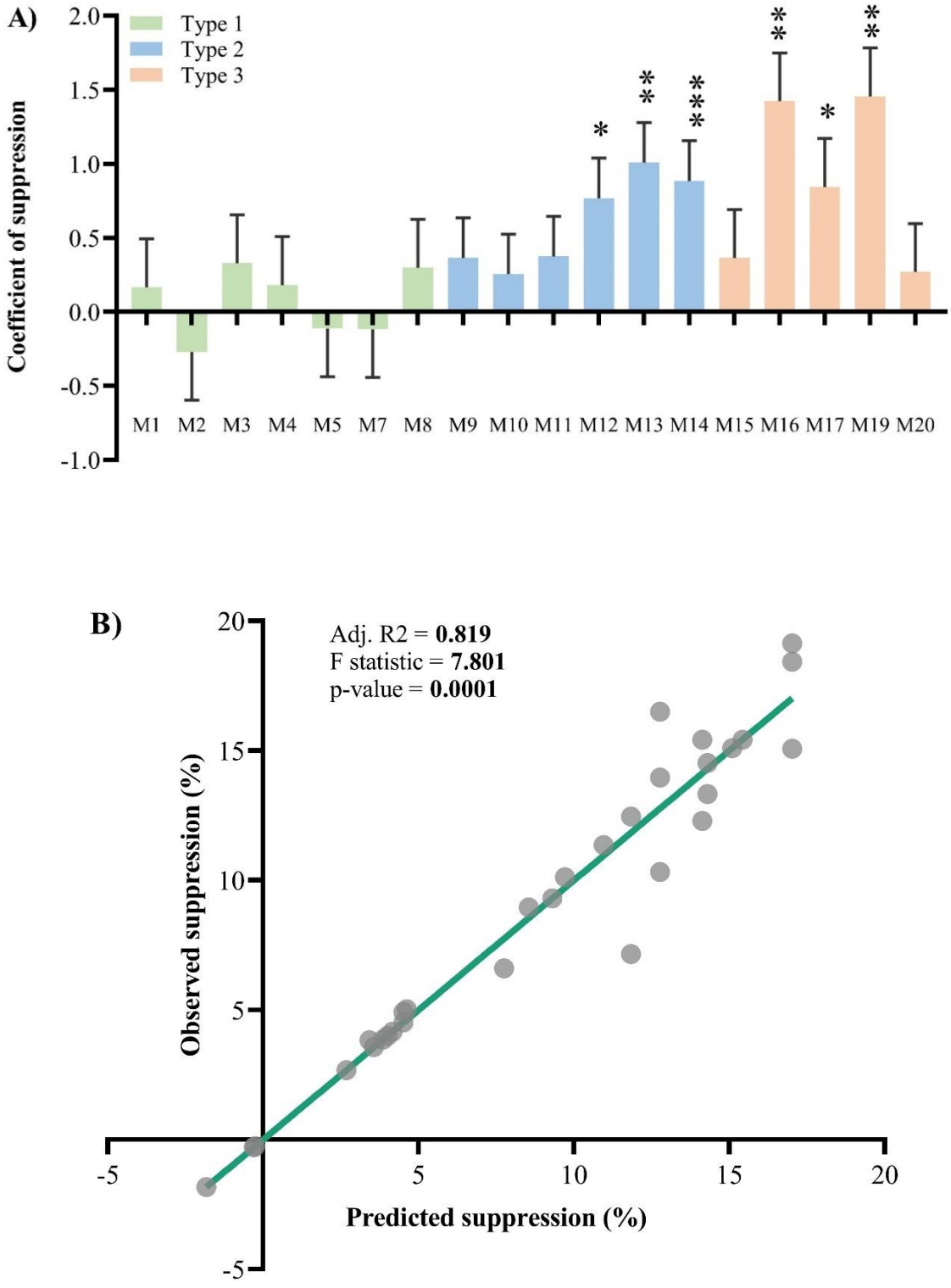

Figure 4.9) OLS modelling identified six statistically significant suppressive motifs. 31 homotypic and heterotypic constructs were modelled using an OLS. A) Motif coefficient values with SD and associated p-values. Statistical significance was defined as $p \leq 0.05$ (*=p≤0.05, **=p≤0.01, ***=p≤0.001, ****=p≤0.0001). B) Observed element suppression (%) was compared to model predicted (%) values.

Within MLR modelling, the number of observations (31) should exceed the number of parameters to be estimated (20), as is true of this model. However, in order to improve its robustness, the model was run again using only the six sequences identified as statistically significant with observed element suppression plotted against new model predictions in Figure 4.10. From this data, a new model with an adjusted R^2 of 0.69, F-statistic of 12.33 and p-values of <0.0001 was calculated (Appendix, Supplementary Table 8). This not only improves model simplicity and interpretability, but also reduces the impact of noise (due to overfitting from too many parameters). Compared to 82% in the previous model, this new iteration shows six motifs account for 69% of total variation. These data increase model confidence and further support the identification of these six motifs as immunosuppressive sequences.

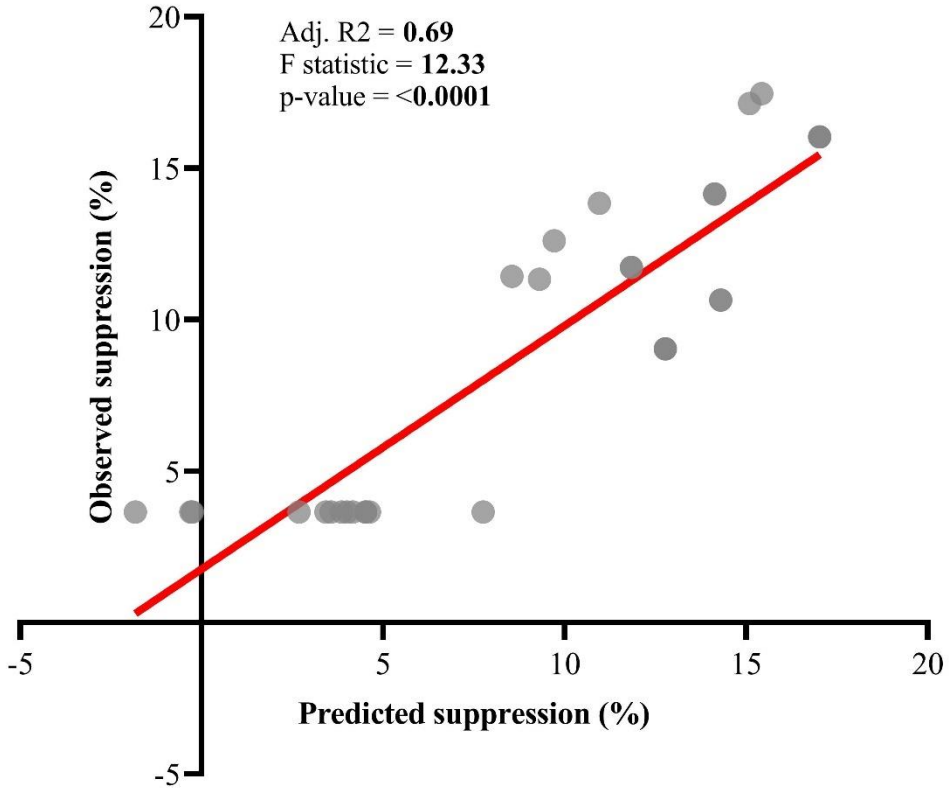

Figure 4.10) Six motifs account for 69% of observed suppression in library 1. 31 homotypic and heterotypic constructs were OLS modelled using six input parameters (M12, M13, M14, M16, M17, M19). Observed element suppression (%) was compared to model predicted (%) values. Statistical significance was defined as $p \leq 0.05$ (*=p≤0.05, **=p≤0.01, ***=p≤0.001, ****=p≤0.0001).

4.2.4 Designing library 2 heterotypic elements

In practise, application of these motifs/ elements in gene therapy vectors would require sequences that were small, easy to synthesise and had minimal impacts on vector activity. First however, to determine whether pDNA motif integration was a valid strategy, suppressive activity was maximised by designing a second library based on library 1 design rules and MLR coefficients. 16 elements were designed, each containing 30 suppressive motifs, producing elements that were larger in length (675–730bp) than library 1. Six sub-groups of elements were constructed, as described in Table 4.2 using on a rational design strategy with the following objectives:

Group 1 objective:

Maximise reduction using only the six statistically significant MLR identified motifs at equal ratios (duo-type elements). Three elements were designed, each containing 5x copies of the same six motifs (M12, M13, M14, M16, M17 and M19) within the following architectures: 1a) types-grouped, motifs-mixed, 1b) types-mixed motifs-mixed and 1c) types-mixed motifs-grouped, excluding unfavourable duo-type architecture types-grouped motifs-mixed.

Group 2 objective:

Maximise reduction using statistically significant MLR identified motifs at model-drive ratios (duo-type elements). This involved assigning copy numbers based on the relative magnitude of coefficient values so higher suppression motifs were present at higher copy numbers. For example, M16 and M19 had the highest coefficient values of 1.4 and 1.5 respectively and so were present at the highest copy number of 7x, whereas M12 had the lowest coefficient value of 0.8 and so was present at only 3x copies. Two elements were designed with the following architectures: 2a) types-mixed, motifs-mixed and 2b) types-grouped, motifs-grouped, as these were the most effective duo-type compositions.

Groups 3 objective:

Maximise reduction using M19 within design limitations. Based on model coefficient values, M19 was the singular most suppressive motif. Elements were designed to include as many copies of M19 as possible alongside other suppressive motifs as 'spacers' to aid DNA synthesis whilst including any additional heterotypic suppression. Three elements were designed: 3a) 20 copies of M19 each separated by a different motif of decreasing strength, 3b) model significant motifs at a 5:2:1 ratio of M19, M16 : M13 : M14, M12, M17 and 3c) MLR significant motifs at a 4:1 ratio of M19, M16, M13 : M12, M14 and M17.

Group 4 objective:

Maximise reduction using only Type3 motifs (mono-type elements). Microsatellites were consistently found to be the most suppressive groups within library 1. To further interrogate their suppressive capacity, four elements were designed excluding M18, as coefficient value could not be derived with confidence. 4a) all five Type3 motifs at model driven ratios, 4b) 12x copies of M19 each separated by other Type3 motifs, 4c) 6x copies of each Type3 motif and 4d) each Type3 motif present at a 4:3:2 ratio of M19, M16 : M17 : M15, M20.

Group 5 objective:

Maximise reduction using motifs from all three Types (trio-type elements). In order to test whether trio-type elements were in-fact limited by the presence of motifs in single copies, the following constructs were designed: 5a) Most suppressive two motifs from each Type present in 5x copies each, 5b) Most suppressive two motifs from each Type present at model driven ratios.

Group 6 objective:

Maximise reduction by optimising the best library 1 architectures. To preserve any positional/ architecture specific effects from previous designs, low coefficient motifs were replaced with those that were higher in two duo elements: 6a) Types2+3 types-grouped, motifs-grouped 6b) Types 2+3 types-mixed motifs-grouped.

All designs were successfully synthesised (GenScript Biotech, Piscataway, US) however in the interest of time and cost, an initial screen of one construct from each group (selected based on coefficient sum and likelihood of success) was conducted (Table 4.2). Given the ultimate goal in establishing whether use of suppressive motifs was a viable strategy for reducing the immune response from pDNA therapy vectors, a reduction in the production of immune-activating cytokines would eventually be required. Therefore, the selected six library 2 constructs (1a, 2a, 3a, 4a, 5b, 6b) were directly screened to quantify changes in cytokine protein production rather than Nanostrings profiling, as detailed in the following section.

Table 4.2) Library 2 Designs. Composition of the 16 heterotypic elements is shown including motif type, copy number and accumulated co-efficient sum (from MLR modelled values). Highlighted constructs (grey) were taken forward for TNFa ELISA testing.

Library 2 Motif Composition																					
	M1	**M2**	**M3**	**M4**	**M5**	**M6**	**M7**	**M8**	**M9**	**M10**	**M11**	**M12**	**M13**	**M14**	**M15**	**M16**	**M17**	**M18**	**M19**	**M20**	**Sum**
1a												5	5	5		5	5		5		32
1b												5	5	5		5	5		5		32
1c												5	5	5		5	5		5		32
2a												3	5	4		7	4		7		34
2b												3	5	4		7	4		7		34
3a	1		1					1	1		1	1	1	1	1	1	1		20		36
3b												2	4	2		10	2		10		38
3c												2	8	2		8	2		8		37
4a															2	10	6		10	2	35
4b															4	5	5		12	4	31
4c															6	6	6		6	6	26
4d															4	8	6		8	4	31
5a	5		5										5	5		5			5		26
5b	1		2										5	6		8			8		34
6a												4	4	4		6	4	2	6		31
6b												4	6	6		6	2	2	4		30

4.2.5 Suppressive motif effects were undetected in cytokine ELISAs

Library 1 and 2 vectors did not suppress TNFa production

Having quantified and characterised synthetically engineered immune-suppressive vectors on the gene level, cytokine ELISAs were performed to investigate if these effects translated to the protein level. TNFa is a potent proinflammatory cytokine produced in response to intracellular viral attack and most commonly analysed in literature-based immune studies. As pDNA also enters through the cell membrane occupying space within the cytoplasm and nucleus, it is detected by immune response pathways similar to those of viral infections (Huerfano et al., 2013). For these reasons, TNFa was chosen to screen some of the most promising library 1 and 2 elements to determine whether motif integration was a viable suppressive strategy.

9 vectors were screened in total including the two best homotypic elements (M16 mono and M19 mono), the best heterotypic element (duo-type 2+3 type-mix motif-mix) and one construct from each library 2 group (1a, 2a, 3a, 4a, 5b, 6b). Vectors were transfected into DC2.4 cells, incubated for 24hrs and quantified for TNFa from supernatants. Relative expression compared to pVAX1 is shown in Figure 4.11A. All vectors produced variable but generally neutral effects except library 1 homotypic M16 (average FC of 0.8, ~20% reduction) and library 2 4a and 5b (average FC of 1.3 and 1.8 respectively). Of all groups tested from library 2, 4a and 5b had a high number of single motif repeats suggesting restrictions in motif diversity along with high single-motif copy numbers may cause immune-stimulation. These data show i) immune-suppression on the gene level from library 1 constructs did not correlate with downregulation of TNFa production, ii) library 2 engineered constructs did not suppress TNFa protein production and iii) library 1 M16 had some downregulatory effects on TNFa. To conclusively determine whether M16 suppression was significant, cytokine production from TNFa and IFNb (an anti-viral cytokine associated with cGAS-STING activation) was quantified across 7 biological replicates to provide enough statistical power to identify small changes (Figure 4.12B). Variation across both cytokines was observed with an average downregulation of 5% (TNFa) and 6% for (IFNb) but this was not statistically significant relative to pVAX1.

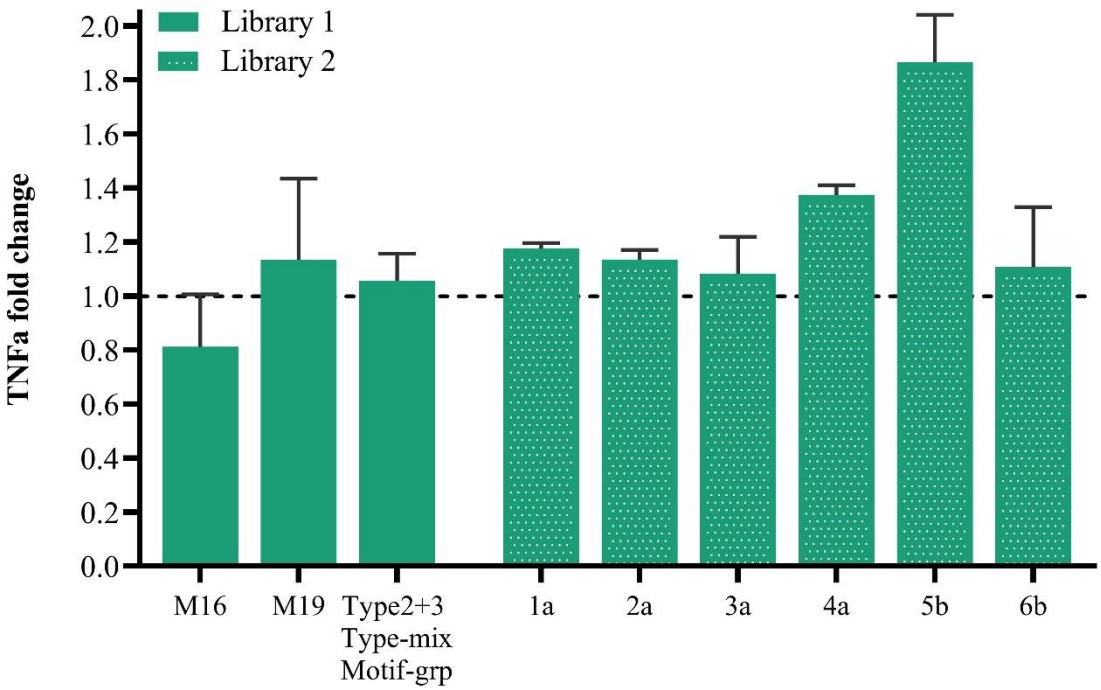

Figure 4.11) TNFa production from library 1 and 2 vectors. 400ng vector DNA was nucleofected into 400,000 DC2.4 cells for 24hrs. TNFa production was quantified and expression relative to pVAX1 control (line at FC 1.0) is shown. Bars represent mean +SD for three biological replicates (except for 1a, 2a, 4a and 5b with two) in technical singlicate.

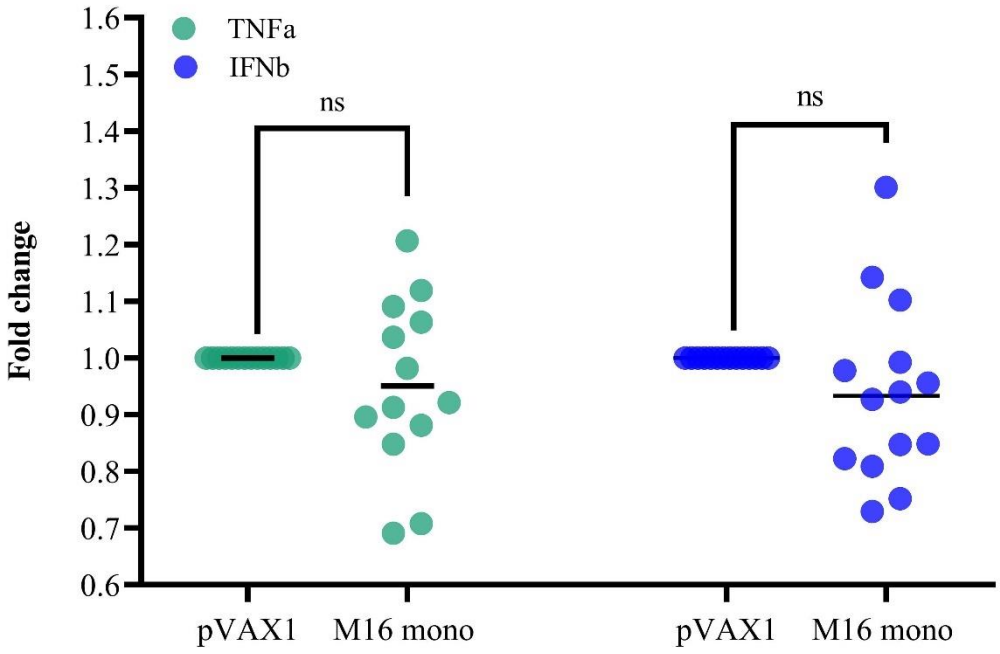

Figure 4.12) Homotypic M16 vector had no suppressive effects on TNFa and IFNb production. 400ng vector DNA was nucleofected into 400,000 DC2.4 cells for 24hrs. TNFa and IFNb production was quantified and expression relative to pVAX1 control is shown. Dots represent each data point for 7 biological replicates in technical duplicate. A two-tailed unpaired t-test on absolute values found no statistical significance (ns).

DNA titration of homotypic M16 vector did not suppress TNFa production

A pVAX1 titration between 50-800ng identified 400ng as an optimal DNA load, producing large quantities of TNFa whilst remaining within the linear range of ELISA detection (see Figure 3.5). In case this concentration was overwhelming the cells system, masking potential suppressive effects, a titration of homotypic vector M16 was conducted between 100-400ng, shown in Figure 4.13. A comparison of TNFa production between pVAX1 and ad M16 found i) decreasing DNA load caused a reduction in TNFa production from both vectors and ii) no discernible difference between control and M16 was observed at lower concentrations, confirming DNA load was not masking M16s suppressive effects on the protein level. Overall, these data confirm no significant suppression from motif integrated suppressive sequences could be observed in the production of TNFa or IFNb, irrespective of pDNA load.

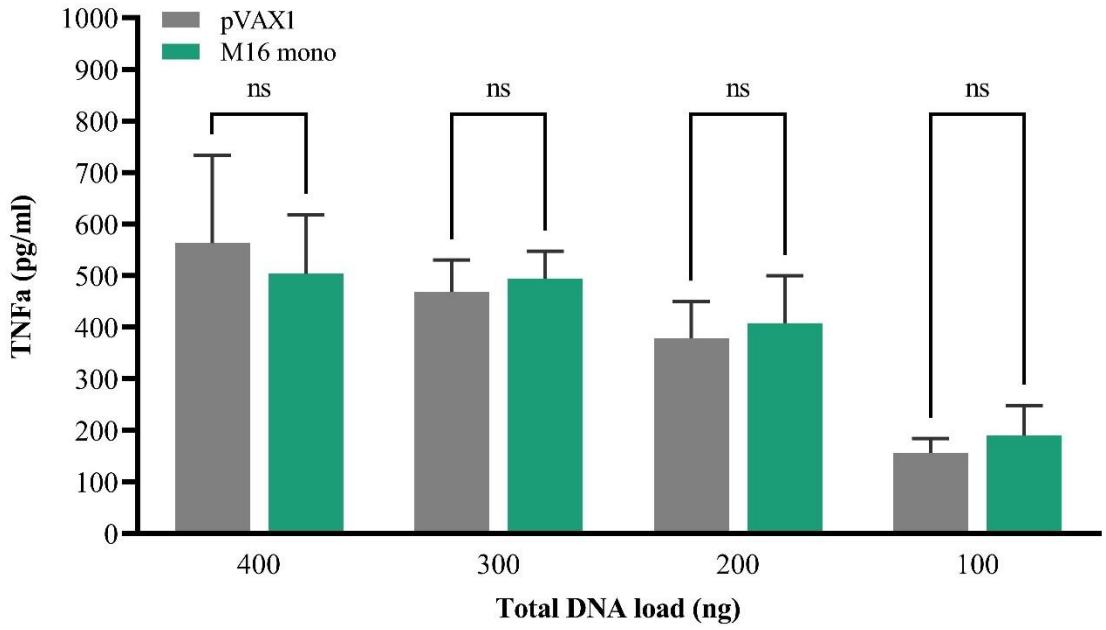

Figure 4.13) DNA titration of homotypic M16 vector did not suppress TNFa production. Vector DNA of varying load was nucleofected into 400,000 DC2.4 cells for 24hrs. TNFa production was quantified, with absolute expression values (pg/ml) shown. Bars represent the mean +SD from three biological replicates in technical duplicate.

4.3 Discussion

The work within this chapter introduces the first-ever large-scale investigation of suppressive motifs within a double-stranded plasmid backbone for application as an immune-suppressing technology in gene therapy vectors. To determine whether this was a viable strategy, 20 of the most promising, literature described immunosuppressive ODNs were tested. Given the novelty of this screen, a number of different variables were tested through the design of a homotypic and heterotypic library, with MLR modelling used to quantify the 'power' of individual motif. Use of novel immune-profiling tool Nanopanel enabled sensitive quantification and characterisation of these sequences within 36 different synthetically designed elements. Without Nanopanel, discrimination of such small sequence-specific effects would propose an extreme challenge. From the results described above, the following 7 design rules were established:

1. Type3 microsatellites were consistently the most suppressive group of sequences, followed by Type2 Dinucleotides and Type1 G-rich motifs.

Interestingly, based on previous literature findings the opposite trend was expected, with G-rich sequences considered to the most potent ODN suppressors followed by CpG dinucleotides and finally Type3 microsatellites (Bayik et al., 2016; Zeuner et al., 2002). In fact, since their discovery in 2009, almost no studies have further investigated the activity of M17, M19 and M20 (Hu et al., 2009). A lack of Type1 suppression may be an effect of the novel pDNA system, with restrictions in the double-stranded backbone preventing formation of G-tetrad secondary structures required for suppressive activity in native ODN form (Gursel et al., 2003). This was however, accounted for, by purposefully integrating motifs upstream of the cmv promoter to enable G-tetrad formation during transcription bubble-dependent DNA strand separation (Duquette et al., 2004). Given the transient and dynamic nature of this process, it may be that duration of the single stranded: double-stranded state was insufficient for significant suppression. Alternatively, the reduction in motif copy number: pDNA ratio may also be responsible, as ODNs are typically used in excess of 1000 molecules per DNA simulant (Kaminski et al., 2013).

2. Duo-type elements were more suppressive than mono-types and trio-types

A consistent increase in immune reduction was observed for elements composed of motifs from two different Types, compared to only one Type. Given these motifs work through different pathways (Bayik et al., 2016), its possible Type variation enables suppressive targeting through multiple pathways. Combination 'power' followed the trend of Type2+3, Type1+3, Type1+2, again suggesting microsatellites were the strongest suppressors. These differences however, were difficult to delineate even with the sensitivity of 30-gene profiling, with all duo-type combinations averaging in suppression to ~15%. Duo-types 2+3 types-mixed motifs-grouped was the singular most suppressive element, exhibiting a~20% downregulation in the average expression of 30 immune-genes.

3. Types-grouped motifs-mixed as an unfavourable duo-type architecture

In order to investigate the positional effects of these motifs within the DNA backbone, multiple architectures were tested. The two most effective arrangements were i) types-mixed and motifs-mixed (alternating between Types whilst also mixing motif duplicate copies and equally, ii) types-grouped and motifs-grouped (keeping different Types separated with their motifs mixed). This was unexpected given the opposition in their design, therefore limiting broader conclusions that can be made regarding optimal grouping/ mixing of motif copy numbers or Types. Interestingly however, architecture types-grouped, motifs-mixed was particularly disadvantageous suggesting something in this arrangement interferes with sequence activity and should therefore be avoided in future designs.

4. Trio-type elements had minimal immune-stimulatory effects.

These elements contained the most sequence heterogeneity, with no motif duplicates, suggesting a minimum of two copies of each motif is required to exhibit suppression. Furthermore, given the low levels of noise within this system (Figure 3.9B), the levels of stimulation detected, although minimal, suggests the presence of these motif sequence induces immune activation when functionality is comprised.

5. M12, M13 M14 (Type2), M16, M17 and M19 (Type3) were statistically significant suppressive motifs, accounting for 69% of observed element suppression.

As observed during homotypic vector screening, MLR modelling confirmed no Type1 motifs were able to exert significantly suppressive effects within the system. Type2 dinucleotides exist in three variations; CpG, GpC and GpG. From these, M12 (GpG), M13 (CpG) and M14 (CpG) were identified as significantly suppressive motifs whilst the remaining GpC-ODN derived sequence had no notable effects. Dinucleotide ODNs generally target TLR9, binding through the C-terminal domain which can distinguish between sequences displaying higher affinities for CpG over GpC variants (Avalos and Ploegh, 2011). This discrimination may explain the system bias towards M13 and M14 induced suppression as opposed to M9 and M11, although M10 suppresses through the TLR7/TRIF axis conferring tolerogenic effects in pDCs that weren't observed in this monocyte-derived model (Volpi et al., 2012). The only GpG-ODN screened (M12) reportedly suppressed through direct TLR9 binding and indirect inhibition of Nf-KB phosphorylation, biasing Th2 over Th1 responses *in vivo* (Ho et al., 2003). Together, these findings show GpC-ODNs do not induce suppression within a dsDNA context regardless of their mechanism of action, with CpG-ODNs found to be the most effective followed by GpG-ODNs.

From the numerous microsatellite derived ODNs initially designed and tested by Hu and colleagues, a small number were found to be effective (Hu et al., 2009). For example M15 was found to inhibit TLR7/9 activation and delay the onset of lupus in murine graft-versus-host-disease (He et al., 2011; Sun et al., 2010) whilst M17 inhibited CpG-ODN induced activation of human PBMCs through cellular uptake/binding competition (Hu et al., 2009). Within this system, M16, M19 and M17 were identified as significantly suppressive motifs, of which the first two exhibited the largest suppressive effects. M16s suppression is well characterised within the literature however MLR modelling has confirmed sequence suppression within a new context whilst also proposing two more motifs, of which one (M19) is equally as suppressive.

Of the 18 motifs screened, these six account for 84% (69/82) of total sequence-dependent effects within a pDNA integrated system

6. M16 and M19 were the two 'strongest' suppressive motifs.

Despite M16s initial use as a neutral ODN (Sun et al, 2010), more recent studies have confirmed potent immunosuppressive activity in numerous mouse models such as; ALI, sepsis, systemic inflammatory response syndrome and myocarditis have been reported (Fang et al., 2011; Gao et al., 2017; Nie et al., 2019; Xiao et al., 2017). Its three key mechanisms of action include i) inhibition of HMGB1 translocation out of the nucleus and into the cytoplasm, preventing DAMP activity, ii) inhibition of IRF5 translocation into the nucleus through consensus competitive binding and iii) NF-kB inhibition, all of which downregulate the expression of TNF-a, IL-6 and IFNa/b (Gao et al., 2017; Nie et al., 2019; Zhang et al., 2022). These findings therefore align with current microsatellite studies and suggest activity in ODN form for these sequences can translated to a pDNA integrated form.

As mentioned earlier, no studies investigating M19 ODN effects post-discovery in 2009 have been reported (Hu et al., 2009). As seen with M16 however, it is possible the downregulatory effects of this ODN have simply not been tested within an appropriate context. Analysis of the M16 monomer AAAG and M19 monomer TTTTG shows some similarities in sequence structure. Zhang and colleagues have hypothesised the presence of a G every 4bps enables M16 to form G-quadruplex-like secondary structures which may also apply to M19 (Zhang et al., 2022). However, given no suppression was observed for the G-rich Type1's, it is unclear whether microsatellite suppression is dependent on the formation of these secondary structures.

7. Larger, overly repetitive and complex designs, cause immune stimulation

The aim of library 2 was to maximise the suppressive capacity of pDNA integrated motifs and determine the limits of this technology. However, the production of more complex and highly repetitive designs instead results in stimulation of TNFa and IFNb. From these data we can conclude over engineered constructs either interfere

with motif functionality and/ or are more readily recognised by host immune-systems and so do not present a viable suppressive design strategy.

To conclude, given the minimal downregulatory effects observed on the protein level, along with the complexities in synthesising such large suppressive elements (>600bp), motif use as pDNA integrated sequences for the inhibition of DNA-driven gene therapy vector responses is not recommended. This screen does however identify six significantly suppressive motifs and seven key design rules to i) inform selection and design of ODN based studies and ii) characterise motifs for the community with pDNA integrated suppressive effects on the gene level, establishing foundational work for future investigations.

As for (i), the outputs from this study were used to guide the design and screen of ODN sequences as immunosuppressants of pDNA-driven responses. Significant and potent effects correlating with the trends and design rules established within this chapter were observed, validating their practical application (see chapter 5).

Chapter 5 : A Sequence Specific Oligodeoxynucleotide Technology Reduces Plasmid DNA Driven Immune Stimulation in Dendritic Cells

This chapter describes the identification of sequence-specific ODNs with novel use as immunosuppressants of pDNA-driven immune responses. Informed screening established a toolbox of eight ODNs with TNFa and IFNb specific modulation, dependent on sequence and concentration. Optimisation of ODN kinetics identified M16; a microsatellite derived ODN with pDNA-CpG counteracting immune activity. Application across multiple vector contexts and concentrations demonstrated the utility of this novel technology, thresholding absolute TNFa production, with a maximum relative inhibition of ~70%. Interrogation within human pDC derived cell line CAL-1 found this model to be ineffective for the study of pDNA immunogenicity, however some condition-specific CpG antagonising M16 suppression was observed. Novel application of M16 presents a technology for the reduction of DNA therapy, vector driven responses. This expands the design space for CpG incorporation, improving the stability and long-term expression of therapeutic transgenes.

5.1 Introduction

As discussed in section 1.1, the immunogenicity of pDNA compromises the safety and efficacy of plasmid-based therapeutics. For example, immune recognition of gene therapy vectors results in i) the death of cells containing 'foreign' DNA/ transgene products, ii) decreased expression of therapeutic proteins and in extreme cases, iii) uncontrolled immune overstimulation resulting in patient death (Sibbald, 2001). A key culprit of these responses is the highly stimulatory CpG-motif present in the genomes of non-viral and viral gene therapy vectors (Bertolini et al., 2021; Rogers et al., 2017; Shirley et al., 2020), The presence of even a single motif within pDNA is sufficient for activation of an inflammatory response (Hyde et al., 2008). Current engineering strategies have found success through methylation (McLachlan et al., 2000), or removal (Hyde et al., 2008; Yew et al., 2000), of these dinucleotides.

Unfortunately, however, CGs have critical methylation-dependent functions in gene regulation. Their presence in high-density unmethylated CpG islands within promoter regions (as well as enhancers, origins of replication and transcriptional start sites) for example, is necessary for the prolonged expression of many housekeeping and tissue-specific genes (Hartl et al., 2019; Larsen et al., 1992). The selection/ design of promoters with fewer CpGs (or even CpG-free) can help reduce immunogenicity, however effects on gene expression can be unpredictable, with reports of increased, (Pringle et al., 2012), decreased (Habib et al., 2020) or null impacts (Ho et al., 2016) on long term transgene production.

Furthermore, the necessity for including intragenic CpGs in three-fold. Firstly, intragenic CGs have regulatory effects similar to those of gene promoters, with depletion causes significant reduction in mRNA transcripts through changes in nucleosome positioning (Bauer et al., 2010). Secondly, the identification of CG overrepresentation within intragenic exons regions, despite its association with increased mutational propensities (Kondrashov et al., 2006), is thought to be essential for the formation of protective mRNA secondary structures (such as stem-loops and hairpins) which stabilise transcripts, facilitating translation (Duan and Antezana, 2003; Shabalina et al., 2006). And finally, due to the degeneracy of the genetic code, a

single amino acid can often be encoded by more than one codon (three consecutive nucleotides), therefore codon-optimisation is often utilised to remove CG's within these regions without affecting the amino acid sequence of therapeutic protein products (Mauro, 2018). These substitutions however are not always neutral and can result in changes to both protein conformation and function due to slower translational rates (Kirchner et al., 2017).

A balance therefore, between unwanted CpG immunogenicity and efficacious functionality in transgene expression must be maintained. This chapter describes novel use of immunosuppressive ODNs to specifically counteract CG activated immunogenicity from pDNA. Application of this technology into gene therapy vectors removes constraints in CpG usage, expanding the design space for use of more effective promoters/ enhancers/ origins of replication/ and coding gene products.

The work in this chapter therefore aims to:

1. Characterise a toolbox of immune-suppressive ODNs, informed from chapter 4, to modulate pDNA driven immune stimulation.
2. Optimise ODN sequence, concentration, and experimental kinetics to maximise suppression.
3. Investigate M16's mechanism of suppression.
4. Examine M16's utility across vectors with varying CpG content and backbone contexts.
5. Screen M16's effects in DC line CAL-1, interrogating its use as a human model for the characterisation of pDNA immunogenicity.

5.2 Results

5.2.1 Characterising a toolbox of immunomodulatory ODNs

ODN selection

Based on the results presented in chapter 4, a small number of ssODNs were investigated to identify potential immune-suppressive effects in DCs exposed to pDNA. From a library of 20 sequences, MLR modelling identified six motifs with statistically significant immune-suppressive effects when pDNA integrated: three Type3 microsatellite (M16, M17, M19) and three Type2 dinucleotide (M12, M13, M14). Based on these findings, and an interest in screening as broad a selection of suppressive ODNs as possible, the following sequences were investigated: MLR motifs with the highest coefficients (M13, M14, M16, M17, M19), literature supported type 1 G-rich ODN (M1), class-C murine activating TLR9 positive control (CpG 2395) and corresponding CG dinucleotides substituted negative control (N 2396) (Table 5.1)

Table 5.1) Immune-suppressive motifs selected for ODN screening. Motif name, type, PS backbone sequence and total nucleotide (nt) length is shown.

	Library of suppressive motifs		
	Motif name	**Sequence**	**Motif length (nt)**
Type 1 (G-rich)	M1	TTAGGGTTAGGGTTAGGGTTAGGG	24
Type 2 (Dinucleotide)	M13	TCCATGTCGTTCCGCCCGCG	20
	M14	TGGCGCGCACCCACGGCCTG	20
Type 3 (Microsatellites)	M16	AAAGAAAGAAAGAAAGAAAGAAAG	24
	M17	TCTCTCTCTCTCTCTCTCTCTCTC	24
	M19	TTTTGTTTTGTTTTGTTTTGTTTTG	25
Controls	C 2395	TCGTCGTTTTCGGCGCGCGCCG	22
	N 2395	TGCTGCTTTTGGGGGGCCCCCC	22

ODN titration against pVAX1

Given no previous literature has investigated the effects of ODNs with pDNA, a methodology was developed to optimise their suppressive interactions using the experimental pipeline described in chapter 4 alongside comparable literature reports. Previously described systems include i) pre-transfection: cells were incubated with suppressive ODNs 24hrs-20mins prior to immune-stimulant exposure, ii) co-transfection: suppressive ODNs and immune-stimulants were introduced simultaneously and iii) post-transfection: cells were first exposed to an immune-stimulant and then incubated with suppressive ODNs immediately (or up to 6hrs) after (Hu et al., 2009; Römmler et al., 2015; Steinhagen et al., 2018; Sun et al., 2010; Valentin et al., 2021; Yamada et al., 2002). Method success was found to be system dependent, however those that used dsDNA-based immune-stimulants or the suppressive ODNs described in Table 5.1 found post-transfection to be most effective and so this method was selected for initial screening experiments (Hu et al., 2009; Sun et al., 2010). ODN concentrations between 0.01–10uM have been reported as efficacious with higher loads inducing greater suppression, however considerations of cost and cell toxicity led to initial experimental titrations between ~0.06–6uM (Römmler et al., 2013).

ODN effects in the absence of DNA were first investigated by mock transfection of DC2.4 cells with endotoxin free water, followed by post-incubation with 5.6uM ODN for 24hrs. TNFa production relative to a 'pVAX1 only' control (a normalisation method used in similar studies (Valentin et al., 2021)) is shown in Figure 5.1A. C 2395 and N2396 induced the largest stimulation followed by M13, M19, M17, M14 and M16. This sequence dependent effect was not unexpected given ODNs in isolation have been reported to induce low levels of cytokine secretion (Römmler et al., 2013). The same system was tested with DNA by transfecting 400ng pVAX1 and incubating with ODNs at either 0.056uM, 0.56uM and 5.6uM (Figure 5.1B). These data show all ODNs including the positive control were suppressive at 0.056uM suggesting this concentration was too low to observe immune modulation. At 0.56uM however, positive control C 2395 was threefold more stimulatory whilst the corresponding

negative control N 2395 behaved as expected (FC ~1), suggesting these ODNs were within their working range. M13 had minimal stimulatory effects whilst M1 remained neutral (FC ~0.93). M19 and M17 exhibited ~20% relative suppression (FC ~0.8) whilst M14 (FC ~0.7) and M16 (FC ~0.6) induced the largest reduction of TNFa, confirming immune-suppressive effects at this concentration. 5.6uM relative to 0.56uM was found to be more stimulatory across all ODNs, with a sixfold increase from N 2395, suggesting higher ODN loads were not more effective within this system and also illustrates difficulties in the design and use of truly neutral controls. M14 and M16 however were the only ODNs to retain relative suppressive effects (FC ~0.8 and 0.7) at 5.6uM, with an overall trend similar to that of ODN only incubation.

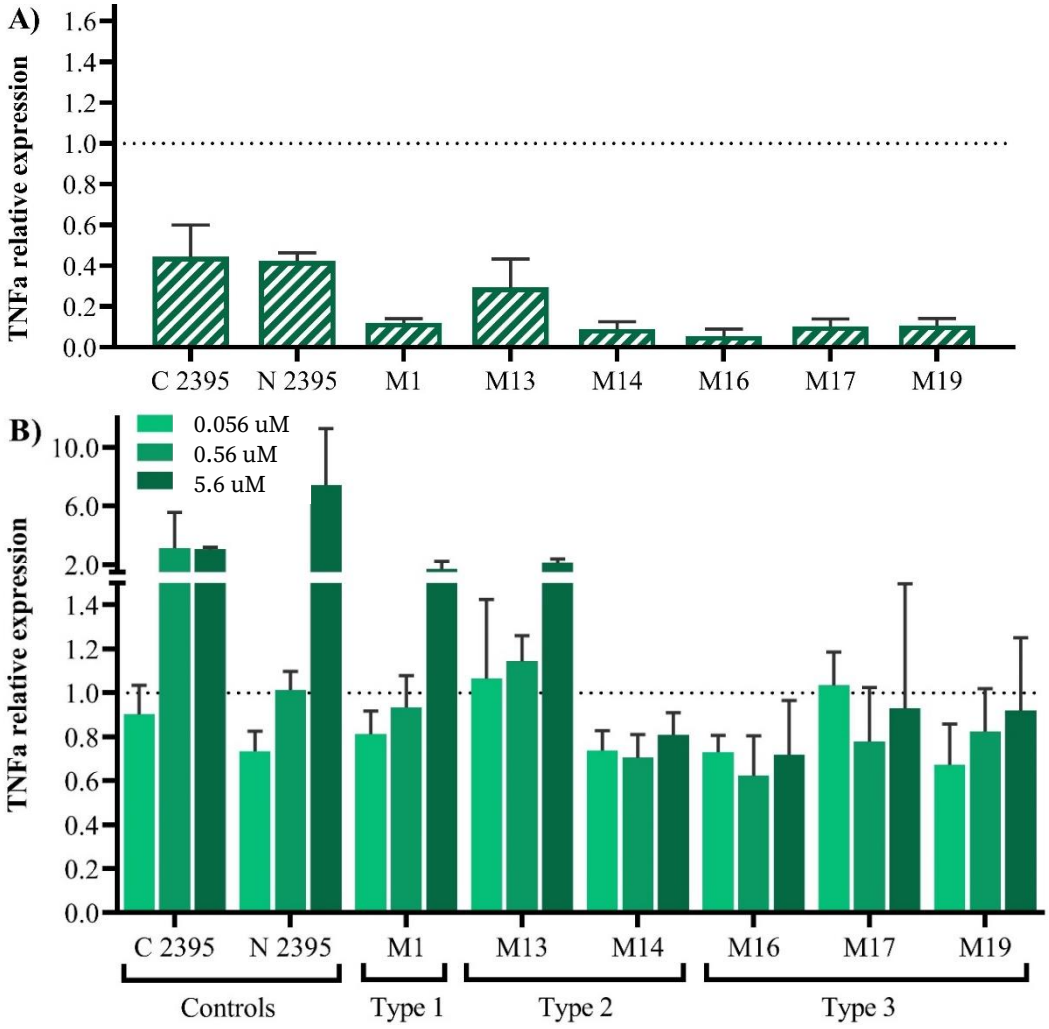

Figure 5.1) Post-incubation ODN titration effects on TNFa production. 400ng pVAX1 or water were nucleofected into 400,000 DC2.4 cells and post-incubated with ssODNs at varying concentrations. TNFa production relative to a 'pVAX1 only' (line at FC 1.0) was quantified at 24hrs. A) No DNA transfection with 5.6uM ODN incubation. B) pVAX1 transfection and ODN incubation. In A and B bars represent mean +SD for three biological replicates tested once.

ODN sequence and concentration modulate TNFa and IFNb production

To characterise the effects of these ODNs on different pathways, TNFa was chosen for its Th1 TLR9 association and IFNb for its Th2 cGAS-STING association. The same conditions described in Figure 5.1B were used to measure IFNb production from ODN incubation at working concentrations of 0.56uM and 5.6uM (Figure 5.2). C 2395 and N 2395 did not behave as expected at 0.56uM, with both ODNs showing 40% and 70% less IFNb expression respectively. All other ODNs show similar levels of suppression, ranked M17 (FC 0.75), M13 (FC 0.7), M14 and M16 (FC ~0.6), and most suppressive M19 and M1 with FCs of ~0.5. At 5.6uM, positive control C 2395 became more stimulatory with a FC closer to neutral whilst N 2395 induced extreme downregulation of IFNb (FC 0.02) further confirming its lack of neutrality. The remaining ODNs were generally neutral, with M14 (FC 0.6) and M1 (FC 0.4) identified as most suppressive although with considerably more sample error. These trends vary dramatically from those observed in TNFa suggesting i) potentially generic PS dependent reduction of IFNb at 0.56uM (see C 2395) and ii) ODN sequence and concentration effect IFNb production.

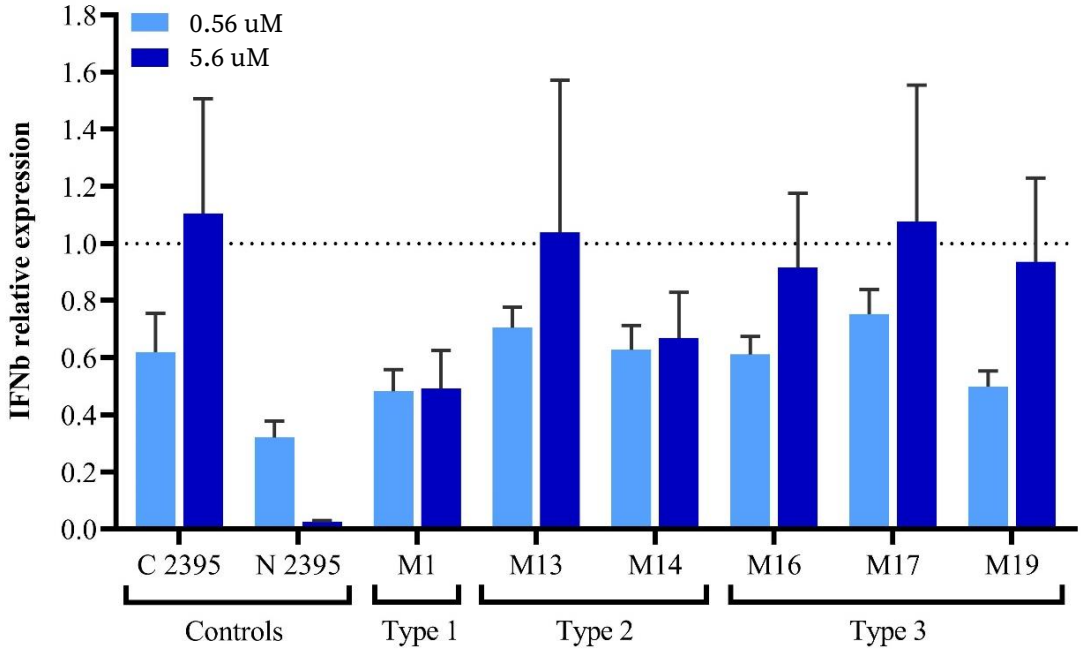

Figure 5.2) Post-incubation ODN titration effects on IFNb production. 400ng pVAX1 DNA was nucleofected into 400,000 DC2.4 cells and post-incubated with ssODNs at 0.56uM or 5.6uM for 24hrs. IFNb production relative to a 'pVAX1 only' control (line at FC 1.0) is shown. Bars represent mean +SD for 3 biological replicates tested once.

Data from Figures 5.1 and 5.2 were combined to produce an immune-modulatory matrix summarising the impact of ODN sequence and concentration on TNFa and IFNb production (Figure 5.3). These data show that within a pDNA immune-stimulated system, M14 and M16 were the strongest suppressors of both cytokines whilst C 2395 (5.6uM) and M13 (5.6uM) stimulated both. N 2395 however, had dramatic modulatory effects, increasing TNFa to ~750% whilst reducing IFNb to ~2%. Similarly, C 2395 (0.56uM) increased TNFa ~250% whilst reducing IFNb by ~40%. These examples present a toolbox of ODNs with sequence and concentration dependent modulatory effects across two key cytokines in response to pDNA. Given the primary objective to identify immune-suppressive ODNs for gene therapy application, M14 (Type2) and M16 (Type3) were selected for further investigation.

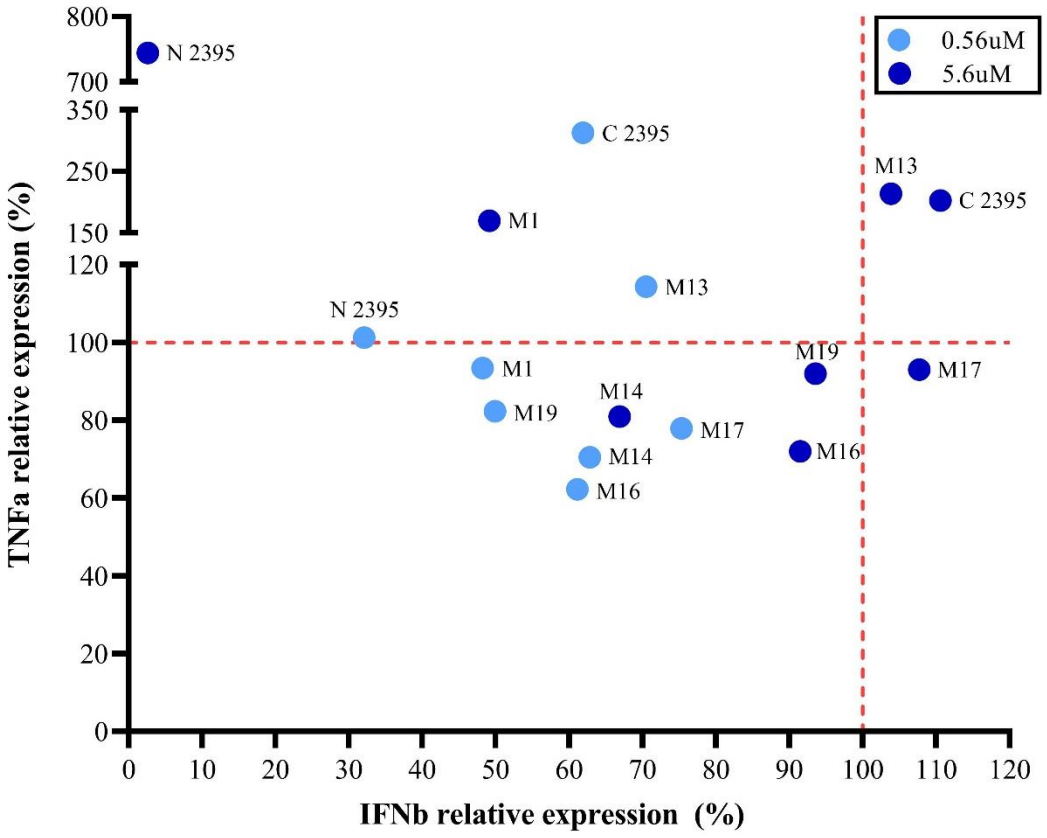

Figure 5.3) ODN sequence and concentration dependent modulation of TNFa and IFNb. 400ng pVAX1 DNA was nucleofected into 400,000 DC2.4 cells and post-incubated with ssODNs at 0.56uM (light blue) or 5.6uM (dark blue) for 24hrs. Relative expression (%) of TNFa and IFNb compared to a 'pVAX1 only' (red line at 100, 100) is shown. Dots represent the mean for three biological replicates tested once.

5.2.2 Optimising ODN kinetics

M14 and M16 combinations were less suppressive than M16 alone

Both M14 and M16 have been found to induce significant suppression in ODN and dsDNA motif form (see Figure 4.2B). M14, known within the literature as CpG-c41, is a Type2 CG dinucleotide with multiple immunosuppressive mechanisms of action including antagonism of membrane-bound TLR9 and inhibition of intracellular TLR7/9 (Liu et al., 2017). M16 on the other hand is a Type3 AAAG microsatellite repeat reported to inhibit NF-kB phosphorylation, antagonise IRF5 and prevent the nuclear translocation of DAMP HMGB-1 (Gao et al., 2017; Nie et al., 2019; Zhang et al., 2022). Given their differing mechanisms and enhanced combinatorial suppression from heterotypic Type2+3 dsDNA elements (see Figure 4.7), it was hypothesised that combining these ODNs may generate additive or synergistic suppressive effects. A minimum total ODN load of 0.56uM and a maximum of 5.6uM were used alongside intermediate concentrations of 2.24uM and 3.92uM. These four values were divided equally between M14 and M16 to generate a full factorial design with varying: 1) M14:M16 ratios and 2) total ODN load as shown in Table 5.2.

Table 5.2) Factorial design of M14:M16 ODN combinations. Individual M14 and M16 concentrations of 0.28uM, 1.12uM, 1.96uM and 2.78uM were combined to calculate all potential combinations including equimolar (grey), M14 biased (orange) and M16 biased (green) loads. Colour gradients represent increasing final concentrations.

		M14 (uM)			
		0.28	**1.12**	**1.96**	**2.78**
M16 (uM)	**0.28**	0.56	1.40	2.24	3.06
	1.12	1.40	2.24	3.08	3.90
	1.96	2.24	3.08	3.92	4.74
	2.78	3.06	3.90	4.74	5.56

Four M14 and M16 combinations of equal molarity were compared to M16 alone using the post-incubation system described previously. 400ng pDNA was nucleofected and incubated with ODN for 24hrs, with TNFa production relative to a 'pVAX1 only' control, shown in Figure 5.4A. These data found M16 alone was always

more suppressive than M14:M16 combinations of equal load except at 0.56uM. The remaining 12 combinations were paired to compare the effects of an M14 bias vs M16 bias of the same total ODN load (Figure 5.4B). For example, a total concentration of 1.4uM had an M16 biased combination (M14 0.3uM: M16 1.1uM) and an M14 biased combination (M14 1.1uM: M16 0.3uM). Although trends were difficult to identify the data suggested i) ratios favouring M16 were generally more suppressive at each total load, ii) there was no clear correlation between TNFa suppression and total ODN load, iii) combining M14:M16 had no additive/ synergistic effects and iv) no combination exceeded the maximum suppression observed from M16 alone at 2.24uM (FC ~0.68).

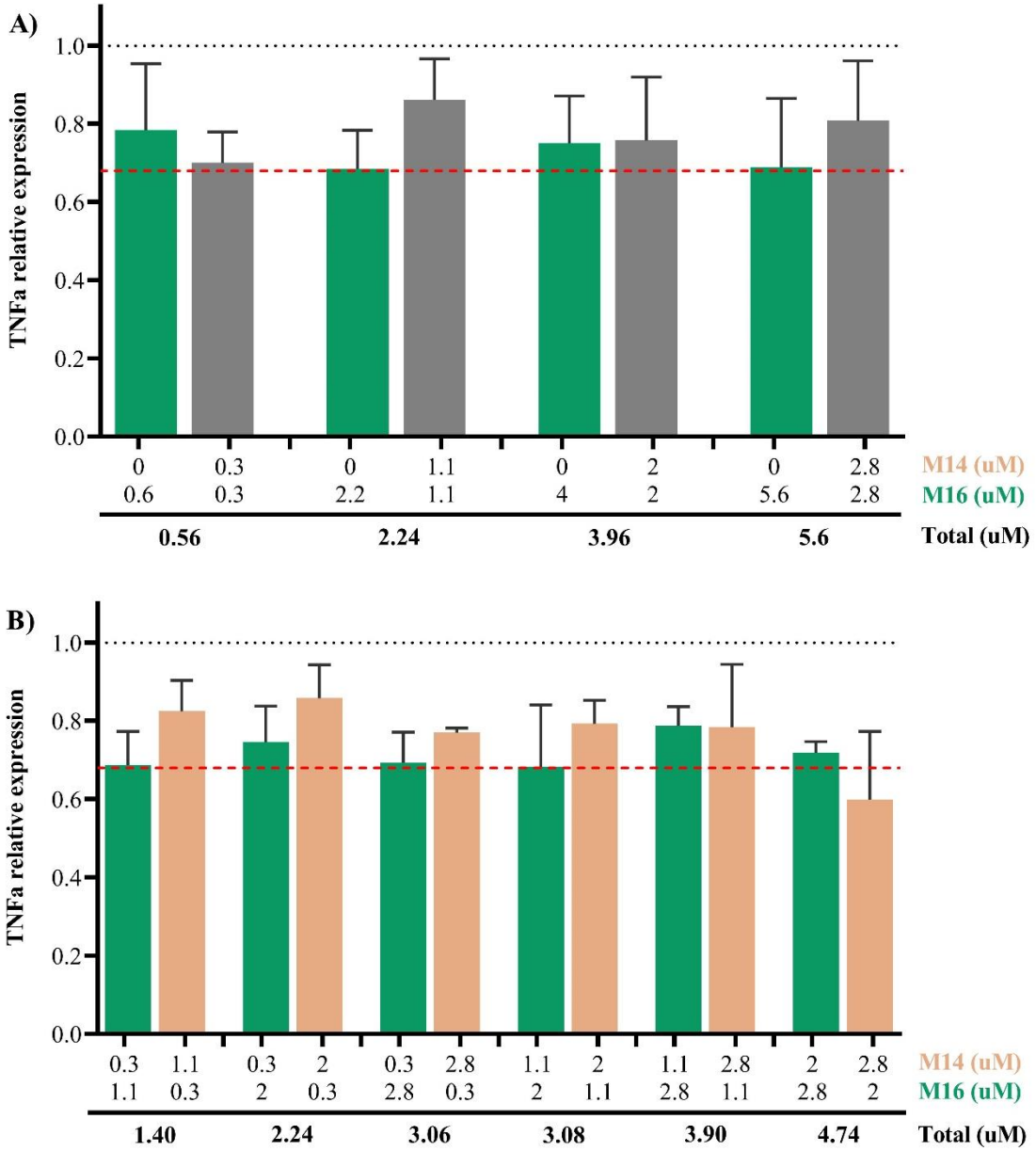

Figure 5.4) M14:M16 ODN combinations were less suppressive than M16 alone. 400ng pVAX1 DNA was nucleofected into 400,000 DC2.4 cells and post-incubated with ssODNs at combinations and concentrations described. TNFa production relative to a 'pVAX1 only' control is shown (black line FC 1.0). A) M16 ODN concentrations (green) compared to M14:M16 load of equal molarity (grey). The maximal suppression observed with M16 alone is represented (dashed red line at ~0.68). B) M14 and M16 combinations at unequal molar ratios but equal ODN load were paired, with M16 bias (green) and M14 bias (orange) shown. In A and B bars represent mean +SD for two biological replicates in technical duplicate.

ODN co-transfection was ineffective compared to post-transfection

Although pDNA transfection followed by 24hr post-incubation with ODN effectively reduced immune stimulation within the system described, a delivery combining administration would be simpler, cheaper, and more applicable for industrial use. A recent study investigating ISD stimulation suggested lipofectamine based co-transfection may enhance ODN activity (Valentin et al., 2021). Although the dynamics of nucleofection based transfection vary compared to chemical methods, a co-transfection was investigated using M16 (the most effective ODN identified thus far) and positive control CpG ODN C 2395. A concentration range between 0.056–2.24uM was tested to prevent overloading the co-transfection system during preliminary investigations, with TNFa production relative to a 'pVAX1 only' control quantified at 24hrs (Figure 5.5). These data show mock transfected controls (no DNA) behaved as expected relative to each other, with C 2395 exhibiting ~3.4-fold more stimulation than M16 at the highest ODN load of 2.24uM. When compared to similar controls from the post-incubation system described earlier (see Figure 5.1A) C 2395 was 2-fold more immune-stimulatory within a co-transfection context, and M16 4-fold more, despite using only half as much ODN. In the presence of pVAX1, C 2395 and M16 were neutral at 0.056uM, suggesting the positive control was not within its working concentration. As ODN load increased, both sequences became immune-stimulatory although CpG more so than M16. Taken together, these data suggest the co-transfection delivery system was inherently more stimulatory than post-incubation, with no observable ODN suppression of pDNA responses, but some sequence dependent immune stimulation.

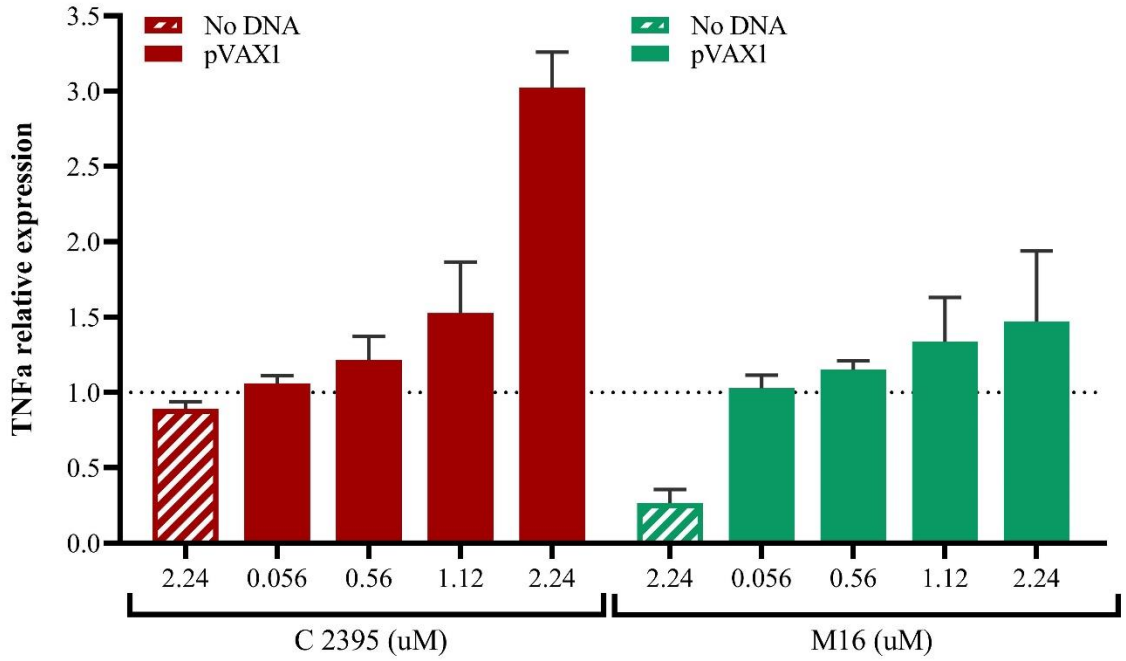

Figure 5.5) Nucleofection based co-transfection did not produce suppressive effects. 400ng pVAX1 DNA and ODNs at concentrations described were nucleofected into 400,000 DC2.4 cells and incubated for 24hrs. TNFa production relative to a 'pVAX1 only' control is shown (line at FC 1.0) for C 2395 ODN (red) and M16 ODN (green) and mock transfected 'no DNA' controls (patterned). All bars represent mean +SD for two biological replicates in technical duplicate.

5.2.3 Investigating M16 suppression dynamics

M16 thresholds TNFa production to ~250pg/ml during pVAX1 titration

Thus far, from the ODN sequences, concentrations and combinations screened, post-incubation of M16 at 2.24uM was identified as the most effective, reducing TNFa and IFNb production from pDNA by 30-40%. To better understand the interplay between M16 and pDNA, a pVAX1 titration between 50-400ng was performed and found TNFa production to increase with DNA load, as expected (Figure 5.6A). Below 200ng, no statistically significant effect on TNFa was observed in the presence of M16 at 2.24uM. At 200ng and above however, M16 consistently reduced TNFa production to a threshold of ~250pg/ml. The same data was re-analysed to better understand the relative effects of M16 at each pDNA load (Figure 5.6B). These results show M16 induced some suppression (~15%) of TNFa between 0-100ng of pVAX1. Interestingly, the introduction of 200ng pVAX1 significantly potentiated the suppressive capacity of

M16 to ~33%, with increased pDNA load further increasing M16 relative suppression up to ~40%. These findings suggest i) M16 required a minimum level of immune activation (~150-250pg/ml) to induce significant downregulation, ii) M16 was thresholding TNFa production to ~250pg/ml irrespective of total plasmid immunogenicity and iii) the relative suppressive effects of M16 varied.

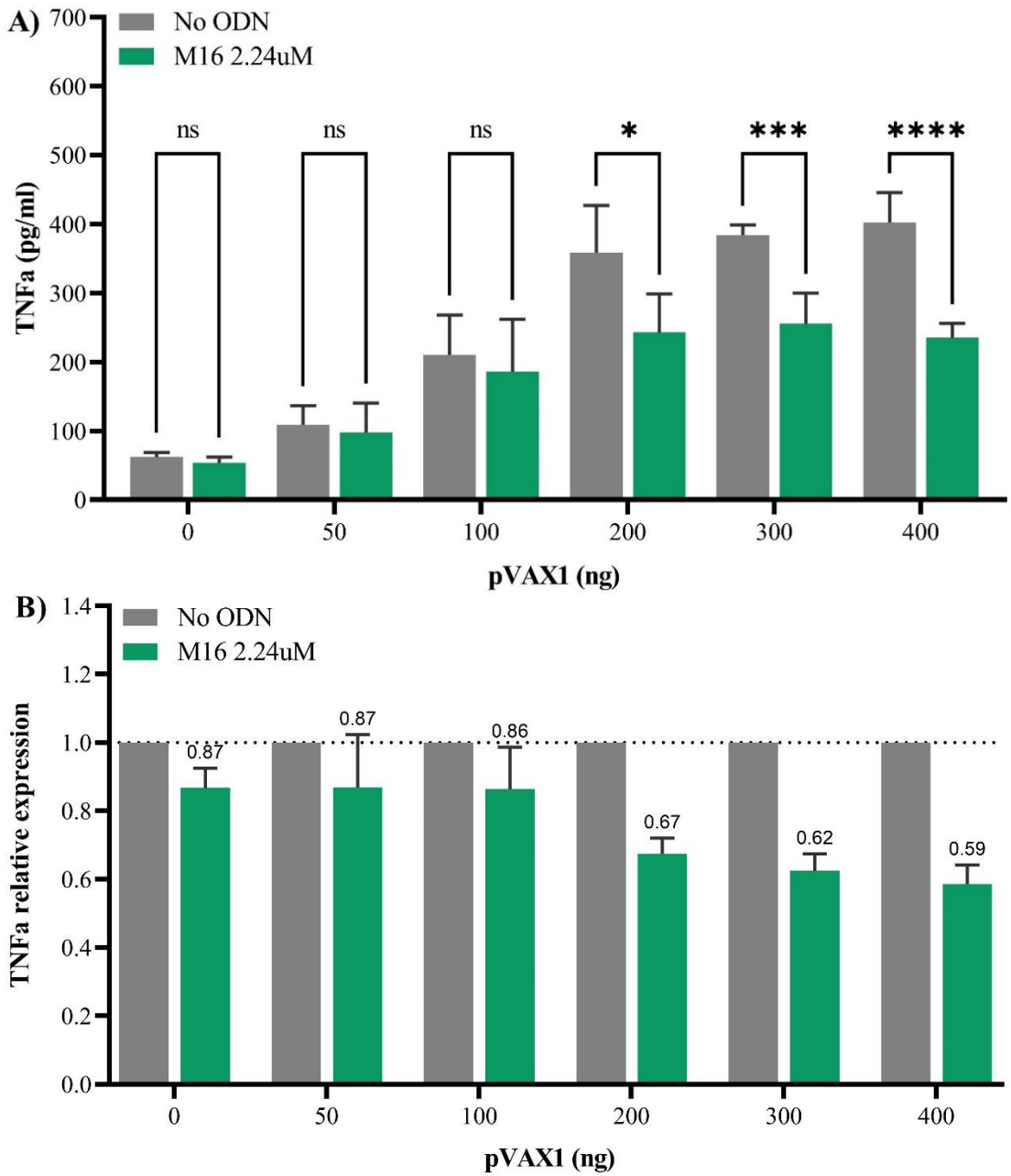

Figure 5.6) M16 suppresses pVAX1 at 200ng and above. pVAX1 at varying DNA loads was nucleofected into 400,000 DC2.4 cells and post-incubated without ODN or with M16 at 2.24uM for 24hrs. A) Absolute TNFa production (pg/ml). Statistical significance was defined as p≤0.05 (*=p≤0.05, **=p≤0.01, ***=p≤0.001, ****=p≤0.0001) and non-significance denoted 'ns'. B) Relative effect of pVAX1 with M16 compared to a 'pVAX1 only' control. In A and B bars represent mean +SD for three biological replicates in technical duplicate.

M16 thresholds TNFa production to ~250pg/ml at 4hrs and onwards

To further investigate the mechanism of M16 thresholding, a time-course analysis of TNFa production between 2-12hrs from 400ng pVAX1 in the presence and absence of M16 (2.24uM) was conducted (Figure 5.7). At 2hrs, M16 had little effect. As TNFa levels increased to ~300pg/ml at 4hrs however, suppressive activity was observed limiting cytokine production to ~250pg/ml even as the 'No ODN' control increased to over 450pg/ml at 24hrs. These findings further support the theory that M16 required a minimal level of TNFa activation (~150-250pg/ml) before limiting cytokine production, regardless of the overall system immunogenicity.

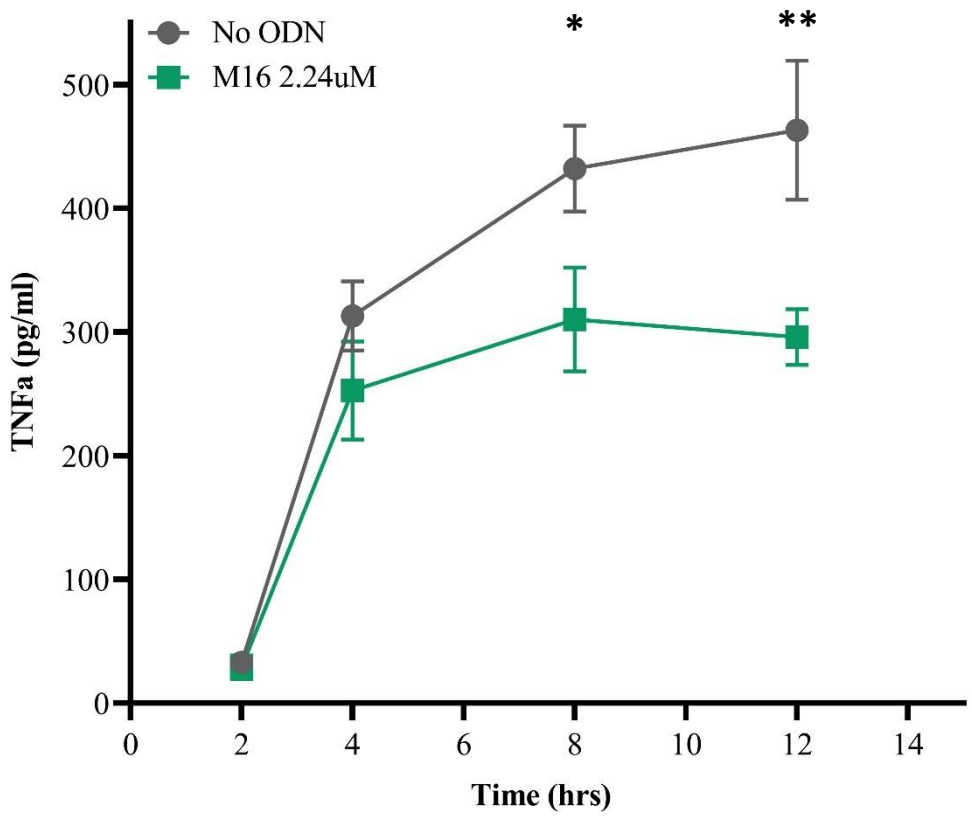

Figure 5.7) M16 suppression plateaus TNFa production over 12hrs. pVAX1 was nucleofected into 400,000 DC2.4 cells and post-incubated without ODN (grey) or with M16 ODN at 2.24uM (green) for 24hrs. Absolute TNFa production (pg/ml) is shown at 2hrs, 4hrs, 8hrs, and 12hrs. Points represent mean +SD for three biological replicates. Statistical significance was defined as p≤0.05 (*=p≤0.05, **=p≤0.01, ***=p≤0.001, ****=p≤0.0001) and non-significance denoted 'ns'.

M16 counteracts CpG stimulating effects across different vectors

To determine whether these observations were specific to pVAX1, M16 was screened against five additional vectors, each with varying CpG content, within two backbone contexts (Figure 5.8). The first vector backbone used pVAX1 derived plasmids including i) 'pVAX1' as described thus far with 251 CG dinucleotides, ii) synthetically engineered immune-stimulatory 'pVAX1-CpG' with 392 CG dinucleotides and iii) a 600bp promoter excised 'pVAX1-cmv' with 219 total CG dinucleotides. The second vector context included three AstraZeneca supplied CpG engineered plasmids: i) CpG-H with 123 CG dinucleotides, ii) CpG-M with 42, and iii) CpG-0 with all CG dinucleotides removed. Although some vectors varied in size, DNA load was normalised to transfect 400ng of each plasmid in the presence or absence of M16 (2.24uM) for 24hrs, which TNFa production relative to a 'pVAX1 only' control quantified for continuity.

In the absence of M16, these data show a clear correlation between the CG dinucleotide content of each vector and the magnitude of TNFa expression, as supported by the literature (Figure 5.8A) (Su et al., 2017; Yu et al., 2015). The ~2.5-fold increase in TNFa from pVAX1-CpG (392) compared to pVAX1 (251), despite only a 1.5-fold increase in CG content, was likely due to the design of these dinucleotides within flanking regions associated with high immunogenicity (CpG-stimulatory motifs) (see 1.2.1). AZ CpG-0 vector produced ~300pg/ml TNFa despite removal of all CG dinucleotides representing the CG independent immune response to pDNA and confirming CG removal alone was not sufficient to completely evade immune activation. Addition of M16 to these vectors caused consistent downregulation of TNFa by ~30-40%, equivalent to ~290-370pg/ml, further supporting the M16 thresholding phenomenon observed thus far (Figure 5.6A and Figure 5.7). Given the CG specific differences within identical vector contexts (e.g., pVAX1 vs pVAX1-CpG and AZ CpG-0 vs CpG-M) these results show M16 specifically counteracted CpG-specific immune activation either directly (inhibiting receptor binding) or indirectly (inhibiting signalling/effector molecules), reducing TNFa levels across all plasmids to those of CpG free pDNA.

To quantify the sequence dependent impact of M16, each vector was normalised to its 'no ODN' control (Figure 5.8B). This method of analysis helps reduce biological noise between samples, allowing better observation of trends in vectors treated with M16 compared to those without. These results show vectors of higher immunogenicity induced statistically significant downregulation of TNFa in the presence of M16, with non-significant effects from AZ CpG-M and CpG-0. The relative suppressive effect of M16 was dependent on CG abundance, with ~70% downregulation in pVAX1-CpG (392), followed by ~40% in pVAX1 (251), ~30% in pVAX1-cmv, ~20% in AZ CpG H (123), 10% in AZ CpG M (42) and ~5% in CpG 0 (0).

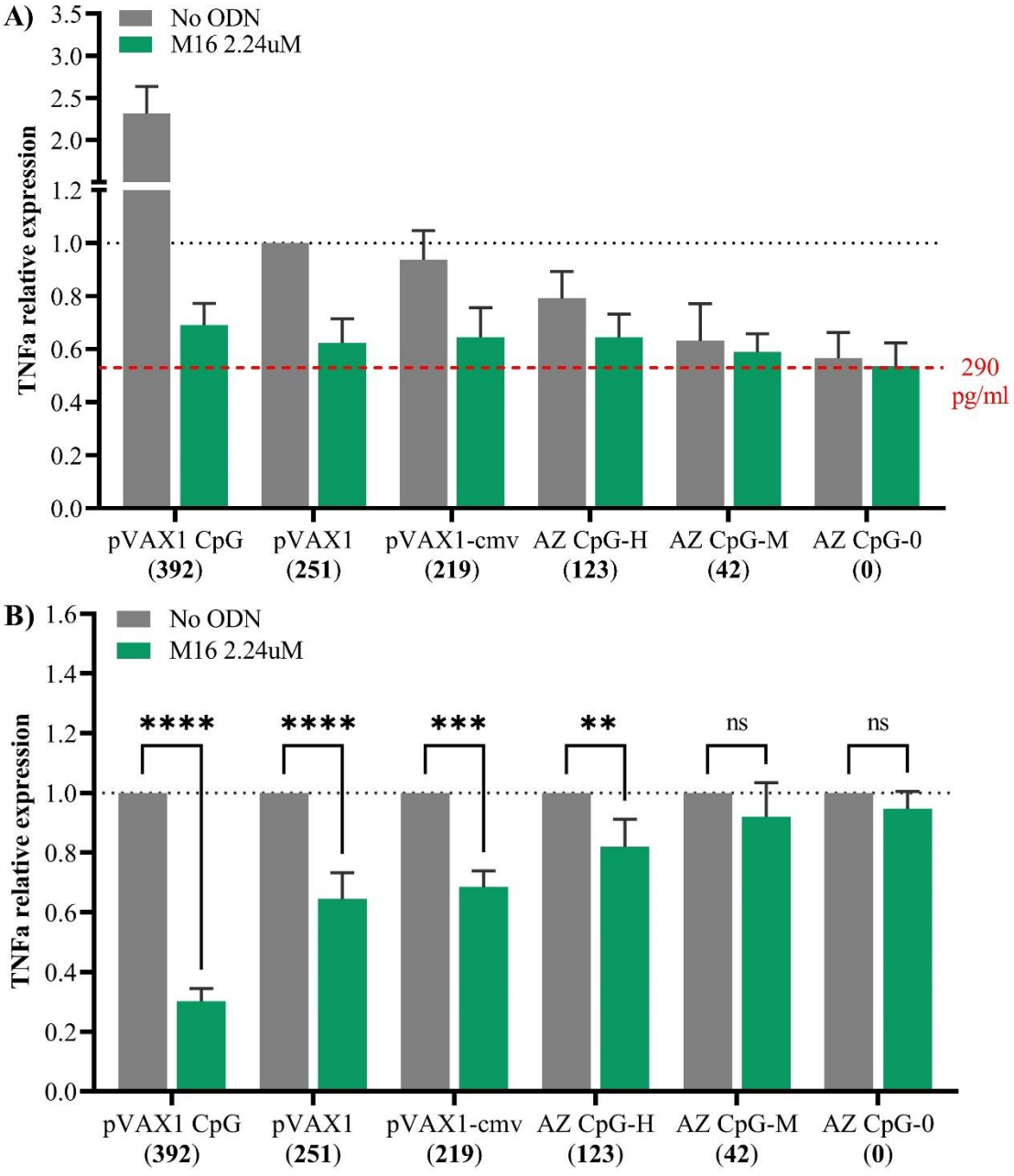

Figure 5.8) M16 counteracts CpG dependent TNFa production. 400ng vector DNA was nucleofected into 400,000 DC2.4 cells and post-incubated with no ODN (grey) or with M16 ODN at 2.24uM (green) for 24hrs. A) TNFa production relative to a 'pVAX1 only' control (black line at FC 1.0). The absolute production of CpG-free DNA at 300pg/ml was highlighted (red line FC at ~0.57). B) M16 TNFa production relative to no ODN controls from each vector. Statistical significance was defined as p≤0.05 (*=p≤0.05, **=p≤0.01, ***=p≤ 0.001, ****=p≤0.0001) and non-significance denoted 'ns'. In A and B bars represent mean +SD for four biological replicates in technical duplicate.

M16 downregulates multiple immune response pathways

To better understand the immune pathways targeted by M16, a Nanostrings analysis was conducted to quantify and characterise its impact across multiple pDNA upregulated pathways (see chapter 3). Cells were transfected with pVAX1 and incubated for 8hrs without ODN or with M16 (2.24uM). RNA analysis using immune-profiling tool Nanopanel found M16 to reduce average expression across 30 immune response genes by an average of ~30%, relative to a 'pVAX1 only' control (Figure 5.9A). The application of a 20% significance threshold found 20/30 genes were downregulated within the panel. A more granular analysis found all 30 were downregulated to some extent, with 40-60% suppression in the production of antivirals *(rsad2, ifit1c, cmpk2),* chemokines *(cxcl10, ccl12),* and PRRs (*ifi205, pyhin1*), demonstrating M16 suppresses a broad range of immune pathways, not just Th1 associated TNFa (Figure 5.9B). Furthermore, with a ~40% reduction in *tnfa* detected, changes in protein production were clearly reflected during gene detection. Taken together, these results describe the sequence specific immunosuppressant effects of M16, reducing pDNA driven responses in DCs.

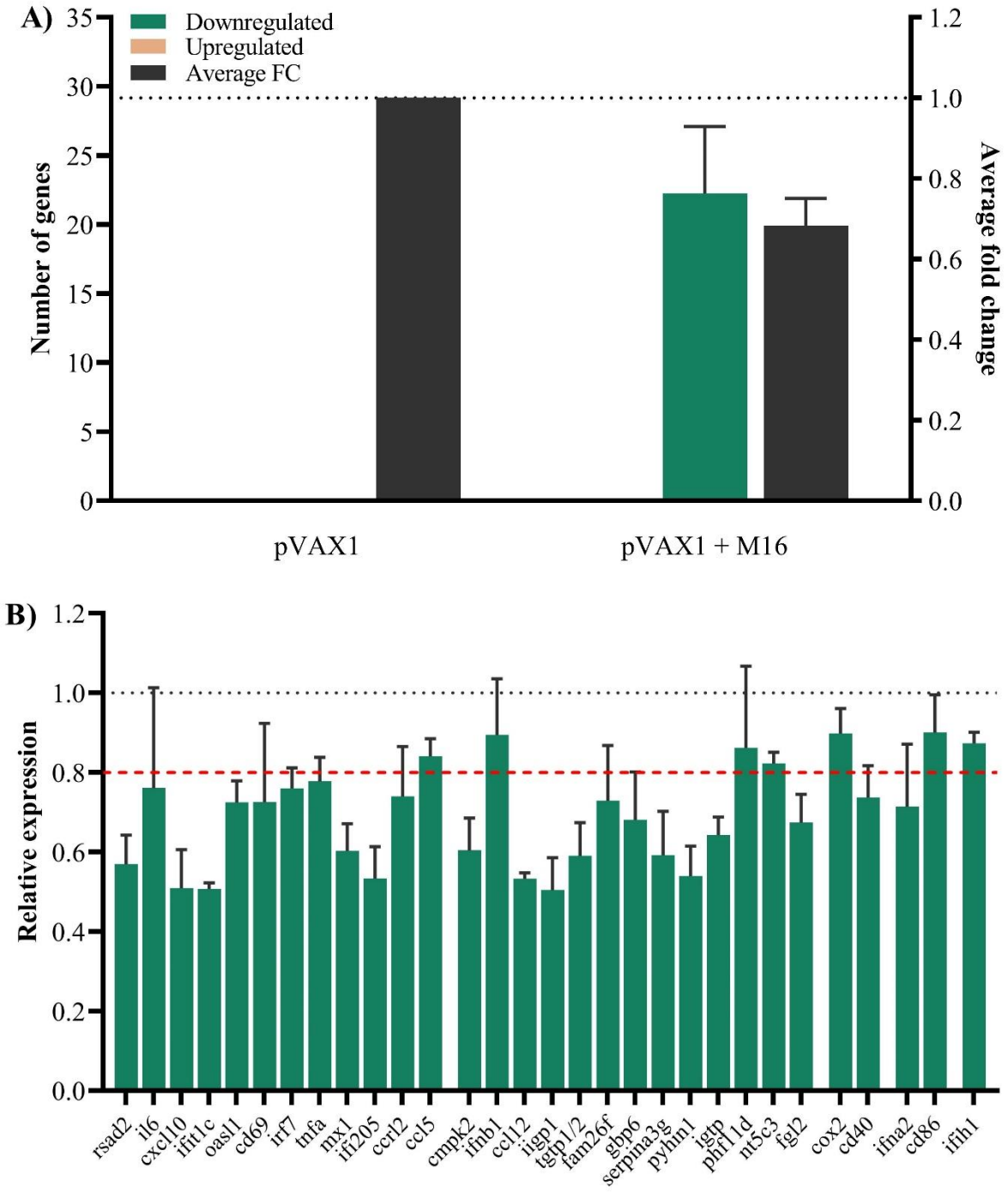

Figure 5.9) M16 downregulates multiple immune-response genes. 400ng pVAX1 DNA was nucleofected into 400,000 DC2.4 cells and post-incubated without ODN or with M16 at 2.24uM (green) for 8hrs. RNA was harvested and analysed using Nanostrings immune-profiling tool Nanopanel. A) Overall average fold change of 30 immune-profiling genes relative to pVAX1 (average FC 1.0), and the number of up/ downregulated genes (20% threshold). B) Relative expression of 30 immune-profiling genes relative to pVAX1 (black line at 1.0). The 20% downregulation threshold (FC 0.8) was highlighted (red line). Bars represent mean +SD across four biological replicates.

5.2.4 Investigating M16 in human dendritic cell line CAL-1

The application of immune-suppressive technology for gene therapy treatment requires testing in both mouse and human cell lines (AstraZeneca, Cambridge, UK). Thus far, M16 has been found to significantly suppress pDNA induced immune activation by ~40% in vaccine vector pVAX1, and over 70% in positive control vector pVAX1-CpG. Investigations of pDNA immunogenicity within human DCs remain limited due to the experimental limitations of using primary cells including; high costs, restricted availability, heterogenous phenotypes and transfection difficulties (Kaur and Dufour, 2012). Immortalised human DCs present a more suitable, cost-effective, and user-friendly alternative for an M16 reduction to practise. Nevertheless, they face their own challenges, including persistent impairment of immune detection and response pathways during the immortalisation process, which can result in immune-tolerance (Rasaiyaah et al., 2017; Tapia-Calle et al., 2017). CAL-1, a recently established human lymphoma derived pDC model, was confirmed to upregulate cytokine production (TNFa, IL-6, IFNs) during incubation with immune-stimulatory ODNs and was successfully nucleofected using an optimised transfection method similar to that of DC2.4 (Maeda et al., 2005; Meng et al., 2011; Steinhagen et al., 2013). This model was therefore selected to investigate whether i) CAL-1 cells had the capability to detect and respond to pDNA, and ii) confirm whether M16 suppression translated to a human system.

Of note, literature investigations of CAL-1 responses to ODN typically involved 'starvation' for 16hrs in which cells were incubated in 0.1% FBS (rather than the standard 10%) overnight, prior to exposure with ODN (Steinhagen et al., 2013, 2016). This process induces cell synchronisation, increases ODN uptake and transfection efficiencies. Given DC2.4 cells were not 'starved', the effects of this method were also interrogated within this CAL-1 model.

pVAX1 nucleofection did not stimulate TNFa production in CAL-1

CAL-1 cells were starved of FBS (0.1%) prior to pDNA transfection/ ODN incubation. pDNA was titrated between 0-1200ng and incubated with 1) no ODN, 2) C 2395 ODN 2.24uM and 3) M16 ODN 2.24uM for 24hrs (Figure 5.10). Across all four conditions, GFP fluorescence increased with pDNA concentration, confirming nucleofection was both successful and effective with maximum transfection efficiencies between 55-70% (Figure 5.10A). Mock transfection controls (no DNA) produced the same basal level of fluorescence (relative fluorescence units ~50 000) across M16 and C 2395 only conditions, confirming addition of ODN did not contribute to background fluorescence. Unexpectedly, ODN incubation seemed to improve GFP expression from pDNA, causing a 10% increase in transfection efficiency with M16 at 1200ng pVAX1 and a 15% increase with C 2395. This suggests ODNs may exert a sequence-dependent effect on pDNA gene expression within the CAL-1 system. Given the novelty of this pDNA interrogation within CAL-1, similar studies measuring ODN effects on pDNA transfection efficiency/ transgene expression could not be compared.

Although nucleofection was successful, subsequent measure of TNFa protein production found CAL-1 to be unresponsive to pDNA without ODN (Figure 5.10B). The addition of M16 had no discernible modulatory effects which was unsurprising given a minimum TNFa level was necessary to observe suppressive activity in the DC2.4 system (see Figure 5.6A) Positive control C 2395 induced a pDNA independent TNFa upregulation of ~3-fold, confirming CAL-1 could both detect and respond to immune-stimulatory CpG-ODN. Interestingly, transfection with 1200ng pVAX1 followed by C 2395 incubation further increased TNFa production that, although statistically non-significant, suggests CAL-1 may be capable of some pDNA detection in a more heightened immune state. This theory was tested using highly immunogenic pDNA vectors pVAX1-CpG (392).

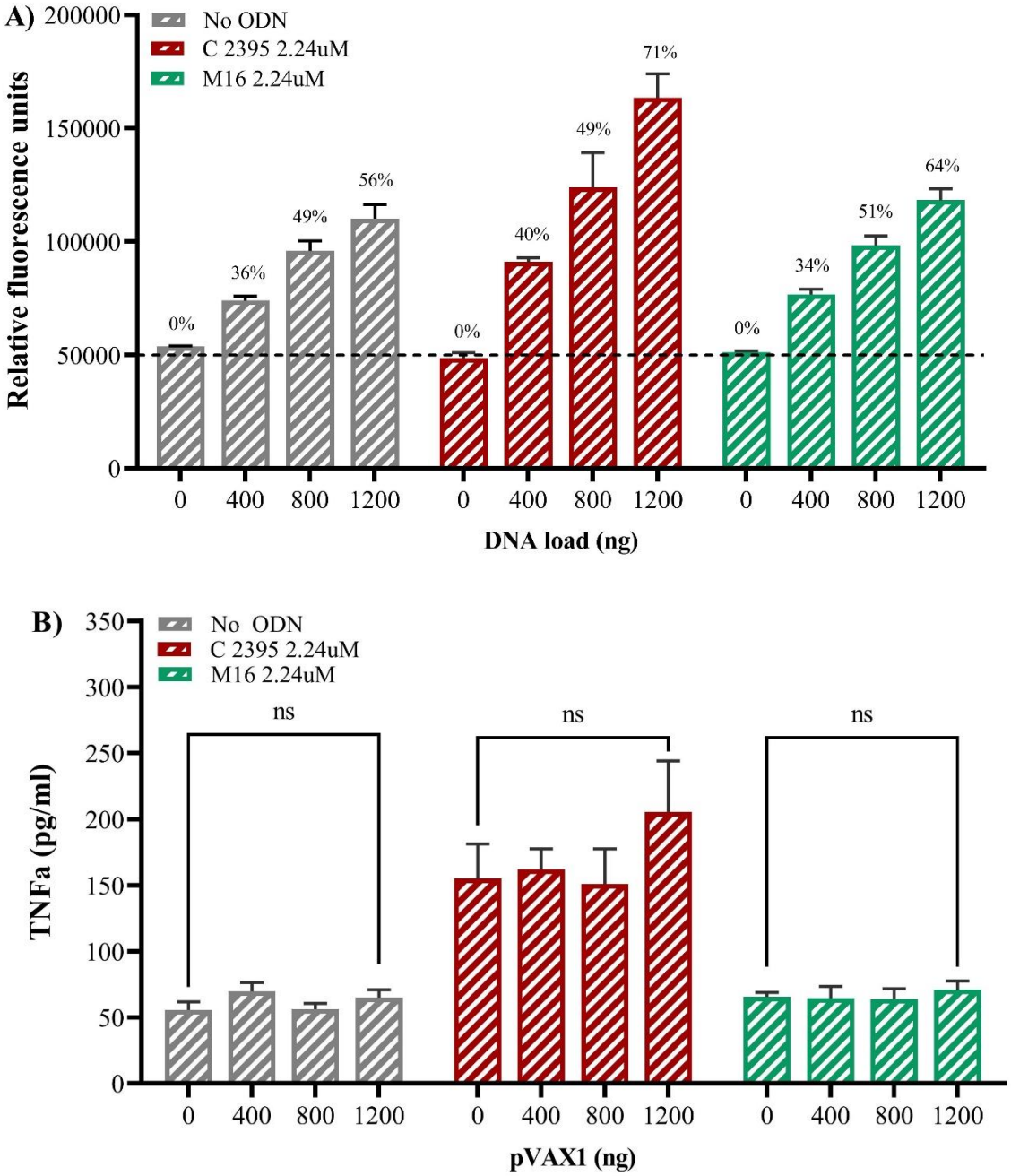

Figure 5.10) pVAX1 nucleofection produced GFP but not TNFa in CAL-1. 1.5 x 10^6 CAL-1 cells were serum starved (FBS 0.1%) for 16hrs prior to nucleofection with varying pDNA loads followed by 24hr incubation with no ODN (grey), C 2395 ODN (red) or M16 ODN (green). A) Relative fluorescence units and transfection efficiencies (denoted as percentages). B) Absolute TNFa production (pg/ml). In A and B bars represent mean +SD for two biological replicates in technical duplicate. Statistical significance was defined as p≤0.05 (*=p≤0.05, **=p≤0.01, ***=p≤0.001, ****=p≤0.0001) and non-significance denoted 'ns'.

pVAX1-CpG nucleofection stimulated TNFa production in CAL-1

To confirm whether CAL-1 could detect and respond to pDNA, highly immunogenic vector pVAX1-CpG (392) was transfected at 2000ng and incubated with either no ODN, C 2395 or M16 at 2.24uM for 24hrs (Figure 5.11). A significant increase in TNFa was detected in all three conditions at ~3.5-FC, ~7-FC and ~2.5-FC respectively, confirming CAL-1 could respond to pDNA at a high enough concentration/ CpG motif content. In terms of absolute values however, for 'no ODN' and 'M16 ODN', TNFa levels remained too low to observe potential M16 dependent immune modulation. Unexpectedly, incubation with C 2395 increased TNFa levels to >1000pg/ml in the presence of pVAX1-CpG (392) DNA, suggesting the presence of both CpG-ODN and a CpG high plasmid had synergistic effects on immune-activation. From these data it is clear CAL-1 can minimally detect pDNA, increasing TNFa in correlation with vector immunogenicity. However, given how small these absolute values were, CAL-1 pDC does not seem to be an appropriate system for the characterisation of pDNA effects on immunity, nor for testing M16 vector suppressing effects within a human system.

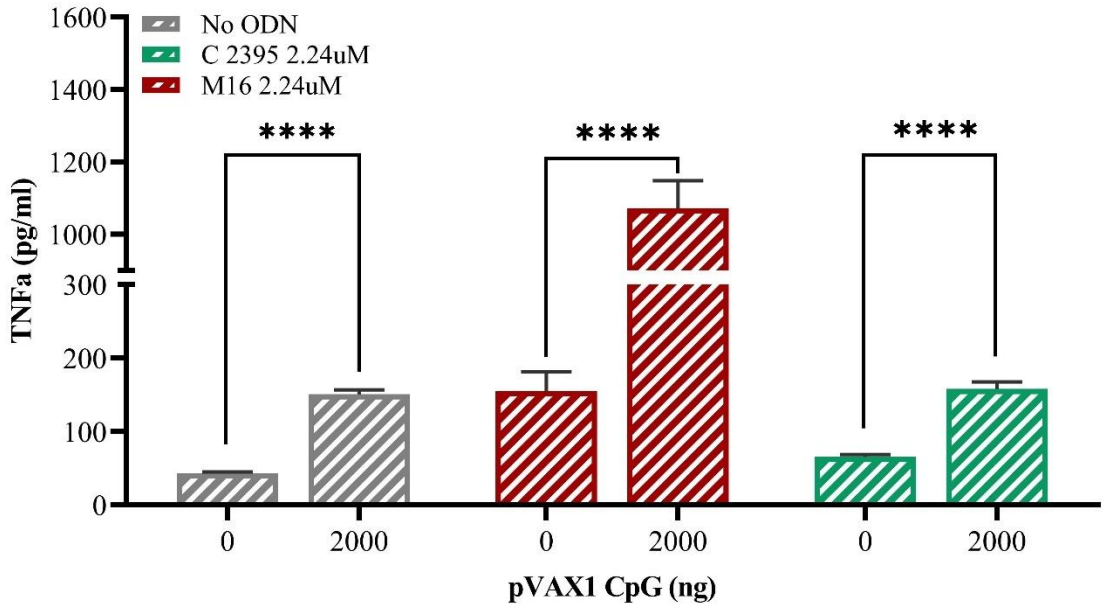

Figure 5.11) pVAX1-CpG nucleofection stimulated TNFa production in CAL-1. 1.5 x 10^6 CAL-1 cells were serum starved (FBS 0.1%) for 16hrs prior to nucleofection with 2000ng pVAX1-CpG followed by 24hrs incubation with no ODN (grey), C 2395 ODN (red) or M16 ODN (green). Absolute TNFa production (pg/ml) is shown. Each bar represents the mean +SD for three biological replicates in technical duplicate. Statistical significance was defined as p≤0.05 (*=p≤0.05, **=p≤0.01, ***=p≤0.001, ****=p≤ 0.0001) and non-significance denoted 'ns'.

Significant M16 suppression was observed in 10% but not 0.1% FBS conditions

In a final attempt to determine whether CAL-1 was capable of detecting M16, the system was modified to include immunogenic CpG-ODN. Although this would mask M16 pDNA effects, the detection of any suppressive activity would help determine whether human DCs were capable of M16 detection, laying the foundation for future optimisation. To examine this, cells were tested in two conditions: 0.1% FBS or 10%FBS, before nucleofection with 2000ng pVAX1-CpG and 24hr post-incubation with ODNs i) M16 (2.24uM), ii) CpG (2.24uM) or iii) equimolar M16: CpG (2.24uM each) (Figure 5.12). A consistent reduction of ~20% GFP expression and ~10-20% transfection efficiency was observed in 10% FBS compared to 0.1% FBS conditions, supporting the standardised use of serum-starvation in CAL-1 to improve cellular uptake (Figure 5.12A) (Steinhagen et al., 2012a, 2016). These trends were magnified in TNFa production, with an average reduction of ~30-50% in 10% FBS compared to 0.1% FBS conditions, within different ODN environments (Figure 5.12B). By comparing TNF levels from C 2395 (2.24uM) to M16: C 2395 (2.24uM each), a downregulation in both conditions was detected, although only non-starved cells were statistically significant, with a ~40% relative decrease (FC 0.63), aligning with previous DC2.4 findings. These data suggest human pDCs to be capable of not only detecting M16 ODN but also responding to its suppressive activity, aligning with previous studies reporting M16 counteraction of CpG-1826 (class-B ODN) stimulation of IFNa from human BMDCs (Sun et al., 2010).

Although serum starvation does improve transfection efficiencies, its impact as an 'environmental stressor' is known to alter cellular activity (Codeluppi et al., 2011). Although poorly understood, starvation of human PBMCs has been found to alter immunoregulatory pathways and lymphocyte populations, causing upregulation of Treg and CD4+ T cell populations (Rahmani et al., 2018). The change in FBS conditions and inclusion of both CpG-ODN and pVAX1-CpG (392) was necessary to better interrogate M16s effects in CAL-1, however data must be considered cautiously given the introduction of multiple variables. These findings do, however, suggest

human pDCs are capable of interacting with M16 ODN, resulting in condition-specific suppression of TNFa from CpG stimulated response pathways.

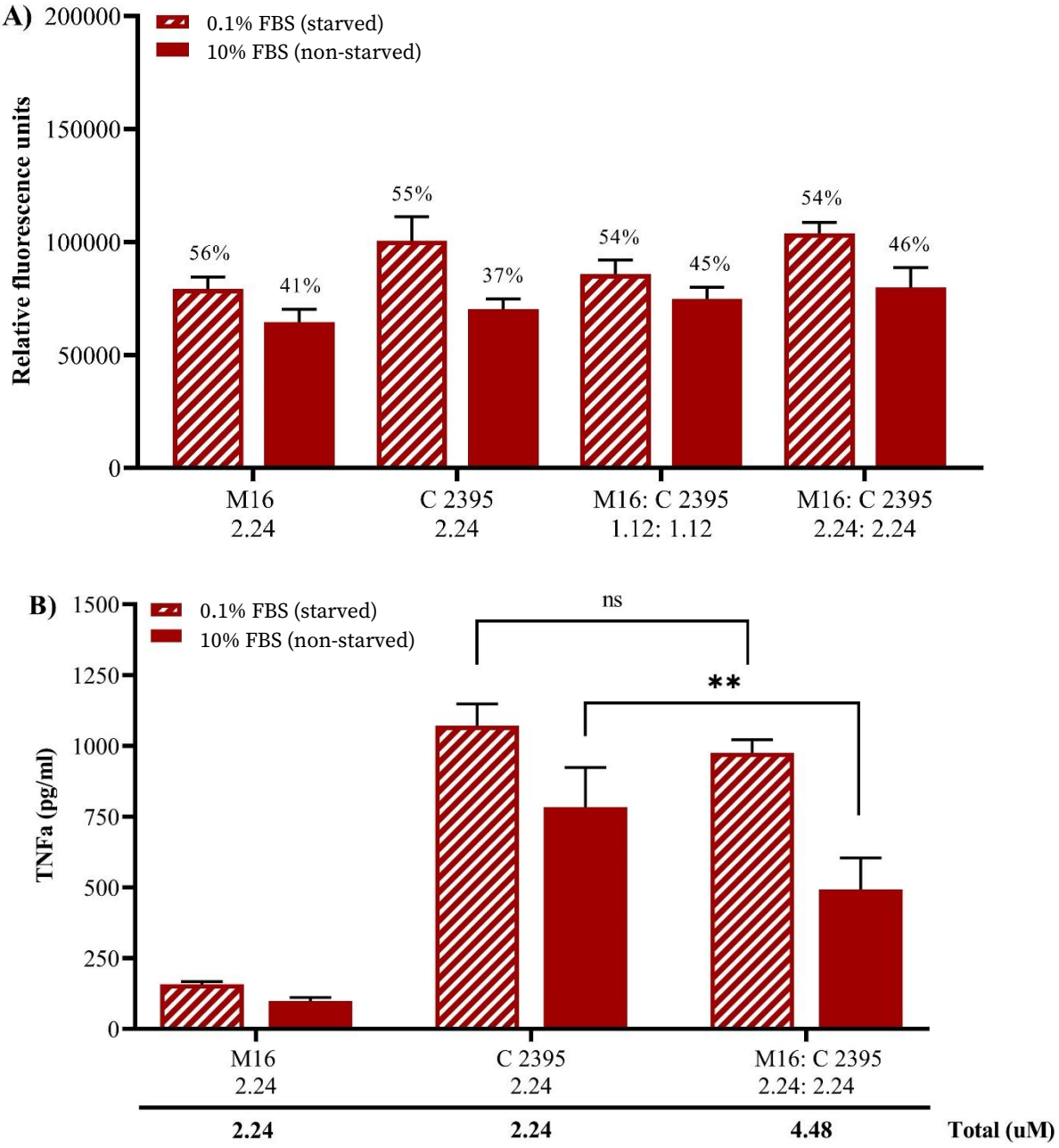

Figure 5.12) M16 ODN induced significant suppression in 10% FBS conditions but not 0.1% FBS conditions. 1.5 x 10^6 CAL-1 cells were serum starved (FBS 0.1%) or non-starved (FBS 10%) for 16hrs prior to nucleofection with pVAX1-CpG followed by 24hr incubation with ODNs of interest. A) Relative fluorescence units and transfection efficiencies (denoted as percentages). B) Absolute TNFa production (pg/ml). In A and B bars represent mean +SD for three biological replicates in technical duplicate. Statistical significance was defined as p≤0.05 (*=p≤0.05, **=p≤0.01, ***=p≤0.001, ****=p≤ 0.0001) and non-significance denoted 'ns'.

5.3 Discussion

5.3.1 pDNA modulating ODNs

pDNA presents a versatile vector and delivery method for use in gene therapy treatments. Depending on the application, its inherent immunogenicity can be advantageous (augmenting immune activation in vaccine therapies) or deleterious (compromising safety and efficacy of gene therapies). With over 88 suppressive motifs reported within the literature, six were found to have statistically significant effects in dsDNA form (from chapter 4) and so were selected for characterisation in ODN form, with M12 (had the lowest coefficient value and so suppressive effect) replaced with M1. Findings from this chapter describe the first ever investigation of immune-modulatory ODNs as pDNA immune-modulators, characterising a toolbox of sequences for application across a range of DNA-based therapeutics. M1 and M13 offer Th1-specific TNF-a upregulation at 5.6uM with minimal effects on IFNb, providing pathway specific targeting beneficial for DNA vaccine applications (Morrow et al., 2010). Alternatively, M14 and M16 exhibit significant downregulation across both cytokines, offering a more generic solution for the suppression of gene therapy vector activated response pathways. M1 was included to compare how this Type1 ODN (the most comprehensively characterised suppressive motif within the literature) behaved with a native PS backbone in this novel system (Gursel et al., 2003). At working concentrations of ≥0.56uM, M1 had neutral or even stimulatory effects on TNFa production despite reports of suppression across multiple immune pathways (TLR9, AIM2, signalling molecules), including a reduction in both TNFa and IFNb mRNA transcripts from exposure to immune-stimulation linear double-stranded poly(dA:dT) (Bayik et al., 2016; Kaminski et al., 2013). These inconsistencies with the literature may be a result of system dependent variation in ODN activity as discussed earlier (see section 4.3) suggesting M1 and by extension all G-rich ODNs may be unable to downregulate pDNA stimulated immune responses in the murine DC2.4 cell line (Fang et al., 2011).

Variation from literature observations were also demonstrated in the extreme immune modulation (TNFa high, IFNb low) of commonly used ‘negative control’ ODN

N 2395 (Invivogen, San Diego, CA). Given the only difference in nucleotide sequence between N 2395 and positive control C 2395 was the substitution of a CpG dinucleotide to GpC, the data suggests system-specific variation from GpC-ODNs. Interestingly, counteraction between TNFa and IFNb has been proposed as a cross-regulatory mechanism to maintain cellular homeostasis, with shifts in cytokine production beyond a certain threshold contributing to immune disorders such as SLE (IFNb upregulation, TNFa downregulation) or RA (TNFa upregulation, IFNb downregulation) (Cantaert et al., 2010). This interplay exploits use of IFN suppressors for SLE treatment and TNFa suppressors for RA treatment, the former of which is enriched within the ODN toolbox screened (all motifs at 0.56uM and N 2395, M1, M14 at 5.6uM). Furthermore, this theory account for the extreme effects observed from N 2395 with low ODN concentration (<0.56uM) enabling a GpC dependent reduction of IFNb whilst higher ODN concentrations (~5.6uM) shift the system beyond an equilibrium threshold, positively upregulating TNFa by ~7.5-fold whilst downregulating IFNb to ~0.02-fold. These findings also demonstrate the challenge in designing appropriate negative ODN controls, with sequence and system specific effects that can be difficult to predict. Of note, Type2 GpC-ODNs tested within the pDNA integrated system of chapter 4 had no significant immune-modulatory effects, although this may be due to significantly higher motif: pDNA ratios described within this ODN system.

5.3.2 Application of M16

Currently, common approaches to reduce vector immunogenicity involve the removal of CG dinucleotides from vector backbone and functional units (Yew et al., 2000). AZ supplied vectors tested within this chapter were engineered to remove these CpGs whilst preserving functionality of control elements. Although promoter activity was retained, intragenic CG removal prevented mRNA translation, inhibiting production of the mCardinal reporter protein in the AZ-CpG (0) vector (AZ unpublished data). This example further highlights the requirement for alternative strategies to retain CpG motifs whilst counteracting their detrimental immune-activating effects for use across DNA therapeutics. Within this system, M16 was found

to be the most effective ODN, thresholding TNFa production to ~250-300pg/ml across increasing DNA load and vector immunogenicity, with a maximum relative downregulation of ~70%. Specific antagonism of CpG motifs was confirmed, with TNFa values consistently reduced to those of CpG free plasmids. Literature descriptions of M16s suppressive effects have been discussed in chapter 4 (where it was also found to exert suppression within a pDNA integrated context). To reiterate however, success in a number of murine models of inflammatory disease have been described (Gao et al., 2017; Nie et al., 2019; Xiao et al., 2017; Zhang et al., 2022). Its mechanism of action involves i) sequence-dependent IRF5 binding which prevents translocation into the nucleus and transcription of pro-inflammatory cytokines, ii) interference of NF-kB phosphorylation restricting TF activation and iii) inhibition of HMGB1 translocation into the cytosol where it can no longer acts as a DAMP to induce sterile inflammation and TNFa production (Gao et al., 2017; Zhang et al., 2022). Extrapolating from these findings, we can speculate that the CpG dependent upregulation of IRF5, NF-KB or HMGB1 was antagonised using M16 within the DC2.4 system described here, offering an alternative ODN based approach to counteract pDNA dependent immune activation for use alongside DNA-based therapeutics. Previous reports of 'thresholding' could not be found, suggesting this phenomenon to be pDNA or system specific.

5.3.3 CAL-1 responses to CpG and M16

A lack of appropriate human pDC models and restrictions in primary human cell sourcing impeded an M16 reduction to practise. Through literature research, cell lines MUTZ-3 (a human DC precursor (Masterson et al., 2002)) and CAL-1 (Maeda et al., 2005) were considered for novel application in screening pDNA activation and M16 ODN suppression. Despite MUTZ-3's effective use as a differentiation model with cytokine secreting abilities (Sakamoto et al., 2018), studies have reported a resistance to TLR activating ligands including vaccine vectors (Tapia-Calle et al., 2017). CAL-1 therefore presented a more responsive, easier-to-culture and already matured (plasmacytoid) alternative, with multiple reports of its cytokine responses to CpG-ODNs. Within this study, CAL-1 was found to be largely unresponsive to vector DNA

producing <60pg/ml TNFa (equivalent to a no DNA response) even at a plasmid load of 1200ng. Exposure to highly immunogenic vector pVAX1-CpG with almost 400 CG dinucleotides at 2000ng (maximal load possible given loss during DNA preparation with extra endotoxin removal wash steps and additional ethanol precipitations (as described in 2.2.2)) did induce a sequence specific increase in TNFa to ~200pg/ml. Although pVAX1 was not tested at a comparable concentration of 2000ng, the trend from its titration between 0-1200ng suggest the increase in response to pVAX1-CpG-H was sequence rather than concentration dependent. Nevertheless, these findings confirm CAL-1 to be an ineffective model for detection and response to pDNA, through TNFa. However, given pDCs are predominantly IFNa producers, dsDNA responses may be better observed through detection and quantification of type I interferon cytokines instead (Steinhagen et al., 2012b).

CAL-1 exposure to C 2395 ODN caused a 3.6-fold (155ng/43ng) increase in TNFa whilst exposure to pVAX1-CpG (392) caused a 3.5-fold (150ng/43ng) increase. By combining both these stimulants within the same system however, a 25-fold (1071ng/43ng) increase in TNFa was detected, surpassing additive or even multiplicative effects. It can be hypothesised therefore, that these distinct CpG systems are either augmenting activity of one another, producing larger synergistic effects or generate enough of a combined stimulatory response as to surpass a certain threshold, resulting in further stimulation of a more significant TNFa response. Interestingly, by adding M16 into this highly immunogenic system, a reduction in TNFa across both 10% FBS and 0.1% FBS conditions was detected. This suppressive effect was much more pronounced in non-starved conditions suggesting that i) M16 can cause some reduction in CpG stimulating activities within human cells and ii) serum starvation affects the cells ability to initiate/ respond to immunomodulatory stimuli (Rahmani et al., 2018).

In conclusion, this chapter characterises a toolbox of ODNs with novel application as immune-modulators of pDNA-driven response pathways. In particular, M16 was identified as a potent sequence-specific suppressor, counteracting vector CpG stimulation providing a novel technology for gene therapy use, expanding the efficacy and diversity of vector designs whilst reducing immunogenicity.

Chapter 6 : Conclusions and Future Work

This chapter summarises the conclusions, industrial application, and recommendations of future work from the results described within this thesis.

6.1 Conclusions

The tools developed in this thesis enable quantification, characterisation, and control of pDNA-driven immune activation within murine DC models. Vector engineers and immunologists can now i) sensitively and rapidly quantify the sequence-specific effects of plasmids and ODNs across multiple DNA response pathways, ii) better inform gene therapy designs by biasing towards the incorporation (or tolerance) of GpG, CpG or microsatellite derived sequences, but not GpC or G-rich motifs, iii) control TNFa and IFNb responses to pDNA using sequence-specific ODNs; stimulating, suppressing or modulating the Th1 proinflammatory and IFN antiviral responses and iv) specifically counteract plasmid-CpG effects using microsatellite derived M16 ODN, expanding the diversity and activity of CpG dependent functional units (promoters/ intragenic sequences) for gene therapy use. The work described here facilitates a more informed and controllable response to pDNA activated immunity, expanding the repertoire of technologies available for safer and more efficacious DNA-based therapeutics.

1. Sensitive characterisation of sequence specific modulation across pDNA-driven immune response pathways

The investigation of ODN-derived suppressive motifs as plasmid integrated dsDNA sequences provides vector engineers with clear design rules to better inform construction of novel therapeutic plasmids. Although not recommended for additional integration to downregulate cytokine production, their effects on the gene level suggest incorporation/ tolerance of Type2 GpG's, CpG's, or Type3 microsatellite sequences, may have more advantageous suppressive effects compared to random spacer usage during vector construction. For the wider community, this screen also provides essential foundational analysis of immune-modulatory dsDNA motifs, highlighting i) the largely overlooked suppressive potential of microsatellite derived sequences (particularly M19 and M17) within this novel context, ii) how different motif Types have variable effects between groups and ODN contexts, and iii) how cell models differ (even within the same species) in their interaction with modulatory dsDNA motifs. The sensitive quantification and characterisation of these sequence-

specific effects was only made possible through development of novel immune-profiling tool Nanopanel. This technology provides immunologists with a method for sensitive and accurate quantification of DNA-driven response pathways. Applications include i) immunogenicity screening of current DNA-therapeutics, providing additional safety screening and a mechanistic understanding, ii) medium-throughput comparison of early vector designs, informing selection of more efficacious plasmids with pathway-specific effects, (e.g. gene therapy downregulation of multiple immune pathways, vaccine-dependent upregulation of either Th1 or Th2 responses, or more fine-tuned observation of receptor/ cytokine/ chemokine specific impacts) and iii) a multiplex RNA quantification method requiring less experimental labour and manual processing, whilst increasing confidence and analytical depth, compared to traditional ELISA methods.

2. Novel application of ODNs as pDNA immune modulators

Literature investigations have previously demonstrated the immune-suppressive activity of ODNs within murine models of inflammatory disease. Within this study, their novel application as modulators of pDNA-driven responses identified a small toolbox of sequences, for use in augmenting the immune activity of DNA-based therapeutics. These technologies enable variable proinflammatory TNFa and antiviral IFNb activity for immunological application alongside gene therapies (suppress both), vaccine vectors (activate both) and even for the potential treatment of SLE symptoms (suppress IFNb). For vector engineers, microsatellites were again demonstrated as the most effective group, further supporting use of these sequences in dsDNA or ODN form for pDNA specific suppression. For the first-time, vector-CpG counteracting M16 activity was characterised for application alongside gene therapies to counteract the detrimental immunogenic effects of these motifs, while preserving their critical requirement for high therapeutic transgene expression. These findings expand the design space available for vector engineers, providing a solution for the development of efficacious, yet safe, therapeutic plasmids.

6.2 Future Work

Further work is required to validate, improve, and apply the novel tools described within this study.

6.2.1 Translation of immune-profiling tool Nanopanel

The use of a literature-based bioinformatics approach enabled hypothesis and data-driven selection of response genes, forming the basis of immune-profiling tool Nanopanel. However, testing this pipeline within *in vivo* mouse models (compared to *in vitro* DC2.4) is required to validate its application and utility in more informative systems.

Given gene therapies must exhibit efficacious activity in murine models before human testing (AstraZeneca, Cambridge, UK), this tool is an appropriate initial screening platform for novel vector designs. However, evolutionary divergence between mouse and human immune systems generates critical differences in the detection and activity of DNA sequences. Incorporation of human transcriptomic data would therefore enable translation of this technology into a human context, enabling similar observation of multiple DNA-driven response pathways. In order to do this, the following is required; i) microarray screening of multiple pDNA conditions within human DC *in vivo*, ii) gene mapping of DNA driven response pathways and subsequent rule-based filtering to identify a small panel of representative genes (as described in chapter 3) and iii) incorporation of Nanostrings-based (or other multiplex technology such as BioMark HD or Luminex) analysis. A similar experimental pipeline would also require development (as detailed in chapter 3) although this presents a number of challenges given current limitation in human DC models capable of pDNA detection. Therefore, proof-of-principle screening of potential *in vitro* systems (as described with CAL-1) or access to primary cell models would be necessary.

The development of Nanopanel describes a methodology for delineating pDNA specific immune effects in DCs, however similar processes can be applied to different stimulant conditions (LPS, mRNA, AAV) within different systems (DC, macrophages,

T/B lymphocytes). This would be particularly useful in characterising AAV specific immune response pathways (most commonly used gene therapy vector) given its highly disadvantageous and restrictive immunogenic effects (Yang et al., 2022).

6.2.2 A mechanistic interrogation of modulatory ODNs

The characterisation of pDNA modulating ODNs presents novel technology for tuneable immune control. However, further investigation into their sequence-specific differential activity would provide a better understanding of their mechanisms, enabling development of more potent and specific modulators. M17 and M19 for example, are poorly characterised and largely overlooked within the literature, despite clear and significant suppressive effects within the murine DC2.4 model as described in this study. Inhibitory ODNs are broadly classified as 'immunosuppressive ODNs' with protein targeting effects, or 'antisense ODNs' with mRNA targeting effects. Whilst no ODNs described within this study have been previously reported to exert antisense-ODN activity, this method of suppression cannot be ruled out and requires further interrogation (Wang et al., 2023).

Thus far, TNFa and IFNb analysis was used to quantify effects on differing immune pathways through TLR9 (proinflammatory) or cGAS-STING (antiviral) activation, respectively. Furthermore, high levels of IFNb have been associated with a Th2 over Th1 bias, while the opposite is true for TNFa. These interactions however, are complex and difficult to discriminate from DC analysis alone. T-cell co-culture would better determine whether these ODNs had sequence/ concentration dependent impacts on Th differentiation pathways. Thus, enriching the understanding and application of this toolbox, enabling control of not just inflammatory and antiviral responses but also Th differentiation bias.

6.2.3 M16 reduction to practice

Mechanism of action

M16's CpG-counteracting effects on TNFa production offers promising application alongside gene therapy vectors, permitting use of more efficacious vector components. Although M16's mechanism of action is more widely understood than

other microsatellite ODNs, its CpG-dependent activity within this system remains to be characterised and therefore requires more detailed analysis to ensure safety and further improve efficacy.

Formulation

Although initially designed for electroporation-based administration, industrial interest has shifted towards lipid nano particle (LNP) based delivery of therapeutic pDNA. M16 is therefore currently undergoing *in vivo* testing within this context (AstraZeneca, Cambridge, UK). To adapt to this change, an experimental plan was developed to outline preliminary testing strategies for M16 within LNPs for *in vivo* murine models. These recommendations were as follow: 1) co-delivery of pDNA and M16 (despite exhibiting neutral/ stimulatory effects in DC2.4), as this provides a simpler experimental approach for initial testing and was reportedly most effective in lipofectamine transfection systems, which more closely resemble LNP delivery mechanisms (Valentin et al., 2021). 2) Co-formulation of pDNA and M16 within LNPs, as similar studies investigating CpG-ODN adjuvant activity found incorporation within LNPs, as opposed to separately, were most efficacious (Luan et al., 2022; Shirai et al., 2020). 3) M16 loads of 10, 25 and 50ug/mouse for initial testing to avoid ODN toxicity and cell death, informed from M16 *in vivo* testing in the literature for the treatment of ALI (Zhang et al., 2022), and similar CpG-ODN studies (Zhao et al., 2022).

Optimisation

The investigation of ODNs within this study were conducted exclusively within a PS backbone context for simplicity. Reports of further modified ODNs with guanine substitution to 7-deaza-guanine (replacement of a carbon atom with nitrogen) or 7-deaza-2′-O-methyl-guanine (addition of a methyl group) were found to increase suppression of TLR7 TNFa, Il12p40 and B cell IL-6 production (Römmler et al., 2013). Additionally, 2'-*O*-methyl-modifications or 2′,4′-methylene-bridging also reportedly increased binding affinities and suppressive activity (Swayze et al., 2007; Yoo et al., 2004). Investigation of these backbone changes to further potentiate M16's suppressive activity is currently underway (AstraZeneca, Cambridge, UK).

Appendix

Supplementary Table 1) Literature reported immune-suppressive motifs. Literature based grouping into six subtypes along with sequence and example references are shown. mE denotes a guanine modified nucleotide.

	Motif name	Sequence	Reference
G-tetrads	A151	TTAGGGTTAGGGTTAGGGTTAGGG	*(Gursel et al, 2002)*
	H154	CCTCAAGCTTGAGGGG	*(Gursel et al, 2002)*
	G-tetrad 1	GGGTGGGTGGGTATTACCATTA	*(Gursel et al, 2002)*
	G-tetrad 2	TGGGCGGTTCAACCTTCA	*(Gursel et al, 2002)*
	G-tetrad 3	TTGGTTGGTTGGTTGG	*(Gursel et al, 2002)*
	G-tetrad 4	CCGGCCGGCCGGCCGG	*(Gursel et al, 2002)*
	G-tetrad 5	TTAGGGTCAACCTTCA	*(Gursel et al, 2002)*
	Sup ODN	TCAAGCTTGA	*(Bouladoux et al, 2012)*
	G' ODN	CTCCTATTGGGGGTTTCCTAT	*(Peter et al, 2008)*
	PolyG	GGGGGGGGGGGGGGGGGGGG	*(Halpern et al, 1995)*
CpG dinucleotides	GpC 1502	GAGCAAGCTGGACCTTCCAT	*(Yamada et al, 2002)*
	GpC 1826a	TCCATGAGCTTCCTGAGCTT	*(Wingender et al, 2005)*
	GpC 1826b	TCCATGAGCTTCCTAAGCTT	*(Avalos and Ploegh, 2011)*
	GpC 1668	TCCATGAGCTTCCTGATGCT	*(Vopli et al, 2012)*
	GpC 2006	TGCTGCTTTTGTGCTTTTGTGCTT	*(Volpi et al, 2012)*
	GpG 1019	TGACTGTGAAGGTTAGAGATGA	*(Ho et al, 2003)*
	ODN 1952	TCCATGTCGTTCCGCGCGCG	*(Krieg et al, 1998)*
	ODN 1953	TCCATGTCGTTCCGCCCGCG	*(Krieg et al, 1998)*
	CpG-c41	TGGCGCGCACCCACGGCCTG	*(Liu et al, 2017)*
Inhibitory ODNs	**INH-ODN 2088 (parent)**	TCCTGGCGGGGAAGT	*(Lenert et al, 2001)*
	INH-ODN 21595	TCCTGGCEGGGAAGT	*(Rommler et al, 2013)*
	INH-ODN 20844	TCCTGGCGEGGAAGT	*(Rommler et al, 2013)*
	INH-ODN 24888	TCCTGGCmEGGGAAGT	*(Rommler et al, 2013)*
	INH-ODN 2114	TCCTGGAGGGGAAGT	*(Lenert et al, 2001)*
	INH-ODN 4031	TCCTGGAGGGG	*(Lenert et al, 2003)*
	INH-ODN 4033	CCTGGAGGGGAAGT	*(Ashman et al, 2011)*
	INH-ODN 4171	CCTGGAGGGG	*(Ashman et al, 2011)*
	INH-ODN 4104	CCTGGAGGGGAA	*(Ashman et al, 2005)*
	INH-ODN 4030	TCCTGGAGGGGAA	*(Ashman et al, 2005)*
	INH-ODN 2144	TCCTGACGGGGAAGT	*(Stuz et al, 2002)*
	INH-ODN 2341	TCCTGGCGGGCAAGT	*(Stuz et al, 2002)*
	INH-ODN 2342	TCCTGGCGGGTAAGT	*(Stuz et al, 2002)*
	INH-ODN 2343	TCCTGGCGGGAAAGT	*(Stuz et al, 2002)*
	INH-ODN 4352	TCCTTCCTGGAGGGGAAG	*(Ashman et al, 2011)*
	INH-ODN 4351	TCCTATCCTATCCTGGAGGGGAAG	*(Ashman et al, 2011)*
	INH-ODN 4005	TCCTGGAGTGGAAGT	*(Lenert et al, 2003)*
	INH-ODN 4024	TCCTGGATGGGAAGT	*(Lenert et al, 2003)*
	INH-ODN 4024F	CCTGGATGGGAA	*(Ashman et al, 2011)*

	INH-ODN 4191	TCCTATCCTGGAGGGGAAG	*(Ashman et al, 2011)*
	INH-ODN 4347	CCTATCCTGGAGGGGAAG	*(Ashman et al, 2011)*
	INH-ODN 4348	TCGTATCCTGGAGGGGAAG	*(Ashman et al, 2011)*
	INH-ODN 4349	TAATATCCTGGAGGGGAAG	*(Ashman et al, 2011)*
	INH-ODN 4350	TCCTATAATGGAGGGGAAG	*(Lenert et al, 2003)*
	INH-ODN 4029	GGAGGGGAAGT	*(Lenert et al, 2009)*
	INH-ODN 1 (R class)	CCTGGATGGGAATTCCCATCCAGG	*(Lenert et al, 2009)*
	INH-ODN 18 (B class)	CCTGGATGGGAACTTACCGCTGCA	*(Lenert et al, 2009)*
	INH 4 (R class)	TTCCCATCCAGGCCTGGATGGGAA	*(Lenert et al, 2009)*
	INH 13 (B class)	CTTACCGCTGCACCTGGATGGGAA	*(Rommler et al, 2013)*
	INH-ODN 21158 (parent)	CCTGGCGGGG	*(Rommler et al, 2013)*
	INH-ODN 24987	CCTGGCEGGG	*(Rommler et al, 2013)*
	INH-ODN 24991	CCTGGCmEGGG	*(Rommler et al, 2013)*
	INH-ODN 20959 (parent)	TAATGGCGGGGAAGT	*(Rommler et al, 2013)*
	INH-ODN 105870	TAATGGCEGGGAAGT	*(Rommler et al, 2013)*
	INH-ODN 105871	TAATGGCmEGGGAAGT	*(Rommler et al, 2013)*
	INH-ODN 533	TGACTGTAGGCGGGGAAGATGA	*(Duramand et al, 2003)*
Immuno-regulatory sequences	IRS 869	TCCTGGAGGGGTTGT	*(Duramand et al, 2003*
	IRS 661	TGCTTGCAAGCTTGCAAGCA	*(Barrat et al, 2005)*
	IRS 967	TGCTTGACAGCTTGACAGCATCCTGGAGGGGTTGT	*(Barrat et al, 2005)*
	IRS 957	TGCTTGACATCCTGGAGGGGTTGT	*(Barrat et al, 2005)*
	IRS 954	TGCTCCTGGAGGGGTTGT	*(Pawar et al, 2004)*
	IRS 986	GCTCCTGGAGGGGTTGT	*(Barrat et al, 2005)*
	IRS 987	CTCCTGGAGGGGTTGT	*(Barrat et al, 2005)*
	IRS 988	AAATCCTGGAGGGGTTGT	*(Barrat et al, 2005)*
Microsatellites	SAT05f	CCTCCTCCTCCTCCTCCTCCTCCT	*(Sun et al, 2010)*
	SAT05f2	CCTCCTCCTCCTCCTCCTCCTCCTCCTCCT	*(Zhang et al, 2012)*
	SAT05f3	CCTCCTCCTCCTCCTCCTCCTCCTCCTCCTCCTCCTCCT	*(Zhang et al, 2012)*
	SAT05f4	CCTCCTCCTCCTCCTCCTAAGAAG	*(Zhang et al, 2012)*
	SAT05f6	AAGAAGCCTCCTCCTCCTCCTCCT	*(Zhang et al, 2012)*
	SAT05f9	AGGAGGCCTCCTCCTCCTCCTCCT	*(Zhang et al, 2012)*
	MS19	AAAGAAAGAAAGAAAGAAAGAAAG	*(Hu et al, 2009)*
	MS08	TCTCTCTCTCTCTCTCTCTCTC	*(Hu et al, 2009)*
	MS03	ACACACACACACACACACACACAC	*(Hu et al, 2009)*
	MS12	TTCTTCTTCTTCTTCTTCTTCTTC	*(Hu et al, 2009)*
	MS13	AGGAGGAGGAGGAGGAGGAGGAGG	*(Hu et al, 2009)*
	MS20	TTTCTTTCTTTCTTTCTTTCTTTC	*(Hu et al, 2009)*
	MS24	TTCCTTCCTTCCTTCCTTCCTTCC	*(Hu et al, 2009)*
	MS28	TTTTGTTTTGTTTTGTTTTGTTTTG	*(Hu et al, 2009)*
	MS32	TTTTTGTTTTTGTTTTTGTTTTTG	*(Hu et al, 2009)*
	MS34	TTTTTCTTTTTCTTTTTCTTTTTC	*(Hu et al, 2009)*
Hybrid Inhibit	iSG0	CCTCATTAGGGTGA	*(Ito et al, 2013)*
	iSG1	CCTCATTAGGGTGAG	*(Ito et al, 2013)*

	iSG2	CCTCATTAGGGTGAGG	*(Ito et al, 2013)*
	iSG3	CCTCATTAGGGTGAGGG	*(Ito et al, 2013)*
	iSG4	CCTCATTAGGGTGAGGGG	*(Ito et al, 2013)*
	iSG5	CCTCATTAGGGTGAGGGGG	*(Ito et al, 2013)*
	iSG6	CCTCATTAGGGTGAGGGGGG	*(Ito et al, 2013)*
	iSG7	CCTCATTAGGGTGAGGGGGGG	*(Ito et al, 2013)*
	IMO-8400	CTATCTNNNNTTCTCTNN	*(Jian et al, 2012)*

Supplementary Table 2) Top 25% of transcriptomic expressers. Statistically significant genes upregulated in Tumour, ISD and CpG conditions (log_2 FC>1, adjusted p-value <0.1) within top 25% of FC and FE expressers are shown along with bottom-up data.

Gene	Tumour	ISD	CpG	Bottom-up	Bottom-up rank
Rsad2					4
Il6					1
Cxcl10					1
Gm14446					
Oasl1					
Cd69					
Irf7					4
Tnf					2
Mx1					
Ifi205 /// Mnda					4
Ccrl2					
Cxcl9					4
Cmpk2					
Ifnb1					1
Ccl12					
Iigp1					
Tgtp1 /// Tgtp2					
Fam26f					
Gbp6					
Serpina3g					
Ms4a4c					
Pyhin1					
Igtp					
Phf11d					
Nt5c3					
Fgl2					
Il12b					3
Ptgs2					
Cd40					2
Ifit1					3
Ifit2					4
Ifit3					
Gm9706 /// Isg15					
Usp18					
Oasl2					
Irg1					
Ccl4					4
Irgm1					
Ifi47					4
Slfn8					
Ifna2					1
Cxcl11					
BC023105					
Slfn3 /// Slfn4					
Slfn4					
Isg20					
Ch25h					
Gm9706					
Cst7					
Mx2					
Tlr3					4
Trim30d					
Serpinb9					

Rgcc				
Gm4951				
Kdr				
Ccnd2				
Slco3a1				
Slc7a2				
Hspa1b				
Pla2g16				
Plac8				
Gbp2				
Il15				4
Nlrc5				
Cflar				
Cd86				2
Peli1				
Daxx				
Stx11				
Trim25				
Zbp1				4
Il13ra1				
Aldh1b1				
Dck				
Slfn5				
Ifih1				3
Irgm2				
Herc6				
Gm16340/Ifi203				
Parp14				
Gm16340/Ifi203				
Xaf1				
Znfx1				
Ddx58				4
Il1a				4
Cxcl1				4
Cxcl3				
Cxcl2				4
Inhba				
Il1b				2
Saa3				
Marco				
Socs3				4
Clec4e				
Rasgef1b				
Hivep3				
Ccl3				

Supplementary Table 3) g:Profiler analysis of 34 key DC response genes to DNA. 34 response genes were analysed using g:profiler with a g:SCS applied q-value of 0.05. Top 30 enriched biological pathways and 17 enriched molecular functions are shown.

Top 30 biological pathways	Associated genes	Adjusted p-value
Response to virus	20	4.8E-27
Defence response to virus	18	1.1E-24
Défense response to symbiont	18	1.2E-24
Negative regulation of viral genome replication	8	1.7E-11
Positive regulation of innate immune response	11	7.4E-11
Cellular response to lipopolysaccharide	11	8.3E-11
Cellular response to molecule of bacterial origin	11	1.1E-10
Positive regulation of response to biotic stimulus	11	1.9E-10
Activation of innate immune response	10	2.1E-10
Cellular response to biotic stimulus	11	2.7E-10
Regulation of viral genome replication	8	6.6E-10
Negative regulation of viral process	8	8.5E-10
Viral genome replication	8	5.4E-09
Regulation of viral life cycle	8	2.9E-08
Pattern recognition receptor signalling pathway	8	7.5E-08
Regulation of viral process	8	9.1E-08
Innate immune response-activating signalling pathway	8	1.2E-07
Regulation of adaptive immune response	8	2.2E-07
Viral life cycle	8	1.2E-06
Cellular response to interferon-beta	5	2.0E-06
Cytosolic pattern recognition receptor signalling pathway	6	2.2E-06
Response to interferon-beta	5	4.8E-06
Regulation of adaptive immune response based on somatic recombination of immune receptors built from immunoglobulin superfamily domains	7	5.2E-06
Regulation of lymphocyte mediated immunity	7	7.4E-06
Positive regulation of tyrosine phosphorylation of STAT protein	5	7.9E-06
Viral process	8	8.2E-06
Regulation of production of molecular mediator of immune response	7	1.2E-05
Positive regulation of adaptive immune response based on somatic recombination of immune receptors built from immunoglobulin superfamily domains	6	1.3E-05
CD4-positive, alpha-beta T cell cytokine production	4	1.4E-05
Response to type II interferon	6	1.7E-05
Top 17 molecular functions	**Associated genes**	**Adjusted p-value**
Cytokine receptor binding	11	2.3E-11
Cytokine activity	10	6.5E-11
Receptor ligand activity	10	1.7E-07
Chemokine receptor binding	5	2.0E-07
Signalling receptor activator activity	10	2.1E-07
Signalling receptor regulator activity	10	4.7E-07
Chemokine activity	4	3.9E-06
Signalling receptor binding	13	1.2E-05
Molecular function activator activity	11	7.8E-05

G protein-coupled receptor binding	5	2.7E-04
CXCR3 chemokine receptor binding	2	4.1E-04
Molecular function regulator activity	12	9.4E-04
CCR chemokine receptor binding	3	1.4E-03
CXCR chemokine receptor binding	2	5.3E-03
Protein binding	15	6.3E-03
GTPase activity	4	3.7E-02
Chemoattractant activity	2	4.4E-02

Supplementary Table 4) Cytoscape characterisation of 34 key response genes. g:Profiler enriched biological pathways were clustered and visualised using Cytoscape Autoannotate functions. q-value < 0.01 and Jaccard Overlap combined coefficient of >0.375.

Cluster	Number of GO terms	Top 3 GO terms
Adaptive Immune System	107	Cellular response to lipopolysaccharide Cellular response to molecular of bacterial origin Defence response to protozoan
Regulation of Defence Response	16	IkB/Nf-kB signalling Regulation of IkB/NF-kB signalling Positive regulation of IkB/Nf-kB signalling
Downregulation of Immune Response	14	Regulation of innate immune response Regulation of response to cytokine stimulus Regulation of cytokine-mediated signalling pathway
Immune Receptor Signalling	12	IFNg mediated signalling pathway Positive regulation of response to cytokine stimulus Cytoplasmic pattern recognition receptor signalling pathway
Viral Response	9	Defence response to virus Defence response to symbiont Negation regulation of viral response
Type I IFN Production	8	Type I IFN Production Regulation of type I IFN production IFN-b production
TLR Signalling	5	Pattern recognition receptor signalling pathway Toll-like receptor signalling pathway Regulation of pattern recognition receptor signalling pathway
IFNg/B Production	4	Response to IFN-b Cellular response to IFN-b Response to IFN-g
Innate Immune Response Activation	4	Positive regulation of defence response Positive regulation of response to biotic stimulus Positive regulation of innate immune response
Antiviral IFN Signalling	3	IFN signalling Antiviral mechanism by IFN-stimulated genes ISG15 antiviral mechanism

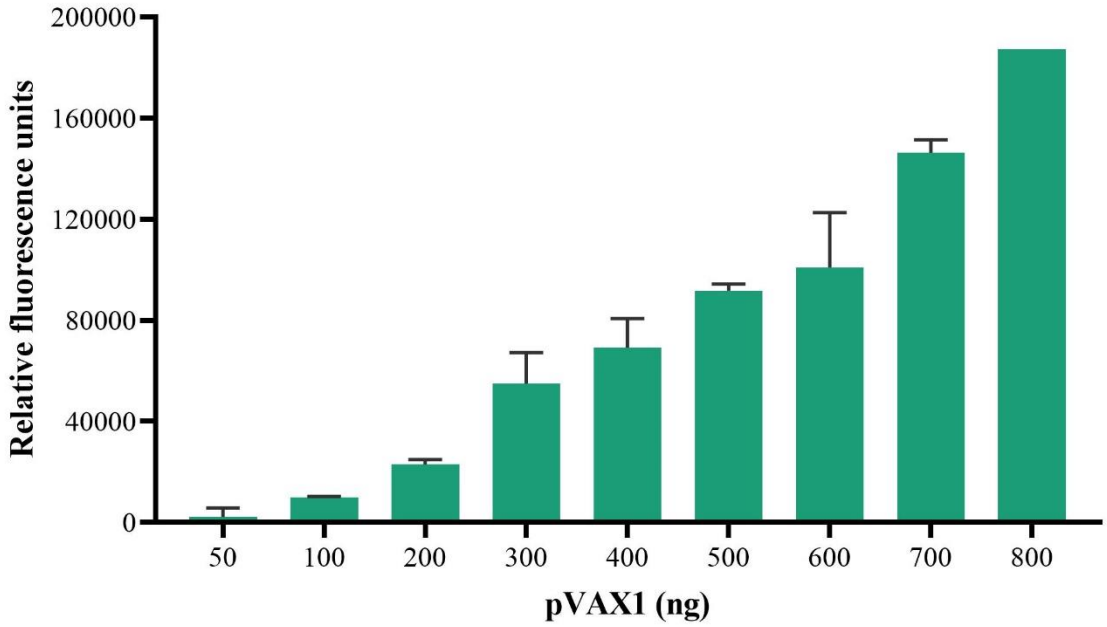

Supplementary Figure 1) GFP expression from pVAX1 DNA titration 50-800ng. Vector DNA at varying concentrations were nucleofected into 400,000 DC2.4 cells and GFP expression quantified at 24hrs. Bars represent relative fluorescence mean +SD from 1 biological replicate in technical duplicate.

Supplementary Table 5) Immune-stimulatory motifs. Literature identified immune-stimulatory motifs used to construct pVAX1-CpG (392).

Immune-stimulatory motifs			
Motif class	**Motif name**	**Motif sequence**	**Motif length (nt)**
CpG A	1585	GGGGTCAACGTTGAGGGGGG	20
CpG B	1668	TCCATGACGTTCCTGATGCT	20
	BW006	TCGACGTTCGTCGTTCGTCGTTC	23
	D-SL01	TCGCGACGTTCGCCCGACGTTCGGTA	26
	minM	TTTTTCGTTTTTTTTTTTTTTT	22
	1555	GCTAGACGTTAGCGT	15
	1826	TCCATGACGTTCCTGACGTT	20
	1466	TCAACGTTGA	10
CpG C	2395	TCGTCGTTTTCGGCGCGCGCCG	22
	M362	TCGTCGTCGTTCGAACGACGTTGAT	25
	D-SL03	TCGCGAACGTTCGCCGCGTTCGAACGCGG	29
CpG P	23617	TCGTCGACGATCGGCGCGCGCCG	23

Supplementary Table 6) Library 1 element motif composition. 20 homotypic and 21 heterotypic elements were constructed with motif identity and copy numbers shown. Elements that could not be synthesised or tested are shown in grey.

Library 1 Element Composition																						
Architecture	**Element**	M1	M2	M3	M4	M5	M6	M7	M8	M9	M10	M11	M12	M13	M14	M15	M16	M17	M18	M19	M20	**Total**
Homotypic Mono-type Mono-motif	Motif1	10																				10
	Motif2		10																			10
	Motif3			10																		10
	Motif4				10																	10
	Motif5					10																10
	Motif6						10															10
	Motif7							10														10
	Motif8								10													10
	Motif9									10												10
	Motif10										10											10
	Motif11											10										10
	Motif12												10									10
	Motif13													10								10
	Motif14														10							10
	Motif15															10						10
	Motif16																10					10
	Motif17																	10				10
	Motif18																		10			10
	Motif19																			10		10
	Motif20																				10	10
Mono-type Motif-mix	Type1	3	3	3	3	3	3	3	3													24
	Type2									3	3	3	3	3	3							18
	Type3															3	3	3	3	3	3	18
Mono-type Motif-grp	Type1	3	3	3	3	3	3	3	3													24
	Type2									3	3	3	3	3	3							18
	Type3															3	3	3	3	3	3	18
Duo Type-mix Motif-mix	Type 1+2	2	2	2	2	2	2	2	2	2	2	2	2	2	2							28
	Type 1+3	2	2	2	2	2	2	2	2							2	2	2	2	2	2	28
	Type 2+3									2	2	2	2	2	2	2	2	2	2	2	2	24
Duo Type-grp Motif-mix	Type 1+2	2	2	2	2	2	2	2	2	2	2	2	2	2	2							28
	Type 1+3	2	2	2	2	2	2	2	2							2	2	2	2	2	2	28
	Type 2+3									2	2	2	2	2	2	2	2	2	2	2	2	24
Duo Type-mix Motif-grp	Type 1+2	2	2	2	2	2	2	2	2	2	2	2	2	2	2							28
	Type 1+3	2	2	2	2	2	2	2	2							2	2	2	2	2	2	28
	Type 2+3									2	2	2	2	2	2	2	2	2	2	2	2	24
Duo Type-grp Motif-grp	Type 1+2	2	2	2	2	2	2	2	2	2	2	2	2	2	2							28
	Type 1+2	2	2	2	2	2	2	2	2							2	2	2	2	2	2	28
	Type 2+3									2	2	2	2	2	2	2	2	2	2	2	2	24
Trio-types All-motifs	Alternating	1	1	1	1	1	1	1	1	1	1	1	1	1	1	1	1	1	1	1	1	20
	Grouped	1	1	1	1	1	1	1	1	1	1	1	1	1	1	1	1	1	1	1	1	20
	Random	1	1	1	1	1	1	1	1	1	1	1	1	1	1	1	1	1	1	1	1	20

Supplementary Table 5) MLR modelling output using 20 motifs. Individual motif coefficient values were calculated along with their standard error, t value and p values (*=0.01, **=0.001 ***=0.0001). Residuals, adjusted R^2, F statistic and the associated global p value are shown.

Motif	Coefficient	SD	t value	p value	
M1	0.167	0.326	0.514	0.619	
M2	-0.27	0.326	-0.828	0.427	
M3	0.329	0.326	1.012	0.336	
M4	0.182	0.326	0.558	0.589	
M5	-0.112	0.326	-0.344	0.738	
M6	1.816	1.298	1.399	0.192	
M7	-0.116	0.326	-0.357	0.728	
M8	0.299	0.326	0.917	0.381	
M9	0.365	0.27	1.353	0.206	
M10	0.256	0.27	0.949	0.365	
M11	0.375	0.27	1.391	0.194	
M12	0.768	0.27	2.847	0.017	*
M13	1.009	0.27	3.74	0.004	**
M14	0.885	0.27	3.281	0.008	**
M15	0.365	0.326	1.121	0.288	
M16	1.423	0.326	4.37	0.001	**
M17	0.844	0.326	2.591	0.027	*
M18	0.064	0.869	0.073	0.943	
M19	1.456	0.326	4.472	0.001	**
M20	0.27	0.326	0.829	0.427	
Intercept	0.864	2.095	0.412	0.689	

Residuals					
Min	**1Q**	**Median**	**3Q**	**Max**	**SE**
-4.675	0	0	0.41	3.728	2.49

Adjusted R2	F statistic	p value
0.819	7.801	0.0001

Supplementary Table 6) MLR modelling output using 6 statistically significant motifs. Individual motif coefficient values were calculated along with their standard error, t value and p values (*=0.01, **=0.001 ***=0.0001). Residuals, adjusted R^2, F statistic and the associated global p value are shown.

Motif	Coefficient	SD	t value	p value	
M12	0.778	0.308	2.526	0.000	*
M13	1.019	0.308	3.308	0.427	**
M14	0.895	0.308	2.906	0.336	**
M16	1.348	0.308	4.370	0.589	***
M17	0.769	0.308	2.492	0.738	*
M19	1.381	0.308	4.478	0.192	***
Intercept	3.6544	0.87	4.200	0.000	***

Residuals					
Min	**1Q**	**Median**	**3Q**	**Max**	**SE**
-5.487	-2.0402	0.1968	1.325	7.4583	3.25

Adjusted R2	F statistic	p value
0.6938	12.33	<0.0001

References

Aalamian, M., Pirtskhalaishvili, G., Nunez, A., Esche, C., Shurin, G. V., Huland, E., Huland, H., and Shurin, M.R. (2001). Human prostate cancer regulates generation and maturation of monocyte-derived dendritic cells. Prostate *46*, 68–75.

Ablasser, A., Bauernfeind, F., Hartmann, G., Latz, E., Fitzgerald, K.A., and Hornung, V. (2009). RIG-I-dependent sensing of poly(dA:dT) through the induction of an RNA polymerase III-transcribed RNA intermediate. Nat. Immunol. *10*, 1065–1072.

Alton, E.W.F.W., Boyd, A.C., Cheng, S.H., Cunningham, S., Davies, J.C., Gill, D.R., Griesenbach, U., Higgins, T., Hyde, S.C., Innes, J.A., et al. (2013). A randomised, double-blind, placebo-controlled phase IIB clinical trial of repeated application of gene therapy in patients with cystic fibrosis. Thorax *68*, 1075–1077.

Arruda, V.R., Favaro, P., and Finn, J.D. (2009). Strategies to modulate immune responses: A new frontier for gene therapy. Mol. Ther. *17*, 1492–1503.

Asakura, Y., Liu, L.J., Shono, N., Hinkula, J., Kjerrström, A., Aoki, I., Okuda, K., Wahren, B., and Fukushima, J. (2000). Th1-biased immune responses induced by DNA-based immunizations are mediated via action on professional antigen-presenting cells to up-regulate IL-12 production. Clin. Exp. Immunol. *119*, 130–139.

Ashman, R.F., Goeken, J.A., Drahos, J., and Lenert, P. (2005). Sequence requirements for oligodeoxyribonucleotide inhibitory activity. Int. Immunol. *17*, 411–420.

Ashman, R.F., Goeken, J.A., Latz, E., and Lenert, P. (2011). Optimal oligonucleotide sequences for TLR9 inhibitory activity in human cells: Lack of correlation with TLR9 binding. Int. Immunol. *23*, 203–214.

Au, H.K.E., Isalan, M., and Mielcarek, M. (2022). Gene Therapy Advances: A Meta-Analysis of AAV Usage in Clinical Settings. Front. Med. *8*, 1–14.

Avalos, A.M., and Ploegh, H.L. (2011). Competition by inhibitory oligonucleotides prevents binding of CpG to C-terminal TLR9. Eur. J. Immunol. *41*, 2820–2827.

Aydin, S. (2015). A short history, principles, and types of ELISA, and our laboratory experience with peptide/protein analyses using ELISA. Peptides *72*, 4–15.

Baghban, R., Ghasemian, A., and Mahmoodi, S. (2023). Nucleic acid-based vaccine platforms against the coronavirus disease 19 (COVID-19). Arch. Microbiol. *205*, 1–15.

Barrat, F.J., Meeker, T., Gregorio, J., Chan, J.H., Uematsu, S., Akira, S., Chang, B., Duramad, O., and Coffman, R.L. (2005). Nucleic acids of mammalian origin can act as endogenous ligands for Toll-like receptors and may promote systemic lupus erythematosus. J. Exp. Med. *202*, 1131–1139.

Bauer, A.P., Leikam, D., Krinner, S., Notka, F., Ludwig, C., Längst, G., and Wagner, R. (2010). The impact of intragenic CpG content on gene expression. Nucleic Acids Res. *38*, 3891–3908.

Bauer, S., Kirschning, C.J., Häcker, H., Redecke, V., Hausmann, S., Akira, S., Wagner, H., and Lipford, G.B. (2001). Human TLR9 confers responsiveness to bacterial DNA via species-specific CpG motif recognition. Proc. Natl. Acad. Sci. U. S. A. *98*, 9237–9242.

Bayik, D., Gursel, I., and Klinman, D.M. (2016). Structure, mechanism, and therapeutic utility of immunosuppressive oligonucleotides. Pharmacol. Res. *105*, 216–225.

Benjamini, Y., and Hochberg, Y. (1995). Controlling the False Discovery Rate : A Practical and Powerful Approach to Multiple Testing. J. R. Stat. Soc. *57*, 289–300.

Bertolini, T.B., Shirley, J.L., Zolotukhin, I., Li, X., Kaisho, T., Xiao, W., Kumar, S.R.P., and Herzog, R.W. (2021). Effect of CpG Depletion of Vector Genome on CD8+ T Cell Responses in AAV Gene Therapy. Front. Immunol. *12*, 1–11.

Bessis, N., GarciaCozar, F.J., and Boissier, M.C. (2004). Immune responses to gene therapy vectors: Influence on vector function and effector mechanisms. Gene Ther. *11*, S10–S17.

Bird, A. (2011). The dinucleotide CG as a genomic signalling module. J. Mol. Biol. *409*, 47–53.

Bird, A.P. (1980). DNA methylation and the frequency of CpG in animal DNA. Nucleic Acids Res. *8*, 1499–1504.

Bode, C., Zhao, G., Steinhagen, F., Kinjo, T., and Klinman, D.M. (2011). CpG DNA as a vaccine adjuvant. Expert Rev. Vaccines *10*, 499-511Manuscript, Author.

Bode, C., Yang, X.P., Kiu, H., and Klinman, D.M. (2013). Suppressive Oligodeoxynucleotides Promote the Development of Th17 Cells. PLoS One *8*, 2–9.

Bode, C., Fox, M., Tewary, P., Steinhagen, A., Ellerkmann, R.K., Klinman, D., Baumgarten, G., Hornung, V., and Steinhagen, F. (2016). Human plasmacytoid dentritic cells elicit a Type I Interferon response by sensing DNA via the cGAS-STING signaling pathway. Eur. J. Immunol. *46*, 1615–1621.

Bonilla, F.A., and Oettgen, H.C. (2010). Adaptive immunity. J. Allergy Clin. Immunol. *125*, S33–S40.

Brazolot Millan, C.L., Weeratna, R., Krieg, A.M., Siegrist, C.A., and Davis, H.L. (1998). CpG DNA can induce strong Th1 humoral and cell-mediated immune responses against hepatitis B surface antigen in young mice. Proc. Natl. Acad. Sci. U. S. A. *95*, 15553–15558.

Brown, A.J., Sweeney, B., Mainwaring, D.O., and James, D.C. (2014). Synthetic promoters for CHO cell engineering. Biotechnol. Bioeng. *111*, 1638–1647.

Bucher, K., Rodríguez-Bocanegra, E., Dauletbekov, D., and Fischer, M.D. (2021). Immune responses to retinal gene therapy using adeno-associated viral vectors – Implications for treatment success and safety. Prog. Retin. Eye Res. *83*, 100915.

Bulcha, J.T., Wang, Y., Ma, H., Tai, P.W.L., and Gao, G. (2021). Viral vector platforms within the gene therapy landscape. Signal Transduct. Target. Ther. *6*.

Bustin, S.A. (2000). Absolute quantification of mrna using real-time reverse transcription polymerase chain reaction assays. J. Mol. Endocrinol. *25*, 169–193.

Bustin, S.A. (2002). Quantification of mRNA using real-time reverse transcription PCR (RT-PCR): Trends and problems. J. Mol. Endocrinol. *29*, 23–39.

Bustin, S.A., Benes, V., Nolan, T., and Pfaffl, M.W. (2005). Quantitative real-time RT-PCR - A perspective. J. Mol. Endocrinol. *34*, 597–601.

Cabrera, A., Edelstein, H.I., Glykofrydis, F., Love, K.S., Palacios, S., Tycko, J., Zhang, M., Lensch, S., Shields, C.E., Livingston, M., et al. (2022). The sound of silence: Transgene silencing in mammalian cell engineering. Cell Syst. *13*, 950–973.

Cai, Y., Dong, Q., and Li, A. (2020). Review of CpG Island Recognition Algorithms. J. Phys. Conf. Ser. *1624*.

Canouil, M., Bouland, G.A., Bonnefond, A., Froguel, P., T'Hart, L.M., and Slieker, R.C. (2019). NACHO: An R package for quality control of Nanostring nCounter data. Bioinformatics *36*, 970–971.

Cantaert, T., Baeten, D., Tak, P.P., and van Baarsen, L.G.M. (2010). Type I IFN and TNFα cross-regulation in immune-mediated inflammatory disease: Basic concepts and clinical relevance. Arthritis Res. Ther. *12*, 1–10.

Carswell, E.A., Old, L.J., Kassel, R.L., Green, S., Fiore, N., and Williamson, B. (1975). An endotoxin induced serum factor that cuases necrosis of tumors. Proc. Natl. Acad. Sci. U. S. A. *72*, 3666–3670.

Chan, Y.K., Wang, S.K., Chu, C.J., Copland, A., Alexander, J., Verdera, H.C., Chiang, J.J., Sethi, M., Wang, M.K., Jr, W.J.N., et al. (2021). Engineering adeno-associated viral vectors to evade innate immune and inflammatory responses. Sci. Transl. Med. *13*, 1–34.

Chang, G.J., Mahanty, H.D., Vincenti, F., Freise, C.E., Roberts, J.P., Ascher, N.L., Stock, P.G., and Hirose, R. (2000). A calcineurin inhibitor-sparing regimen with sirolimus, mycophenolate mofetil, and anti-CD25 mAb provides effective immunosuppression in kidney transplant recipients with delayed or impaired graft function. Clin. Transplant. *14*, 550–554.

Chaplin, D.D. (2010). Overview of the Immune Response. J. Allergy Clin. Immunol. *125*, 826–828.

Chattopadhyay, P.K., Gierahn, T.M., Roederer, M., and Love, J.C. (2014). Single-cell technologies for monitoring immune systems. Nat. Immunol. *15*, 128–135.

Chaudhry, A., Samstein, R.M., Treuting, P., Liang, Y., Pils, M.C., Heinrich, J.M., Jack, R.S., Wunderlich, F.T., Brüning, J.C., Müller, W., et al. (2011). Interleukin-10 Signaling in Regulatory T Cells Is Required for Suppression of Th17 Cell-Mediated Inflammation. Immunity *34*, 566–578.

Chen, L., Koyanagi, M., Fukada, K., Imanishi, K., Yagi, J., Kato, H., Miyoshi-Akiyama, T., Zhang, R., Miwa, K., and Uchiyama, T. (2002). Continuous Exposure of Mice to Superantigenic Toxins Induces a High-Level Protracted Expansion and an Immunological Memory in the Toxin-Reactive CD4+ T Cells. J. Immunol. *168*, 3817–3824.

Chen, L., Grabowski, K.A., Xin, J., Coleman, J., Huang, Z., Espiritu, B., Alkan, S., Xie, H.B., Zhu, Y., White, F.A., et al. (2004). IL-4 Induces Differentiation and Expansion of Th2 Cytokine-Producing Eosinophils. J. Immunol. *172*, 2059–2066.

Chen, Y., Xiang, L.X., and Shao, J.Z. (2007). Construction of a recombinant plasmid containing multi-copy CpG motifs and its effects on the innate immune responses of aquatic animals. Fish Shellfish Immunol. *23*, 589–600.

Clinical Trials <https://clinicaltrials.gov/> accessed July 2023

Coban, C., Ishii, K.J., Gursel, M., Klinman, D.M., and Kumar, N. (2005). Effect of plasmid backbone modification by different human CpG motifs on the immunogenicity of DNA vaccine vectors. J. Leukoc. Biol. *78*, 647–655.

Codeluppi, S., Gregory, E.N., Kjell, J., Wigerblad, G., Olson, L., and Svensson, C.I. (2011). Influence of rat substrain and growth conditions on the characteristics of primary cultures of adult rat spinal cord astrocytes. J. Neurosci. Methods *197*, 118–127.

Coffman, R., and Carty, J. (1986). A T cell activity that enhances polyclonal IgE production and its inhibition by IFN-g. J. Immunol. *136*, 949–954.

Cooper, E.L. (1992). Overview of immunoevolution. Ital. J. Zool. *59*, 119–128.

Corthay, A. (2009). How do regulatory t cells work? Scand. J. Immunol. *70*, 326–336.

Costa, L.T., Kerkmann, M., Hartmann, G., Endres, S., Bisch, P.M., Heckl, W.M., and Thalhammer, S. (2004). Structural studies of oligonucleotides containing G-quadruplex motifs using AFM. Biochem. Biophys. Res. Commun. *313*, 1065–1072.

Culley, F.J., Pennycook, A.M.J., Tregoning, J.S., Dodd, J.S., Walzl, G., Wells, T.N., Hussell, T., and Openshaw, P.J.M. (2006). Role of CCL5 (RANTES) in Viral Lung Disease. J. Virol. *80*, 8151–8157.

Czerkinsky, C., Nilsson, L.Å., Nygren, H., Ouchterlony, Ö., and Tarkowski, A. (1984). Solid-phase enzyme-linked immunospot (ELISPOT) assay for enumeration of IgG rheumatoid factor-secreting cells. J. Immunol. Methods *72*, 451–459.

Dangouloff, T., and Servais, L. (2019). Clinical evidence supporting early treatment of patients with spinal muscular atrophy: Current perspectives. Ther. Clin.

Risk Manag. *15*, 1153–1161.

Danielsson, R., and Eriksson, H. (2021). Aluminium adjuvants in vaccines – A way to modulate the immune response. Semin. Cell Dev. Biol. *115*, 3–9.

Dhanda, S.K., Mahajan, S., Paul, S., Yan, Z., Kim, H., Jespersen, M.C., Jurtz, V., Andreatta, M., Greenbaum, J.A., Marcatili, P., et al. (2019). IEDB-AR: immune epitope database - analysis resource in 2019. Nucleic Acids Res. *47*, W502–W506.

Dias Junior, A.G., Sampaio, N.G., and Rehwinkel, J. (2019). A Balancing Act: MDA5 in Antiviral Immunity and Autoinflammation. Trends Microbiol. *27*, 75–85.

Diehl, S., and Rincón, M. (2002). The two faces of IL-6 on Th1/Th2 differentiation. Mol. Immunol. *39*, 531–536.

Doytchinova, I.A., and Flower, D.R. (2007). VaxiJen: A server for prediction of protective antigens, tumour antigens and subunit vaccines. BMC Bioinformatics *8*, 1–7.

Drescher, H., Weiskirchen, S., and Weiskirchen, R. (2021). Flow cytometry: A blessing and a curse. Biomedicines *9*, 1–12.

Du, J., Jin, J., Wang, J., and Sun, H. (2020). Mechanisms of mixed Th1/Th2 responses in mice induced by albizia julibrissin saponin active fraction by in silico analysis. Vaccines *8*, 1–21.

Duan, J., and Antezana, M.A. (2003). Mammalian Mutation Pressure, Synonymous Codon Choice, and mRNA Degradation. J. Mol. Evol. *57*, 694–701.

Duquette, M.L., Handa, P., Vincent, J.A., Taylor, A.F., and Maizels, N. (2004). Intracellular transcription of G-rich DNAs induces formation of G-loops, novel structures containing G4 DNA. Genes Dev. *18*, 1618–1629.

Duramad, O., Fearon, K.L., Chang, B., Chan, J.H., Gregorio, J., Coffman, R.L., and Barrat, F.J. (2005). Inhibitors of TLR-9 Act on Multiple Cell Subsets in Mouse and Man In Vitro and Prevent Death In Vivo from Systemic Inflammation. J. Immunol. *174*, 5193–5200.

Elnifro, E.M., Ashshi, A.M., Cooper, R.J., and Klapper, P.E. (2000). Multiplex PCR: Optimization and application in diagnostic virology. Clin. Microbiol. Rev. *13*, 559–570.

Engvall, E., and Perlmann, P. (1971). Enzyme-linked immunosorbent assay (ELISA) quantitative assay of immunoglobulin G. Immunochemistry *8*, 871–874.

Excler, J.L., Saville, M., Berkley, S., and Kim, J.H. (2021). Vaccine development for emerging infectious diseases. Nat. Med. *27*, 591–600.

Fang, M., Wan, M., Guo, S., Sun, R., Yang, M., Zhao, T.S., Yan, Y., Zhang, Y., Huang, W., Wu, X., et al. (2011). An oligodeoxynucleotide capable of lessening acute lung inflammatory injury in mice infected by influenza virus. Biochem. Biophys. Res. Commun. *415*, 342–347.

Fischer, T., Büttner, M., and Rziha, H.J. (2000). T helper 1-type cytokine transcription

in peripheral blood mononuclear cells of pseudorabies virus (Suid herpesvirus 1)-primed swine indicates efficient immunization. Immunology *101*, 378–387.

Fitzpatrick, Z., Leborgne, C., Barbon, E., Masat, E., Ronzitti, G., van Wittenberghe, L., Vignaud, A., Collaud, F., Charles, S., Simon Sola, M., et al. (2018). Influence of Pre-existing Anti-capsid Neutralizing and Binding Antibodies on AAV Vector Transduction. Mol. Ther. - Methods Clin. Dev. *9*, 119–129.

Frazier, K.S. (2015). Antisense Oligonucleotide Therapies:The Promise and the Challenges from a Toxicologic Pathologist's Perspective. Toxicol. Pathol. *43*, 78–89.

Gajewski, T.F., and Fitch, F.W. (1988). Anti-proliferative effect of IFN-gamma in immune regulation. I. IFN-gamma inhibits the proliferation of Th2 but not Th1 murine helper T lymphocyte clones. J. Immunol. *140*, 4245–4252.

Gao, J., Hussain, R.M., and Weng, C.Y. (2020). Voretigene neparvovec in retinal diseases: A review of the current clinical evidence. Clin. Ophthalmol. *14*, 3855–3869.

Gao, S., Li, X., Nie, S., Yang, L., Tu, L., Dong, B., Zhao, P., Wang, Y., Yu, Y., Wang, L., et al. (2017). An AAAG-rich oligodeoxynucleotide rescues mice from bacterial septic peritonitis by interfering interferon regulatory factor 5. Int. J. Mol. Sci. *18*.

Gary, E.N., and Weiner, D.B. (2020). DNA vaccines: prime time is now. Curr. Opin. Immunol. *65*, 21–27.

Gentili, M., Lahaye, X., Nadalin, F., Fachinetti, D., and Manel, N. (2019). The N-Terminal Domain of cGAS Determines Preferential Association with Centromeric DNA and Innate Immune Activation in the Nucleus.

Gershon, R.K., and Kondo, K. (1970). Cell interactions in the induction of tolerance: the role of thymic lymphocytes. Immunology *18*, 723–737.

Ginn, S.L., Amaya, A.K., Alexander, I.E., Edelstein, M., and Abedi, M.R. (2018). Gene therapy clinical trials worldwide to 2017: An update. J. Gene Med. *20*.

Graham, K.L., Lee, L.Y., Higgins, J.P., Steinman, L., Utz, P.J., and Ho, P.P. (2010). Treatment with a Toll-like receptor inhibitory GpG oligonucleotide delays and attenuates lupu nephritis in NZB/W mice. Autoimmunity *43*, 140–155.

Grakoui, A., Bromley, S.K., Sumen, C., Davis, M.M., Andrey, S., Allen, P.M., Dustin, M.L., Grakoui, A., Bromley, S.K., Sumen, C., et al. (1999). The Immunological Synapse : A Molecular Machine Controlling T Cell Activation. Science (80-.). *285*, 221–227.

Graves, C.L., Norloff, E., Thompson, D., Kosyk, O., Sang, Y., Chen, A., Zannas, A.S., and Wallet, S.M. (2023). Chronic early life stress alters the neuroimmune profile and functioning of the developing zebrafish gut. Brain, Behav. Immun. - Heal. *31*, 100655.

Gursel, I., Gursel, M., Yamada, H., Ishii, K.J., Takeshita, F., and Klinman, D.M.

(2003). Repetitive Elements in Mammalian Telomeres Suppress Bacterial DNA-Induced Immune Activation. J. Immunol. *171*, 1393–1400.

Gursel, M., Klinman, D.M., and Gursel, I. (2013). Plasmacytoid dendritic cell response to CpG ODN correlates with CXCL16 expression and is inhibited by ox-LDL. Mediators Inflamm. *2013*.

Gürtler, C., and Bowie, A.G. (2013). Innate immune detection of microbial nucleic acids. Trends Microbiol. *21*, 413–420.

Habib, O., Sakri, R.M., Ghazalli, N., Chau, D.M., Ling, K.H., and Abdullah, S. (2020). Limited expression of non-integrating CpG-free plasmid is associated with increased nucleosome enrichment. PLoS One *15*.

Hamilton, B.A., and Wright, J.F. (2021). Challenges Posed by Immune Responses to AAV Vectors: Addressing Root Causes. Front. Immunol. *12*, 1–8.

Harrington, L.E., Hatton, R.D., Mangan, P.R., Turner, H., Murphy, T.L., Murphy, K.M., and Weaver, C.T. (2005). Interleukin 17-producing CD4+ effector T cells develop via a lineage distinct from the T helper type 1 and 2 lineages. Nat. Immunol. *6*, 1123–1132.

Hartl, D., Krebs, A.R., Grand, R.S., Baubec, T., Isbel, L., Wirbelauer, C., Burger, L., and Schübeler, D. (2019). CG dinucleotides enhance promoter activity independent of DNA methylation. Genome Res. *29*, 554–563.

He, C., Zhou, L., Sun, R., Zhao, T., Zhang, Y., Fu, Y., Wang, L., and Yu, Y. (2011). Effects of oligodeoxynucleotide with CCT repeats on chronic graft versus host disease induced experimental lupus nephritis in mice. Clin. Immunol. *140*, 300–306.

Hemmi, H., Takeuchi, O., Kawai, T., Kaisho, T., Sato, S., Sanjo, H., Matsumoto, M., Hoshino, K., Wagner, H., Takeda, K., et al. (2000). A Toll-like receptor recognizes bacterial DNA. Nature *408*, 740–745.

Herzner, A.M., Hagmann, C.A., Goldeck, M., Wolter, S., Kübler, K., Wittmann, S., Gramberg, T., Andreeva, L., Hopfner, K.P., Mertens, C., et al. (2015). Sequence-specific activation of the DNA sensor cGAS by Y-form DNA structures as found in primary HIV-1 cDNA. Nat. Immunol. *16*, 1025–1033.

Ho, P.P., Fontoura, P., Ruiz, P.J., Steinman, L., and Garren, H. (2003). An Immunomodulatory GpG Oligonucleotide for the Treatment of Autoimmunity via the Innate and Adaptive Immune Systems. J. Immunol. *171*, 4920–4926.

Ho, P.P., Fontoura, P., Platten, M., Sobel, R.A., DeVoss, J.J., Lee, L.Y., Kidd, B.A., Tomooka, B.H., Capers, J., Agrawal, A., et al. (2005). A Suppressive Oligodeoxynucleotide Enhances the Efficacy of Myelin Cocktail/IL-4-Tolerizing DNA Vaccination and Treats Autoimmune Disease. J. Immunol. *175*, 6226–6234.

Ho, S.C.L., Koh, E.Y.C., Soo, B.P.C., Chao, S.H., and Yang, Y. (2016). Evaluating the use of a CpG free promoter for long-term recombinant protein expression stability in Chinese hamster ovary cells. BMC Biotechnol. *16*, 1–13.

Honda, K., Hideyuki, Y., Hideo, N., Asagiri, M., Sato, M., Mizutani, T., Shimada, N., Yusuke, O., Takaoka, A., Yoshida, N., et al. (2005). IRF-7 is the master regulator of type-I interferon-dependent immune responses. Nature *434*.

Hornung, V., Rutering, J., Ilmer, M., Recio, A., Coleman, M., Vykoukal, J., Alt, E., and Orleans, N. (2009). AIM2 recognizes cytosolic dsDNA and forms a caspase-1 activating inflammasome with ASC. Nature *458*.

Hsieh, C., Macatonia, S.E., Tripp, C.S., Wolf, S.F., Hsieh, C., Macatonia, S.E., Tripp, C.S., Wolf, S.F., Garra, A.O., and Murphy, K.M. (1993). Development of TH1 CD4+ T Cells Through IL-12 Produced by Listeria-Induced Macrophages. Science (80-.). *260*, 547–549.

Hu, D., Su, X., Sun, R., Yang, G., Wang, H., Ren, J., Sun, L., Wu, X., Hu, X., Yu, Y., et al. (2009). Human microsatellite DNA mimicking oligodeoxynucleotides down-regulate TLR9-dependent and -independent activation of human immune cells. Mol. Immunol. *46*, 1387–1396.

Hu, J., Yan, J., Ganesh, R., Latha, K., Overwijk, W.W., Heimberger, A.B., and Li, S. (2016). The duality of fgl2 - secreted immune checkpoint regulator versus membrane-associated procoagulant: therapeutic potential and implications. Int. Rev. Immunol. *35*, 325–339.

Huerfano, S., Ryabchenko, B., and Forstová, J. (2013). Nucleofection of expression vectors induces a robust interferon response and inhibition of cell proliferation. DNA Cell Biol. *32*, 467–479.

Hyde, S.C., Pringle, I.A., Abdullah, S., Lawton, A.E., Davies, L.A., Varathalingam, A., Nunez-Alonso, G., Green, A.M., Bazzani, R.P., Sumner-Jones, S.G., et al. (2008). CpG-free plasmids confer reduced inflammation and sustained pulmonary gene expression. Nat. Biotechnol. *26*, 549–551.

Ishikawa, H., and Barber, G.N. (2008). STING is an endoplasmic reticulum adaptor that facilitates innate immune signalling. Nature *455*, 674–678.

Ito, Y., Shigemori, S., Sato, T., Shimazu, T., Hatano, K., Otani, H., Kitazawa, H., and Shimosato, T. (2013). Class I/II hybrid inhibitory oligodeoxynucleotide exerts Th1 and Th2 double immunosuppression. Fed. Eur. Biochem. Soc. *3*, 41–45.

Iwamoto, S., Iwai, S., Tsujiyama, K., Kurahashi, C., Takeshita, K., Naoe, M., Masunaga, A., Ogawa, Y., Oguchi, K., and Miyazaki, A. (2007). TNF-α Drives Human CD14+ Monocytes to Differentiate into CD70+ Dendritic Cells Evoking Th1 and Th17 Responses. J. Immunol. *179*, 1449–1457.

Jaluria, P., Konstantopoulos, K., Betenbaugh, M., and Shiloach, J. (2007). A perspective on microarrays: Current applications, pitfalls, and potential uses. Microb. Cell Fact. *6*, 1–14.

Jin, T., Perry, A., Jiang, J., Smith, P., Curry, J.A., Unterholzner, L., Jiang, Z., Horvath, G., Rathinam, V., Ricky, W., et al. (2001). Structures of The HIN Domain:DNA Complexes Reveal Ligand Binding and Activation Mechanisms of The AIM2 Inflammasome and IFI16 Receptor. *36*, 561–571.

Johnson, A.O., Fowler, S.B., Webster, C.I., Brown, A.J., and James, D.C. (2022). Bioinformatic Design of Dendritic Cell-Specific Synthetic Promoters. ACS Synth. Biol. *11*, 1613–1626.

Jooss, K., Yang, Y., Fisher, K.J., and Wilson, J.M. (1998). Transduction of Dendritic Cells by DNA Viral Vectors Directs the Immune Response to Transgene Products in Muscle Fibers. J. Virol. *72*, 4212–4223.

Junt, T., and Barchet, W. (2015). Translating nucleic acid-sensing pathways into therapies. Nat. Rev. Immunol. *15*, 529–544.

Jutel, M., Akdis, M., Budak, F., Aebischer-Casaulta, C., Wrzyszcz, M., Blaser, K., and Akdis, C.A. (2003). IL-10 and TGF-β cooperate in the regulatory T cell response to mucosal allergens in normal immunity and specific immunotherapy. Eur. J. Immunol. *33*, 1205–1214.

Kaminski, D.A., Wei, C., Qian, Y., Rosenberg, A.F., and Sanz, I. (2012). Advances in human B cell phenotypic profiling. Front. Immunol. *3*, 1–15.

Kaminski, J.J., Schattgen, S.A., Tzeng, T.-C., Bode, C., Klinman, D.M., and Fitzgerald, K.A. (2013). Synthetic Oligodeoxynucleotides Containing Suppressive TTAGGG Motifs Inhibit AIM2 Inflammasome Activation. J. Immunol. *191*, 3876–3883.

Kanehisa, M., and Goto, S. (1999). KEGG: Kyoto Encyclopedia of Genes and Genomes. Nucleic Acids Res. *28*, 27–3.

Kaur, G., and Dufour, J.M. (2012). Cell lines. Spermatogenesis *2*, 1–5.

Kawabata, S., Terao, Y., Fujiwara, T., Nakagawa, I., and Hamada, S. (1999). Targeted salivary gland immunization with plasmid DNA elicits specific salivary immunoglobulin A and G antibodies and serum immunoglobulin G antibodies in mice. Infect. Immun. *67*, 5863–5868.

Kawai, T., and Akira, S. (2010). The role of pattern-recognition receptors in innate immunity: Update on toll-like receptors. Nat. Immunol. *11*, 373–384.

Kawai, T., Takahashi, K., Sato, S., Coban, C., Kumar, H., Kato, H., Ishii, K.J., Takeuchi, O., and Akira, S. (2005). IPS-1, an adaptor triggering RIG-I- and Mda5-mediated type I interferon induction. Nat. Immunol. *6*, 981–988.

Khan, I., MacLean, J.A., Lee, F.S., Casciotti, L., DeHaan, E., Schwartzman, J.D., and Luster, A.D. (2000). IP-10 is critical for effector T cell trafficking and host survival in Toxoplasma gondii infection. Immunity *12*, 483–494.

Kim, T., Pazhoor, S., Bao, M., Zhang, Z., Hanabuchi, S., Facchinetti, V., Bover, L., Plumas, J., Chaperot, L., Qin, J., et al. (2010). Aspartate-glutamate-alanine-histidine box motif (DEAH)/RNA helicase a helicases sense microbial DNA in human plasmacytoid dendritic cells. Proc. Natl. Acad. Sci. U. S. A. *107*, 15181–15186.

Kirchner, S., Cai, Z., Rauscher, R., Kastelic, N., Anding, M., Czech, A., Kleizen, B., Ostedgaard, L.S., Braakman, I., Sheppard, D.N., et al. (2017). Alteration of protein function by a silent polymorphism linked to tRNA abundance. PLoS

Biol. *15*.

Kis-Toth, K., Szanto, A., Thai, T.-H., and Tsokos, G.C. (2011). Cytosolic DNA-Activated Human Dendritic Cells Are Potent Activators of the Adaptive Immune Response. J. Immunol. *187*, 1222–1234.

Klinman, D.M., Yi, A.K., Beaucage, S.L., Conover, J., and Krieg, A.M. (1996). CpG motifs present in bacterial DNA rapidly induce lymphocytes to secrete interleukin 6, interleukin 12, and interferon γ. Proc. Natl. Acad. Sci. U. S. A. *93*, 2879–2883.

Klinman, D.M., Zeuner, R., Verthelyi, D., Zeuner, R., Gursel, I., and Gursel, M. (2006). Method of treating inflammatory arthropathies with suppressors of CpG oligonucleotides.

Kojima, Y., Xin, K.Q., Ooki, T., Hamajima, K., Oikawa, T., Shinoda, K., Ozaki, T., Hoshino, Y., Jounai, N., Nakazawa, M., et al. (2002). Adjuvant effect of multi-CpG motifs on an HIV-1 DNA vaccine. Vaccine *20*, 2857–2865.

Kondrashov, F.A., Ogurtsov, A.Y., and Kondrashov, A.S. (2006). Selection in favor of nucleotides G and C diversifies evolution rates and levels of polymorphism at mammalian synonymous sites. J. Theor. Biol. *240*, 616–626.

Korn, T., and Hiltensperger, M. (2021). Role of IL-6 in the commitment of T cell subsets. Cytokine *146*, 155654.

Kouwenhoven, M., Özenci, V., Teleshova, N., Hussein, Y., Huang, Y.M., Eusebio, A., and Link, H. (2001). Enzyme-linked immunospot assays provide a sensitive tool for detection of cytokine secretion by monocytes. Clin. Diagn. Lab. Immunol. *8*, 1248–1257.

Krieg, A.M. (2002). CpG Motifs in Bacterial DNA and Their Immune Effects. Annu. Rev. Immunol. *20*, 709–760.

Krieg, A.M. (2006). Therapeutic potential of toll-like receptor 9 activation. Nat. Rev. Drug Discov. *5*, 471–484.

Krieg, A.M., Yi, A.K., Matson, S., Waldschmidt, T.J., Bishop, G.A., Teasdale, R., Koretzky, G.A., and Klinman, D.M. (1995). CpG motifs in bacterial DNA trigger direct B-cell activation. Nature *374*, 546–549.

Krieg, A.M., Wu, T., Weeratna, R., Efler, S.M., Love-Homan, L., Yang, L., Yi, K., Short, D., and Davis, H.L. (1998). Sequence motifs in adenoviral DNA block immune activation by stimulatory CpG motifs. Proc. Natl. Acad. Sci. U. S. A. *95*, 12631–12636.

Krinner, S., Heitzer, A., Asbach, B., and Wagner, R. (2015). Interplay of promoter usage and intragenic CpG content: Impact on GFP reporter gene expression. Hum. Gene Ther. *26*, 826–840.

Kucera, M., Isserlin, R., Arkhangorodsky, A., and Bader, G.D. (2016). AutoAnnotate: A Cytoscape app for summarizing networks with semantic annotations. Research *5*, 1–12.

Kulkarni, M.M. (2011). Digital multiplexed gene expression analysis using the Nanostring ncounter system. Curr. Protoc. Mol. Biol. 1–17.

Kupper, T.S., and Fuhlbrigge, R.C. (2004). Immune surveillance in the skin: Mechanisms and clinical consequences. Nat. Rev. Immunol. *4*, 211–222.

Langrish, C.L., Chen, Y., Blumenschein, W.M., Mattson, J., Basham, B., Sedgwick, J.D., McClanahan, T., Kastelein, R.A., and Cua, D.J. (2005). IL-23 drives a pathogenic T cell population that induces autoimmune inflammation. J. Exp. Med. *201*, 233–240.

Larsen, F., Gundersen, G., Lopez, R., and Prydz, H. (1992). CpG islands as gene markers in the human genome. Genomics *13*, 1095–1107.

Lašťovička, J., Budinský, V., Špíšek, R., and Bartůňková, J. (2009). Assessment of lymphocyte proliferation: CFSE kills dividing cells and modulates expression of activation markers. Cell. Immunol. *256*, 79–85.

Lee, H., Yoon, S.E., Kim, S.J., Kim, W.S., and Cho, J. (2023). A unique expression pattern of LAG3 distinct from that of other immune checkpoints in diffuse large B-cell lymphoma. Cancer Med. 1–11.

Lenert, P., Yasuda, K., Busconi, L., Nelson, P., Fleenor, C., Ratnabalasuriar, R.S., Nagy, P.L., Ashman, R.F., Rifkin, I.R., and Marshak-Rothstein, A. (2009). DNA-like class R inhibitory oligonucleotides (INH-ODNs) preferentially block autoantigen-induced B-cell and dendritic cell activation in vitro and autoantibody production in lupus-prone MRL-Faslpr/lpr mice in vivo. Arthritis Res. Ther. *11*, 1–16.

Leng, S.X., McElhaney, J.E., Walston, J.D., Dongxu, X., Fedarko, N.S., and Kuchel, G.A. (2008). Elisa and Multiplex Technologies for Cytokine Measurement in Inflammation and Aging Research. J. Gerontol. *63*, 879–884.

Li, G.-W., and Xie, S. (2011). Central dogma at the single-molecule level in living cells. Nature *7356*, 308–315.

Li, G., Iyer, B., Prasath, V.B.S., Ni, Y., and Salomonis, N. (2021). DeepImmuno: Deep learning-empowered prediction and generation of immunogenic peptides for T-cell immunity. Brief. Bioinform. *22*, 1–10.

Li, J., Ge, M., Lu, S., Shi, J., Li, X., Wang, M., Huang, J., Shao, Y., Huang, Z., Zhang, J., et al. (2017). Pro-inflammatory effects of the Th1 chemokine CXCL10 in acquired aplastic anaemia. Cytokine *94*, 45–51.

Li, X., Shu, C., Yi, G., Chaton, C.T., Shelton, C.L., Diao, J., Zuo, X., Kao, C.C., Herr, A.B., and Li, P. (2013a). Cyclic GMP-AMP Synthase Is Activated by Double-Stranded DNA-Induced Oligomerization. Immunity *39*, 1019–1031.

Li, X., Shu, C., Yi, G., Chaton, C.T., Shelton, C.L., Diao, J., Zuo, X., Kao, C.C., Herr, A.B., and Li, P. (2013b). Cyclic GMP-AMP Synthase is Activated by Double-stranded DNA-Induced Oligomerization. Immunity *39*.

Li, Y., Cao, H., Wang, N., Xiang, Y., Lu, Y., Zhao, K., Zheng, J., and Zhou, H. (2011). A

novel antagonist of TLR9 blocking all classes of immunostimulatory CpG-ODNs. Vaccine *29*, 2193–2198.

Liu, W., Yang, X., Wang, N., Fan, S., Zhu, Y., Zheng, X., and Li, Y. (2017). Multiple Immunosuppressive Effects of CpG-c41 on Intracellular TLR-Mediated Inflammation. Mediators Inflamm.

Lopes, A., Vandermeulen, G., and Préat, V. (2019). Cancer DNA vaccines : current preclinical and clinical developments and future perspectives. J. Exp. Clin. Cancer Res. *7*, 1–24.

Luan, N., Cao, H., Wang, Y., Lin, K., and Liu, C. (2022). Virologica Sinica LNP-CpG ODN-adjuvanted varicella-zoster virus glycoprotein E induced comparable levels of immunity with Shingrix ™ in VZV-primed mice. Virol. Sin. *37*, 731–739.

Luecke, S., Holleufer, A., Christensen, M.H., Jønsson, K.L., Boni, G.A., Sørensen, L.K., Johannsen, M., Jakobsen, M.R., Hartmann, R., and Paludan, S.R. (2017). cGAS is activated by DNA in a length-dependent manner . EMBO Rep. *18*, 1707–1715.

Ma, D.Y., and Clark, E.A. (2010). The role of CD40 and CD40L in Dendritic Cells. Semin. Immunol. *21*, 265–272.

Maeda, T., Murata, K., Fukushima, T., Sugahara, K., Tsuruda, K., Anami, M., Onimaru, Y., Tsukasaki, K., Tomonaga, M., Moriuchi, R., et al. (2005). A novel plasmacytoid dendritic cell line, CAL-1, established from a patient with blastic natural killer cell lymphoma. Int. J. Hematol. *81*, 148–154.

Marshall, J.S., Warrington, R., Watson, W., and Kim, H.L. (2018). An introduction to immunology and immunopathology. Allergy, Asthma Clin. Immunol. *14*, 1–10.

Martinon, F., Burns, K., and Tschopp, J. (2002). The Inflammasome: A molecular platform triggering activation of inflammatory caspases and processing of proIL-β. Mol. Cell *10*, 417–426.

Masterson, A.J., Sombroek, C.C., De Gruijl, T.D., Graus, Y.M.F., Van Der Vliet, H.J.J., Lougheed, S.M., Van Den Eertwegh, A.J.M., Pinedo, H.M., and Scheper, R.J. (2002). MUTZ-3, a human cell line model for the cytokine-induced differentiation of dendritic cells from CD34+ precursors. Blood *100*, 701–703.

Mauro, V.P. (2018). Codon Optimization in the Production of Recombinant Biotherapeutics: Potential Risks and Considerations. BioDrugs *32*, 69–81.

Mbongue, J., Nicholas, D., Firek, A., and Langridge, W. (2014). The role of dendritic cells in tissue-specific autoimmunity. J. Immunol. Res. *2014*.

McKinnon, K.M. (2019). Flow cytometry: an overview. Curr. Protoc. Immunol. *5*, 56–61.

McLachlan, G., Stevenson, B.J., Davidson, D.J., and Porteous, D.J. (2000). Bacterial DNA is implicated in the inflammatory response to delivery of DNA/DOTAP to

mouse lungs. Gene Ther. *7*, 384–392.

Meager, A. (1998). Interferons Alpha, Beta, and Omega. Cytokines 361–389.

Mears, H. V, and Sweeney, T.R. (2020). Mouse Ifit1b is a cap1-RNA – binding protein that inhibits mouse coronavirus translation and is regulated by complexing with Ifit1c. J. Biol. Chem. *295*, 17781–17801.

Mellman, I. (2013). Dendritic cells: master regulators of the immune response. Cancer Immunol. Res. *1*, 145–149.

Mendell, J.R., Rodino-Klapac, L.R., Rosales, X.Q., Coley, B.D., Galloway, G., Lewis, S., Malik, V., Shilling, C., Byrne, B.J., Conlon, T., et al. (2010). Sustained alpha-sarcoglycan gene expression after gene transfer in limb-girdle muscular dystrophy, type 2D. Ann. Neurol. *68*, 629–638.

Meng, W., Yamazaki, T., Nishida, Y., and Hanagata, N. (2011). Nuclease-resistant immunostimulatory phosphodiester CpG oligodeoxynucleotides as human Toll-like receptor 9 agonists. BMC Biotechnol. *11*.

Meng, X., Sun, W., Ren, Y., Xiao, Y., Zhao, P., Lu, W., Hua, L., Wang, L., Wang, L., and Yu, Y. (2017). Protective role of surface Toll-like receptor 9 expressing neutrophils in local inflammation during systemic inflammatory response syndrome in mice. Mol. Immunol. *90*, 74–86.

Mirjam, P., Bode, K., Lipford, G.B., Eberle, F., Heeg, K., and Dalpke, A.H. (2011). Characterization of suppressive oligodeoxynucleotides that inhibit Toll-like receptor-9-mediated activation of innate immunity. Eur. J. Immunol. *41*, 1–7.

Morrow, M.P., Yan, J., Pankhong, P., Ferraro, B., Lewis, M.G., Khan, A.S., Sardesai, N.Y., and Weiner, D.B. (2010). Unique Th1/Th2 phenotypes induced during priming and memory phases by use of interleukin-12 (IL-12) or IL-28B vaccine adjuvants in rhesus macaques. Clin. Vaccine Immunol. *17*, 1493–1499.

Mosmann, T.R., Cherwinski, H., Bond, M.W., Giedlin, M.A., and Coffman, R.L. (1986). Two types of murine helper T cell clone I. J. Immunol. *136*, 2348–2357.

Motwani, M., Pesiridis, S., and Fitzgerald, K.A. (2019). DNA sensing by the cGAS–STING pathway in health and disease. Nat. Rev. Genet. *20*, 657–674.

Muldoon, L.L., Alvarez, J.I., Begley, D.J., Boado, R.J., Del Zoppo, G.J., Doolittle, N.D., Engelhardt, B., Hallenbeck, J.M., Lonser, R.R., Ohlfest, J.R., et al. (2013). Immunologic privilege in the central nervous system and the blood-brain barrier. J. Cereb. Blood Flow Metab. *33*, 13–21.

Nagae, G., Isagawa, T., Shiraki, N., Fujita, T., Yamamoto, S., Tsutsumi, S., Nonaka, A., Yoshiba, S., Matsusaka, K., Midorikawa, Y., et al. (2011). Tissue-specific demethylation in CpG-poor promoters during cellular differentiation. Hum. Mol. Genet. *20*, 2710–2721.

Nie, S., Dong, B., Gao, S., Zhou, Y., Lu, W., Fang, M., Hua, S., Yu, Y., and Wang, L. (2019). The protective effect of interfering TLR9-IRF5 signaling pathway on the development of CVB3-induced myocarditis. Clin. Immunol. *207*, 24–35.

O'Connor, W., Kamanaka, M., Booth, C.J., Town, T., Nakae, S., Iwakura, Y., Kolls, J.K., and Flavell, R.A. (2009). A protective function for interleukin 17A in T cell-mediated intestinal inflammation. Nat. Immunol. *10*, 603–609.

O'Garra, A. (1998). Cytokines induce the development of functionally heterogeneous T helper cell subsets. Immunity *8*, 275–283.

Olkhov-Mitsel, E., Yu, Y., Lajkosz, K., Liu, S.K., Vesprini, D., Sherman, C.G., and Downes, M.R. (2022). Development of a Clinically Applicable Nanostring-Based Gene Expression Classifier for Muscle-Invasive Bladder Cancer Molecular Stratification. Cancers (Basel). *14*, 1–13.

Paludan, S.R. (2015). Activation and Regulation of DNA-Driven Immune Responses. Microbiol. Mol. Biol. Rev. *79*, 225–241.

Pandya, A., Shah, Y., Kothari, N., Postwala, H., Shah, A., Parekh, P., and Chorawala, M.R. (2023). The future of cancer immunotherapy: DNA vaccines leading the way (Springer US).

Park, H., Li, Z., Yang, X., Chang, S.H., Nurieva, R., Yi-Hong, W., Wang, Y., Hood, L., Zhu, Z., Tian, Q., et al. (2005). A distinct lineage of CD4 T cells regulates tissue inflammation by producing interleukin 17. Nat. Immunol. *6*, 1133–1141.

Patente, T.A., Pinho, M.P., Oliveira, A.A., Evangelista, G.C.M., Bergami-Santos, P.C., and Barbuto, J.A.M. (2019). Human dendritic cells: Their heterogeneity and clinical application potential in cancer immunotherapy. Front. Immunol. *10*, 1–18.

Paul, W.E., and Zhu, J. (2010). How are Th2-type immune responses initiated and amplified. Annu. Rev. Immunol. *28*, 445–489.

Pawar, R.D., Ramanjaneyulu, A., Kulkarni, O.P., Lech, M., Segerer, S., and Anders, H.J. (2007). Inhibition of Toll-like receptor-7 (TLR-7) or TLR-7 plus TLR-9 attenuates glomerulonephritis and lung injury in experimental lupus. J. Am. Soc. Nephrol. *18*, 1721–1731.

Perez, B.A., Shutterly, A., Chan, Y.K., Byrne, B.J., and Corti, M. (2020). Management of neuroinflammatory responses to AAV-mediated gene therapies for neurodegenerative diseases. Brain Sci. *10*.

Peter, M., Bode, K., Lipford, G.B., Eberle, F., Heeg, K., and Dalpke, A.H. (2008). Characterization of suppressive oligodeoxynucleotides that inhibit Toll-like receptor-9-mediated activation of innate immunity. Immunology *123*, 118–128.

Phetsouphanh, C., Zaunders, J.J., and Kelleher, A.D. (2015). Detecting antigen-specific T cell responses: From bulk populations to single cells. Int. J. Mol. Sci. *16*, 18878–18893.

Pisetsky, D.S., and Reich, C.F. (2000). Inhibition of murine macrophage IL-12 production by natural and synthetic DNA. Clin. Immunol. *96*, 198–204.

Pontarollo, R.A., Babiuk, L.A., Hecker, R., and van Drunen Littel-van den Hurk, S.

(2002). Augmentation of cellular immune responses to bovine herpesvirus-1 glycoprotein D by vaccination with CpG-enhanced plasmid vectors. J. Gen. Virol. *83*, 2973–2981.

Prazeres, D.M.F., and Monteiro, G.A. (2014). Plasmid Biopharmaceuticals. Am. Soc. Microbiol. *2*, 669–688.

Pringle, I.A., Hyde, S.C., Connolly, M.M., Lawton, A.E., Xu, B., Nunez-Alonso, G., Davies, L.A., Sumner-Jones, S.G., and Gill, D.R. (2012). CpG-free plasmid expression cassettes for cystic fibrosis gene therapy. Biomaterials *33*, 6833–6842.

Rahmani, M., Mohammadnia-Afrouzi, M., Nouri, H.R., Fattahi, S., Akhavan-Niaki, H., and Mostafazadeh, A. (2018). Human PBMCs fight or flight response to starvation stress: Increased T-reg, FOXP3, and TGF-β1 with decreased miR-21 and Constant miR-181c levels. Biomed. Pharmacother. *108*, 1404–1411.

Ramamoorth, M., and Narvekar, A. (2015). Non viral vectors in gene therapy - An overview. J. Clin. Diagnostic Res. *9*, GE01–GE06.

Rasaiyaah, J., Noursadeghi, M., Kellam, P., and Chain, B. (2017). Transcriptional and functional defects of dendritic cells derived from the MUTZ-3 leukaemia line. Immunology *5*.

Rasmussen, S., Horan, K.A., Holm, C.K., Amanda, J.S., Thomas, C.M., Simon, A.K., Søren, B.J., Frazer, J.R., Bin, H., and Søren, P. (2011). Activation of autophagy by alpha-herpesviruses in myeloid cells is mediated by cytoplasmic viral DNA through a mechanism dependent on STING. J. Immunol. *187*, 1–7.

Raudvere, U., Kolberg, L., Kuzmin, I., Arak, T., Adler, P., Peterson, H., and Vilo, J. (2019). G:Profiler: A web server for functional enrichment analysis and conversions of gene lists (2019 update). Nucleic Acids Res. *47*, W191–W198.

Razin, A., and Cedar, H. (1983). DNA methylation and gene expression. Biomed. Pharmacother. *37*, 173–175.

Rea, I.M., McNerlan, S.E., and Alexander, H.D. (1999). CD69, CD25, and HLA-DR activation antigen expression on CD3+ lymphocytes and relationship to serum TNF-α, IFN-γ, and sIL-2R levels in aging. Exp. Gerontol. *34*, 79–93.

Rehli, M. (2002). Of mice and men: Species variations of Toll-like receptor expression. Trends Immunol. *23*, 375–378.

Rehwinkel, J., and Gack, M.U. (2020). RIG-I-like receptors: their regulation and roles in RNA sensing. Nat. Rev. Immunol. *20*, 537–551.

Reimand, J., Kull, M., Peterson, H., Hansen, J., and Vilo, J. (2007). G:Profiler-a web-based toolset for functional profiling of gene lists from large-scale experiments. Nucleic Acids Res. *35*, 193–200.

Restifo, N.P., Ying, H., Hwang, L., and Leitner, W.W. (2000). The promise of nucleic acid vaccines. Gene Ther. *7*, 89–92.

Reyes-Sandoval, A., and Ertl, H.C.J. (2004). CpG methylation of a plasmid vector

results in extended transgene product expression by circumventing induction of immune responses. Mol. Ther. *9*, 249–261.

Rishi, V., Bhattacharya, P., Chatterjee, R., Rozenberg, J., Zhao, J., Glass, K., Fitzgerald, P., and Vinson, C. (2010). CpG methylation of half-CRE sequences creates C/EBPα binding sites that activate some tissue-specific genes. Proc. Natl. Acad. Sci. U. S. A. *107*, 20311–20316.

Ritchie, M.E., Phipson, B., Wu, D., Hu, Y., Law, C.W., Shi, W., and Smyth, G.K. (2015). Limma powers differential expression analyses for RNA-sequencing and microarray studies. Nucleic Acids Res. *43*, e47.

Rogers, G.L., Shirley, J.L., Zolotukhin, I., Kumar, S.R.P., Sherman, A., Perrin, G.Q., Hoffman, B.E., Srivastava, A., Basner-Tschakarjan, E., Wallet, M.A., et al. (2017). Plasmacytoid and conventional dendritic cells cooperate in crosspriming AAV capsid-specific CD8+ T cells. Blood *129*, 3184–3195.

Romagnani, S. (1996). TH1 and TH2 in human diseases. Clin. Immunol. Immunopathol. *80*, 225–235.

Römmler, F., Jurk, M., Uhlmann, E., Hammel, M., Waldhuber, A., Pfeiffer, L., Wagner, H., Vollmer, J., and Miethke, T. (2013). Guanine Modification of Inhibitory Oligonucleotides Potentiates Their Suppressive Function. J. Immunol. *191*, 3240–3253.

Römmler, F., Hammel, M., Waldhuber, A., Müller, T., Jurk, M., Uhlmann, E., Wagner, H., Vollmer, J., and Miethke, T. (2015). Guanine-modified inhibitory oligonucleotides efficiently impair TLR7- and TLR9-mediated immune responses of human immune cells. PLoS One *10*, 1–19.

Rosenfeld, A.M., Meng, W., Luning Prak, E.T., and Hershberg, U. (2018). ImmuneDB, a novel tool for the analysis, storage, and dissemination of immune repertoire sequencing data. Front. Immunol. *9*, 1–13.

Rusinova, I., Forster, S., Yu, S., Kannan, A., Masse, M., Cumming, H., Chapman, R., and Hertzog, P.J. (2013). INTERFEROME v2 . 0 : an updated database of annotated interferon-regulated genes. Nucleic Acids Res. *41*, 1040–1046.

Sack, B.K., and Herzog, R.W. (2009). Evading the immune response upon in vivo gene therapy with viral vectors. Curr. Opin. Mol. Ther. *11*, 493–503.

Sakamoto, S., Putalun, W., Vimolmangkang, S., Phoolcharoen, W., Shoyama, Y., Tanaka, H., and Morimoto, S. (2018). Enzyme-linked immunosorbent assay for the quantitative/qualitative analysis of plant secondary metabolites. J. Nat. Med. *72*, 32–42.

Sampaolesi, M., Blot, S., D'Antona, G., Granger, N., Tonlorenzi, R., Innocenzi, A., Mognol, P., Thibaud, J.L., Galvez, B.G., Barthélémy, I., et al. (2006). Mesoangioblast stem cells ameliorate muscle function in dystrophic dogs. Nature *444*, 574–579.

Samulowitz, U., Weber, M., Weeratna, R., Uhlmann, E., Noll, B., Krieg, A.M., and Vollmer, J. (2010). A novel class of immune-stimulatory cpg

oligodeoxynucleotides unifies high potency in type i interferon induction with preferred structural properties. Oligonucleotides *20*, 93–101.

Saraswat, P., Soni, R.R., Bhandari, A., and Nagori, B.P. (2009). DNA as therapeutics; An update. Indian J. Pharm. Sci. *71*, 488–498.

Sasai, M., Linehan, M.M., and Iwasaki, A. (2010). Bifurcation of Toll-Like Receptor 9 Signaling by Adaptor Protein 3. Science (80-.). *329*, 1530–1534.

Scharner, J., and Aznarez, I. (2021). Clinical Applications of Single-Stranded Oligonucleotides: Current Landscape of Approved and In-Development Therapeutics. Mol. Ther. *29*, 540–554.

Schmidt, B.Z., Haaf, J.B., Leal, T., and Noel, S. (2016). Cystic fibrosis transmembrane conductance regulator modulators in cystic fibrosis: Current perspectives. Clin. Pharmacol. Adv. Appl. *8*, 127–140.

Schneeberger, A., Wagner, C., Anja, Z., Lhrs, P., Kutil, R., Goos, M., Stingl, G., and Wagner, S.N. (2004). CpG Motifs Are Efficient Adjuvants for DNA Cancer Vaccines. J. Invest. Dermatol. 371–379.

Schuessler-Lenz, M., Enzmann, H., and Vamvakas, S. (2020). Regulators' Advice Can Make a Difference: European Medicines Agency Approval of Zynteglo for Beta Thalassemia. Clin. Pharmacol. Ther. *107*, 492–494.

Sean, D., and Meltzer, P.S. (2007). GEOquery: A bridge between the Gene Expression Omnibus (GEO) and BioConductor. Bioinformatics *23*, 1846–1847.

Seder, R.A., Paul, W.E., Davis, M.M., and Fazekas de St. Groth, B. (1992). The presence of interleukln 4 during in vitro priming determines the lymphoklne-producing potential of CD4+ T cells from T cell receptor transgenic mice. J. Exp. Med. *176*, 1091–1098.

Šega, S., Wraber, B., Mesec, A., Horvat, A., and Ihan, A. (2004). IFN-β1a and IFN-β1b have different patterns of influence on cytokines. Clin. Neurol. Neurosurg. *106*, 255–258.

Shabalina, S.A., Ogurtsov, A.Y., and Spiridonov, N.A. (2006). A periodic pattern of mRNA secondary structure created by the genetic code. Nucleic Acids Res. *34*, 2428–2437.

Shannon, P., Markiel, A., Ozier, O., Baliga, N.S., Wang, J.T., Ramage, D., Amin, N., Schwikowski, B., and Ideker, T. (2019). Cytoscape: A Software Environment for Integrated Models. Genome Res. *13*, 426.

Shen, Z., Reznikoff, G., Dranoff, G., and Rock, K. (1997). Cloned dendritic cells can present exogenous antigens on both MHC class I and class II molecules. J. Immunol. *158*, 2723–2730.

Shirai, S., Shibuya, M., Kawai, A., Tamiya, S., and Munakata, L. (2020). Lipid Nanoparticles Potentiate Vaccine for Influenza Virus. Frounties Immunol. *10*.

Shirley, J.L., de Jong, Y.P., Terhorst, C., and Herzog, R.W. (2020). Immune Responses to Viral Gene Therapy Vectors. Mol. Ther. *28*, 709–722.

Shirota, H., Gursel, M., and Klinman, D.M. (2004). Suppressive Oligodeoxynucleotides Inhibit Th1 Differentiation by Blocking IFN-γ- and IL-12-Mediated Signaling. J. Immunol. *173*, 5002–5007.

Sibbald, B. (2001). Death but one unintended consequence of gene-therapy trial. Can. Med. Assoc. J. *164*, 1612.

Steinhagen, F., Meyer, C., Tross, D., Gursel, M., Maeda, T., Klaschik, S., and Klinman, D.M. (2012a). Activation of type I interferon-dependent genes characterizes the " core response " induced by CpG DNA. J. Leukoc. Biol. *92*, 775–785.

Steinhagen, F., Meyer, C., Tross, D., Gursel, M., Maeda, T., Klaschik, S., and Klinman, D.M. (2012b). Activation of type I interferon-dependent genes characterizes the "core response" induced by CpG DNA. J. Leukoc. Biol. *92*, 775–785.

Steinhagen, F., Mcfarland, A.P., Rodriguez, L.G., Tewary, P., Jarret, A., Savan, R., and Klinman, D.M. (2013). IRF-5 and NF-κB p50 co-regulate IFN-β and IL-6 expression in TLR9-stimulated human plasmacytoid dendritic cells. Eur. J. Immunol. *43*, 1896–1906.

Steinhagen, F., Rodriguez, L.G., Tross, D., Tewary, P., Bode, C., and Klinma, D.M. (2016). IRF5 and IRF8 modulate the CAL-1 human plasmacytoid dendritic cell line response following TLR9 ligation. Eur. J. Immunol. *46*, 647–655.

Steinhagen, F., Zillinger, T., Peukert, K., Fox, M., Thudium, M., Barchet, W., Putensen, C., Klinman, D., Latz, E., and Bode, C. (2018). Suppressive oligodeoxynucleotides containing TTAGGG motifs inhibit cGAS activation in human monocytes. Eur. J. Immunol. *48*, 605–611.

Steinman, R.M., and Cohn, Z.A. (1973). Identification of a novel cell type in peripheral lymphoid organs of mice. J. Exp. Med. *137*, 1142–1162.

Stetson, D.B., and Medzhitov, R. (2006). Recognition of cytosolic DNA activates an IRF3-dependent innate immune response. Immunity *24*, 93–103.

Streilein, J.W., Ksander, B.R., and Taylor, A.W. (1997a). Immune deviation in relation to ocular immune privilege. J. Immunol. *158*, 3557–3560.

Streilein, J.W., Takeuchi, M., and Taylor, A.W. (1997b). Immune privilege, T-cell tolerance, and tissue-restricted autoimmunity. Hum. Immunol. *52*, 138–143.

Stunz, L.L., Lenert, P., Peckham, D., Yi, A.K., Haxhinasto, S., Chang, M., Krieg, A.M., and Ashman, R.F. (2002). Inhibitory oligonucleotides specifically block effects of stimulatory CpG oligonucleotides in B cells. Eur. J. Immunol. *32*, 1212–1222.

Su, H., Liao, Z., Yuan, G., and Su, J. (2017). A plasmid containing CpG ODN as vaccine adjuvant against grass carp reovirus in grass carp Ctenopharyngodon idella. Oncotarget *8*, 86576–86591.

Sun, R., Sun, L., Bao, M., Zhang, Y., Wang, L., Wu, X., Hu, D., Liu, Y., Yu, Y., and Wang, L. (2010). A human microsatellite DNA-mimicking oligodeoxynucleotide with CCT repeats negatively regulates TLR7/9-mediated innate immune responses via selected TLR pathways. Clin. Immunol. *134*,

262–276.

Suschak, J.J., Williams, J.A., and Schmaljohn, C.S. (2017). Advancements in DNA vaccine vectors, non-mechanical delivery methods, and molecular adjuvants to increase immunogenicity. Hum. Vaccines Immunother. *13*, 2837–2848.

Suzuki, Y., Orellana, M.A., Schreiber, R.D., Jack, S., and Remington, J.S. (1988). Interferon-g : The Major Mediator of Resistance against Toxoplasma gondii Published. Science (80-.). *240*, 516–518.

Sved, J., and Bird, A. (1990). The expected equilibrium of the CpG dinucleotide in vertebrate genomes under a mutation model (DNA methylation/factor IX/a-globin gene/pseudogene/neutral hypothesis). Evolution (N. Y). *87*, 4692–4696.

Swain, S.L., Weinberg, A.D., English, M., Huston, G., and Huston, G. (1990). IL-4 directs the development of Th2-like helper effectors. J. Immunol. *145*, 3796–3806.

Swayze, E.E., Siwkowski, A.M., Wancewicz, E. V., Migawa, M.T., Wyrzykiewicz, T.K., Hung, G., Monia, B.P., and Bennett, C.F. (2007). Antisense oligonucleotides containing locked nucleic acid improve potency but cause significant hepatotoxicity in animals. Nucleic Acids Res. *35*, 687–700.

Takaoka, A., Yanai, H., Kondo, S., Duncan, G., Negishi, H., Mizutani, T., Kano, S.I., Honda, K., Ohba, Y., Mak, T.W., et al. (2005). Integral role of IRF-5 in the gene induction programme activated by Toll-like receptors. Nature *434*, 243–249.

Tapia-Calle, G., Stoel, M., de Vries-Idema, J., and Huckriede, A. (2017). Distinctive responses in an in vitro human dendritic cell-based system upon stimulation with different influenza vaccine formulations. Vaccines *5*.

Tate, P.H., and Bird, A.P. (1993). Effects of DNA methylation on DNA-binding proteins and gene expression. Curr. Opin. Genet. Dev. *3*, 226–231.

Tesmer, L.A., Lundy, S.K., Sarkar, S., and Fox, D.A. (2008). Th17 cells in human disease. Immunol. Rev. *223*, 87–113.

Tighe, P.J., Ryder, R.R., Todd, I., and Fairclough, L.C. (2015). ELISA in the multiplex era: Potentials and pitfalls. Proteomics - Clin. Appl. *9*, 406–422.

Touzot, M., Grandclaudon, M., Cappuccio, A., Satoh, T., Martinez-Cingolani, C., Servant, N., Manel, N., and Soumelis, V. (2014). Combinatorial flexibility of cytokine function during human T helper cell differentiation. Nat. Commun. *5*, 1–9.

Unterholzner, L., Keating, S.E., Baran, M., Horan, K.A., Jensen, S.B., Sharma, S., Sirois, C.M., Jin, T., Latz, E., Xiao, T.S., et al. (2010). IFI16 is an innate immune sensor for intracellular DNA. Nat. Immunol. *11*, 997–1004.

Vaissière, T., Sawan, C., and Herceg, Z. (2008). Epigenetic interplay between histone modifications and DNA methylation in gene silencing. Mutat. Res. - Rev. Mutat. Res. *659*, 40–48.

Valentin, R., Wong, C., Alharbi, A.S., Pradeloux, S., Morros, M.P., Lennox, K.A.,

Ellyard, J.I., Garcin, A.J., Ullah, T.R., Kusuma, G.D., et al. (2021). Sequence-dependent inhibition of cGAS and TLR9 DNA sensing by 2′-O-methyl gapmer oligonucleotides. Nucleic Acids Res. *49*, 6082–6099.

Vandivort, T.C., Horton, D.B., and Johnson, S.B. (2020). Regulatory and strategic considerations for addressing immunogenicity and related responses in biopharmaceutical development programs. J. Clin. Transl. Sci. *4*, 547–555.

Verthelyi, D., Gursel, M., Kenney, R.T., Lifson, J.D., Liu, S., Mican, J., and Klinman, D.M. (2003). CpG Oligodeoxynucleotides Protect Normal and SIV-Infected Macaques from Leishmania Infection . J. Immunol. *170*, 4717–4723.

Vignali, D.A.A., Collison, L.W., and Workman, C.J. (2008). How regulatory T cells work. Nat. Rev. Immunol. *8*, 523–532.

Vollmer, J., Weeratna, R., Payette, P., Jurk, M., Schetter, C., Laucht, M., Wader, T., Tluk, S., Liu, M., Davis, H.L., et al. (2004). Characterization of three CpG oligodeoxynucleotide classes with distinct immunostimulatory activities. Eur. J. Immunol. *34*, 251–262.

Volpi, C., Fallarino, F., Bianchi, R., Orabona, C., De Luca, A., Vacca, C., Romani, L., Gran, B., Grohmann, U., Puccetti, P., et al. (2012). A GpC-Rich Oligonucleotide Acts on Plasmacytoid Dendritic Cells To Promote Immune Suppression. J. Immunol. *189*, 2283–2289.

Wang, H., Su, Y., Chen, D., Li, Q., Shi, S., Huang, X., Fang, M., and Yang, M. (2023). Advances in the mechanisms and applications of inhibitory oligodeoxynucleotides against immune-mediated inflammatory diseases. Front. Pharmacol. *14*, 1–12.

Wang, Y., Yamamoto, Y., Shigemori, S., Watanabe, T., Oshiro, K., Wang, X., Wang, P., Sato, T., Yonekura, S., Tanaka, S., et al. (2015). Inhibitory/suppressive oligodeoxynucleotide nanocapsules as simple oral delivery devices for preventing atopic dermatitis in mice. Mol. Ther. *23*, 297–309.

Wang, Z., Kuhr, C.S., Allen, J.M., Blankinship, M., Gregorevic, P., Chamberlain, J.S., Tapscott, S.J., and Storb, R. (2007). Sustained AAV-mediated dystrophin expression in a canine model of duchenne muscular dystrophy with a brief course of immunosuppression. Mol. Ther. *15*, 1160–1166.

Wang, Z., Gerstein, M., and Snyder, M. (2010). RNA-Seq: a revolutionary tool for transcriptomics. Nat. Rev. Genet. *10*, 57–63.

Warga, E., Anderson, J., Tucker, M., Harris, E., and Elmer, J. (2023). Transcriptomic analysis of the innate immune response to in vitro transfection of plasmid DNA. Mol. Ther. - Nucleic Acids *31*, 43–56.

Warneck, L. (2021). Gene Therapy Industry Report 2021 a growing market, current challenges, and an exciting future.

Weemen, B.K. Van, and Schuurs, A.H.W.M. (1971). Immunoasssay Using Antigen-Enzyme Conjugates. FEBS Lett. *15*, 445–555.

Weeratna, R.D., Wu, T., Efler, S.M., Zhang, L., and Davis, H.L. (2001). Designing gene therapy vectors: Avoiding immune responses by using tissue-specific promoters. Gene Ther. *8*, 1872–1878.

Woo, S., Fuertes, M.B., Corrales, L., Spranger, S., Furdyna, M.J., Leung, M.Y.K., Duggan, R., Wang, Y., Barber, G.N., Fitzgerald, K.A., et al. (2014). STING-Dependent Cytosolic DNA Sensing Mediates Innate Immune Recognition of Immunogenic Tumors. Immunity *41*, 830–842.

Wu, J., Sun, L., Chen, X., Du, F., Shi, H., Chen, C., and Chen, Z. (2013). Cyclic-GMP-AMP Is An Endogenous Second Messenger in Innate Immune Signaling by Cytosolic DNA. Science (80-.). *339*.

Wu, Y., Han, B., Luo, H., Shi, G., and Wu, J. (2004). Dipeptide boronic acid, a novel proteasome inhibitor, prevents islet-allograft rejection. Transplantation *78*, 360–366.

Xiao, Y., Lu, W., Li, X., Zhao, P., Yao, Y., Wang, X., Wang, Y., Lin, Z., Yu, Y., Hua, S., et al. (2017). An oligodeoxynucleotide with AAAG repeats significantly attenuates burn-induced systemic inflammatory responses by inhibiting interferon regulatory factor 5 pathway. Mol. Med. *23*, 166–176.

Xu, Y.D., Cheng, M., Shang, P.P., and Yang, Y.Q. (2022). Role of IL-6 in dendritic cell functions. J. Leukoc. Biol. *111*, 695–709.

Yamada, H., Gursel, I., Takeshita, F., Conover, J., Ishii, K.J., Gursel, M., Takeshita, S., and Klinman, D.M. (2002). Effect of Suppressive DNA on CpG-Induced Immune Activation. J. Immunol. *169*, 5590–5594.

Yang, L., Pang, Y., and Moses, H.L. (2010). TGF-β and immune cells: an important regulatory axis in the tumor microenvironment and progression. Trends Immunol. *31*, 1–7.

Yang, T. yuan, Braun, M., Lembke, W., McBlane, F., Kamerud, J., DeWall, S., Tarcsa, E., Fang, X., Hofer, L., Kavita, U., et al. (2022). Immunogenicity assessment of AAV-based gene therapies: An IQ consortium industry white paper. Mol. Ther. - Methods Clin. Dev. *26*, 471–494.

Yang, Y., Su, Q., and Wilson, J.M. (1996). Role of viral antigens in destructive cellular immune responses to adenovirus vector-transduced cells in mouse lungs. J. Virol. *70*, 7209–7212.

Yew, N.S., Zhao, H., Wu, I.H., Song, A., Tousignant, J.D., Przybylska, M., and Cheng, S.H. (2000). Reduced Inflammatory Response to Plasmid DNA Vectors by Elimination and Inhibition of Immunostimulatory CpG Motifs. Mol. Ther. *1*, 255–262.

Yew, N.S., Zhao, H., Przybylska, M., Wu, I., Tousignant, J.D., Scheule, R.K., and Cheng, S.H. (2002). CpG-Depleted Plasmid DNA Vectors with Enhanced Safety and Long-Term Gene Expression in Vivo. Mol. Ther. *5*, 731–738.

Yoo, B.H., Bochkareva, E., Bochakarev, A., Mou, T.C., and Gray, D.M. (2004). 2′-O-methyl-modified phoshorothioate antisense oligonucleotides have reduced

non-specific effects in vitro. Nucleic Acids Res. *32*, 2008–2016.

Yu, Y.Z., Ma, Y., Xu, W.H., Wang, S., and Sun, Z.W. (2015). Combinations of various CpG motifs cloned into plasmid backbone modulate and enhance protective immunity of viral replicon DNA anthrax vaccines. Med. Microbiol. Immunol. *204*, 481–491.

Zeuner, R.A., Ishii, K.J., Lizak, M.J., Gursel, I., Yamada, H., Klinman, D.M., and Verthelyi, D. (2002). Reduction of CpG-induced arthritis by suppressive oligodeoxynucleotides. Arthritis Rheum. *46*, 2219–2224.

Zhang, C., Wang, H., Wang, H., Shi, S., Zhao, P., Su, Y., Wang, H., Yang, M., and Fang, M. (2022). A microsatellite DNA-derived oligodeoxynucleotide attenuates lipopolysaccharide-induced acute lung injury in mice by inhibiting the HMGB1-TLR4-NF-κB signaling pathway. Front. Microbiol. *13*, 1–15.

Zhang, Z., Yuan, B., Bao, M., Lu, N., Kim, T., and Liu, Y.J. (2011). The helicase DDX41 senses intracellular DNA mediated by the adaptor STING in dendritic cells. Nat. Immunol. *12*, 959–965.

Zhao, D., Thi, A., Tu, T., Shobo, M., Bui, N., Le, T., Yoshikawa, C., Sugai, K., Hakamata, Y., and Yamazaki, T. (2022). Non-Modified CpG Oligodeoxynucleotide Forming Guanine-Quadruplex Structure Complexes with ε -Poly- L -Lysine Induce Antibody Production as Vaccine Adjuvants. Mol. Med. *9*.

Zhao, Y., Ye, X., Dunker, W., Song, Y., and Karijolich, J. (2018). RIG-I like receptor sensing of host RNAs facilitates the cell-intrinsic immune response to KSHV infection. Nat. Commun. *9*, 1–14.